Durham University

Durham E-Theses

Synthesis and Evaluation of Small Molecules for Controlling Stem Cell Development

GARR LAYY ZHOU

How to cite:

ZHOU, GARR LAYY (2014) Synthesis and Evaluation of Small Molecules for Controlling Stem Cell Development. Doctoral thesis, Durham University.

Use policy

The full-text may be used and/or reproduced, and given to third parties in any format or medium, without prior permission or charge, for personal research or study, educational, or not-for-profit purposes provided that:

- a full bibliographic reference is made to the original source
- a https://etheses.durham.ac.uk/id/eprint/10761/ is made to the metadata record in Durham E-Theses
- the full-text is not changed in any way

The full-text must not be sold in any format or medium without the formal permission of the copyright holders.

Please consult the full Durham E-Theses policy for further details.

Academic Support Office, The Palatine Centre, Durham University, Stockton Road, Durham, DH1 3LE
e-mail: e-theses.admin@durham.ac.uk Tel: +44 0191 334 6107
https://etheses.durham.ac.uk

Department of Chemistry

Synthesis and Evaluation of Small Molecules for Controlling Stem Cell Development

Garr-Layy Zhou

Supported by:

High Force Research

A thesis submitted for the degree of Doctor of Philosophy

2014

Declaration

The work described in this thesis was carried out in the Department of Chemistry at Durham University and High Force Research Ltd in Bowburn between October 2010 and September 2013. All of the work is attributed to the author, except where specifically stated otherwise. No part has previously been submitted for a degree at this or any other university.

Statement of Copyright

The copyright of this thesis rests with the author. No quotation from it should be published without the author's prior written consent, and information derived from it should be acknowledged.

Abstract

Retinoids are a class of signalling molecules that includes vitamin A along with its natural and synthetic analogues. Retinoids regulate important biological pathways from embryogenesis through to adult homeostasis, and influence the proliferation and differentiation of a variety of cell types. The effects of retinoids are primarily mediated through binding to and activation of the retinoic acid receptors (RARs) and retinoid X receptors (RXRs). Three subtypes of RARs exist: RARα, RARβ and RARγ. Isoforms for each of these receptor subtypes are known, with the RARβ2 isoform in particular known to stimulate neurite outgrowth.

The design of isoform-selective ligands is thus an important area to allow investigation into the mechanism of activity of the individual RAR isoforms. Syntheses of the proposed RARβ2 agonists containing phenyl- and tetramethyltetrahydronaphthyl-substituted side chains are described herein. These thiazole-containing small molecules were assessed for activity in inducing the differentiation of human pluripotent TERA2.cl.SP12 embryonal carcinoma (EC) cells, with the more bulky tetramethyltetrahydronaphthyl analogue able to induce differentiation of this cell line to a level comparable to that of the natural retinoid, ATRA. Furthermore, at 0.1 μM, this analogue promoted enhanced neural commitment and neurite outgrowth over ATRA, with levels similar to that observed with the synthetic retinoid EC23.

The second part of this thesis concerns the synthesis of a fluorescent retinoid, **GZ108**, and preliminary assessments of its fluorescence and biological activities. In an effort to optimise the synthetic route and to improve compound stability, the preparation of *N*-acetyl, amide, and oxazoline analogues are also discussed.

Acknowledgements

I would like to thank my supervisors Prof. Andy Whiting and Prof. Todd Marder for their enthusiasm and guidance, which have been an inspiration and a motivation during my time at Durham.

Special thanks also to High Force Research for funding towards this project, to the directors Bob Redfern, Roy Valentine, and Stuart Penny for the enjoyable time spent at the company. Particular thanks to Nicola, Barry, Stephen, Owen, Ben, and Craig for generously giving their time and advice.

With thanks also to Prof. Stefan Przyborski, Bridie Murray, and Daniel Tams for help and assistance in biological techniques.

To the members of the Marder group who are now in different parts of the world: Jon, Marie-Hélène, Bianca, Andrew, Nim, Hazmi, Anna, Ji Lei, and Dongxia - thank you for a great introduction to postgraduate life.

It has been a pleasure to get to know all members past and present of the Whiting group. My thanks and best wishes go to: Andy, Ben, Hayley, Irene, Ricardo, Louis, Alex, Farhana, Adam, Hesham, Wade, David, Kate, Alba, and Serge.

Finally, I will always be grateful to my family for their continued support, encouragement, and love.

獻給

爸爸,媽媽和弟弟

Table of Contents

Declaration i
Abstract ii
Acknowledgements iii
Table of Contents v
Abbreviations ix
Publication xiv
1. INTRODUCTION 1
1.1. Retinoids 2
Cellular uptake of retinoids 2
Metabolism of retinoids 3
Retinoid signalling 3
Effects of retinoids 4
1.2. Retinoic acid receptors 6
Receptor structure 6
Receptor subtypes 7
Receptor functions 8
1.3. Retinoic acid receptor β (RARβ) 9
Role in cancer 9
Isoform-specific effects 9
1.4. Synthetic retinoids 12
Toxicity of natural retinoids 12
General structure of retinoids 12
Arotinoids and heteroarotinoids 13
Subtype-selective ligands 17
RARβ isoform selectivity 19
1.5. Summary 21
1.6. Project Aims 21
2. SYNTHESIS AND BIOLOGICAL EVALUATION OF THIAZOLE-CONTAINING RETINOIDS. 22
2.1. Background and Aims 23
2.2. Synthesis of 2,4-disubstituted thiazole derivatives 25
2.3. Effect of thiazole retinoid-like small molecules on the differentiation of human pluripotent stem cells 29

Cell culture 29
Cell viability assay 31
Differentiated-cell assay 33
Effect on neurite outgrowth 36
2.4. Stability study 38
2.5. Conclusions and Outlook 38
3. FLUORESCENCE IMAGING 40
3.1. Cell imaging 41
3.2. Fluorescence 42
3.3. Fluorescence microscopy 43
3.4. Fluorophores 45
Small organic dyes 46
Fluorescent proteins 48
Quantum dots 50
3.5. Factors influencing fluorescence 51
Photobleaching 51
Quenching 52
3.6. Tracking in live cells 54
Membrane proteins 55
Cytoplasmic proteins 56
Other Single Objects 59
3.7. Summary 61
4. DESIGN AND SYNTHESIS OF FLUORESCENT RETINOIDS 62
4.1. Background and Aims 63
4.2. Aza-EC23 64
Synthetic route 65
Light stability study 66
Proposed degradation routes 67
4.3. Synthesis of an aza-EC23 derivative (GZ108) 68
Construction of the hydrophobic core 68
Direct iodination approach 70
Aromatic bromination 72
Synthesis of an enamine species 74
Synthesis of a dibromide species 76

Reactions of the dibromide species....81
Synthesis of the polar terminus....85
Halogen-exchange reaction....87
Sonogashira reactions with an aromatic bromide....89
Base desilylation....92
Second Sonogashira coupling....92
Ester hydrolysis....93
4.4. Stability and purification of GZ108....94
Photodehydrogenation....94
Proposed light-promoted radical mechanisms....98
Oxidation reactions....100
Separation by HPLC....101
4.5. Initial fluorescence data and biological evaluation....103
4.6. Synthesis of a bromine-containing retinoid....107
4.7. Synthesis of a fluorescent retinoid *via* an *N*-acetyl compound....110
Proposed synthetic route....111
Acetylation....112
Alkylation....113
Cyclisation....114
Iodination....125
Low-energy conformation calculations....126
4.8. Synthesis of an amide-containing retinoid....129
Target hydrophobic core....130
N-Alkylation....131
Cyclisation reactions....133
Derivatisation reactions....136
Sonogashira coupling and hydrolysis....136
4.9. Synthesis of an amide retinoid *via* an oxazoline compound....141
4.10. Conclusions and Outlook....144
5. CONCLUDING REMARKS AND FUTURE WORK....145
5.1. Concluding remarks....146
5.2. Future work....148
6. EXPERIMENTAL....149
6.1. General experimental....150

6.2. Synthetic procedures for thiazole-containing retinoids 151
6.3. Biological procedures 156
Tissue culture 156
Neurite outgrowth assay 157
Cell viability assay 158
Flow cytometric analysis of pluripotent TERA2.cl.SP12 EC cells 158
Immunocytochemistry with human pluripotent TERA2.cl.SP12 EC cells and neuroprogenitor ReN197 VM cells 159
6.4. Synthetic procedures for a fluorescent retinoid 160
6.5. Synthetic procedures for a bromine-containing retinoid 172
6.6. Synthetic procedures for *N*-acetyl compounds 174
6.7. Synthetic procedures for amide-containing retinoids 178
6.8. Synthetic procedures for oxazoline-containing compounds 186
7. REFERENCES 190

Abbreviations

AAV	adeno-associated virus
aq.	aqueous
AF-1	ligand-independent activation function
AF-2	ligand-dependent activation function
ATRA	all-*trans*-retinoic acid
br s	broad singlet
BSA	bovine serum albumin
c.	concentrated
cAMP	cyclic adenosine monophosphate
CCD	charge-coupled device
CDK	cyclin-dependent kinase
CNS	central nervous system
CRABP	cellular retinoic acid-binding protein
CRBP	cellular retinol-binding protein
CST	corticalspinal tract
CYP	cytochrome
δ	chemical shift
d	doublet
Da	dalton
DAPI	4’,6-diamidino-2-phenylindole

DBD	DNA-binding domain
DCM	dichloromethane
dd	doublet of doublets
ddd	doublet of doublet of doublets
DDQ	2,3-dichloro-5,6-dicyano-1,4- benzoquinone
DIPEA	*N*,*N*-diisopropylethylamine
DMAP	4-dimethylaminopyridine
DMEDA	dimethylethylenediamine
DMEM	Dulbecco's modified eagle's medium
DMF	dimethylformamide
DMSO	dimethyl sulfoxide
DNA	deoxyribonucleic acid
DNPH	2,4-dinitrophenylhydrazine
DRG	dorsal root ganglia
EC	embryonal carcinoma
ECFP	enhanced cyan fluorescent protein
EGF	epidermal growth factor
ES	electrospray
Et	ethyl
EYFP	enhanced yellow fluorescent protein
FGF	fibroblast growth factor

FIONA	fluorescence imaging with one nanometer accuracy
FITC	fluorescein isothiocyanate
FP	fluorescent protein
FRET	Förster resonance energy transfer
GC	gas chromatography
GFP	green fluorescent protein
HPLC	high-performance liquid chromatography
HRMS	high-resolution mass spectrometry
HTS	high-throughput screening
IC	import complex
IR	infrared
J	coupling constant
LBD	ligand-binding domain
LBP	ligand-binding pocket
LCMS	liquid chromatography-mass spectrometry
LRAT	lecithin:retinol acyl transferase
m	multiplet
m.p.	melting point
ms	millisecond
min	minutes
Me	methyl

MS	mass spectrometry
MW	microwave
NCS	*N*-chlorosuccinimide
NE	nuclear envelope
NIS	*N*-iodosuccinimide
nm	nanometer
NMR	nuclear magnetic resonance
NPC	nuclear pore complex
PBS	phosphate-buffered saline
PPA	polyphosphoric acid
QD	quantum dot
r.t.	room temperature
RA	retinoic acid
Ral	retinal
RALDH	retinal dehydrogenase
RAR	retinoic acid receptor
RARE	retinoic acid response element
RBP	retinol-binding protein
R_f	retention factor
RDH	retinol dehydrogenase
RNA	ribonucleic acid

R-SAT	Receptor Selection and Amplification Technology
RT	room temperature
RXR	retinoid X receptor
s	singlet
SAR	structure-activity relationship
SEM	standard error of the mean
SNR	signal to noise ratio
sRBP / RBP	serum retinol-binding protein
SSEA-3	stage-specific embryonic antigen 3
TF	transcription factor
TFA	trifluoroacetic acid
Tf	triflyl, CF_3SO_2
TLC	thin layer chromatography
THF	tetrahydrofuran
TMS	tetramethylsilyl
TMSA	trimethylsilylacetylene
unsymmet. d	unsymmetrical doublet
UV	ultraviolet
VAD	vitamin A deficiency
w/v	% weight per volume
YFP	yellow fluorescent protein

Publication

"Synthesis and applications of 2,4-disubstituted thiazole derivatives as small molecule modulators of cellular development"

- Garr-Layy Zhou, Daniel M. Tams, Todd B. Marder, Roy Valentine, Andrew Whiting and Stefan A. Przyborski, *Org. Biomol. Chem.*, 2013, **11**, 2323-2334.

1. INTRODUCTION

1.1. Retinoids

Vitamin A (retinol) and its derivatives belong to a class of compounds known as retinoids. This term encompasses a group of signalling molecules that regulates many important biological pathways from embryogenesis through to adult homeostasis, and controls many aspects of cell development, proliferation, differentiation, and apoptosis.[1] There are over 4000 natural and synthetic molecules that are structurally and/or functionally related to vitamin A; naturally occurring retinoids possessing biological activity include all-*trans*-retinoic acid (ATRA, or simply RA), 9-*cis*-retinoic acid (9-*cis*-RA), 11-*cis* retinaldehyde, and 3,4-didehydro retinoic acid.[2] ATRA is the most abundant endogenous retinoid and has been widely studied for many years; ATRA isomerises under physiological and experimental conditions, with different isomers activating different receptors, thus accounting for the variety of biological effects observed with these small molecules.

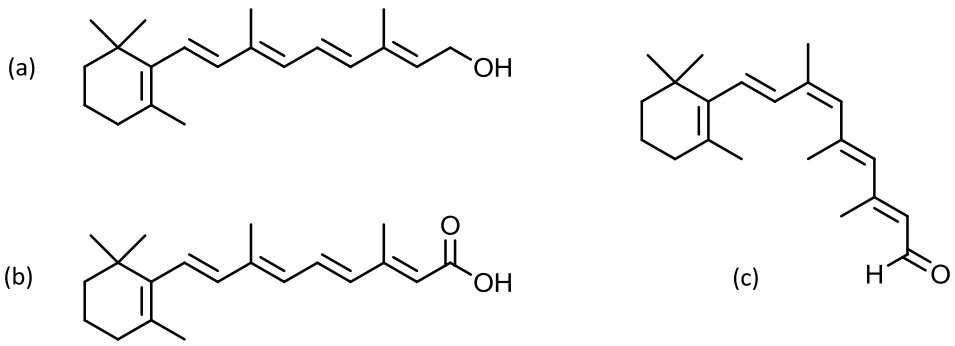

Fig. 1 Examples of some naturally occurring retinoids: (a) retinol (vitamin A); (b) all-*trans*-retinoic acid (ATRA); (c) 9-*cis*-retinoic acid (9-*cis*-RA).

Cellular uptake of retinoids

Since animal species are unable to synthesise vitamin A, it is therefore obtained solely through the diet in the form of retinol, retinyl esters, or β-carotene. Ingested vitamin A is stored as retinyl esters in the liver, as well as in various extrahepatic sites including the heart, kidney, lung, adipose tissue, skeletal muscle, bone marrow, spleen, eye, and testis.[3,4] Retinol is secreted from these areas and is transported in the blood bound to

the serum retinol-binding protein 4 (RBP4), where it is taken up by target cells through interacting with STRA6, a widely expressed multi-transmembrane receptor protein.[5] An enzyme responsible for esterifying vitamin A within the cell, lecithin:retinol acyl transferase (LRAT), is also required for effective uptake of vitamin A *via* this pathway.[6] High levels of STRA6 are expressed at blood/organ barriers, as well as in various embryonic and adult cell types during development,[7] which is indicative of a necessity for retinoid action at these sites; vitamin A can thus be delivered to defined cell types according to requirement.

Metabolism of retinoids

Upon entering the cytoplasm, retinol is either stored or converted into a form that is able to regulate gene transcription. In the latter case, retinol binds to the cellular retinol-binding protein 1 (CRBP1) and is subsequently metabolised in two steps to ATRA: in many cell types the enzyme retinol dehydrogenase 10 (RDH10) reversibly oxidises retinol to retinal, which may then be irreversibly oxidised to ATRA by retinal dehydrogenases (RALDHs).[8] The cytoplasmic proteins cellular RA-binding proteins 1 and 2 (CRABP1 and CRABP2) bind to the newly synthesised RA; CRABP1 is known to inhibit retinoid activity by sequestering free RA, while CRABP2 appears to regulate RA transport and metabolism both in the developing embryo and throughout adult life.[9] Thus, the *in vivo* regulation of vitamin A metabolism by these binding proteins to generate biologically active retinoids is an important area for investigation.

Retinoid signalling

Inside the cell, CRABP2-bound RA is transported to the nucleus and exerts its physiological effects through interacting with the retinoic acid receptors (RARs) and retinoid X receptors (RXRs).[10] These heterodimerise and bind specific DNA sequences termed retinoic acid response elements (RAREs) in the promoter region of target genes; the ternary complex of ligand-bound RAR with RXR and a RARE regulates gene transcription through altering the binding of corepressors and coactivators. ATRA binds predominately to RARs, while other retinoids such as 9-*cis*-RA exhibit a greater

affinity for RXRs.[11] Following RAR activation, ATRA is released, exits the nucleus, and is oxidised for degradation and removal in the cytoplasm of cells expressing cytochrome P450, CYP26 (Fig. 2).

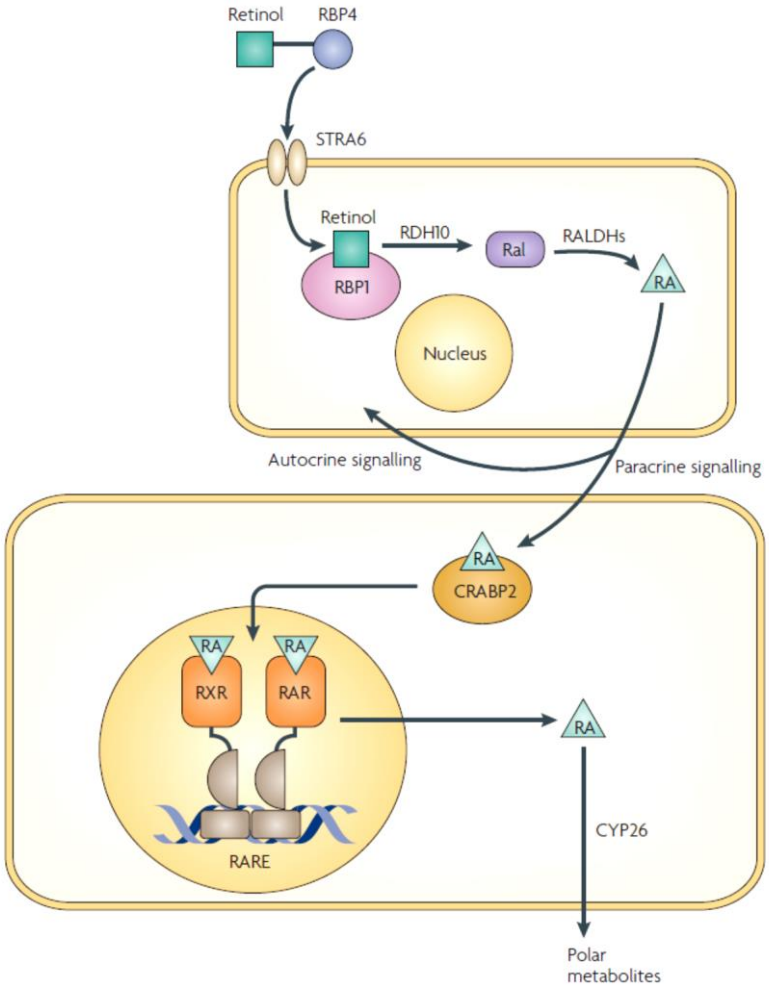

Fig. 2 Pathways involved in the generation, action and catabolism of RA.[12]

Reprinted by permission from Macmillan Publishers Ltd: NATURE REVIEWS NEUROSCIENCE (M. Maden, 2007, **8**, 755-765), copyright 2007.

Effects of retinoids

By regulating gene expression through binding their nuclear receptors, retinoids control the development and maintain the functions of numerous biological systems. Important processes regulated by these signalling molecules include reproduction (spermatogenesis, conception, placental formation), embryogenesis (patterning of the

body axis, development of the nervous system, formation of digits), bone remodelling, epithelial differentiation, and the immune system.

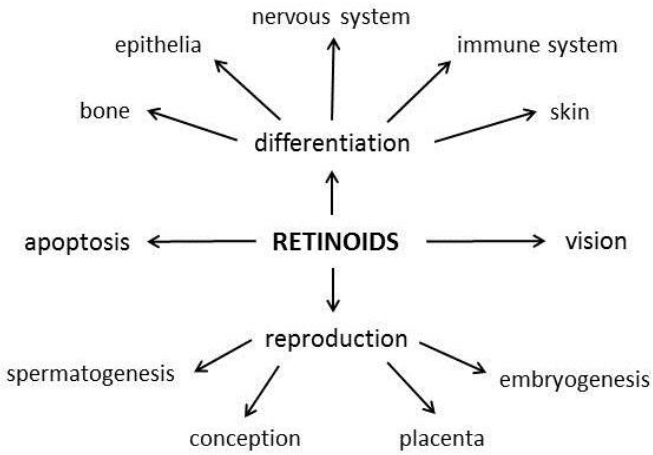

Fig. 3 Functions of naturally-occurring retinoids.

Retinoids are vital for cell proliferation, differentiation, and apoptosis in both normal and cancerous cells. A particular area of interest concerns the role of RA in the survival and differentiation of vertebrate central nervous system (CNS) neurons in the developing embryo.[13] While many factors are involved in the regulation of neurogenesis, recent studies indicate that RA is able to induce differentiation of progenitor cells into neuronal cells.[14] Similarly, RA is known to induce differentiation of various types of neurons and glia through transcriptional activation of genes encoding transcription factors, cell signalling molecules, structural proteins, enzymes, and cell-surface receptors.[15,16] RA also plays a role in maintaining the differentiated state of adult neurons and neural stem cells, with altered RA signalling levels contributing to the symptoms of some neurodegenerative diseases.[17]

The generation of specific classes of neurons from neural progenitor cells in response to RA has been studied extensively,[18] including the differentiation of neuroepithelial cells into ventral spinal progenitors and postmitotic motorneurons after treatment with RA followed by an additional small molecule, purmorphamine.[19] It is interesting

to note that, while the role of RA in directing a high specification of distinct cell types has been established in various progenitor stem cell lines, there is a lack of compelling evidence thus far to support comparable retinoid activity at the level of the pluripotent stem cell.

Retinoids are widely used in the treatment of visual and dermatological conditions, and they have also gained considerable attention in the field of cancer research, specifically as chemopreventive and chemotherapeutic agents, due to their differentiation, anti-proliferative, pro-apoptotic, and anti-oxidant effects. Retinoids were found to suppress carcinogenesis in studies using animal models for bladder, breast, lung, oral, ovarian, prostate, and skin cancer.[20-26] In humans, retinoid treatment reversed premalignant human epithelial lesions and prevented lung, liver, and breast cancers.[27-30]

1.2. Retinoic acid receptors

Receptor structure

Retinoids exert their physiological effects primarily through binding to and activating the ligand-dependent transcription factors RAR and RXR, leading to transcriptional activation of their downstream target genes. These two distinct classes of receptors belong to the superfamily of nuclear receptors, the common structure of which is shown in Fig. 4: the *N*-terminal A/B region is the ligand-independent transactivation domain, AF-1, that associates with co-activators and other transcription factors; the DNA-binding domain (DBD) contains two zinc finger motifs that bind specific DNA target sequences (RARE); the ligand-binding domain (LBD) consists of twelve α-helices forming a ligand-binding pocket (LBP) and is highly conserved among the nuclear receptor family. This latter region also contains the ligand-induced activation function, AF-2, that is critical in receptor interaction with transcriptional coregulators.[31]

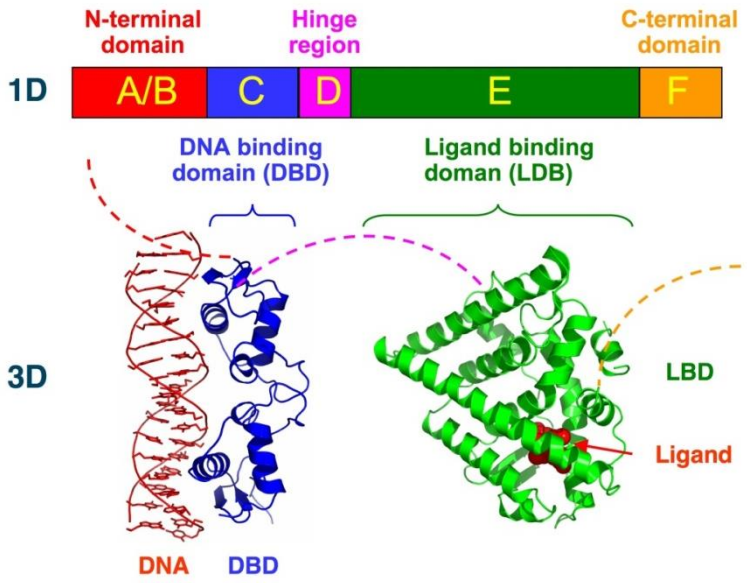

Fig. 4 Structural organisation of nuclear receptors.

(Reproduced from: http://en.wikipedia.org/wiki/Nuclear_receptor)

Receptor subtypes

RARs and RXRs each consist of three subtypes: α, β, γ, which are encoded by separate genes on six different chromosomes.[32,33] As a result of the differential usage of two promoters and alternative splicing, isoforms of each subtype exist in a tissue-related pattern. These isoforms differ in their *N*-terminal regions; there are two major isoforms for RARα (α1 and α2) and RARγ (γ1 and γ2), and five major isoforms for RARβ (β1-β4 and β1'). Two major isoforms for RXRα (α1 and α2), RXRβ (β1 and β2), and RXRγ (γ1 and γ2) are also known.

RARs and RXRs are expressed in a tissue-specific manner during development: RARα is expressed ubiquitously in adult tissue and in the developing embryo, while RARβ and RARγ display highly regionalised and/or cell type-specific expression: RARβ is prevalent in neural tissues and RARγ is expressed predominately in the skin. RXRα is found in limited adult and embryo tissues including the liver, skin, kidney, spleen, and lung. RXRβ is more widely expressed in both the adult and embryo, while RXRγ expression appears to be restricted to mainly muscle and brain tissues.[34]

Receptor functions

Numerous knockout studies using mice have been carried out in order to determine the *in vivo* functions of RAR and RXR: spermatogenesis was inhibited in RARα-null males, rendering the subjects sterile; abnormalities in the vitreous body of the eye, and impaired movement and motor coordination were observed in RARβ-null mice; RARγ knockout animals displayed both skeletal and epithelial defects.[35-37] Targeted disruption of the RXRα gene resulted in embryonic lethality due to incomplete development of the ventricular chambers of the heart; foetuses lacking RXRα displayed ocular malformations, and it appears that this gene is also involved in mediating the teratogenic effects of retinoids.[38-40] Ablation of RXRβ in mice gave rise to approximately 50% lethality in utero; similar to RARα-knockout mice, RXRβ-null mice are also sterile: however, this is due to testicular defects and abnormal spermatid maturation.[41] RXRβ also appears to be involved with other nuclear receptors in the control of lipid metabolism.[42] Disruption of RXRγ produced no adverse effects on growth, fertility, viability, and behaviour in mice, suggesting that this gene does not exert any essential functional that is not also performed by the other RXR subtypes.[43]

In addition to the knockout approach, selective activation with retinoids is able to provide further insight into the individual functions of these receptors. For example, abnormalities observed in RARα and RARβ double null mice in the area of early lung morphogenesis include unilateral lung agenesis and unilateral or bilateral lung hypoplasia,[44] however, these effects are not observed in RAR single knockout mice.[45.46] Thus, in order to define specific roles for the individual receptors, synthetic retinoids were used to selectively activate RARα and RARβ signalling in RALDH2-null mice: activation of RARβ, but not RARα, induced expression of the fibroblast growth factor FGF10 and bud morphogenesis in the lung field. RARα activity was required to maintain overall RA signalling, and to assist in the effects mediated by RARβ.[47]

1.3. Retinoic acid receptor β (RARβ)

Role in cancer

Due to their involvement in regulating gene networks that control cell growth, differentiation, survival, and death, RARs are linked to the cancer chemotherapeutic and chemopreventive properties of retinoids. RARβ has received considerable attention in this field, and many studies have documented the critical role of this receptor subtype in mediating the retinoid growth-inhibitory effect in various types of cancer cells, including breast cancer, lung cancer, ovarian cancer, prostate cancer, neuroblastoma, renal cell carcinoma, pancreatic cancer, and liver cancer.[48-55] Expression of RARβ is often lost in many abnormal tissues, and in certain cases this may be attributed to gene silencing through epigenetic modifications such as DNA methylation, histone hypermethylation, and deacetylation.[56-58] Treatments that reverse these alterations have thus been highly successful in restoring the retinoid-induced anti-proliferative effect in various types of tumours.[58,59] Similarly, transfection of RARβ into RARβ-null cervical, breast, and lung cancer cells also increased responsiveness to the growth inhibitory and apoptosis action of retinoids.[60-62] Since expression of RARβ inversely correlates with tumour grade, this receptor is an important target for anticancer research, and ligands that exhibit RARβ-selective agonist activities constitute highly desirable targets for synthesis and application in this field.

Isoform-specific effects

In humans, the tumour-suppressive properties of retinoids are thought to be mediated primarily through the RARβ2 isoform, which is the most abundant of the RARβ isoforms.[63] The promoter region of the gene encoding this receptor contains a very high affinity RA-responsive element,[64] which directly accounts for the rapid RA-induced transcriptional activation of RARβ2 in various cell types.[65]

RARβ2 is thought to be the crucial transducer of the RA signal in neurons, and holds particular interest in the area of neurodegenerative disease research. Following

treatment with RA, upregulation of RARβ2 was observed in both embryonic and adult mouse dorsal root ganglia (DRG) neurons, along with stimulation of neurite outgrowth in both cell cultures.[66] Strikingly, it was an RARβ-specific ligand that induced these effects, rather than an RARα or RARγ agonist. A failure to regenerate axonal projections in these tissues could, therefore, be attributed to the absence, or reduced level, of RARβ; this theory is supported by the lack of peripheral axonal regeneration observed in adult RARβ-null mice.[67]

Compelling evidence to support isoform-specific receptor activity was observed when a viral vector expressing RARβ2 was transduced with non-regenerative adult mouse and rat spinal cord.[68] This produced a large number of neurites in both mouse and rat cords, which was not observed in spinal cords transfected with empty or mutated vectors, when different RAR isoforms were used, or when the cells were treated with nerve growth factor. Overexpression of RARβ2 by lentiviral vectors in adult DRG or corticospinal tract (CST) neurons has also resulted in axonal outgrowth and functional recovery in models of CNS injury.[69,70]

Since the gene for RARβ contains an RARE that can bind RARβ2, introduction of an RARβ agonist may be expected to give rise to *in vivo* autoregulation of RARβ2 expression in neurons. This concept has been applied in a rodent model of spinal cord injury in order to demonstrate that both axonal outgrowth and functional recovery are induced in response to an RARβ agonist, CD2019.[71] These results indicate that loss of RA-driven signalling pathways arising from a lack of an appropriate ligand to activate RARβ2/RXR heterodimers may be a contributing factor in the failure of axonal outgrowth in the injured CNS. The ligand may be administered at the time of spinal cord injury, with enhanced neurite outgrowth evident in DRG explants from CD2019-treated lesioned animals (Fig. 5). Moreover, studies have shown that RARβ agonists are able to stimulate proliferation and differentiation of neural progenitor cells,[72] which may also be a contributing factor in the functional recovery observed with the CD2019-treated lesioned animals. Ligand therapy thus presents a simpler and more practical alternative to using lentiviral vectors overexpressing RARβ2: the dosage of,

and length of exposure to, the agonist may be controlled, and the small size and lipophilicity of the ligand means that potentially all affected neurons may be reached.

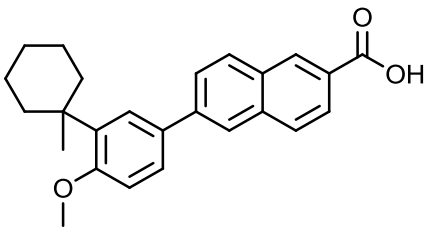

CD2019 (RARβ-agonist)

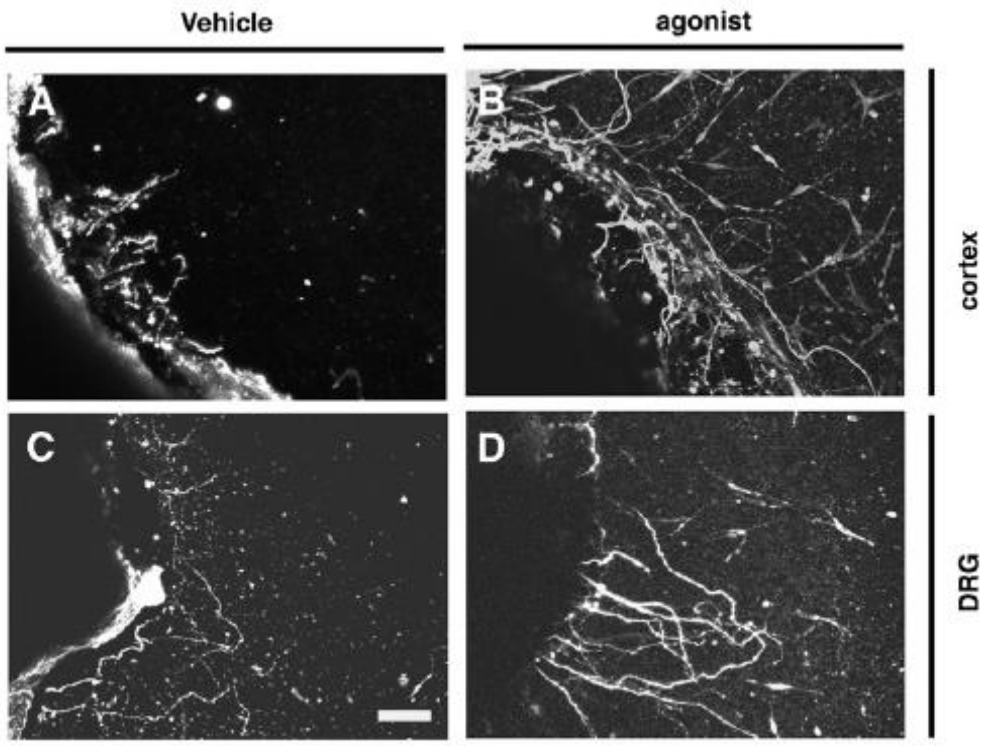

Fig. 5 Stimulation of neurite outgrowth observed in the cortex and DRG explants obtained from lesioned animals treated with the RARβ agonist CD2019. A control vehicle was included consisting of 10% DMSO in PBS.[71]

1.4. Synthetic retinoids

Toxicity of natural retinoids

Due to the diverse functions of the retinoic acid receptors (discussed in sections 1.2 and 1.3), the non-selective receptor activation exhibited by natural retinoids is accompanied by a high toxicity profile, with severe side-effects observed when administering RA and its derivatives in various clinical trials.[73] Toxicities associated with long-term retinoid treatment affect the skin, mucous membranes, hair, eyes, gastrointestinal system, liver, neuromuscular system, endocrine system, kidneys, and bone.[74] The adverse effects of vitamin A are well documented in the medical community, with reports of patients presenting with unusual symptoms, notably hepatic congestion and fibrosis, after ingesting large doses of vitamin A.[75] Patients with increased risk of hypervitaminosis A include those with severe type I hyperlipidaemia, causing an impaired ability to metabolise retinoids,[76] and a familial clustering of individuals exhibiting characteristic symptoms of toxicity despite only a modest retinol intake implies a genetic predisposition towards intoxication.[77] Natural retinoids are thus unsuitable for long-term clinical studies, and the synthesis of analogues possessing enhanced receptor-selective agonist activity and, as a result, a reduced level of toxicity, is highly desirable for facilitating such studies.

General structure of retinoids

Retinoids can be considered to have three units: a bulky hydrophobic region, a linker unit, and a polar terminus, which is usually a carboxylic acid (Fig. 6). The small size and amphiphilic nature of retinoids means they may be effectively transported across lipid cell membranes and into the nucleus, where receptor binding initiates a signalling cascade that produces the physiological effects observed with these biomolecules.

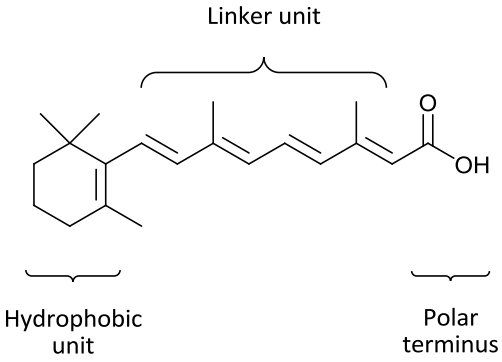

Fig. 6 The general structure of retinoids (exemplified by ATRA).

The presence of a long-chain conjugated polyene unit in natural retinoids renders these molecules sensitive to oxidation and isomerisation in response to acid, light, or heat. Furthermore, the susceptibility of retinoids to metabolic removal, and a poor solubility in aqueous media, limits their pharmacological utility.[78] Thus, the design and synthesis of ligands that are stable under both laboratory and metabolic conditions will assist in a more thorough analysis of the effects and therapeutic potential of retinoids.

Arotinoids and heteroarotinoids

It was recognised that structures without the classic polyene chain could also be effective as retinoid substitutes, which led to the dramatic expansion of the range of molecules synthesised for biological evaluation. 4-[(1*E*0-2-(5,5,8,8-Tetramethyl-5,6,7,8-tetrahydro-2-naphthalenyl)-1-propen-1-yl]benzoic acid, TTNPB (Fig. 7), is generally viewed as the first stable and highly potent RAR-selective agonist.[79] This molecule contains the 1,1,4,4-tetramethyl-1,2,3,4-tetrahydronaphthalene moiety, which is structurally similar to the trimethylcyclohexenylvinyl unit present in natural retinoids. Since the number of atoms exposed to enzymatic digestion is reduced, this building block is more resistant to radical oxidation and epoxidation, and there is also less potential for conformational isomerisation. The successful substitution of aromatic rings into retinoid structures, giving rise to a class of compounds known as arotinoids, have afforded RAR-selective agonists exhibiting remarkable chemical

stability along with improved bioavailability. Hence, in biological assays, TTNPB was found to be 10-fold more potent than ATRA, but also considerably more toxic, when used as a pharmacological agent.[80]

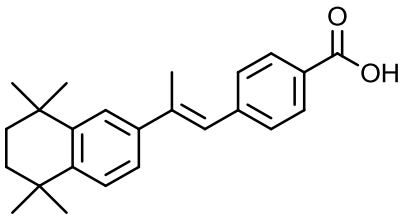

Fig. 7 TTNPB, a RAR-selective synthetic retinoid.[80]

Retinoids selective to each RAR subtype have also been reported: the TTNPB derivative Am80 demonstrates selective activity towards RARα as well as RARβ, and led to the development of further RARα-selective retinoids, such as Am555S and AGN-193836; BMS961 was developed as a RARγ-selective retinoid (Fig. 8).[81-83] It is interesting to note in these structures the presence of an amide linking group between two aromatic rings.

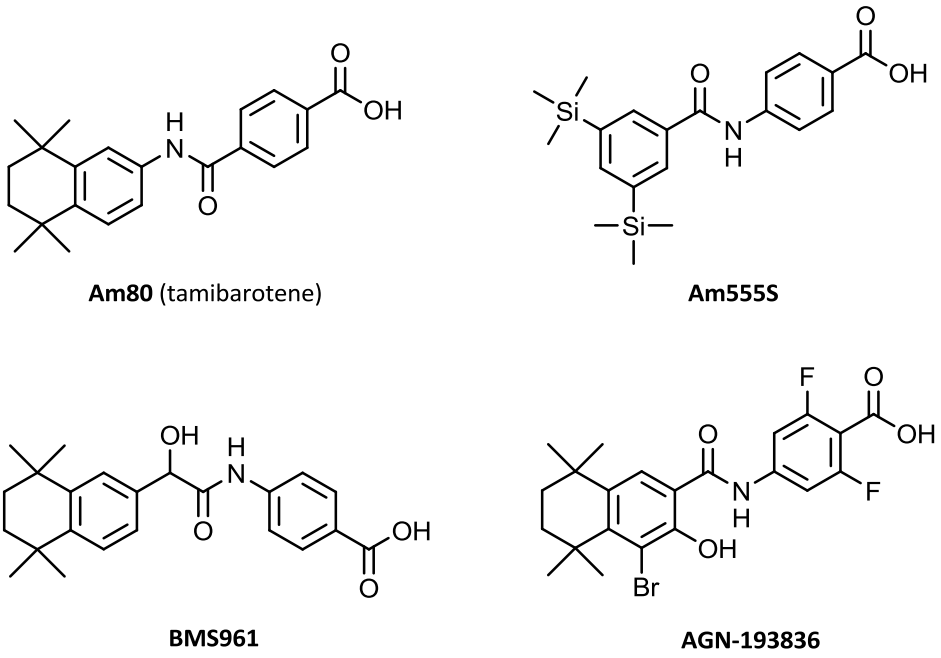

Fig. 8 RAR-subtype selective arotinoids: Am80 (RARα- and RARβ-selective); Am555S and AGN-193836 (RARα-selective); BMS961 (RARγ-selective).[81-83]

The substitution of one of the *gem*-dimethyl groups on the tetrahydronaphthalene ring of TTNPB with oxygen or sulphur produces a group of compounds known as heteroarotinoids (Fig. 9). Similar biological activities of these molecules compared to ATRA were observed,[84] along with reduced toxicities,[85] which may be attributed to the presence of an electronegative heteroatom.[86] However, the reported lower activities of some heteroarotinoids can be due to the increased susceptibility of the molecules towards metabolic removal: for example, TTNPB may be expected to be more active than its thia-analogue, since the sulphur atom present in the latter can potentially be oxidised to a sulfone or sulfoxide. Although beyond the scope of this introduction, it is worth noting that RXR-selective ligands are also known.[87,88]

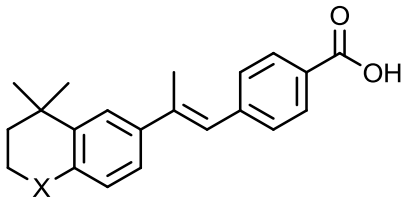

TTNPB analogues (X = O, S, NR)

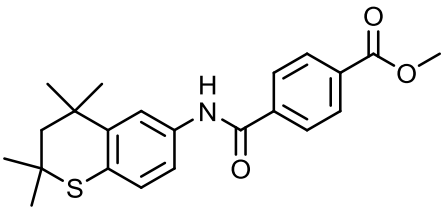

SHet50
RAR and RXR pan-agonist

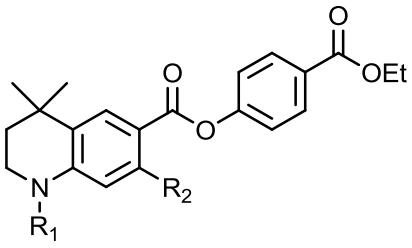

NHet17: $R_1 = CH(CH_3)_2$, $R_2 = H$
NHet86: $R_1 = CH_3$, $R_2 = H$
RARα/β and RXRα/β/γ active, RARγ inactive

NHet90: $R_1 = CH_3$, $R_2 = CH_3$
RARα/β/γ and RXRα/β/γ active

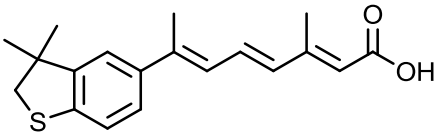

SHet65
RARγ-selective

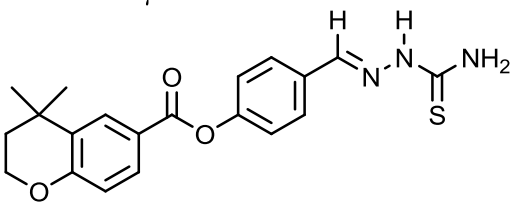

OHet72
RXR-specific

Fig. 9 Examples of heteroarotinoids.[84-88]

Most potent synthetic retinoids consist of a benzoic acid or other aromatic carboxylic group in place of the unstable polyenecarboxylic acid present in natural retinoids. Additionally, the structure of the hydrophobic region and linking group may be varied while retaining high activity. However, replacing the terminal carboxylic acid with other functional groups such as an aminosulfonyl, amidino, or tetrazolyl, is generally accompanied by a significant decrease, or loss, of activity.[81] However, a thiazolidinedione moiety (such as TZ335, Fig. 10a) has been suggested as an effective replacement,[89] as well as a tropolone ring (for example, Tp80, Fig. 10b).[90] The latter moiety, 2-hydroxy-2,4,6-cycloheptatrien-1-one, is an isomer of benzoic acid, consisting of a seven-membered, non-benzenoid aromatic molecule containing three double bonds conjugated with a carbonyl group. Furthermore, a novel retinoid structure has recently been reported containing a 1,2,4-oxadiazol-5-one group as the polar terminus, with one compound in particular displaying significant activity towards RARβ (Fig. 10c).[91]

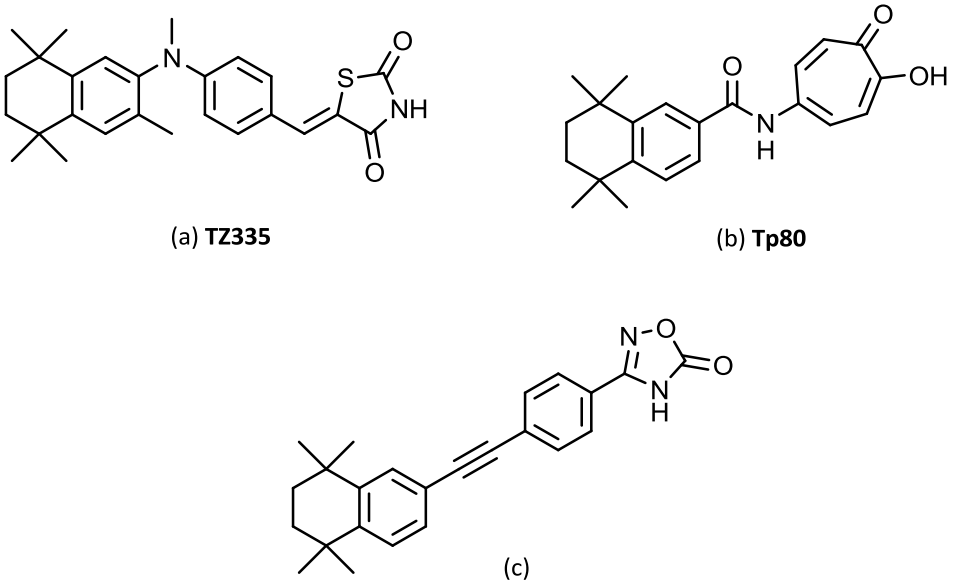

(a) **TZ335** (b) **Tp80**

(c)

Fig. 10 Synthetic retinoids containing (a) thiazolidinedione[89], (b) tropolone[90], and (c) 1,2,4-oxadiazol-5-one[91] functional groups in place of a carboxylic acid terminus.

Subtype-selective ligands

A ligand exhibiting an affinity difference greater than 100-fold between its primary target and other receptors may be considered as selective for this particular receptor.[92] Below this threshold, the ligand is defined as showing preference for the given receptor. The advantages of producing RAR-selective agonists for the purposes of investigating the physiological function of these receptors, as well as to provide novel tools for research and therapeutic exploitation, are clear: synthetic ligands with reduced toxicity profiles and increased stabilities compared to natural retinoids will greatly assist in the application and study of these compounds in the context of biological systems.

The individual RAR subtypes are associated with different phenotypes: RARγ is linked to skin,[93] bone and teratogenic toxicity,[94] whereas RARα is associated with elevated triglyceride levels.[95] Examples of synthetic retinoids that selectively target these subtypes are known.[82,96] RARβ exhibits a more restricted expression profile[97] and appears to be a promising anticancer target due to its ability to supress proliferation of specific cell types.[98] The major toxicity issues associated with the other RARs mean that the use of an RARβ-selective ligand can potentially circumvent these problems. However, the design of these subtype-selective ligands is complicated by the similarity of the RAR LBDs: the LBD of RARβ differs from that of RARα and RARγ by only one and two residues, respectively.

In order to gain more insight into the distinguishing structural features of the RAR isotypes, the 3D-structure of the RARβ LBD was determined (Fig. 11), and superposition with the RARγ LBD revealed the former to be significantly larger.[99] Rather than being due to a conformational adaptation in response to ligand-binding, this reflects a different architecture of the LBDs: In RARβ, the I263 side chain is in a position that allows for the creation of an additional cavity between H5 and H10. This is not possible in the case of the RARγ LBD, since the residue M272 is directed towards the interior of the binding-pocket.[100] From these findings, it can be inferred that

ligands able to occupy the additional space in RARβ may acquire selectivity for this subtype.

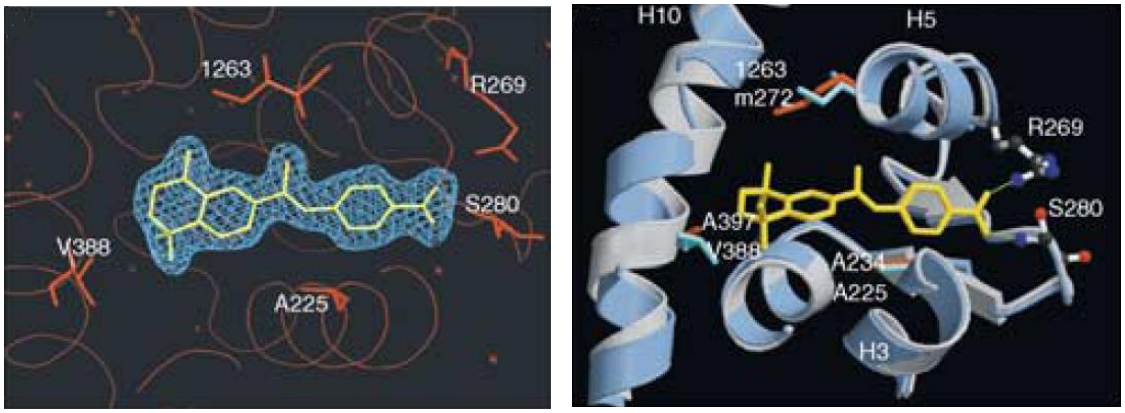

Fig. 11 Left: Electron density map of TTNPB in RARβ LBD; Right: Superposition of TTNPB-RARβ (blue) and 9-*cis*-RA-RARγ (grey) LBDs. Isotype-specific residues are shown in cyan (RARβ) and orange (RARγ), and TTNPB in yellow (*reproduced with permission*).[99]

Through screening a panel of synthetic retinoids using an *in vivo* reporter cell system, BMS641 (Fig. 12) was found to exclusively activate RARβ with an affinity 100 times greater than that for RARα or RARγ.[99] Since the non-chlorinated analogue was able to bind to all three RARs with similar affinity profiles, the presence of a halogen at the C3 position was thought to be a crucial determinant for generating RARβ selectivity.

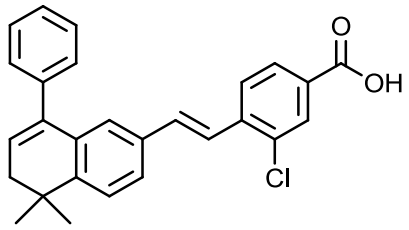

Fig. 12 RARβ-selective agonist, BMS641.[99]

RARβ isoform selectivity

It is evident that ligands selectively targeting RARβ2 would be of great advantage in exploring conditions associated with an absence, or lack of function, of this receptor; however, the design of these isoform-selective agonists represents an even more challenging prospect: The LBDs of the isoforms are identical and differ only in their *N*-terminus, in a region encompassing the ligand-independent activation domain AF-1. Therefore, rational drug design based on the current crystal structures of RARβ is unlikely to be extended to include isoform selectivity.

Despite these difficulties, isoform-selective agonists have been identified using a high throughput screening assay, namely, receptor selection and amplification technology (R-SAT). Thus, a chemical library of over 160,000 compounds was assessed for activity against the RARβ2 receptor, and led to the identification of 4'-octyl-4-biphenylcarboxylic acid, AC-55649 (Fig. 13) as an RARβ2-selective ligand, which displayed 100-fold activity for RARβ2 over other RARs, along with a potency of 100 nM.[101] Studies of structure-activity relationships of these biphenyl compounds revealed the importance of chain length for activity, with the octyl to nonyl chain analogues displaying optimal RARβ2-agonist activity. A hit-to-lead optimisation led to the synthesis of a more potent RARβ2 agonist possessing drug-like properties, the thiazole-containing compound AC-261066 (Fig. 13).

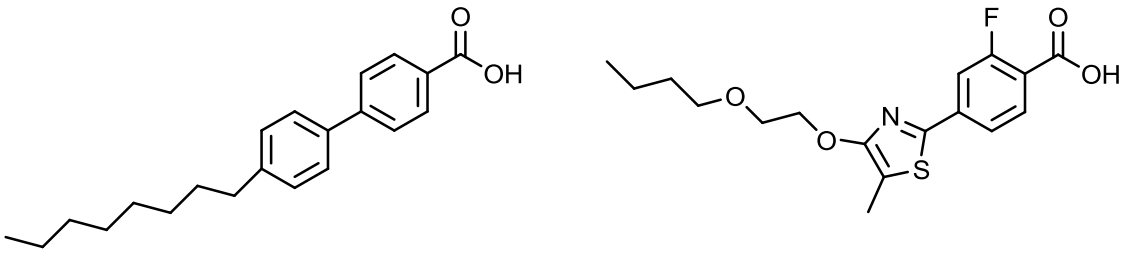

AC-55649 **AC-261066**

Fig. 13 RARβ2-selective agonists.[101]

Docking studies with AC-55649 and thiazole AC-261066, along with ATRA, were carried out in a model of the ligand-binding domain of the RARβ receptor (Fig. 14):[101] The polar carboxy-aromatic section of the molecules can be seen to overlap, where a network of hydrogen bonds is formed between the negatively-charged carboxylate and the polar amino acid residues Arg278 and Ser289. The aliphatic side chains and cyclohexenyl ring were positioned in the lipophilic pocket, and it was suggested that favourable interactions with Leu407, Met406, and Ile403 contributed to the agonist activity observed with AC-55649 and AC-261066. Thus, it was concluded that the lower activity observed with ligands containing shorter side chains was due to insufficient contact with the residues in the LBP. However, since molecular docking studies with these small molecules were carried out using the RARγ subtype, the basis for their receptor-selective activity should be further investigated.

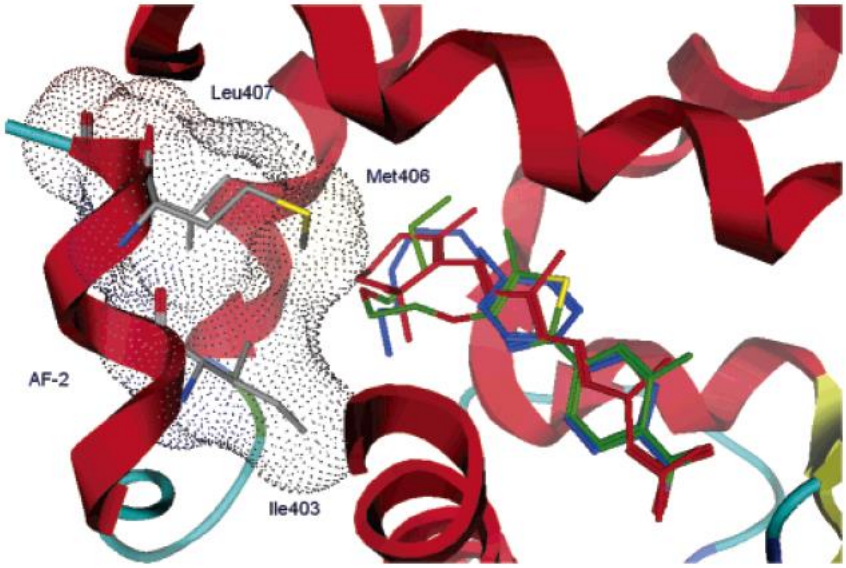

Fig 14 Docking of AC-55649 (blue), AC-261066 (green) and ATRA (red) in a model of the ligand-binding domain of the RARβ receptor.[101]

(Reprinted with permission from: B. W. Lund, F. Piu, N. K. Gauthier, A. Eeg, E. Currier, V. Sherbukhin, M. R. Brann, U Hacksell and R. Olsson, *J. Med. Chem.*, 2005, **48**, 7517-7519. Copyright 2005 American Chemical Society.)

1.5. Summary

The present challenge lies in the integration of structural and molecular biological information for the study of the physiological significance of retinoid receptor signalling, which will facilitate the development of investigative tools for research and therapeutic applications. Well-documented evidence has identified retinoic acid and its derivatives as potential agents for treating neurodegenerative diseases; a prominent target is RARβ2, with the discovery of a number of molecules exhibiting potent agonistic properties towards this receptor. Thus, if a particular receptor isoform could be selectively targeted for activation, specific biological outcomes could, potentially, be promoted, along with reduced unwanted and/or toxic side effects. It remains to be seen if such selectively could be achieved in the design and synthesis of synthetic retinoids, and, if successful, to what extent these molecules may be manipulated in biological systems in order to produce the desired result.

1.6. Project Aims

The synthesis of thiazole-containing small molecules is described in the following chapter, along with an evaluation of their activity in the TERA2.cl.SP12 EC stem cell line, in order to ascertain if enhancement of neural differentiation may be induced by these compounds, and if these effects may be attributed to activation of the RARβ2 receptor.

In the second part of this thesis, the synthesis and characterisation of a fluorescent analogue of EC23, which is a highly stable and potent synthetic retinoid developed in our laboratory,[115] is described. The ultimate goal was to produce a fluorescent probe which would also be an active small molecule modulator of stem cell differentiation: this would allow the pathway of retinoid transport to be followed in live-cell tracking studies, and could potentially constitute a powerful tool in the field of retinoid research.

2. SYNTHESIS AND BIOLOGICAL EVALUATION OF THIAZOLE-CONTAINING RETINOIDS

2.1. Background and Aims

A cell-based functional assay using R-SAT identified 4-[4-(2-ethoxy-ethoxy)-5-methyl-thiazol-2-yl]-benzoic acid (**A**, Fig. 15) as displaying 78% of the activity for RARβ2 compared to the reference compound, AM580.[102] The thiazole moiety is present in naturally-occurring molecules possessing important antibiotic,[103] antitumour,[104] and immunosuppressive properties.[105] The presence of a sulphur atom means that thiazole-containing compounds may be susceptible to metabolic oxidation and removal, in which case they will be inherently less toxic than synthetic retinoids that are unable to be metabolised.

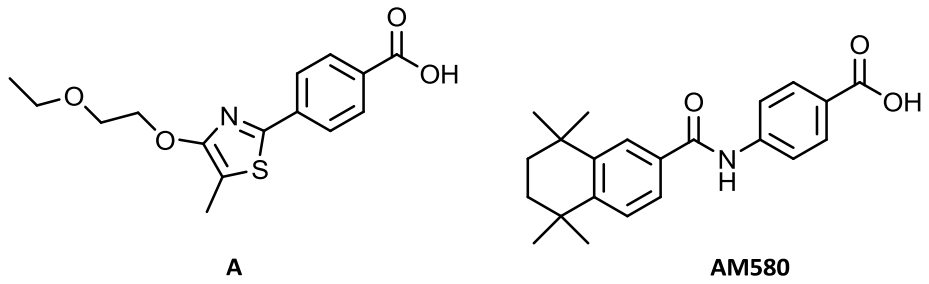

Fig. 15 RARβ2-selective 4-[4-(2-ethoxy-ethoxy)-5-methyl-thiazol-2-yl]-benzoic acid (**A**) and reference compound AM580.[102]

Compound **A** was duly synthesised in our laboratory and assessed for its ability to induce cellular differentiation of the human pluripotent embryonal carcinoma (EC) stem cell line, TERA2.cl.SP12.[106] However, a comparison of cell morphology between cell cultures treated with thiazole **A** and those treated with the natural retinoid ATRA showed that the synthetic molecule was unable to arrest cell proliferation and direct differentiation at the concentration used. Quantification of the effects of this compound on inducing differentiation of this cell line by analysing for expression of known markers for stem cell and differentiated cell phenotypes further confirmed that compound **A** was unable to induce the differentiation of EC stem cells.

The ability of compound **A** to modulate the differentiation of the neuroprogenitor cell line, ReNcell 197VM, was also assessed: after 7 days, cultures exposed to thiazole **A**

appeared similar to the control differentiation cultures, while cells treated with ATRA displayed predominately neuronal morphology compared to the control cultures. Immunocytochemical staining to record the expression of the pan-neuronal marker β-III-tubulin, and the marker of mature neurons, NF-200, was then performed (Fig. 16).

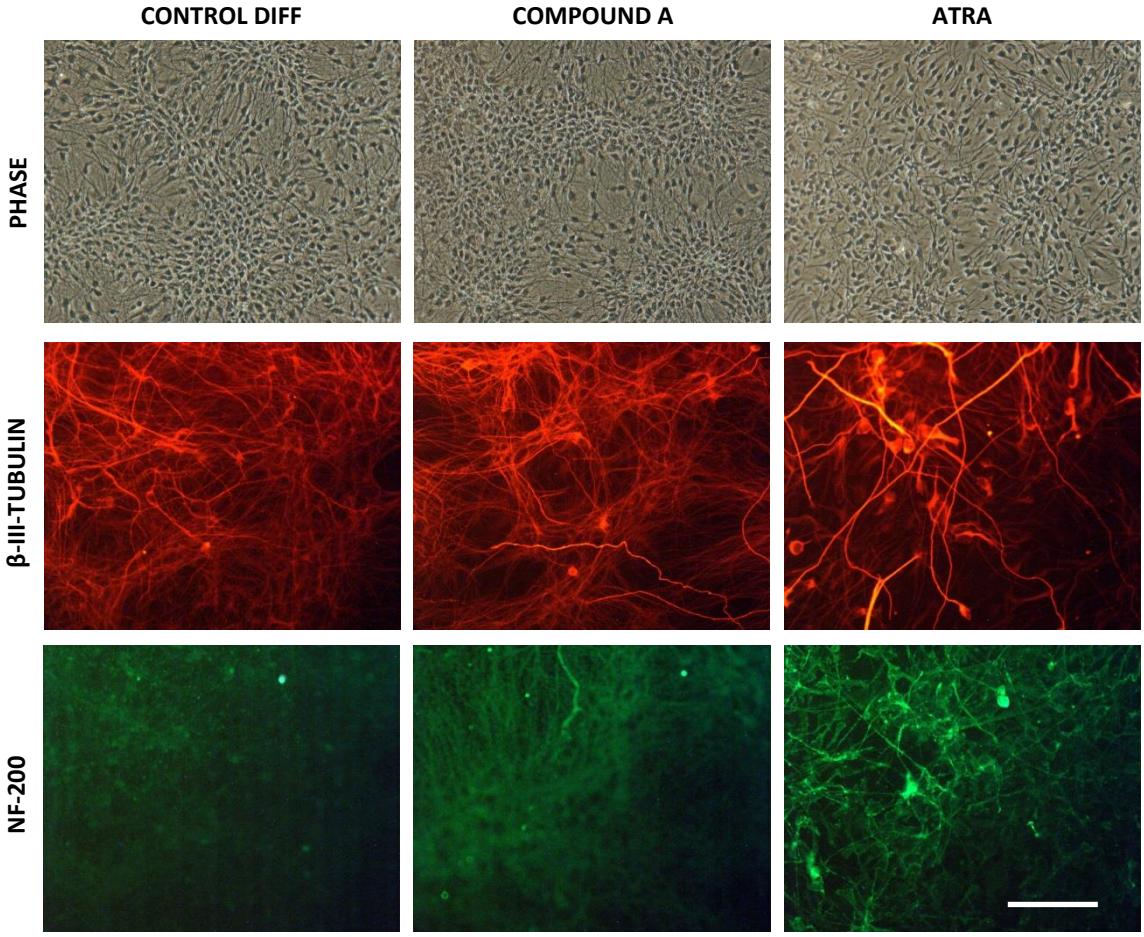

Fig. 16 Effect of supplementation of ReNcell 197VM culture media with 1 μM compound **A** or ATRA on the induction of neural differentiation as observed by immunocytochemical staining for markers for β-III-tubulin (a general neuronal marker protein) and neurofilament protein NF-200 (a 200 kDa protein expressed in mature neurons), compared to differentiated (control diff) control cultures. *Scale bar represents 100 μm*.[106]

Quantification of positively stained cells for these markers showed that, compared to the differentiated control cultures, compound **A** did not induce significant neuronal differentiation in this cell line: Control differentiation cultures stained for the general neuronal marker β-III-tubulin, and showed minimal levels of NF-200 expression, which

was indicative of an immature neuronal phenotype. In contrast, cultures exposed to ATRA displayed an approximately 1.5-fold increase in cells staining positive for β-III-tubulin, along with a 3-fold increase in those staining positive for NF-200.

It was hypothesised that modification of the side chain to a more bulky hydrophobic group may mean that the molecule is better able to bind in the larger cavity of the RARβ2 receptor, thereby eliciting a more effective retinoid response. Hence, in order to determine if such analogues are capable of inducing cellular differentiation, the synthesis of two thiazole derivatives containing phenyl and 1,1,4,4-tetramethyl-1,2,3,4-tetrahydronaphthalene groups (Fig. 17), and their biological evaluation in the TERA2.cl.SP12 EC stem cell line, are described in the following sections.

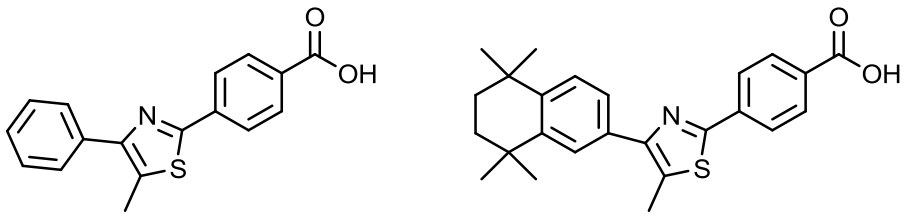

1 **2**

Fig. 17 Proposed novel 2,4-disubstituted thiazole derivatives with bulky phenyl (**1**) and 1,1,4,4-tetramethyl-1,2,3,4-tetrahydronaphthalene (**2**) side chains.

2.2. Synthesis of 2,4-disubstituted thiazole derivatives

Ethyl 4-cyanobenzoate (**3**) was heated with equimolar equivalents of 2-mercaptopropionic acid (**4**) and pyridine under microwave (MW) conditions to provide the desired hydroxythiazole **5a** after recrystallisation (Equation 1). The reaction appeared to be reversible, with the product reverting back to the starting material if not isolated immediately.

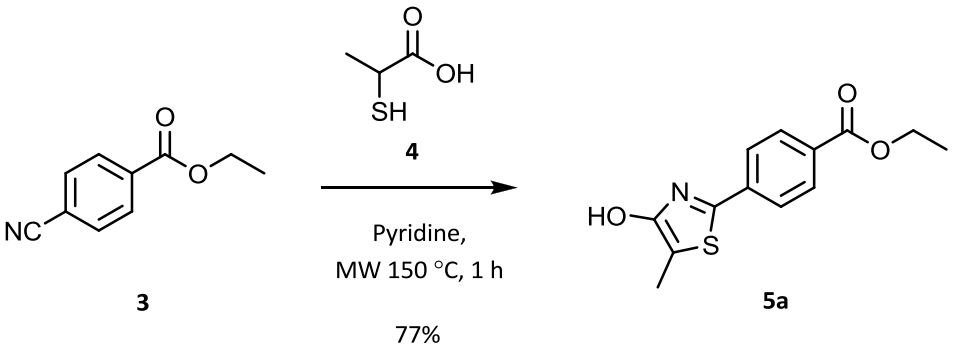

Equation 1

Despite TLC and MS analyses indicating the presence of only one product, two species were observed by ^{1}H NMR spectroscopy, and were found to be inseparable by either recrystallisation or column chromatography. The overlapping ethyl signals, along with an additional doublet and quartet peak in the alkyl region of the spectrum, were deduced to be consistent with the keto-tautomer **5b** (Scheme 1). This occurrence was not reported previously, and compound **5b** constituted a significant proportion of the mixture (approximately 15%).

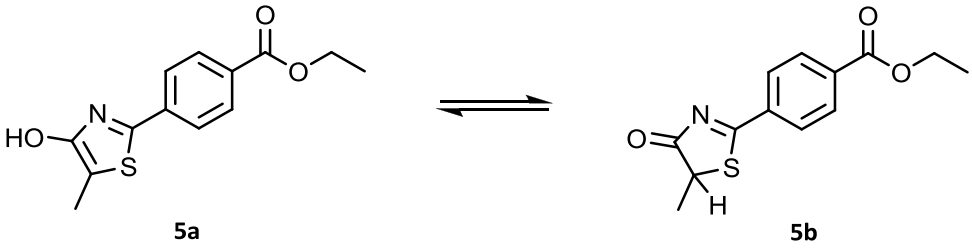

Scheme 1 Keto-enol tautomerism of **5a**.

4-Hydroxy-1,3-thiazoles are known as active inhibitors of 5-lipoxygenase[107] and CDK5,[108] and exist in different tautomeric forms: the enol-form is favoured in polar solvents and the keto-form in non-polar solvents.[109] In this case, the lower energy of the aromatic 4-hydroxythiazole structure, as well as the presence of an aromatic substituent at the 2-position, is likely to account for the predominance of the enol tautomer.[110] Furthermore, functionalising the hydroxyl group of compound **5a** would

be expected to 'lock' the product in the aromatic form; indeed, this was observed when the keto-enol mixture was treated with triflic anhydride to provide triflate **6**, and loss of signals associated with the keto-tautomer was accordingly observed by ^{1}H NMR analysis of the product.

Procedures for the conversion of hydroxythiazoles to triflates are known,[111] and have been employed in the derivatisation of these compounds to give biologically-useful agents.[112] Initially, the Comin's reagent was stirred with the hydroxythiazole in tetrahydrofuran, however, a TLC analysis after 6 h showed predominately a mixture of starting materials was present. The use of triflic anhydride with pyridine as base was similarly ineffective in promoting product formation; however, when pyridine was replaced by triethylamine, triflate **6** was obtained in 20% yield after purification by silica-gel chromatography. The yield was improved by the use of a more hindered base, diisopropylethylamine (DIPEA), which provided compound **6** in 81% yield following purification (Equation 2).

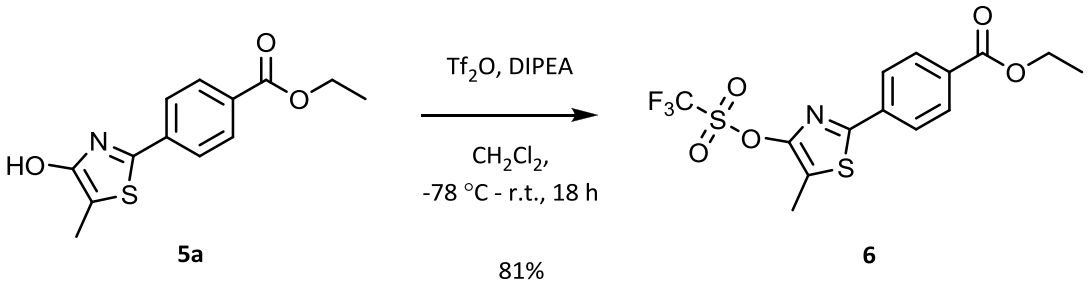

Equation 2

With triflate **6** in hand, Suzuki-Miyaura cross couplings were performed in order to provide small molecules with retinoid-like structures (Scheme 2). Commercially-available 4,4,5,5-tetramethyl-2-phenyl-[1,3,2]-dioxaborolane (**7**) was reacted with triflate **6** in DMF/H_2O, using K_3PO_4 and 3 mol% $Pd(dppf)Cl_2$ as catalyst. After heating to 80 °C for 18 h, an aqueous workup was performed, and the residue was purified by silica-gel chromatography to give 4-(5-methyl-4-phenyl-thiazol-2-yl)-benzoic acid ethyl ester **9** in 69% yield. Compound **10** was prepared in an analogous manner using

4,4,5,5-tetramethyl-2-(5,5,8,8-tetramethyl-5,6,7,8-tetrahydro-naphthalen-2-yl)-[1,3,2]-dioxaborolane (**8**), and the product was obtained in 87% yield following purification by column chromatography.

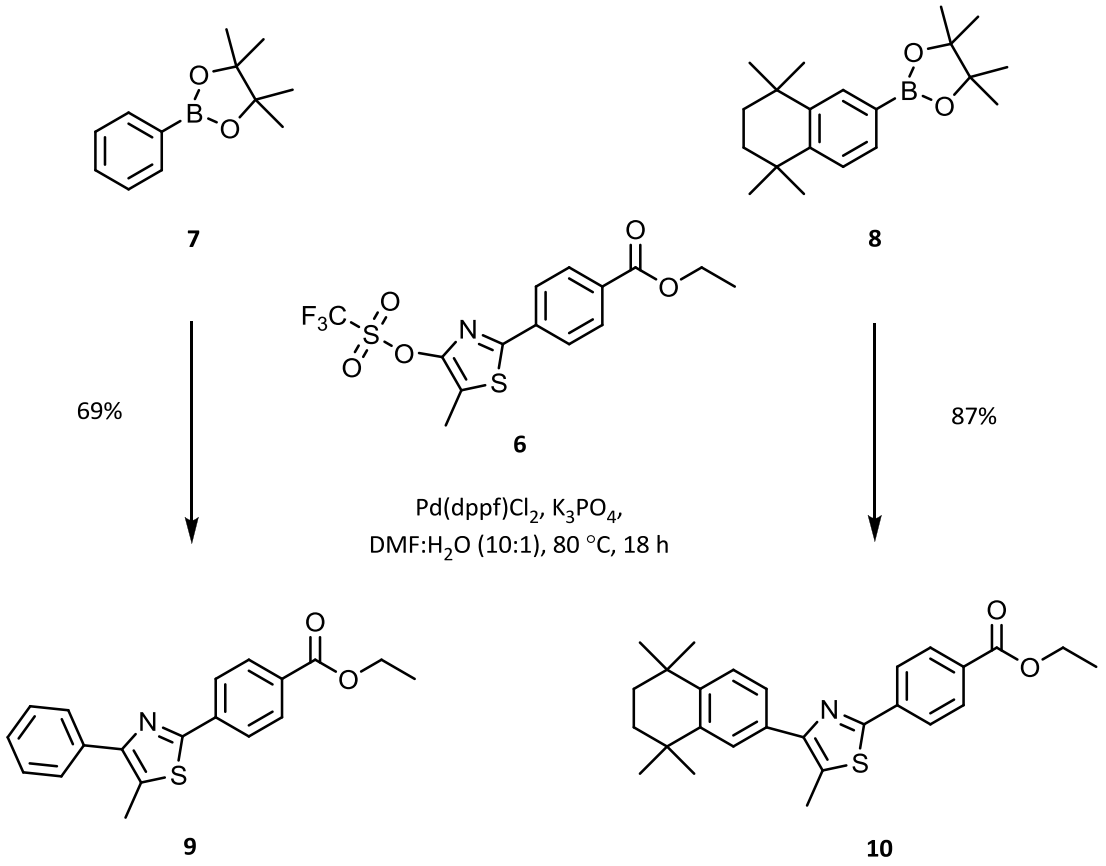

Scheme 2 Suzuki-Miyaura coupling reactions to give retinoid-like structures containing bulky phenyl (**9**) and 1,1,4,4-tetramethyl-1,2,3,4-tetrahydronaphthalene (**10**) side chains.

Base hydrolyses of esters **9** and **10** were attempted using the conventional method of stirring in THF with $LiOH{\cdot}H_2O$ at ambient temperature. However, the reactions were slow and poor-yielding, despite the addition of more base and heating for a period of a few days. Instead, a microwave-assisted method of heating to 160 °C for 15 min provided the desired acids **1** and **2** in good yields (88% and 85%, respectively) following aqueous workup and recrystallisation.

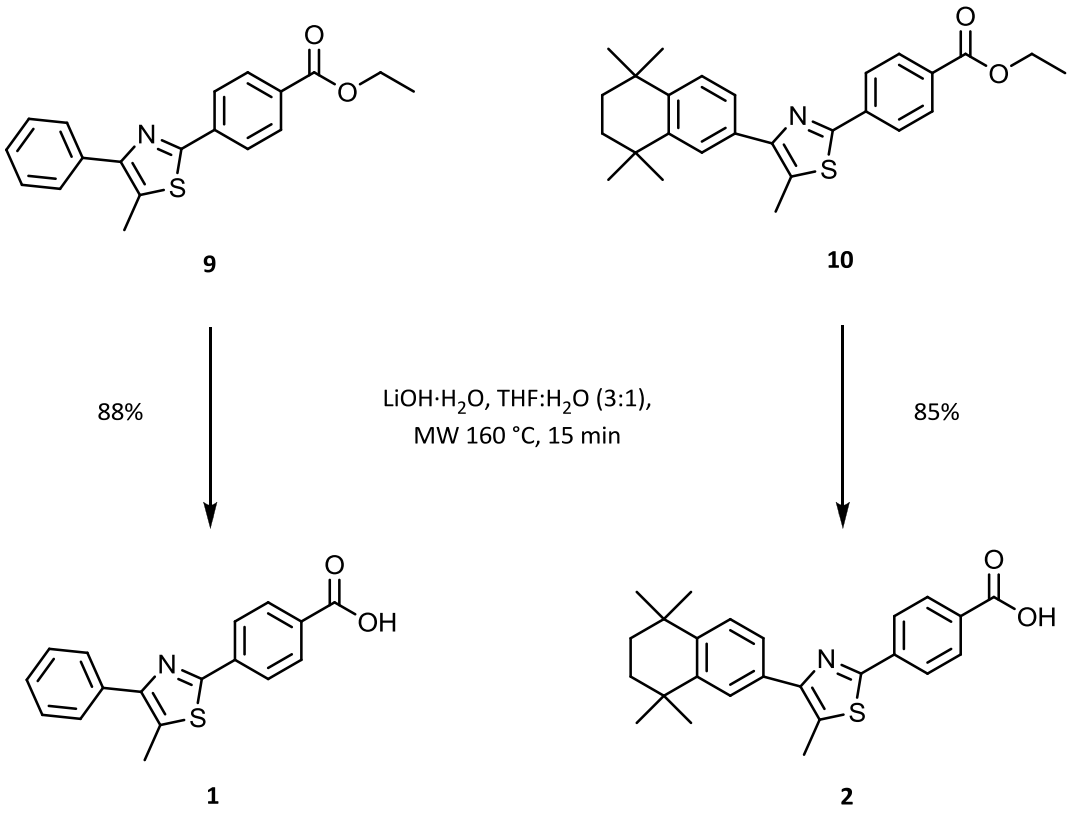

Scheme 3 Hydrolysis reactions of esters **9** and **10**.

2.3. Effect of thiazole retinoid-like small molecules on the differentiation of human pluripotent stem cells

Cell culture

Having prepared the 2,4-disubstituted thiazole molecules **1** and **2**, they were assessed for their ability to induce differentiation of the pluripotent human embryonal carcinoma stem cell line, TERA2.cl.SP12. Cells of this lineage are proven models of human embryonic development,[113] and have been used to study neural differentiation.[114] Cultures of TERA2.cl.SP12 EC cells were duly incubated with compounds **1** or **2** supplemented in the culture media to a final concentration of 10 μM for up to 14 days.

The effects of the test compounds on inducing stem cell differentiation were compared with the effect of the natural retinoid ATRA, which acted as a positive control. Hence, cultures consisting of cells treated with 10 µM ATRA in the growth media were also established and incubated alongside the test cultures. Cell cultures supplemented with the loading vehicle DMSO were also set up to act as a negative differentiation control, and these were processed for analysis after 3 days. In order to minimise ATRA degradation and isomerisation, all culture flasks were handled under reduced light conditions. Furthermore, for reproducibility of results, cell cultures for each compound were set up in triplicate for each time point, and these were processed for analysis after 3, 7, and 14 days.

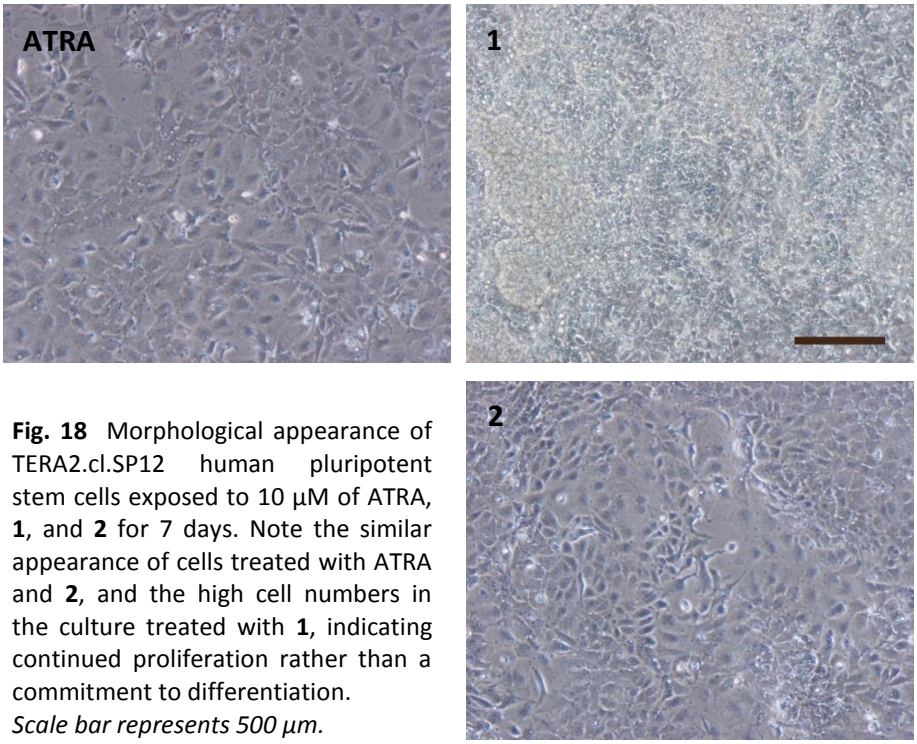

Fig. 18 Morphological appearance of TERA2.cl.SP12 human pluripotent stem cells exposed to 10 µM of ATRA, **1**, and **2** for 7 days. Note the similar appearance of cells treated with ATRA and **2**, and the high cell numbers in the culture treated with **1**, indicating continued proliferation rather than a commitment to differentiation.
Scale bar represents 500 µm.

After 7 days, it became apparent that cell proliferation in cultures exposed to ATRA and compound **2** had slowed considerably, which was consistent with cells committing to differentiate. In contrast, cells treated with compound **1** continued to proliferate, and very high cell numbers were observed (Fig. 18), which was a clear indication that these molecules were unable to arrest cell proliferation and induce cell differentiation

at the concentration used. The appearance of the cells after 14 days followed a similar trend, *i.e.* cell proliferation slowed in response to ATRA and compound **2**, whereas cultures exposed to compound **1** became over-confluent due to continued cell proliferation (Fig. 19).

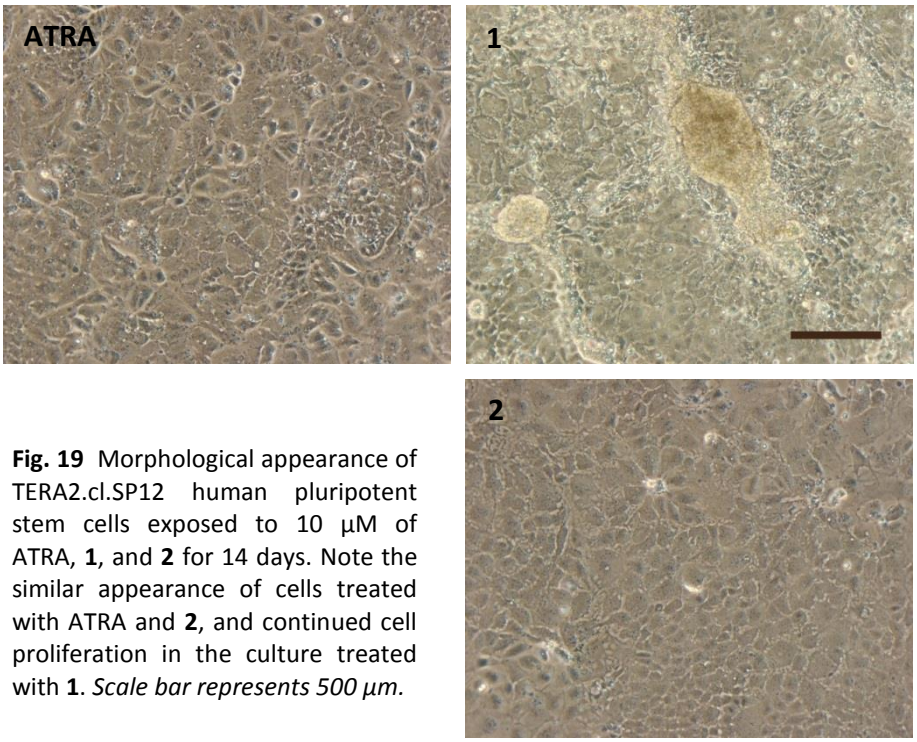

Fig. 19 Morphological appearance of TERA2.cl.SP12 human pluripotent stem cells exposed to 10 µM of ATRA, **1**, and **2** for 14 days. Note the similar appearance of cells treated with ATRA and **2**, and continued cell proliferation in the culture treated with **1**. *Scale bar represents 500 µm.*

Cell viability assay

After incubating for 7 days in compound-supplemented media, cells were prepared for an assay of cell viability by combining culture media containing any potentially detached or dead cells, with trypsinised live cells from each experimental condition. The resulting cell solution from each flask was centrifuged, then re-suspended in 0.1% BSA solution to allow cells to be counted. Cells from cultures exposed to ATRA and comppounds **1** and **2** were diluted in a staining solution, and the proportion of live (intact cytoplasmic membranes excluded the dye) to dead (compromised cell membranes stained positive for the dye) cells was determined using a Viacount assay on a Guava EasyCyte cytometer. The number of viable cells, percentage viability, and total cell counts were thus determined (Fig. 20).

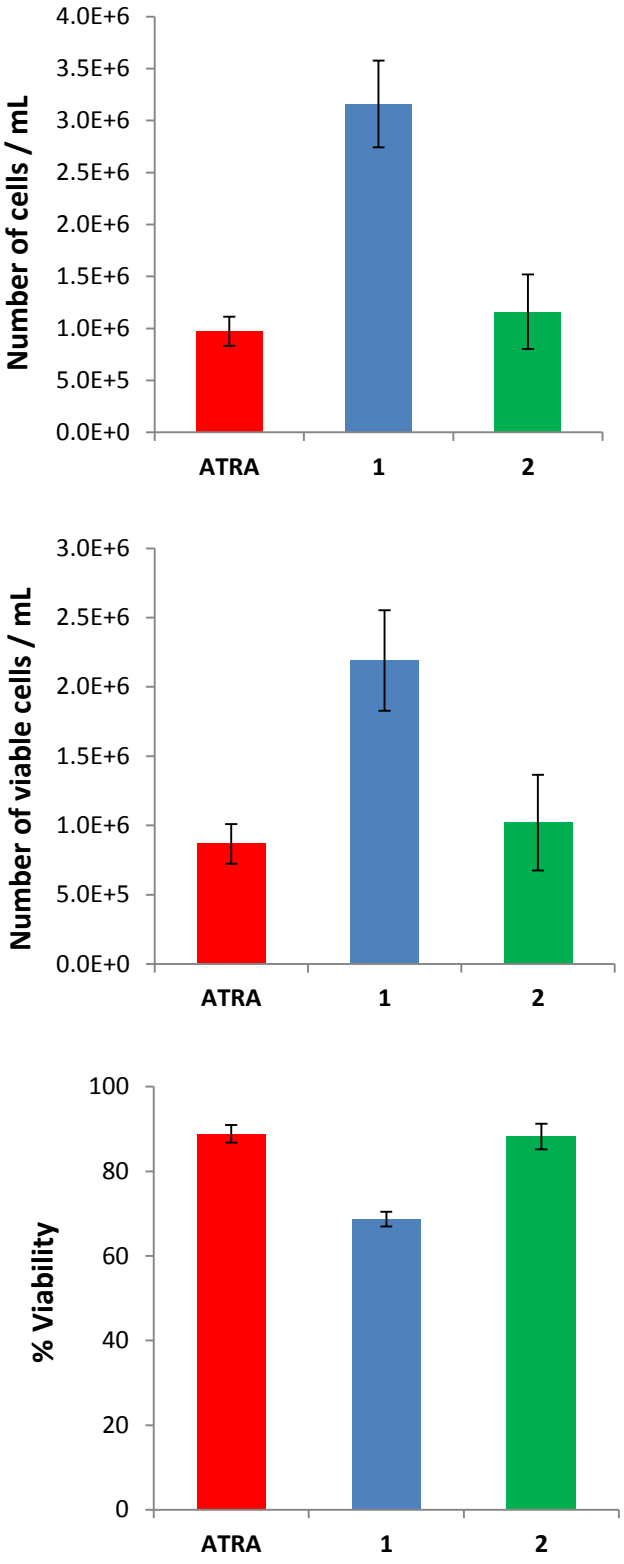

Fig. 20 TERA2.cl.SP12 EC stem cells incubated for 7 days in culture media supplemented with 10 µM of ATRA, compound **1**, or compound **2**. The number of viable cells, percentage viability, and total cell counts were determined using a Viacount assay and these are represented in graphical format (for reproducibility, results are the average of triplicate assays ± SEM for each culture condition, *n* = 3).

Continued cell proliferation in cultures treated with compound **1** was reflected in the high cell count and number of viable cells, whereas with ATRA and compound **2**, these values were lower due to cells exiting the cell cycle and committing to differentiation. However, cells exposed to compound **1** proved less viable than those treated with ATRA and compound **2**, which was consistent with suboptimal culture conditions due to high cell numbers and over-proliferation. The similarity of cell viability values observed in the cultures treated with ATRA and compound **2** supports the earlier observation from cell morphology that these compounds act in a comparable fashion when exposed to the TERA2.cl.SP12 EC cell line.

Differentiated-cell assay

In order to quantify the effects of the thiazole-containing compounds on inducing differentiation of the TERA2.cl.SP12 cell line, cells were analysed for expression of known markers for stem cell and differentiated cell phenotypes. Cells from each experimental condition were incubated with antibodies for the stem cell antigens SSEA-3 (globoseries stage-specific embryonic antigen-3) and TRA-1-60 (a keratin-sulphate-associated glycoprotein stem surface marker). Following this, incubation with a secondary fluorescent antibody allowed the proportion of cells expressing the marker to be determined through flow cytometry (Fig. 21, **SSEA-3** and **TRA-1-60**).

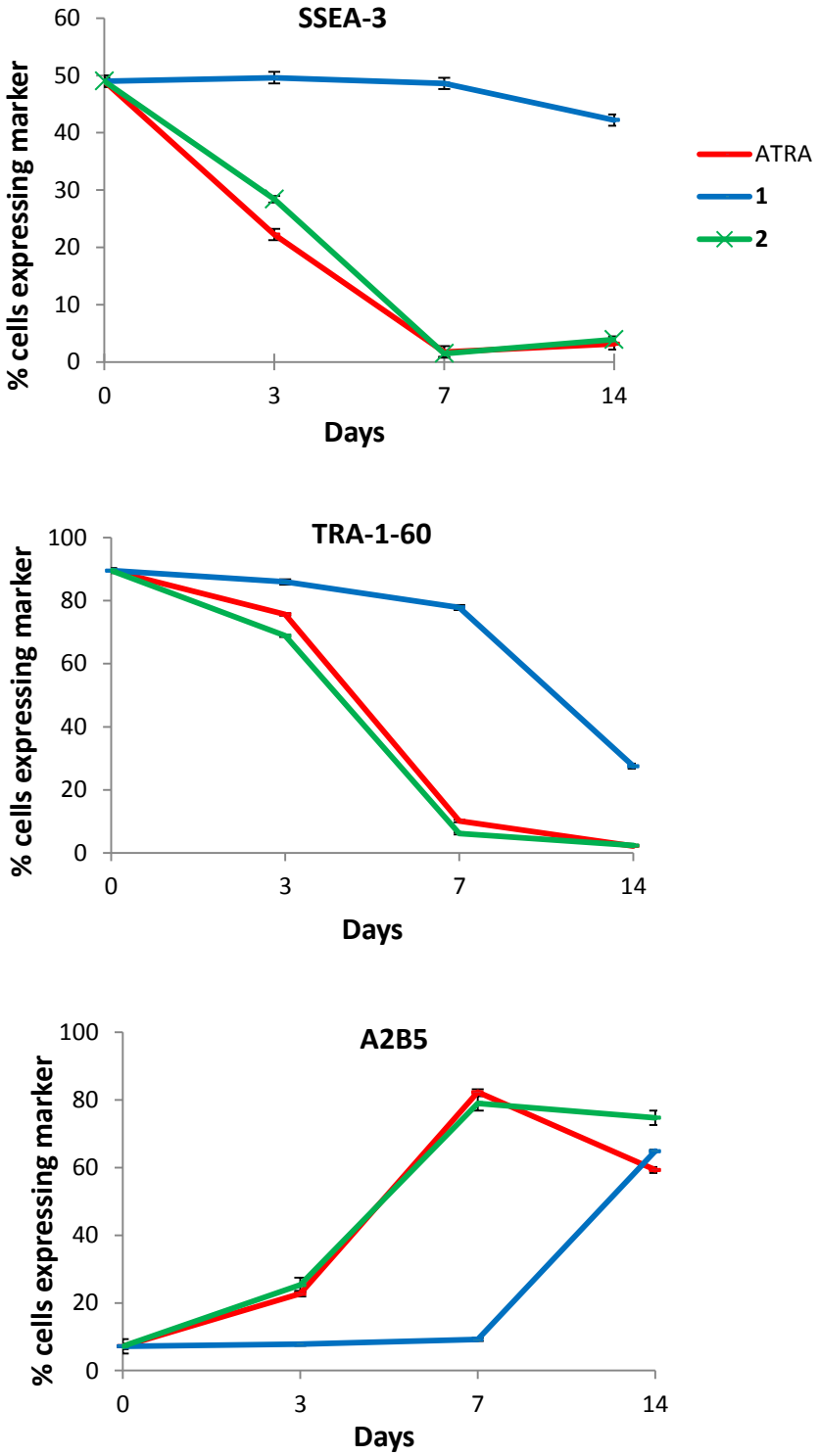

Fig. 21 TERA2.cl.SP12 EC cells were exposed to 10 µM of ATRA, **1**, and **2** for 14 days and analysed for expression of stem cell markers (SSEA-3 and TRA-1-60) and a neural marker (A2B5). Expression of SSEA-3 and TRA-1-60 decreased significantly in cultures exposed to ATRA and compound **2**, with a corresponding increase in A2B5 expression. Conversely, a high level of stem cell character was observed for compound **1**, with minimal A2B5 expression, indicating the compound does not induce differentiation. After 14 days, spontaneous differentiation of cell cultures exposed to compound **1** could account for the reduced SSEA-3 and TRA-1-60 levels, along with the elevated expression of A2B5. (For reproducibility, results are the average of triplicate assays ± SEM for each culture condition, *n* = 3).

After 3 days, expression of SSEA-3 and TRA-1-60 in cultures treated with ATRA and compound **2** began to decrease compared to the negative DMSO control. This was especially clear for SSEA-3 where levels decreased by approximately 55% and 42% in the cultures exposed to ATRA and compound **2**, respectively. These data provide a strong indication of TERA2.cl.SP12 stem cells committing to differentiate in response to these compounds. However, no significant change in expression of these stem cell markers was observed for cells exposed to compound **1**, suggesting that these cells retained a more stem cell-like phenotype. After 7 days, expression of SSEA-3 and TRA-1-60 in the cultures treated with ATRA and compound **2** was greatly reduced, and remained minimal after 14 days. At this point it was surprising to note also the dramatic reduction in TRA-1-60 expression in cells treated with compound **1**, indicating that differentiating cells may be present in these cultures.

Since TERA2.SP12 cells are known to form neurons in response to exposure to ATRA,[111] the expression of the antigen A2B5 (ganglioseries antigen marking early-stage neural cells), which is associated with differentiating neural cell types, was also monitored by flow cytometry (Fig. 21, **A2B5**). As expected, the expression of A2B5 increased in response to ATRA over the course of the study period. A very similar pattern of expression was recorded in cultures treated with compound **2**, suggesting that the compound is capable of inducing differentiation of TERA2.cl.SP12 cells with a level of activity comparable to that of the natural retinoid. After 7 days, no significant increase in antigen expression was observed in response to compound **1**, yet by day 14, an elevated A2B5 expression was recorded that was similar to the levels observed with ATRA and compound **2**. It would appear that differentiated cell types were now present in these cultures; however, further investigation would be required to determine if this was the result of spontaneous differentiation in the cultures due to sub-optimal growth conditions, rather than due to any effects induced by compound **1**. Nonetheless, given the length of time required before a change in cell phenotype was observed, it was unlikely that compound **1** behaved as a true inducer of differentiation.

Effect on neurite outgrowth

(Assay carried out by Daniel M. Tams)

Since the thiazole retinoid-like small molecule **2** was shown to induce neural commitment by flow cytometric analysis, it was hypothesised that these differentiated stem cells would subsequently form neurites. Thus, to assess neurite outgrowth, a human model of neurite formation was used: suspension aggregates of TERA2.cl.SP12 cells were differentiated with 0.1 μM of compound **2**, ATRA, or EC23. The latter is a photo-stable synthetic retinoid that has been found to exhibit a higher level of activity towards the induction of neural differentiation compared to ATRA.[115,116] After 21 days, neurospheres from each treatment group were placed on laminin and poly-D-lysine coated substrates to induce neurite formation. The neurospheres were maintained for 10 days prior to analysis.

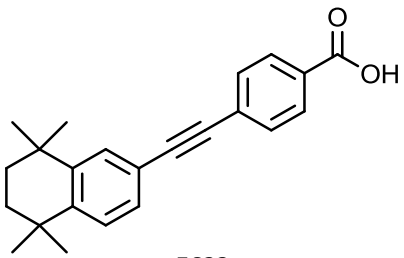

EC23

To visualise neurite outgrowth from each cell aggregate, immunocytochemical analysis of the neuronal marker β-III-tubulin was performed: staining for the marker showed that in cultures treated with compound **2** or EC23, many individual neurites were formed that projected from the central neurosphere. Quantification of the neurite number revealed a significant enhancement of neuritogenesis in these treatment groups compared to ATRA and the undifferentiated control (Fig. 22).

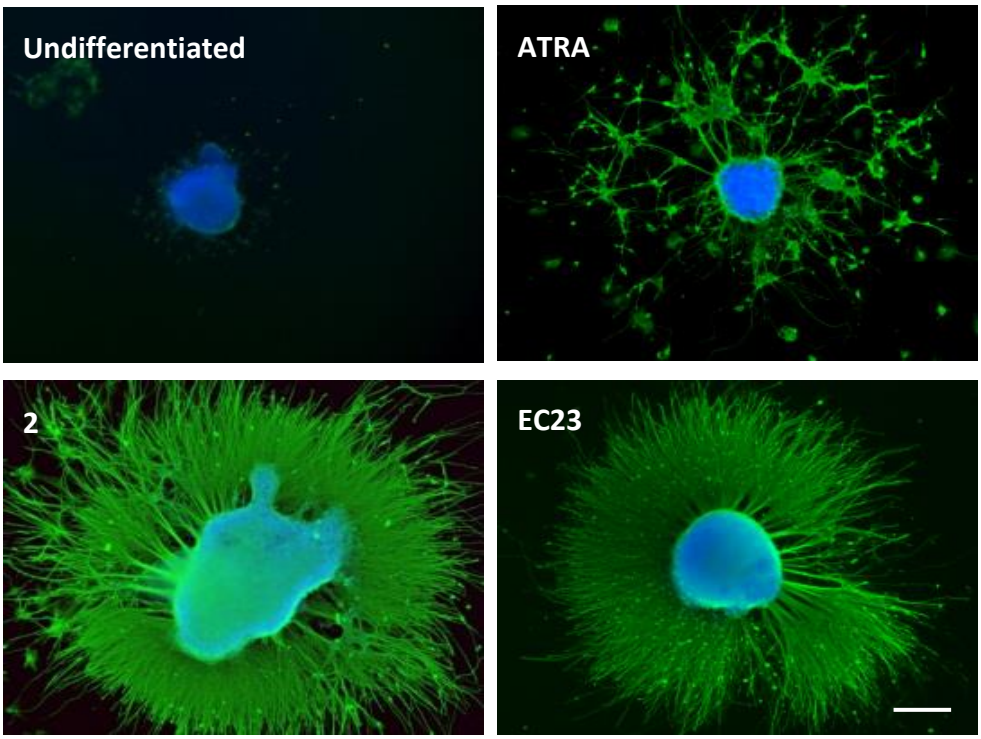

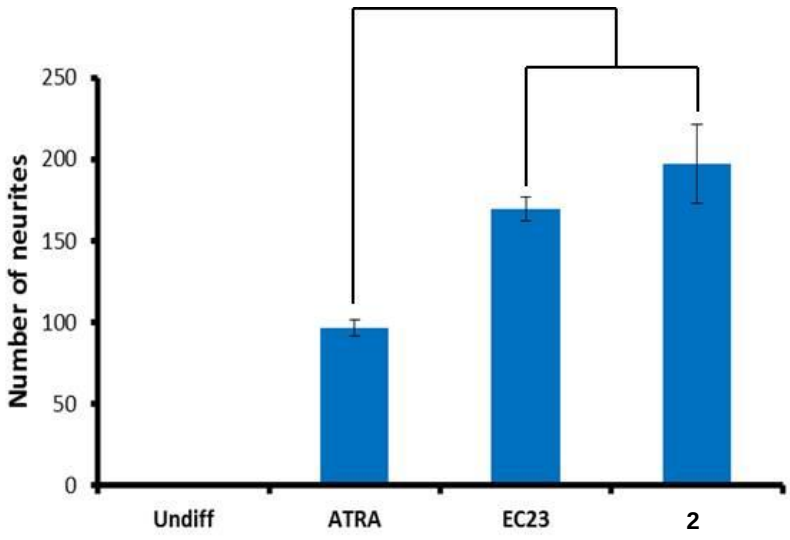

Fig. 22 Neurite outgrowth from differentiated TERA2.cl.SP12 EC stem cells. Cell aggregates were differentiated with 0.1 µM ATRA, EC23, or compound **2** for 21 days. Differentiated aggregates were placed onto a laminin poly-D-lysine substrate for 10 days to allow neurites to form. Neurites were stained with the pan-neuronal marker β-III-tubulin (green), and cell bodies were stained with DAPI (blue). Results are the average of triplicate assays. Error bars represent ± SEM, $*p < 0.05$. Scale bar represents 50 µm.

The ability of EC23 or compound **2** to promote neurite outgrowth in this model was likely due to the stability of these compounds, which could give rise to enhanced retinoic acid receptor activation. Furthermore, the lack, or reduced level, of metabolite formation could contribute to eliciting a more homogeneous biological response, along with a corresponding decrease in undesirable side effects: this could potentially constitute an interesting area for future investigation into the biological activities of these synthetic retinoids.

2.4. Stability study

ATRA is known to be susceptible to isomerisation and degradation, particularly when exposed to light. This is an important area where retinoid activity and potency may be compromised. While the structure of the thiazole-containing compounds does not suggest any potential for instability or isomerisation, a light experiment was nevertheless conducted in order to confirm their stability. Compounds **1** and **2** were dissolved in DMSO-d_6 in NMR tubes, and exposed to a white fluorescent light source at a distance of 40 cm for a period of 30 days. ^{1}H NMR spectra were recorded at various time intervals and compared to the spectrum from day 1. No signs of decomposition, or loss of integrity, of the signals were observed over the course of the investigation, and the compounds can therefore be considered stable towards light exposure.

2.5. Conclusions and Outlook

The experimental evidence demonstrates clearly that compound **2** is able to induce the differentiation of human TERA2.cl.SP12 EC stem cells on a level comparable to that of the natural retinoid ATRA. Furthermore, at 0.1 μM, compound **2** promotes enhanced neural commitment and neurite outgrowth over ATRA, with levels similar to that observed with the synthetic retinoid EC23. Further characterisation would be required to determine if compound **2** exhibits selectivity for a particular retinoic acid receptor subtype, and if this could account for the positive results observed.

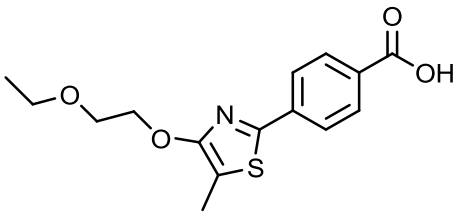

A

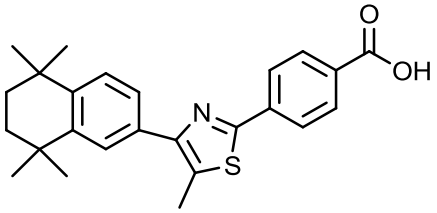

2

Despite the alkoxythiazole-containing compound **A** having previously been identified as an RARβ2 agonist,[102] earlier studies found that this molecule showed limited ability to modulate the differentiation of either the pluripotent TERA2.cl.SP12 or the neuroprogenitor ReNcell 197VM cell lines.[106] Although RARβ2 signalling is understood to play a significant role in neurite outgrowth,[66,69,70] activation of this receptor thus did not appear to result in a positive effect on neuritogenesis when compared to ATRA or EC23 under the conditions tested. It remains possible that activation of RARβ2 is a necessary, but not sufficient, factor for neuronal differentiation in these types of human cells.

Overall, these results show how subtle modifications to the structures of small molecules, specifically the incorporation of bulky hydrophobic side chains, can have a significant impact on their biological activity. Such information concerning structure-activity relationships will advance our ability to design new compounds for specific biological applications.

3. FLUORESCENCE IMAGING

3.1. Cell imaging

A great challenge of this post-genome age lies in determining the biological significance of intracellular molecules in living cells. The visualisation of cellular molecules will provide information concerning their location and function, and the design and synthesis of chemical tools which will be suitable for these purposes will, therefore, prove to be highly valuable areas for investigation and development. The field of cell imaging has become increasingly important in chemical biology research over the last two decades, and fluorescent molecules have thus been synthesised and successfully applied for imaging cellular structures,[117] which has led to the commercialisation of many probes for a wide variety of biological applications.

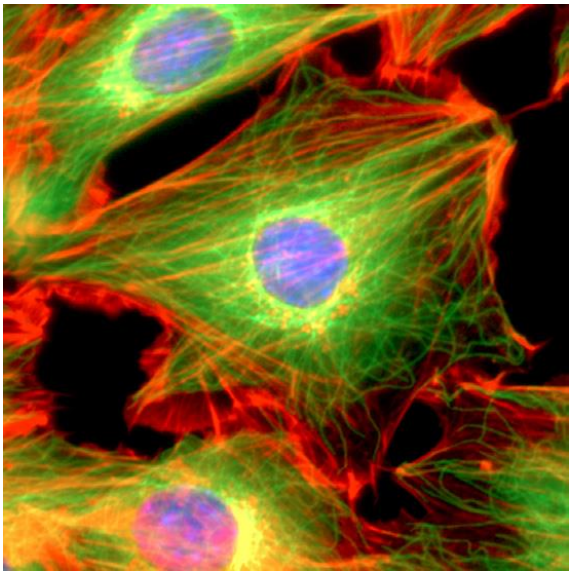

Fig. 23 Fluorescence image of a mouse NIH3T3 fibroblast cell fixed and stained for DNA (blue), and the major cytoskeletal filaments actin (red) and α-tubulin (green).[118]

Reprinted from Acta Materialia, **55**, S. Suresh, Biomechanics and biophysics of cancer cells, 3989-4014, copyright 2007, with permission from Elsevier.

3.2. Fluorescence

Fluorescence is a form of luminescence in which a substance that has absorbed light or other electromagnetic radiation emits light from electronically excited states. The electromagnetic spectrum is outlined in Fig. 24, and gives the range of all possible frequencies of electromagnetic radiation.

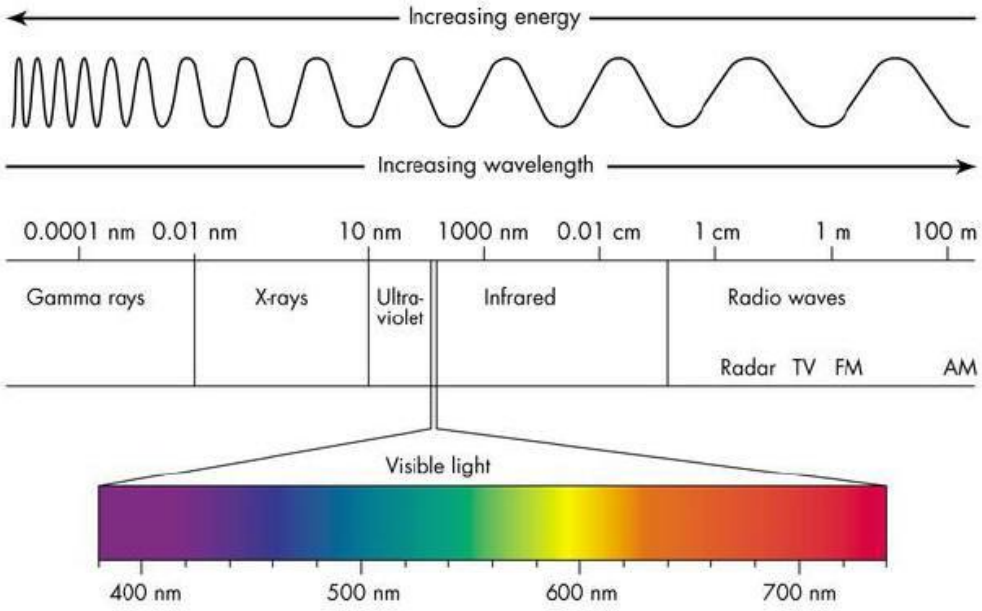

Fig. 24 The electromagnetic spectrum.

(Reproduced with permission from: http://www.cyberphysics.co.uk/topics/light/emspect.htm)

In fluorescence, the emitted light is usually of a longer wavelength (and lower energy) than the absorbed light. This phenomenon is known as Stokes shift, and is attributed to the loss of energy, usually *via* vibrational relaxation to the lowest energy level of the first excited state (S_1), before an absorbed photon is emitted. The quantum yield gives the efficiency of the fluorescence process: it is defined as the ratio of the number of photons emitted to the number of photons absorbed (maximum value = 1, *i.e.* every absorbed photon results in an emitted photon). The fluorescence lifetime refers to the average length of time a molecule remains in an excited state before undergoing relaxation back to the ground state. In phosphorescence, a longer excited state

lifetime is observed, followed by radiative decay (*i.e.* photon emission) from an excited triplet state. A summary of the various transitions between the electronic states of a molecule is given in the Jablonski diagram (Fig. 25).

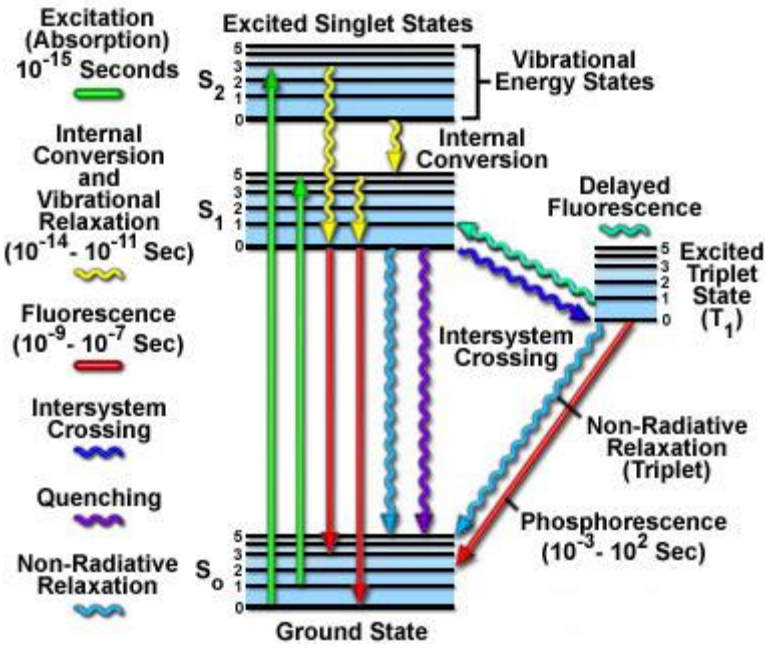

Fig. 25 Jablonski diagram.

(Reproduced from: http://www.olympusmicro.com/primer/java/jablonski/jabintro/)

Fluorescence has wide-ranging and important applications in a variety of fields such as minerology, gemology, geology, fluorescence spectroscopy, fluorescence labelling, microscopy, medicine, forensics, and most commonly, in fluorescent lamps.

3.3. Fluorescence microscopy

Fluorescence microscopy has become an important tool for investigating biological molecules, pathways, and processes in living cells, tissues, and organisms. The compatibility of fluorescence microscopy with live cells confers an advantage over other imaging techniques, and dynamic and non-invasive studies may be carried out.

Specific applications employing fluorescence include cellular and molecular imaging, cell labelling and tracking, and DNA detection.[119]

The sample is placed under the objective lens of a fluorescence microscope and illuminated with light of a specific wavelength. This is absorbed by the fluorophores (fluorescent chemical compounds, see section 3.4.) present in the sample, which subsequently emit light of longer wavelengths (*i.e.* different colours) to the absorbed light. A spectral emission filter separates the weaker emitted fluorescence from the illuminating light. Typical components of a fluorescence microscope include: a light source (commonly a xenon arc or mercury-vapour lamp, or, in more advanced instruments, high-power LEDs and lasers); the excitation filter; the dichroic mirror; and the emission filter (Fig. 26). Different filters and dichroic mirrors are selected based on the excitation and emission characteristics of the fluorophore. Hence, the distribution of each fluorophore in a sample may be visualised separately, and multi-colour images may be generated by overlaying the single-colour images.

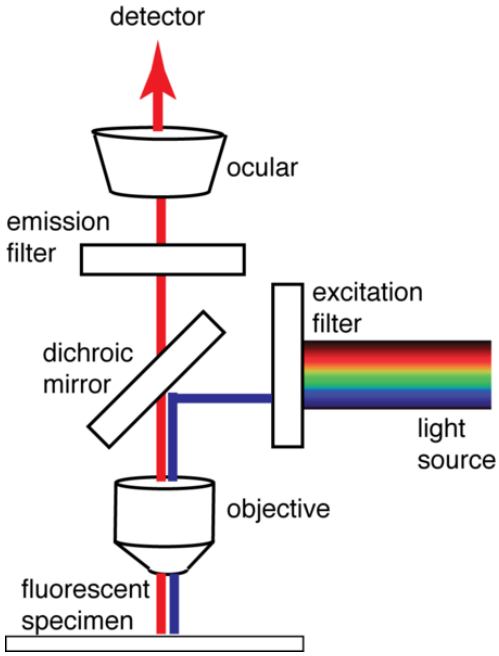

Fig. 26 Schematic diagram of the typical components of a fluorescence microscope, exemplified by the epifluorescence microscope, where excitation and emission of the sample are both focused by the objective lens.

(Reproduced from: http://biologywiki.apps01.yorku.ca/index.php?title=Main_Page/BIOL_4160/Visualizing_the_Photosynthetic_Apparatus)

Wide-field and confocal microscopy represent the two most widely used fluorescence imaging methods: In wide-field microscopy, the entire sample is evenly flooded in light from a mercury or xenon source, and the resulting fluorescence may be viewed directly by eye or projected onto a camera, along with a large unfocused background. Confocal microscopy uses a focused laser beam that is scanned laterally along the *x* and *y* axes of the sample; point illumination and a pinhole in an optically conjugate plane in front of the detector eliminate out-of-focus signals, offering improved optical resolution compared to conventional wide-field microscopy. However, since much of the fluorescence is blocked at the pinhole, long exposure times are often required in order to compensate for a reduced signal intensity.

Autofluorescence is the natural emission of light by biological structures, such as mitochondria and lysosomes, when they have absorbed light. This can interfere with visualisation of samples using fluorescence microscopy, since the structures of interest may be less discernible as a result. Hence, it is desirable to use fluorescent markers which are easily detectable despite cellular autofluorescence, and the latter may be excluded in some microscopes by making use of the different excited state lifetimes of individual fluorophores.

3.4. Fluorophores

Fluorophores are fluorescent chemical compounds, usually organic small molecules (ranging from 200 to 1000 Dalton), and typically contain several aromatic groups or π-bonds in conjugation; an ideal fluorophore has a high absorption and fluorescence quantum yield, shows steady emission intensity, is biocompatible and non-toxic to the sample, does not perturb the host molecule, and stays photoactive over a long period under intense illumination (*i.e.* is stable to photobleaching, see section 3.5.). The various classes of fluorophore used in cell imaging studies are considered in the following subsections.

Small organic dyes

Synthetic organic dyes, such as fluorescein and its major derivatives (fluorescein isothiocyanate, FITC, and 6-FAM phosphoramidite; Fig. 27), were the first fluorescent compounds to be used in biological research. The small size of these fluorophores means they have versatile applications, and they may be cross-linked to macromolecules without interfering with normal biological functions.

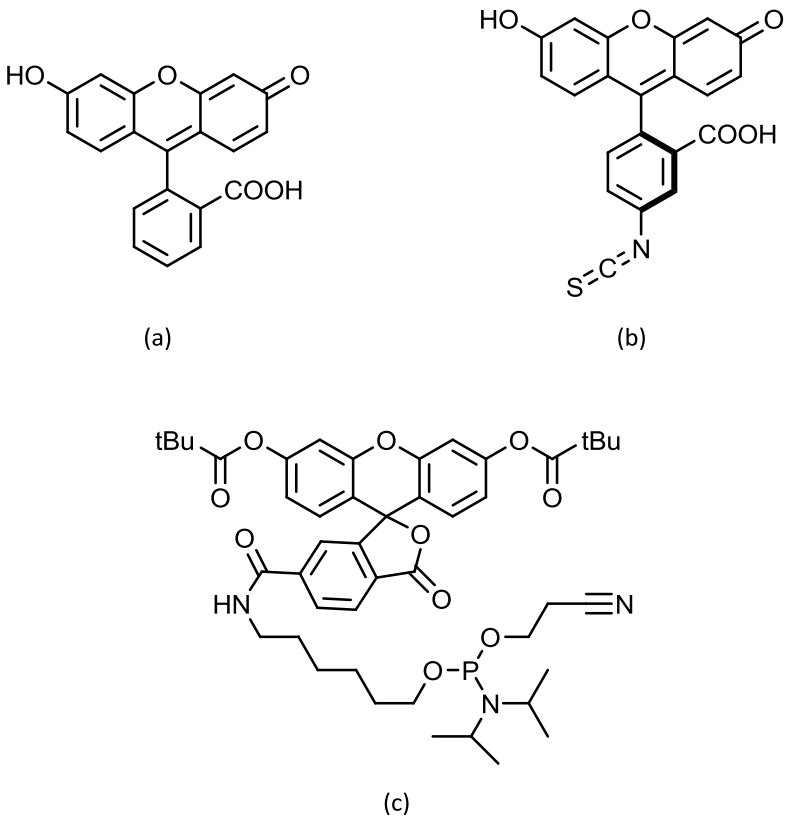

Fig. 27 First fluorescent dyes: fluorescein (a), fluorescein isothiocyanate, FITC (b), and 6-FAM phosphoramidite (c), which is used in the preparation of fluorescein-labelled oligonucleotides.

Cyanine and rhodamine dyes comprise the two important families of fluorophore currently employed in the majority of *in vitro* studies. These types of small organic fluorophores (<1 kDa) are covalently attached to the macromolecule of interest, and industrial optimisation has been in the areas of wavelength range, brightness, photostability, and reduction in self-quenching. Structural modifications to the small molecules include: the extension of double-bond conjugation, rigidification through

extra rings, and the incorporation of electron-withdrawing or charged substituents, such as fluorines or sulfonates. Thus, hundreds of dyes with characteristic excitation/emission spectra and optimal quantum yields are commercially available for any fluorescence application. Such dyes are often used in conjunction with antibody labels in order to target specific proteins of interest in both fixed and permeabilised cells.

Cy3 and Cy5 are the most popular cyanine dyes (Fig. 28): Cy3 dyes fluoresce yellow-green (~550 nm excitation, ~570 nm emission), while Cy5 dyes absorb in the orange region (~649 nm), and are fluorescent in the red region (~650/670 nm).[120] The side chains may be non-identical, and usually consist of short aliphatic chains, one or both ending in highly reactive groups which may be chemically linked to nucleic acids or proteins for various applications, such as proteomics and RNA localisation.

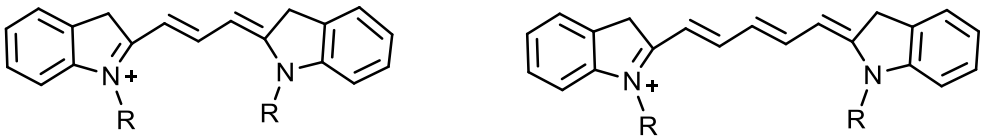

Cy3 **Cy5**

Fig. 28 General structure of the most popular cyanine dyes, Cy3 and Cy5.

Popular dyes in the rhodamine family include tetramethylrhodamine, rhodamine 6G, Texas Red, and Alexa546 (Fig. 29). The excitation and emission spectra of these dyes span across 500-700 nm, and several exhibit high quantum yield, low intersystem crossing, and high photostability properties.[121] Rhodamine dyes are generally toxic, and they are typically soluble in water, methanol, and ethanol.

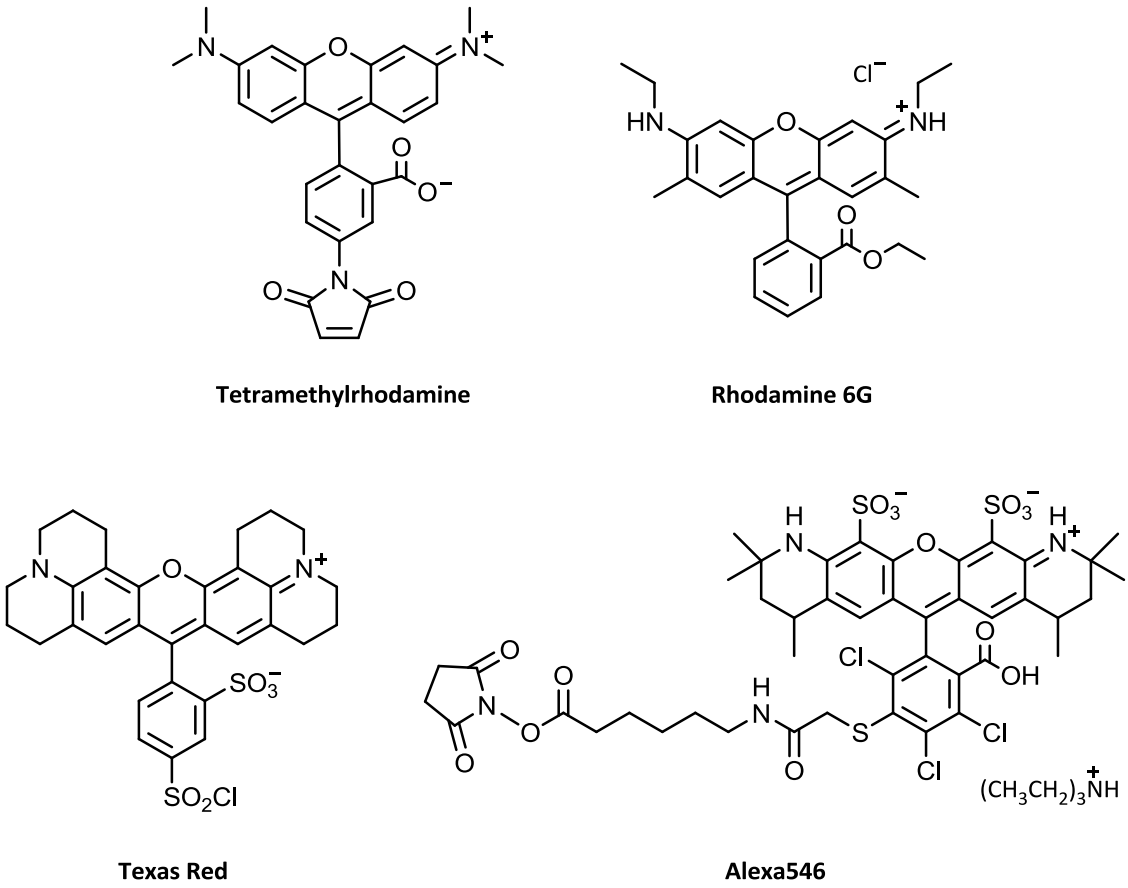

Fig. 29 Examples of popular rhodamine dyes.

Fluorescent proteins

The use of autofluorescent proteins in cell-imaging studies can circumvent the modification and labelling steps that are required for attaching small organic dyes to structures of interest. The discovery, gene cloning, and heterologous gene expression of the green fluorescent protein (GFP) from the jellyfish *Aequorea victoria* has revolutionised fluorescence microscopy and its applications in cell biology.[122] GFP is a protein consisting of 238 amino acid residues (26.9 kDa), and exhibits bright green fluorescence (at wavelength 509 nm) when exposed to light in the blue to ultraviolet range (major excitation peak at 395 nm, minor at 475 nm), with a high fluorescence quantum yield (0.79). GFP belongs to a large family of homologous fluorescent proteins (FPs),[123,124] and different colours are observed due to variations in chromophore covalent structure and the nonconvalent environment.[125]

The low toxicity of fluorescent proteins means they are compatible in live-cell studies, and GFP labelling is particularly useful for the study of protein localisation and mobility in living cells. The GFP gene is spliced into the genome of the organism, in a region that encodes the target protein. GFP is subsequently expressed along with the protein of interest, resulting in production of the fluorescent protein, thus allowing for visualisation using fluorescence microscopy.

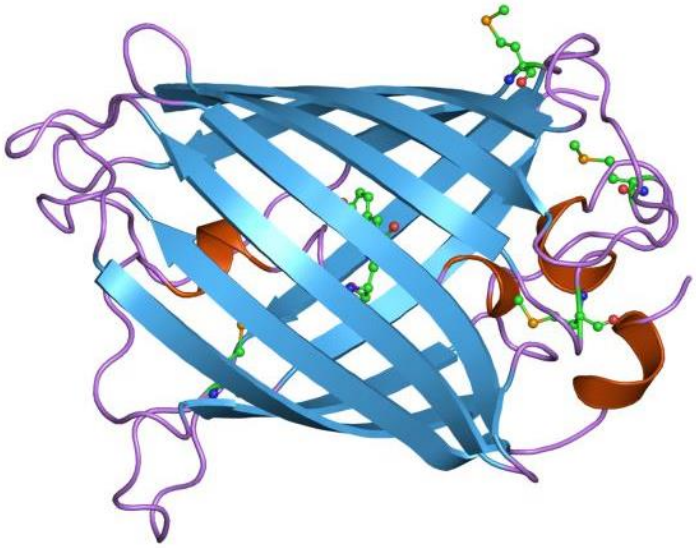

Fig. 30 Crystal structure of the *Aequorea victoria* green fluorescent protein.[126]

The use of GFP has proved valuable in the area of retinoid research and discovery: in one study, a reporter assay system used two GFP derivatives, one (enhanced yellow fluorescent protein (EYFP)) to measure the induction of gene expression, and the other (enhanced cyan fluorescent protein (ECFP)) as an internal control. This enabled fluorescence measurements to be obtained in cells expressing the target protein in response to ligand-induced transcriptional activation, and after screening a library of over 140 compounds, several were identified as activators of RARs.[127]

Quantum dots

Quantum dots (QDs) are inorganic nanocrystals typically consisting of a CdSe or CdTe core and ZnS shell, and range from 2-10 nm in diameter (Fig. 31). QDs possess good quantum yields, and fluoresce at sharp and discrete wavelengths depending on their size: hence, specific wavelengths of emission may be generated by modifying the core size, resulting in emission of any colour of light desired. This wavelength-tunable property of QDs is called the 'size quantisation effect'. The high photostability of QDs allows for repeated imaging of single molecules, and in this respect QDs have been found to be superior to traditional organic dyes: it has been estimated that QDs are 20 times brighter and 100 times more stable than conventional fluorescent labels.[128] Indeed, one study found that quantum dots were able to be observed in the lymph nodes of mice for more than 4 months.[129]

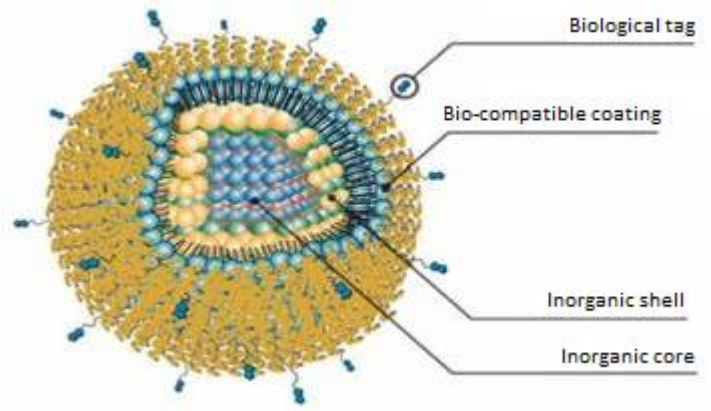

Fig. 31 General structure of quantum dots.

(Reproduced from http://ceramics.org; credit: H. R. Patel.)

The development of coatings to confer water soluble properties to QDs has expanded their role in biological applications, preventing quenching by water, and allowing conjugation to antibodies targeting specific proteins in live cell studies. However, the relatively large size of these conjugates (~10-30 nm) render them unsuitable for transmembrane transport studies, and permeabilised cells or extracellular proteins must be therefore be employed. Nevertheless, the far-reaching potential of QDs in the

study of intracellular processes, and in the areas of tumour targeting and diagnostics, have been highlighted.[130]

In general, the low QD concentrations used in live-cell and animal studies have no reported adverse effects on cell viability, morphology, function, or development. However, higher concentrations appear to affect embryonic development,[131] and when QDs with less protected cores were used, the release of Cd^{2+} or Se^{2-} ions was observed, along with abnormalities in cell viability or function.[132] Therefore, careful optimisation of the use of QDs in medical procedures will be required in order to avoid these undesired outcomes.

3.5. Factors influencing fluorescence

Photobleaching

Photobleaching describes the irreversible destruction of a fluorophore, leading to loss of fluorescence, through photon-induced chemical damage and covalent modification. The susceptibility of a molecule towards photobleaching, therefore, affects its suitability for use in fluorescence imaging experiments. Loss of fluorescence may be attributed to an oxidation reaction between the excited triplet state of the fluorophore and a nearby reactive species,[133,134] or excitation of the molecule already in the excited state, leading to an unstable form.[135,136] The total number of photons emitted before photobleaching, N_{pb}, is thus reduced, and this can be a limiting factor in time resolution imaging. Efforts to maximise N_{pb} have been made, including the use of pulse excitation to avoid double excitation,[137] removing reactive oxygen species through oxygen scavenger systems,[138] and using triplet-state quenchers, such as β-mercaptoethanol (BME) or Trolox, a water-soluble vitamin E analogue.[139] The rate of photobleaching may also be controlled by reducing the intensity or time-span of light exposure, reducing the frequency (and hence the energy) of light, or using fluorophores that are less susceptible to photobleaching. Excited[140] and ground[141] state transitions may also occur, resulting in reversible darkening of the fluorophore in

a process known as photoblinking; in such cases the molecule switches between a photoactive and photoinactive form. An example of the loss of fluorescence intensity due to photobleaching a GFP-tagged cell is shown in Fig. 32.

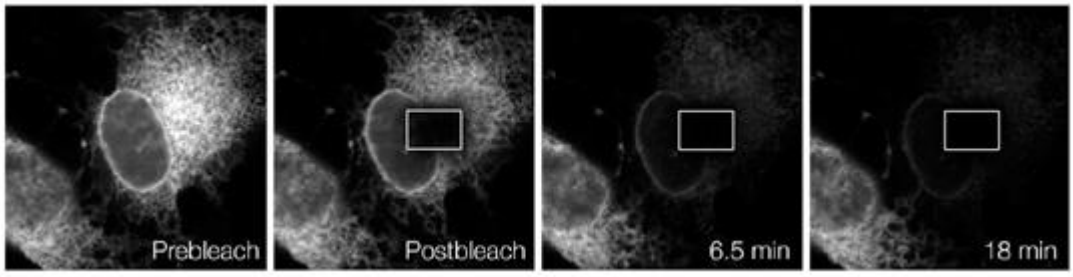

Fig. 32 Protein fluorescence in a small area (box) of a COS-7 cell is bleached repetitively every 40 s. Loss of fluorescence in areas outside the box indicates that the fluorescent protein diffuses between the bleached and unbleached areas. After 18 min, the entire fluorescence was depleted, indicating the highly mobile nature of the GFP-tagged protein.[142]

Reprinted by permission from Macmillan Publishers Ltd: NATURE REVIEWS MOLECULAR CELL BIOLOGY (J. Lippincott-Schwartz, E. Snapp and A. Kenworthy, 2001, **2**, 444-456), copyright 2001.

Quenching

Fluorescence emission of a fluorophore may also be influenced by its interaction with other fluorescent or non-fluorescent molecules, resulting in 'quenching' of fluorescence. This is an important area for consideration when choosing a fluorophore for performing experiments, either in solution, or in the aqueous media used for maintaining cell cultures. The extent of quenching depends on the nature of the quencher molecule, the type of interaction, and the wavelength of energy that is emitted by the fluorophore. The types of fluorescence quenching include fluorescence resonance energy transfer (FRET), contact quenching, and collision quenching (Fig. 33).

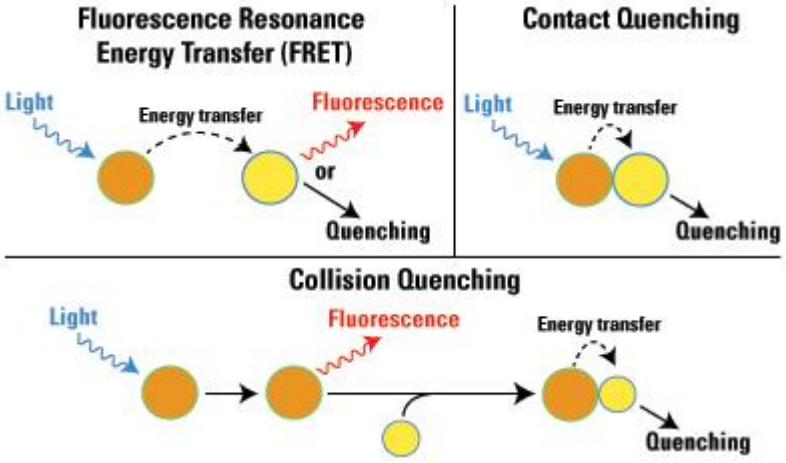

Fig. 33 Types of fluorescence quenching.

(Reproduced with permission from Thermo Fisher Scientific Inc.: http://www.piercenet.com/method/fluorescent-probes; copyright 2014.)

Fluorescence resonance energy transfer (FRET)

In FRET (also known as Förster resonance energy transfer), the photon emitted from the excited state of a donor fluorophore is absorbed by a neighbouring acceptor molecule. When a non-fluorescent acceptor is used, the emitted light from the donor is effectively quenched. In the case of a fluorescent acceptor molecule, if the absorbed photon is within the excitation wavelength range of the acceptor, the latter is raised to an excited state, and releases a photon at the wavelength corresponding to relaxation to its ground state. Thus, instead of observing fluorescence at the wavelength of the original fluorophore, the emission wavelength of the quenching fluorophore is now detected. FRET is extremely sensitive to small distances, since the efficiency of energy transfer is inversely proportional to the sixth power of the distance between donor and acceptor. The distance between two fluorophores may therefore be determined by measuring the FRET efficiency.[143]

Contact quenching

In contact quenching (also referred to as static quenching), the fluorophore is complexed with a quenching molecule prior to excitation. Upon excitation, the energy is immediately transferred to the contact molecule, and is subsequently lost as heat.

Collision quenching

Collision, or dynamic, quenching occurs when the excited fluorophore reacts in solution with a quencher molecule, resulting in the immediate transfer of energy to the latter, and relaxation of the excited fluorophore.

3.6. Tracking in live cells

While the *in vitro* approach of analysing cells has been of great importance in developing the understanding of molecular reactions in cells, the use of processed cell solutions in these studies means that information concerning the effect of the endogenous cellular environment is often lost. The challenge that remains is to observe biochemical reactions in living cells, and optical imaging is a powerful technique for this purpose, offering millisecond time resolution and nanometer spatial precision, single-molecule sensitivity, and, crucially, biochemical specificity.[144]

In order to visualise small molecules in living cells, several obstacles must be overcome: first, bright fluorophores should be employed to improve the signal to noise ratio (SNR), which would facilitate their detection over the high autofluorescence of the cell;[145] exciting the cell with an evanescent wave may also minimise cellular autofluorescence. Second, given the crowded nature of the cell environment, high specificity in labelling the structure of interest is required. Third, in order to be able to discern molecules separately, a low concentration of fluorescent probe should be used to avoid co-localisation of fluorescing molecules within the diffraction limit. Finally, the rapid diffusion and translocation of molecules in three dimensions, as well as high ATP and oxygen concentrations, necessitate a high temporal resolution and low excitation level.[146]

Nevertheless, advances have been made in the areas of probing gene expression, active transport, and metabolism in living cells through the application of optical imaging techniques (reviewed in ref. 144).

Membrane proteins

Lateral diffusion

Single green fluorescent protein molecules have been successfully imaged in living cells through linking GFPs to E-cadherin (E-cad-GFP), which is a calcium-dependent cell-cell adhesion molecule. Using objective-type total internal reflection fluorescence microscopy, it was possible to image individual E-cad-GFP molecules in the membrane of live cells (Fig. 34, *bottom left*).[147] By measuring the fluorescence intensities of the GFP spots, it was found that more than 50% exhibited greater fluorescence compared to monomers, suggesting that the majority of E-cad-GFP molecules are in oligomeric complexes of sizes ranging from dimers to decamers, and that oligomerisation of E-cadherin takes place before its assembly at cell-cell adhesion sites. It was suggested that enhanced membrane-tethering effects trap these E-cad-GFP oligomers in place on the free cell surface, thus accounting for the greatly reduced (by a factor of 10 to 40) translational diffusion rate observed. Similar characterisation for other transmembrane proteins has also been achieved,[145] as well as for anchored proteins such as Ras, which were tagged with EYFP or GFP.

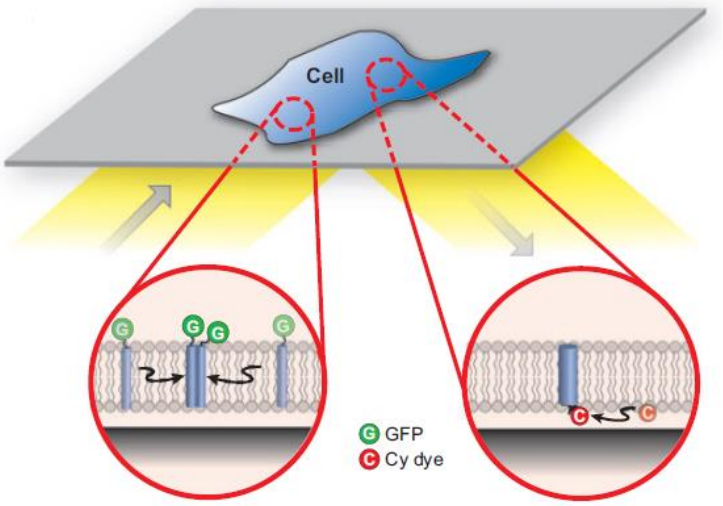

Fig. 34 Live-cell imaging for tracking membrane proteins in lateral diffusion *via* total internal reflection microscopy.[146]

Improved SNR was achieved through the use of synthetic dyes: for example, dye-labelled epidermal growth factor (EGF) was used to observe the movement and dimerisation of its receptor target as the latter bound the extracellular ligand (Fig. 34, *bottom right*).[148] A similar approach was also used to study cAMP receptor systems[149] and peptide-binding proteins.[150] Additional signal improvement was attained by tagging glycine receptors with QDs, which allowed tracking over extended periods (>20 min).[151]

Protein translation

Many *in vitro* single-molecule experiments have provided valuable insights into the mechanistics of protein transcription[152] and translation.[153] However, the 3D nature of protein translation in the cytoplasm means that the process is more difficult to detect in live cells compared to the activity of a membrane protein. However, real-time observation of the production of single protein molecules has been achieved, recently in individual *Escherichia coli* cells.[144] The YFP variant, Venus, was used, and in order to avoid excess fluorescence signals due to the rapid diffusion of the protein through the cytoplasm, a membrane protein, Tsr, was attached to the *N*-terminus of Venus (*tsr-venus*): once produced, the YFP-fusion localises to the cell membrane where its fluorescence signal may be unambiguously detected with single-molecule sensitivity. Thus, a strain of *E. coli* was established containing a single copy of the *tsr-venus* gene in the *E. coli* chromosome, replacing the native *lacZ* gene, and production of YFP during cell growth was imaged through the use of an epifluorescence microscope and a charged-coupled device (CCD) camera. The fusion proteins were counted by photobleaching the fluorophores after their detection: it was found that cells from each cell cycle generally produced up to five fluorescent protein molecules per cell, and that these gene expression bursts lasted between 3 to 15 minutes.

Cytoplasmic proteins

Several studies have identified and tracked cytoplasmic proteins as they diffuse in the 3D volume of the cell, these are highlighted in the following paragraphs.

Transcription factor binding

Along with other transcription factors (TFs), the *in vivo* kinetics of the *lac* repressor has formerly been studied indirectly, through monitoring the gene products. Thus, information concerning the underlying dynamics of TF-mediated gene regulation is often lost. A recent study utilising living *E. coli* cells has followed the kinetics of gene binding and dissociation of the *lac* repressor (LacI) in response to a metabolic signal (Fig. 35, *left*).[154] The repressor was expressed from the native chromosomal *lacI* locus as a fusion with the Venus YFP at the *C*-terminus, thereby allowing for DNA-binding at the *N*-terminal domain. Imaging with a wide-field fluorescence microscope and a CCD camera revealed that fluorescence from TFs that are not specifically bound to DNA were obscured by strong cellular autofluorescence due to rapid diffusion of the proteins throughout the cytoplasm. In contrast, fluorescence from single TFs specifically bound to the relatively stationary DNA proved visible above the background autofluorescence, and could be visualised from highly localised regions. Timescales for LacI binding to, and dissociation from, a DNA target sequence were measured by taking snapshots at 1 to 1000 ms time resolution intervals. As a result, it was observed that LacI spends approximately 90% of the time diffusing along DNA in a non-specific association, with a residence time of less than 5 ms. This approach may thus be applied for the study of other nucleic acid binding proteins.

Transport through the nuclear pore complex

Molecular transport between the nucleus and cytoplasm is made possible by the nuclear pore complexes (NPCs), which span across the double-membrane nuclear envelope (NE). While small molecules (less than ~20-40 kDa) may transit NPCs through a passive diffusion process, larger molecules and complexes (up to ~25-50 MDa) are transported *via* carrier-mediated, signal-dependent processes (facilitated translocation).[155] Single-molecule fluorescence microscopy was used to monitor the nucleocytoplasmic transport process with import complexes (ICs), which consisted of the transport substrate and importin(s), through the NPC in permeabilised cells.[156] A nuclear localisation sequence was tagged with synthetic dyes, and interaction with the NPC temporarily mobilised the molecule to within 200 nm, enabling the fluorescence

to be identified with high spatial (30 nm) and temporal (3 ms) resolution. Tracking of this fluorescence revealed that movement of ICs along the central pore axis is bidirectional and rapid, thus having the characteristics of a random walk.

Motor proteins on linear tracks

Fluorescence imaging with one nanometer accuracy (FIONA) was used to analyse organelle movement by kinesin and cytoplasmic dynein within a cell.[157] These proteins are microtubule-dependent molecular motors that are responsible for intracellular trafficking and cell division (Fig. 35, *right*); long-distance organelle transport occurs in both directions along the microtubule tracks. A GFP-tagged peroxisome in culture *Drosophila* S2 cells were visualised to within 1.5 nm in 1.1 ms, which determined the average step size for movement of this organelle along the microtubule tracks to be approximately 8 nm for both kinesin and dynein. It was also found that the two proteins work in a cooperative manner, at a speed ten times greater compared to the previously observed speed *in vitro*.

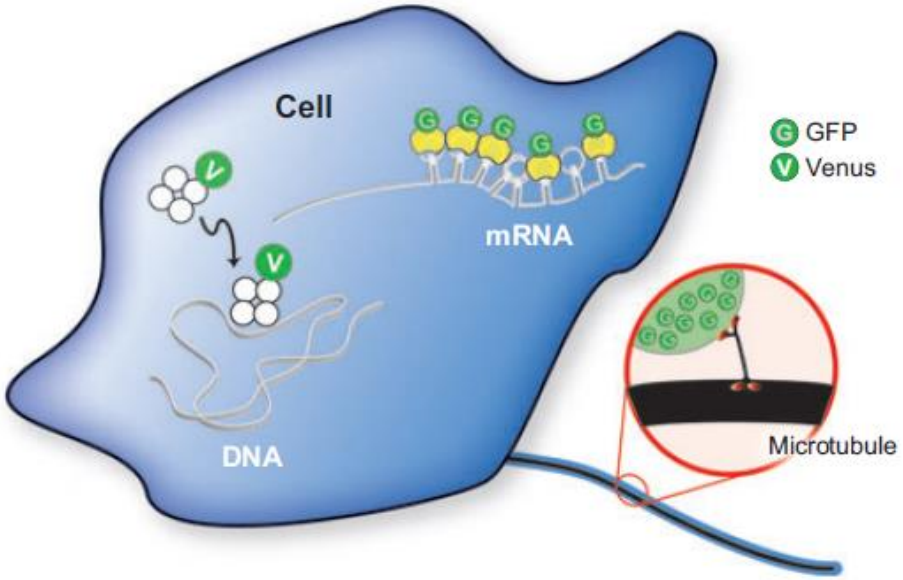

Fig. 35 Live cell imaging for detecting TF-binding onto DNA (*left*);[154] for identifying the presence of mRNA in the cytoplasm (*top*);[158] and for tracking a motor protein (*right*).[157] (*Image reproduced from ref. 146.)*

Other Single Objects

Detection of single molecules in live cells is not limited to proteins: by attaching many copies of a fluorophore to the same object, mRNA molecules and viruses are also able to be visualised and tracked by fluorescence microscopy.

RNA transcript

Most mRNA molecules can be found throughout the cytoplasm[159] and their movement within the cell is essential for determining the spatial distribution of protein synthesis. Complex transport systems involving the cytoskeleton,[160] and in some cases molecular motors,[161] are necessary for the localisation and movement of mRNA. Since RNA molecules may not be covalently labelled with fluorophores, a method was developed for the real-time visualisation of single mRNA molecules in living mammalian cells, with the aim of elucidating the mechanism of movement of these molecules, and to provide information concerning their intracellular localisation.[158]

A MS2 (coat protein) and GFP fusion (MS2-GFP) was used along with a reporter mRNA containing tandemly repeated MS2 binding sites: when these were coexpressed, MS2-GFP that was bound to the reporter mRNA was exported to the cytoplasm (Fig. 35, *top*); when only the MS2-GFP fusion was expressed, the protein was confined to the nucleus by a nuclear localisation signal. Quantification of fluorescence revealed that most GFP-labelled mRNA particles contained 20-50 molecules of GFP. In addition, four types of motility of the mRNA reporters within a single living cell were observed: some molecules appeared to remain stationary; a minority of particles travelled linearly over long distances (>1.5 μm) and at a constant speed; some of the latter molecules occasionally changed direction abruptly and followed a second path of movement, which suggested the involvement of a motor protein; the remaining particles moved significantly, either around a central position, or exhibiting a diffusive pattern of movement, but never travelling more than 1.5 μm continuously in a single direction. Thus, the movement of single RNA transcripts was able to be followed with a time resolution of 10 ms. Individual mRNA molecules were observed frequently switching

among the movements described above, suggesting that they undergo continuous cycles of anchoring, diffusion, and active transport.

Viruses

The viral infection pathway begins with contact between the virus and cell membrane, resulting in transport of the virus into the nucleus and eventual gene expression. In order to effectively design antiviral drugs, and to assist in the development of gene therapy techniques, it is essential to understand the process of viral infection. In the past, electron microscopy was used for investigating the different stages of the infection pathway, however, it was not suitable for analysing living cells with high time resolution.[162] The detection of viruses in fixed cells using conventional fluorescence microscopy was also possible, however, this required high concentrations of viruses and/or many copies of fluorophore, which not only masked the detection of single-molecule processes, but which was also not representative of the real physiological conditions of virus-cell interaction.[163] Thus, real-time visualisation of the infection pathway of single viruses in living cells was achieved by labelling each virus (adeno-associated virus, AAV) with only one fluorescent dye molecule.[164] The trajectories of single AAV-Cy5 particles in 74 living HeLa cells at different stages of infection were then analysed (Fig. 36). Ultimately, the tracing measurements allowed for a detailed observation and quantitative description of the infectious entry pathway of virus particles into living cells.

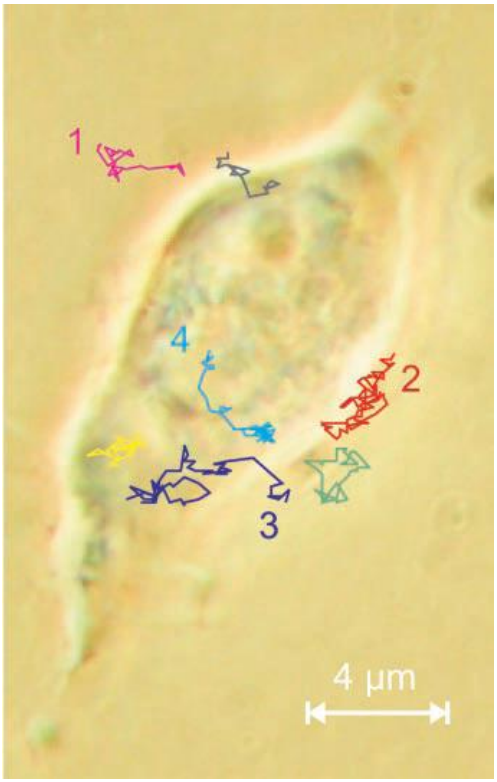

Fig. 36 Trajectories of single AAV-Cy5 particles showing virus entry pathways into a living HeLa cell. Traces showing single diffusing virus particles were recorded at different times, and describe the different stages of infection: diffusion in solution (1 and 2); touching cell membrane (2); penetrating cell membrane (3); diffusion in the cytoplasm (3 and 4); penetrating nuclear envelope, and diffusion in the nucleoplasm (4).[164]

From G. Seisenberger, M. U. Reid, T. Endreß, H. Büning, M. Hallek and C. Bräuchle, *Science*, 2001, **294**, 1929-1932 . Reprinted with permission from AAAS.

3.7. Summary

Fluorescence imaging has rapidly become a powerful tool for investigating biological processes, particularly in living cells where cellular events may be observed in their physiological contexts. The development of single-molecule visualisation techniques has greatly enhanced the usefulness of fluorescence microscopy for such applications, enabling the tracking of proteins and small molecules in their endogenous environments, thus offering a new dimension to understanding their activity and function, at which *in vitro* experiments of the past have only hinted. Improvements in this field lie in the areas of conjugation chemistry, photophysics and photochemistry, and methodology and instrumentation. However, the great diversity of fluorescent probes, and the limitless potential for their modification to provide fluorophores with specific properties (wavelength, fluorescence intensity, and stability), will be a source of great interest for many years to come.

4. DESIGN AND SYNTHESIS OF FLUORESCENT RETINOIDS

4.1. Background and Aims

Doxorubicin (DOX) is a popular chemotherapeutic drug used in the treatment of a wide range of cancers,[165] including leukaemia, Hodgkin's lymphoma, bladder, breast, stomach, lung, ovarian, and thyroid cancers. The amphiphilic and amphoteric nature of the molecule means that the drug is able to bind to both cell membranes and proteins. The main mechanism of DOX cytotoxicity is proposed to be due to its ability to intercalate DNA and inhibit the enzyme topoisomerase II, which unwinds DNA for transcription, thus leading to cell death.

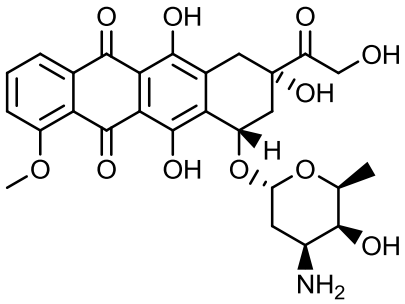

Doxorubicin (DOX)
Trade name: Adriamycin

Due to the inherent fluorescence of the compound, DOX has also become a popular research tool in the field of fluorescence imaging, and its distribution has accordingly been visualised in various cells and tissues. Since the fluorescence intensity of DOX was found to be dependent on its concentration and microenvironment,[166,167] the intracellular uptake and trafficking of the drug in ovarian carcinoma A2780 cells was able to be characterised by taking into account its interaction with cellular components such as DNA, histones, and phospholipids.[168] The ultimate aim was to enhance DOX targeting to tumours, to improve the therapeutic index of the drug, and to reduce systemic toxicity.

At present, DOX is the only known molecule possessing intrinsic fluorescence emission along with significant biological activity. It was recognised that this is an area which has hitherto been unexplored in the field of retinoid research. Thus, if fluorescence

could be incorporated into a small molecule modulator of stem cell development, this would in itself constitute a powerful probe, and would negate the need for the use of fluorescent dyes, proteins, and quantum dots (reviewed in Chapter 3). In particular, the use of live-cell tracking techniques would provide invaluable information concerning cellular uptake and localisation, thereby offering new insights into retinoid activity and metabolism. Furthermore, since it would no longer be necessary to attach a large fluorescent entity to the molecule of interest, the latter may be followed in the physiological context of its natural environment.

Thus, the aim of the project was to design and synthesise a stable fluorescent retinoid, after which its fluorescence emission in various solvents would be measured, the capacity for cellular detection and visualisation determined, and any biological effects induced would be assessed. If results proved favourable, synthesis of a library of fluorescent compounds could then be considered, firstly to derivatise our current set of synthetic retinoids, and then to develop other novel structures.

4.2. Aza-EC23

EC23 is a potent inducer of stem cell differentiation: biological evaluation in the embryonal carcinoma stem cell model TERA2.cl.SP12 revealed that this synthetic retinoid acts in a comparable fashion to ATRA, and induces a higher level of neural differentiation compared to the natural retinoid.[115,116]

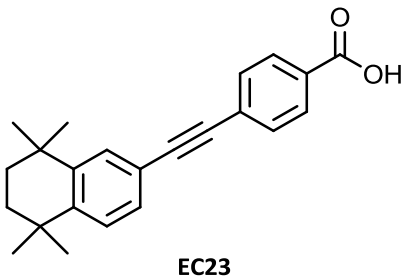

EC23

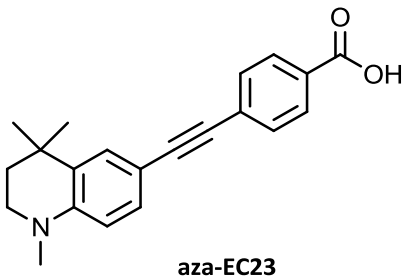

aza-EC23

In order to extend its application to the field of fluorescence imaging, a derivative of EC23 containing an *N*-methyl group within the hydrophobic core was proposed: aza-EC23 (above). The presence of an electron donating and accepting group, as well as the resulting conjugation of electrons throughout the molecule, means that aza-EC23 should, therefore, be fluorescent.

Synthetic route

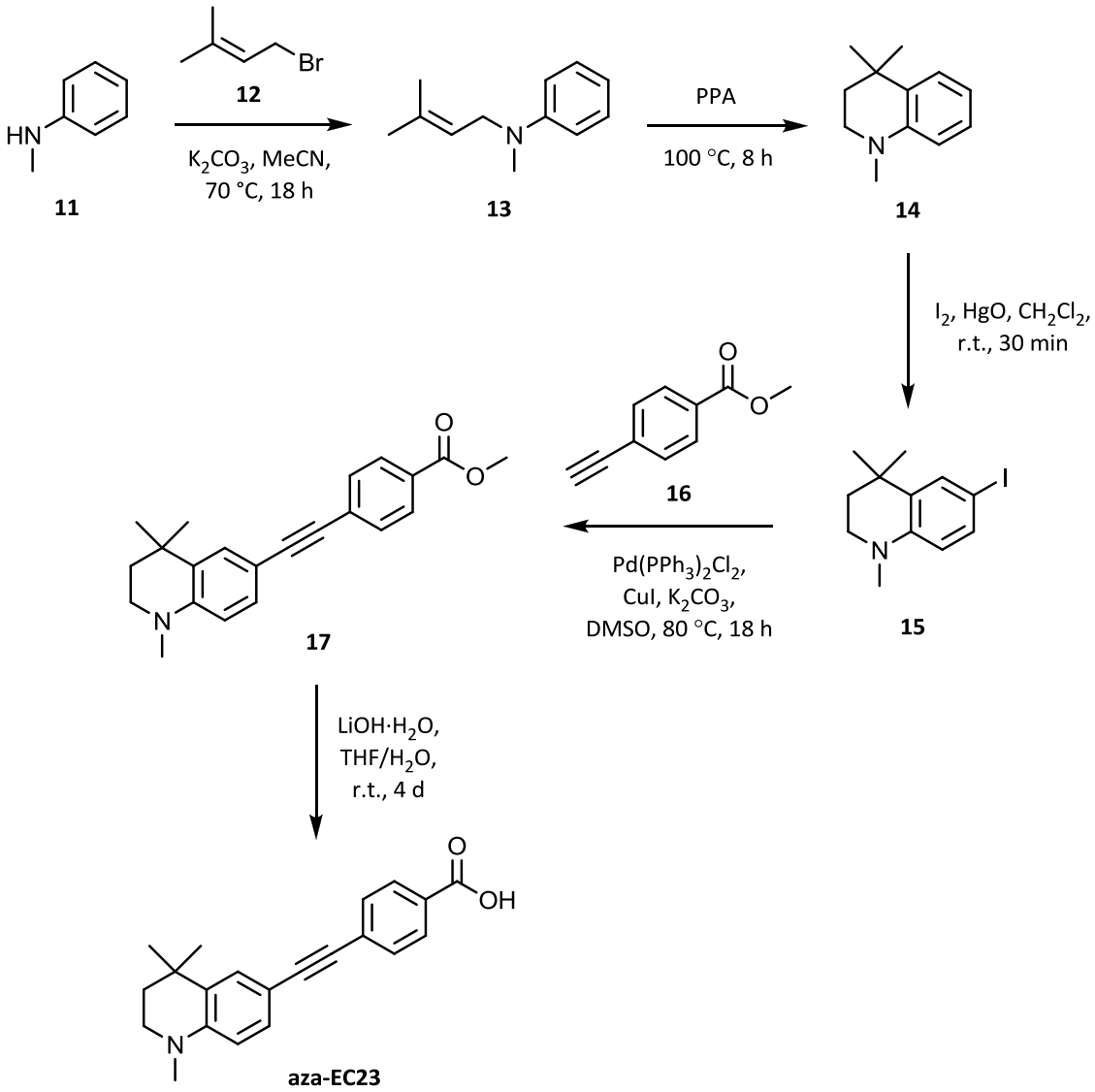

Scheme 4 Synthetic route to aza-EC23.

Aza-EC23 was previously synthesised according to Scheme 4:[169] alkylation of *N*-methylaniline with 3,3'-dimethylallylbromide was followed by cyclisation with polyphosphoric acid (PPA) to provide the tetrahydroquinoline-type structure **14**. Aromatic iodination was then performed, which allowed compound **15** to be coupled to alkyne **16** in a Sonogashira reaction. Saponification of ester **17** then afforded aza-EC23 as a yellow crystalline solid.

Light stability study

An experiment was carried out to determine the stability of aza-EC23 towards light exposure: a sample of the compound in DMSO-d_6 was placed under a white fluorescent light source at a distance of 40 cm for up to 28 days.[170]

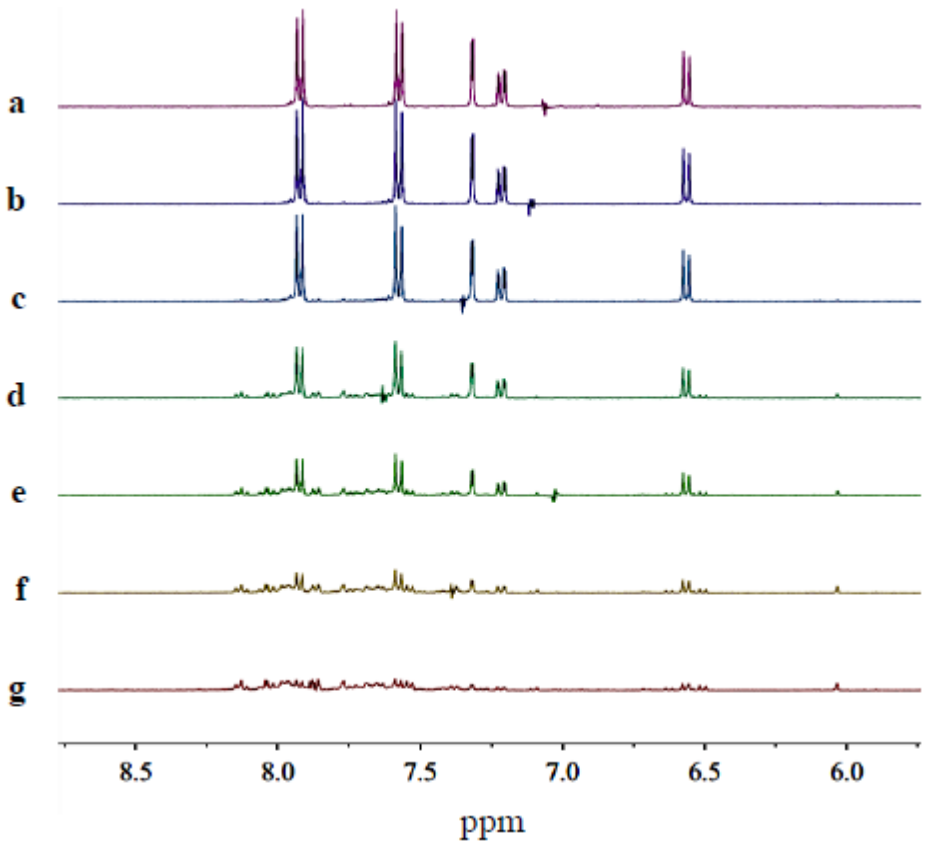

Fig. 37 ^{1}H NMR spectra of aza-EC23 in DMSO-d_6 (recorded at 400 MHz), exposed to a white fluorescent light source at a distance of 40 cm: (**a**) 0 h; (**b**) 24 h; (**c**) 72 h; (**d**) 7 d; (**e**) 14 d; (**f**) 21 d; (**g**) 28 d.

^{1}H NMR spectra were recorded at various time intervals, and the aromatic signals of aza-EC23 over the course of the study were compared in Fig. 37; substantial degradation of the signals was clearly observed, most notably after 7 days light exposure. It was thus clear that the stability of EC23 (in an analogous light experiment, no change in its ^{1}H NMR signals was observed) was not retained in the aza analogue.

Proposed degradation routes

Several oxidation routes of the hydrophobic core of aza-EC23 were proposed (Scheme 5), namely, to give *N*-oxide (**18**), enamine (**19**), and epoxide (**20**) structures. Such species have previously been reported as metabolites of important pharmaceutical compounds,[171] and the biological effects of these *N*-alkyl derivatives have been studied, particularly the relationship between structure, antimicrobial, and cytolytic activity effects on the growth and metabolism of microorganisms. [172,173] It was, therefore, possible that oxidation of aza-EC23 could account for the loss of ^{1}H NMR signals observed, and since the molecule was expected to be fluorescent, light may also have been a contributing factor in the degradation process.

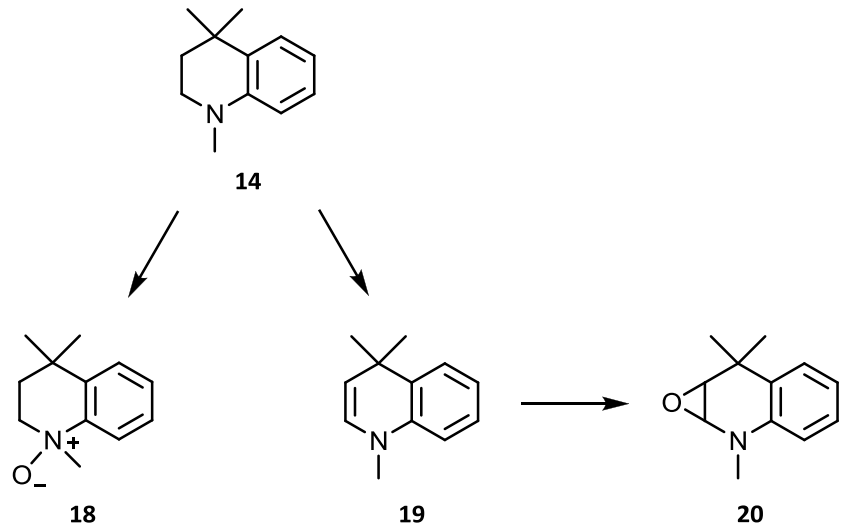

Scheme 5 Proposed degradation routes of the hydrophobic region of aza-EC23.

4.3. Synthesis of an aza-EC23 derivative (GZ108)

Due to the instability of aza-EC23 towards exposure to light for extended periods, some modifications to the structure were proposed, involving the incorporation of a more bulky *N*-isopropyl moiety, as well as a methyl group on the aromatic ring (compound **21**). These would be expected to stabilise the molecule by disfavouring *N*-oxidation, as well as by increasing the electron-donating, and hence fluorescence, properties of the molecule.

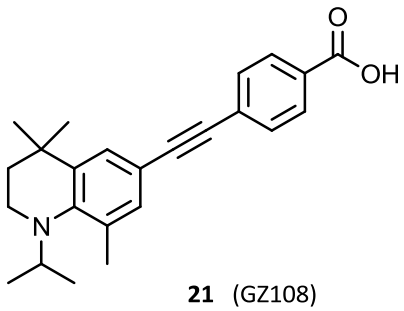

21 (GZ108)

Construction of the hydrophobic core

The synthetic route to compound **21** was proposed to be analogous to that for aza-EC23. The first step involved the reaction of commercially-available *o*-toluidine with 2-iodopropane in order to provide compound **24** (Equation 3). The use of sodium hydroxide in powder form, as opposed to pellets, was found to promote a faster reaction.

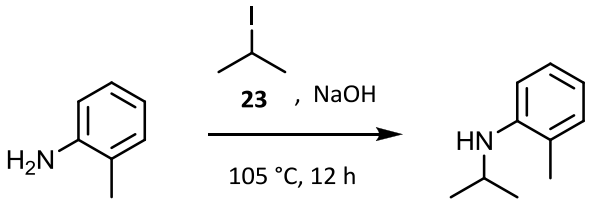

22 82% **24**

Equation 3

It was observed by ^{1}H NMR analyses on all repeats of the reaction that a small amount of the disubstituted product was formed (up to 15%), and attempts at separation by distillation was only successful in removing the lower boiling point unreacted iodopropane. The monosubstituted and disubstituted products were not effectively resolved, and appeared as one spot by TLC analysis when silica gel plates were used; however, on alumina plates, distinct R_f values for the two products were observed. Hence, compound **24** was obtained as a yellow oil in 82% yield following purification by column chromatography on basic alumina.

A second *N*-alkylation was then carried out by heating compound **24** and 3,3'-dimethylallylbromide with potassium carbonate (Equation 4); this hindered substitution reaction did not go to completion, and some unreacted starting material remained despite heating for an extended period (up to 2 days, after which additional side-products were observed). Therefore, after overnight reflux, an aqueous workup was performed, and the crude product was purified by column chromatography on basic alumina to afford compound **25** as a yellow oil in 70% yield.

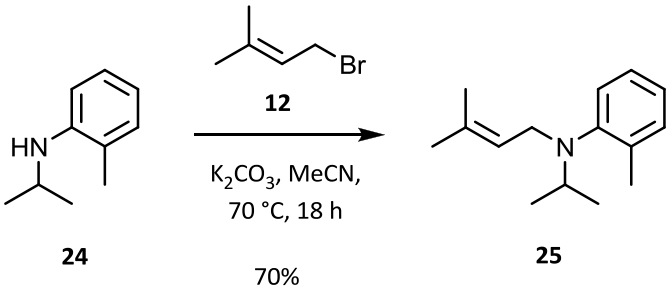

Equation 4

With compound **25** in hand, a cyclisation reaction was then performed using PPA (Equation 5). After heating to 120 °C for 24 h, with vigorous stirring due to the highly viscous mixture, an aqueous workup was carried out, and the residue was filtered through a pad of silica to afford compound **26** as a yellow oil in 78% yield.

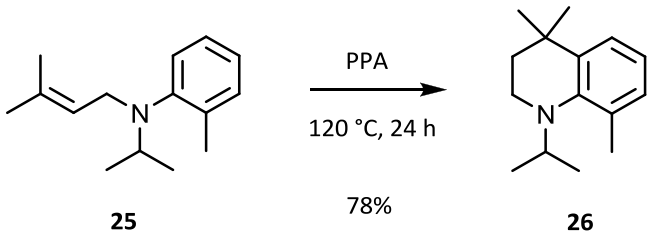

Equation 5

Direct iodination approach

Despite the unreactive nature of iodine towards electrophilic substitution, procedures for successful aromatic iodination reactions have nevertheless been reported.[174] Thus, direct iodination reactions using compound **26** were attempted: Firstly, as for the synthesis of aza-EC23, the starting material was stirred in a mixture of iodine and mercury(II) oxide in dichloromethane (Equation 6, Method **A**). At various timepoints, an aqueous workup was performed on an aliquot of the reaction mixture, and a ^{1}H NMR analysis was obtained; however, only starting material was observed, despite stirring for up to 18 h. Secondly, a Lewis acid-catalysed method based on a reported procedure[175] was also attempted (Equation 6, Method **B**); this was somewhat successful, and approximately 30% conversion to the desired product was observed by ^{1}H NMR analysis after stirring for 72 h.

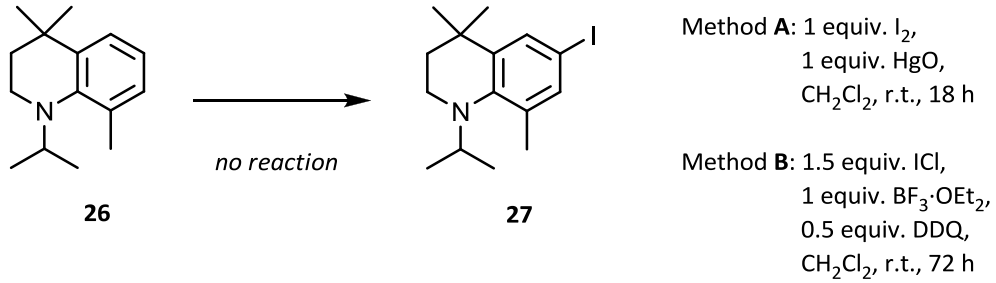

Equation 6

Various other iodination reactions using reported literature procedures were also attempted in order to synthesise the target iodide **27** (Table 1): No reaction was observed when compound **26** was heated with ICl in acetic acid (Table 1, Reaction 1).

Similarly, no iodide was formed when *N*-iodosuccinimide (NIS) and trifluoroacetic acid (TFA) were used (Table 1, Reaction 2).[176] When compound **26** was treated with a mixture of KI and KIO_3 in acetic acid (Table 1, Reaction 3),[177] approximately 30% conversion to the iodide was observed by GC-MS analysis; however, multiple side-products were also present. Finally, equimolar amounts of compound **26**, *N*-chlorosuccinimide (NCS), and sodium iodide were stirred in 0.1 M acetic acid at room temperature:[178] after 4 h, 25% conversion to the iodide was observed (Table 1, Reaction 4); however, when the reaction was stirred for 48 h, a minimal amount of product (approx. 5%) was observed by GC-MS analysis (Table 1, Reaction 5). Evidently, the reaction conditions assessed were insufficiently activating to promote iodination of compound **26**. This was surprising, given that iodination of the *N*-methyl analogue (see synthesis of aza-EC23, Scheme 4) proceeded relatively easily. Thus, it can only be surmised that the presence of the additional methyl groups in compound **26** deactivate the structure towards aromatic iodination.

Table 1 Iodination reactions attempted with compound **26**.

Reaction	Reagents	Solvent	Temp. (°C)	Time (h)	Product observed?
1	ICl (1.2 equiv.)	AcOH	120	5	no
2	NIS (1.1 equiv.) TFA (0.3 equiv.)	MeCN	20	4	no
3	KI (1.0 equiv.) KIO_3 (1.0 equiv.)	AcOH	80	2	30%[a]
4	NCS (1.0 equiv.) NaI (1.0 equiv.)	AcOH (0.1 M)	20	4	25%[b]
5	NCS (1.0 equiv.) NaI (1.0 equiv.)	AcOH (0.1 M)	20	48	5%[b]

[a]Approx. value as observed by GC-MS analysis in comparison to starting material, mix of other products also apparent.
[b]Approx. value compared to starting material as observed by GC-MS analysis.

Aromatic bromination

Given the difficulties in carrying out direct aromatic iodination of compound **26**, the synthesis of bromide **28** was proposed (Equation 7), with the aim of then performing a halogen-exchange reaction to afford the desired iodide product.

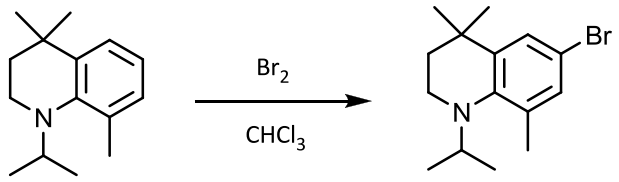

26 **28**

Equation 7

Bromination was initially carried out by cooling a flask containing a solution of compound **26** in chloroform to 0 °C, followed by the dropwise addition of 1.1 equivalents of bromine. After 10 min, consumption of the starting material was apparent by ^{1}H NMR analysis. The mixture was then washed with 1 M aqueous $NaHCO_3$ solution, and the organic layer was dried over $MgSO_4$. Following *in vacuo* solvent removal, the residue was filtered through a pad of alumina using hexane:EtOAc, 9:1, as eluent. However, in addition to the expected brominated product, an alkene species with a similar structure was also present (approx. 10% by ^{1}H NMR analysis), with two doublet signals at δ 6.02 and 4.87 in the ^{1}H NMR spectrum. It became apparent that this species was inseparable from bromide **28**, despite attempts at purifying the oil by column chromatography using different solvent systems. This mixture of products was used in subsequent reactions for synthesis of the target structure (compound **21**); however, despite purification of the product from each step by column chromatography and recrystallisation, the characteristic doublet signals in the alkene region remained by ^{1}H NMR analysis.

It was deduced that the minor species must be the dehydrogenated side-product (compound **29**) formed from bromide **28** during the course of the reaction. This would account for the similarity of the two products by TLC and ^{1}H NMR analyses, and the difficulty in their separation by chromatographic means.

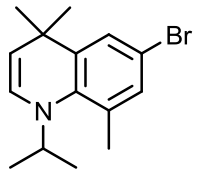

29

It was proposed that once formed, bromide **28** undergoes an addition-elimination reaction in the presence of excess bromine to give an iminium ion, which subsequently eliminated during aqueous workup to give the enamine structure (Scheme 6).

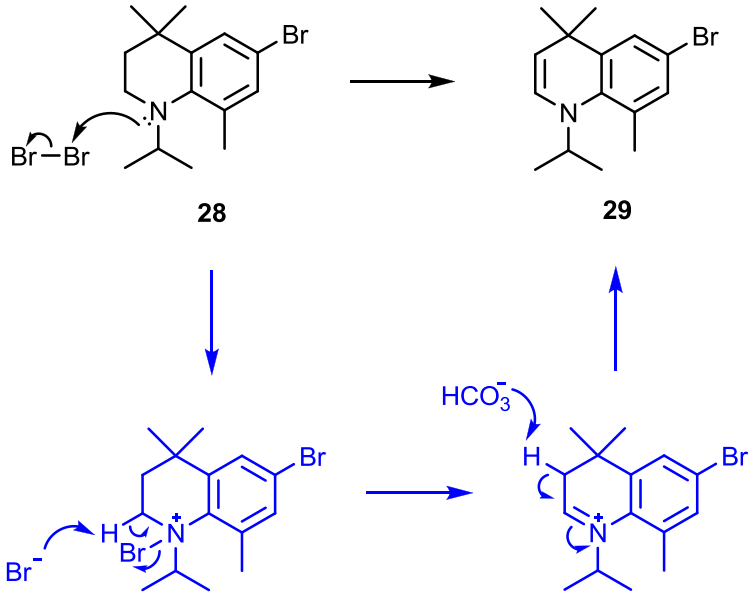

Scheme 6 Proposed mechanism for the formation of compound **29**.

Since the relative integral peaks of major to minor product in the ^{1}H NMR spectrum indicated approximately 10% of the enamine product was present, this would correlate with the 0.1 equivalents of excess bromine used for carrying out bromination of compound **26**. Thus, in order to obtain pure bromide **28**, the reaction was repeated using both 1 and 0.9 equivalents of bromine, at 0 °C and at room temperature, respectively. In both cases, formation of the enamine product was still observed: evidently, the side reaction appeared to be highly competitive.

Pure bromide **28** was eventually obtained by cooling a stirred solution of compound **26** in chloroform using a cryostat set to -60 °C, followed by the addition of 0.95 equivalents of Br_2 (Equation 8). The flask was warmed slowly to -30 °C over 1 h, after which ^{1}H NMR analysis of an aliquot of the reaction mixture after aqueous workup showed the reaction to be complete, and no enamine side-product was observed. However, it was observed that if the crude product was stored without purifying, some side-product would be formed. Thus, in order to remove any residual oxidising bromine species, compound **28** was filtered through a pad of alumina using hexane:EtOAc, 9:1, as eluent, affording the pure bromide as a colourless oil in 62% yield. A fast flow rate was preferred in order to compensate for the tendency of the product to streak on the column, thereby reducing the number of fractions in which the bromide eluted.

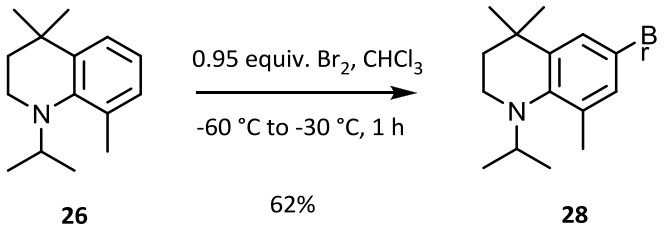

26 62% **28**

Equation 8

Synthesis of an enamine species

It was recognised that if enamine **29** could be exclusively obtained, this could allow for the synthesis of another fluorescent retinoid derivative, compound **30**.

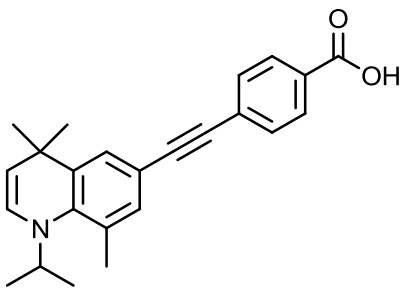

30

The additional double bond and increased conjugation present in this compound should result in enhanced fluorescence properties for this molecule compared to the tetrahydroquinoline structure. Thus, synthesis of enamine **29** was attempted using 2.2 equivalents of bromine in order to ensure complete conversion to the desired product. The reaction was monitored by TLC analyses, and found to be complete after stirring at 30 °C overnight. ^{1}H NMR analysis of the crude product following aqueous workup showed that, as expected, the starting material had been fully consumed, and two doublet peaks associated with the enamine double bond were observed. However, an additional unexpected singlet peak at 6.36 ppm was also present, which appeared to constitute the major product. GC-MS analysis of the mixture suggested that a dibrominated species was present, and the major product was, therefore, determined to be compound **31** (Equation 9).

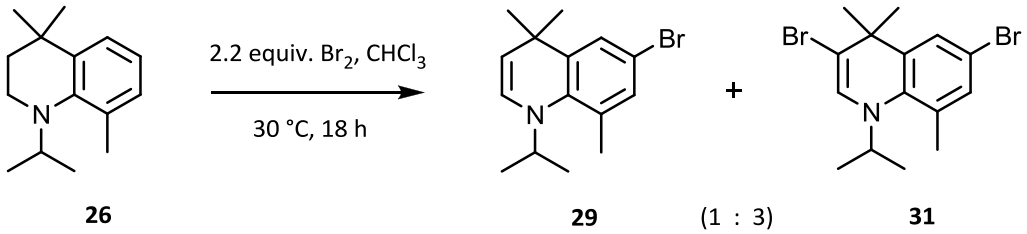

26 **29** (1 : 3) **31**

Equation 9

Chemical shift comparisons and mechanistic considerations (discussed below) suggested the bromine atom to be in the 3-position, rather than in the alpha-position (**32**).

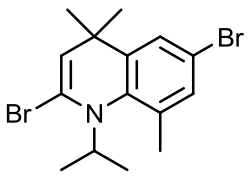

32

Synthesis of a dibromide species

A review of NMR data from previous reactions in which enamine **29** was formed revealed that the dibromide compound was also present following aqueous workup of the bromination reactions. Thus, loss of the singlet peak associated with compound **31** in ^{1}H NMR analyses of the product following purification by column chromatography was likely due to the less-mobile dibromide remaining on the stationary phase. It would appear that excess bromine could react with the enamine product by adding across the double bond, which would give a tribromide species (**33**); Elimination of HBr during aqueous workup would then provide dibromide **31** (Scheme 7).

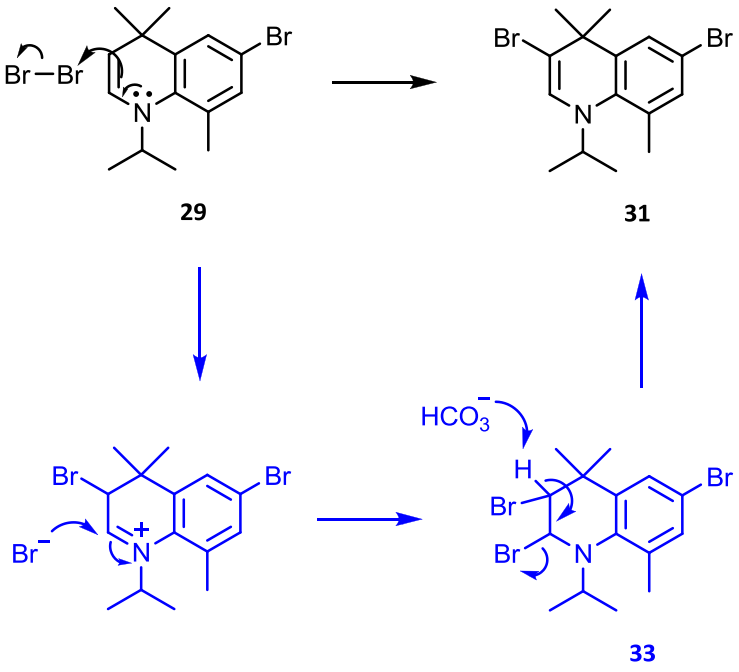

Scheme 7 Proposed mechanism for formation of the dibromide species **31**.

Thus, in the presence of excess bromine as well as a base, enamine **29** would be expected to be a very reactive intermediate to undergo addition-elimination, and should be fully consumed during the course of the reaction. This was accordingly assessed by using 2,6-lutidine as an *in situ* base in order to promote elimination from the tribromide adduct, and to provide exclusively the dibromide species. Indeed, after stirring compound **26** with 2.2 equivalents of bromine and 2,6-lutidine overnight at 30

°C (Equation 10), no enamine was present by ^{1}H NMR analysis. However, the dibromide species in fact constituted the minor product, and the major product was observed to be the monobromide (ratio of 1:2, respectively, as observed by ^{1}H NMR analysis).

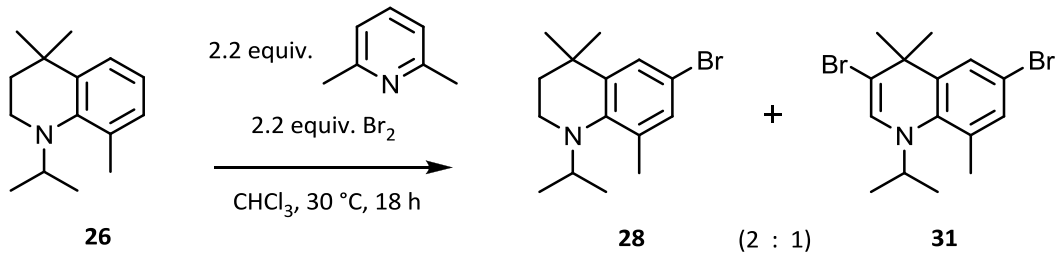

Equation 10

It was recognised that dibromide **31** would provide scope for derivatisation and functionalisation of the molecule at the 3-position, making it an attractive synthetic target. A literature search revealed that if compound **31** could be exclusively obtained, this would provide an interesting, simple, and direct route to a biochemically important and novel dihydroquinoline-type structure.[179] 1,4-Dihydroquinolines have been employed as carriers for the delivery of biologically-active compounds to the brain, however, their use is hampered by poor stability towards oxidation and hydration reactions, which limit investigations *in vivo*.[180] In this case, the fully substituted 4-position of compound **31** renders the molecule stable towards isomerisation, which is a major issue for synthetic control in dihydroquinolines (Fig. 38).[181]

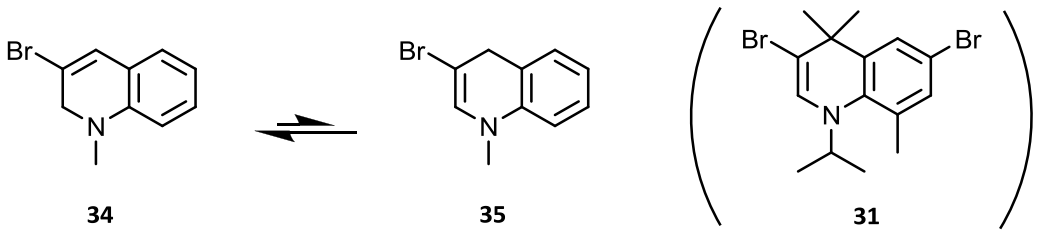

Fig. 38 Spontaneous isomerisation of 1,2 (**34**)- and 1,4 (**35**)-dihydroquinolines possessing electron-withdrawing substituents in the 3-position. Compare with the 'locked' structure of the *gem*-dimethyl group in compound **31**.

Thus, based on the mechanisms outlined in Schemes 6 and 7, it was concluded that the use of 3 equivalents of bromine should provide the desired dibromide product **31**, and the inclusion of a hindered base such as 2,6-lutidine would also be expected to promote product formation *via* the intermediates. Accordingly, 3 equivalents each of bromine and 2,6-lutidine were added to a stirred solution of compound **26** in chloroform. The flask was maintained at 30 °C, and following overnight stirring, a mixture of products was observed by ^{1}H NMR analysis (Fig. 39). It was determined that the major product was still the monobromide, with some dibromide compound present, as well as two distinctive doublets indicative of tribromide **33** (approximate ratio of 55:30:15, respectively; Table 2, Reaction 1).

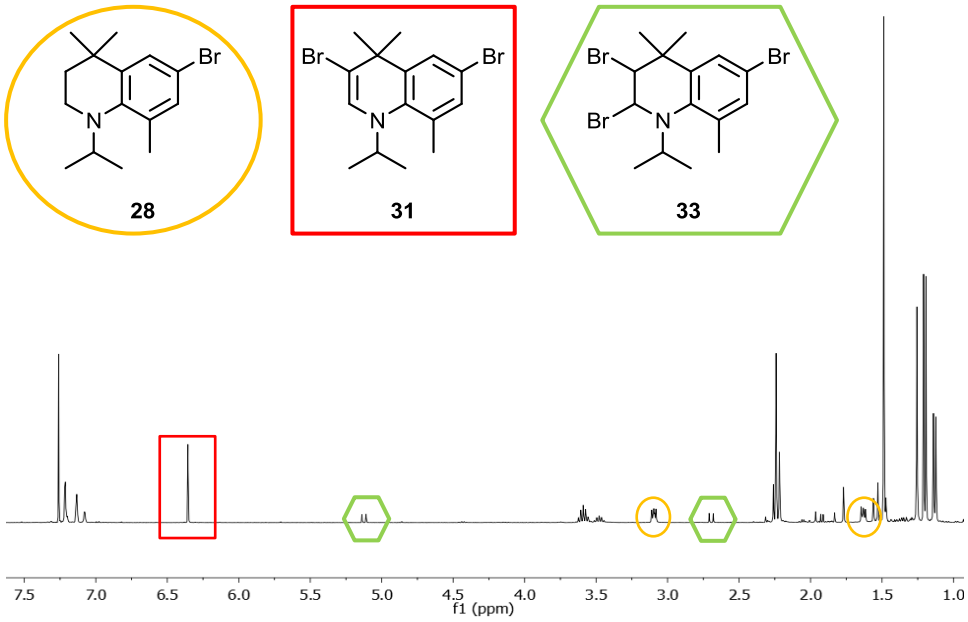

Fig. 39 ^{1}H NMR spectrum showing distinctive signals associated with monobromide **28** (circled); dibromide **31** (rectangle); tribromide **33** (hexagon) - *recorded in $CDCl_3$ at 400 MHz.*

A few drops of lutidine were added to the NMR sample and mixed thoroughly, whereupon ^{1}H NMR analysis showed that signals associated with the tribromide product had disappeared, which was consistent with the suggestion that the dibromide species was the product of basic elimination of HBr from the tribromide intermediate.

A series of reactions were then attempted in order to obtain exclusively the dibromide product, these are summarised below (Table 2).

Table 2 Approximate percentages of monobromide **28**, dibromide **31** and tribromide **33** as observed by ^{1}H NMR analysis following reaction with bromine and 2,6-lutidine.

Reaction	Br_2	2,6-lutidine	Temp.	% mono **28**	% di **31**	% tri **33**
1	3 equiv.	3 equiv.	30 °C	55	30	15
2	1 equiv. x 3	1 equiv. x 3	30 °C	25	25	50
3	4 equiv.	8 equiv.	30 °C	0	33	67
4	4 equiv.	8 equiv.	60 °C	0	100	0

*In all cases, reagents were added to 1 equiv. of compound **26** in chloroform, and stirred for 18 h.*

Since the reaction to give the dibromide product evidently did not go to completion, despite using sufficient equivalents of bromine and 2,6-lutidine, the limiting factor was thought to be consumption of the base (namely, that a lutidine-bromide complex was formed during the course of the reaction). Thus, in order to promote a more efficient reaction, 1 equivalent each of bromine and 2,6-lutidine were added at 0, 4, and 8 h to a stirred solution of compound **26** at 30 °C (Table 2, Reaction 2). Following overnight reaction, the ratio of the mono-, di-, and tri-bromide products was observed by ^{1}H NMR analysis to be 25:25:50, respectively. The addition of a further 1.5 equivalents of bromine followed by 5 equivalents of 2,6-lutidine only resulted in complete formation of the tribromide intermediate, and the addition of more base at this point was ineffective in promoting elimination to give exclusively the dibromide product. It would appear, therefore, that the tribrominated species was in fact more stable than previously expected.

Next, a reaction employing 4 equivalents of Br_2 was set up, and, for effective elimination from the tribromide, 8 equivalents of 2,6-lutidine were also used (Table 2, Reaction 3). After stirring overnight at 30 °C with 1 equivalent of compound **26**, ^{1}H NMR analysis of an aliquot of the reaction mixture (following aqueous workup to remove base and bromine species) showed that no monobromide product was

present. Instead, a 2:1 ratio of tribromide to dibromide products was observed, and subsequent addition of 2,6-lutidine to the reaction mixture was not successful in increasing the ratio of the dibromide product. Since there should have been more than sufficient bromine and base for formation of the dibromide product, the reaction was repeated with heating to 60 °C (Equation 11; Table 2, Reaction 4).

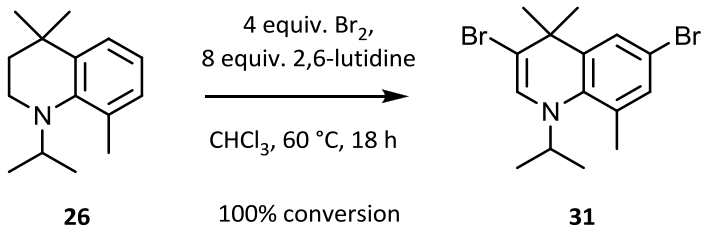

26 **31**

Equation 11

After 18 h, an aqueous workup was performed, and complete conversion to dibromide **31** was observed by ^{1}H NMR analysis, with no monobromide or tribromide species present (Fig. 40).

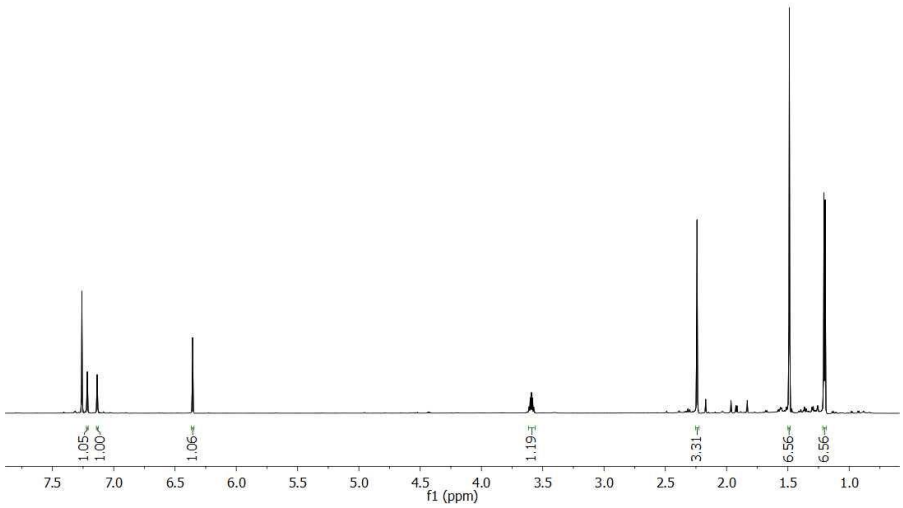

Fig. 40 ^{1}H NMR spectrum of dibromide **31** (recorded in $CDCl_3$ at 400 MHz) from Equation 11 after reaction workup. *Note loss of signals associated with the mono- and tri-bromide products.*

Reactions of the dibromide species

Dibromide **31** was synthesised according to Equation 11, and purification of the compound was performed by filtering the crude product through a pad of alumina. However, ^{1}H NMR analysis of the residue following *in vacuo* removal of the solvent revealed that a species in addition to the expected product was present. The signals did not correlate with either the simple loss of a bromide ion from the product, or with the starting material. Evidently, the presence of the vinyl bromide in conjugation with the nitrogen atom conferred an element of instability to the molecule, which became apparent upon further handling and purification. Some proposed reactions of dibromide **31** are considered below.

Addition-elimination?

The most likely reaction of compound **31** would be the addition of water across the double bond, followed by elimination of HBr (Scheme 8).

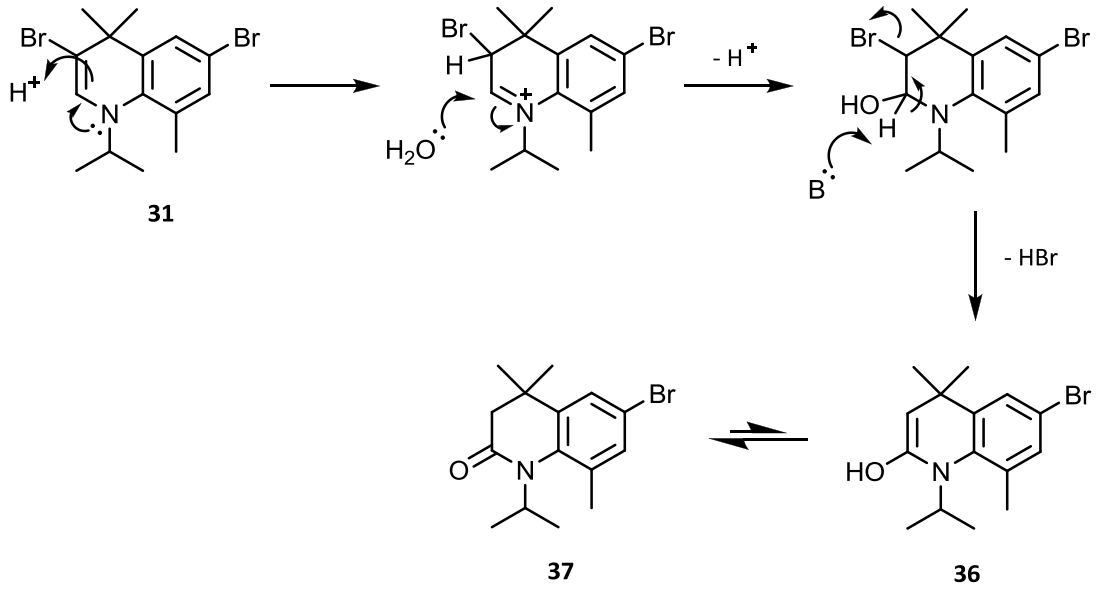

Scheme 8 Proposed mechanism for addition-elimination of compound **31**.

Thus, an overall loss of a bromine atom along with a gain of an oxygen atom would be expected, and GC-MS analysis of the mixture confirmed that this was the case.

Furthermore, a sharp carbonyl signal was present in the IR spectrum of the material (ν_{max} 1723 cm^{-1}), with no peak indicative of a hydroxyl group. The product of the addition-elimination reaction was, therefore, deduced to be the amide compound **37**, rather than the enol product (**36**).

Radical migration?

Compound **36** may undergo a further addition-rearrangement reaction, in which loss of a bromine radical would be stabilised by a 1,2-methyl migration as depicted in Scheme 9.

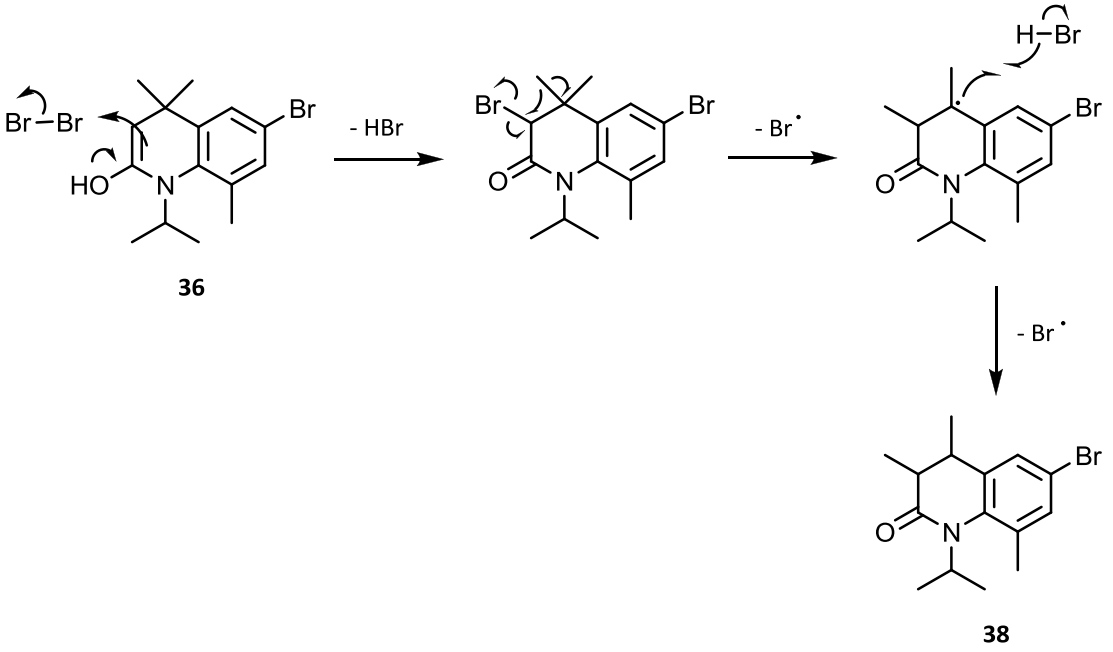

Scheme 9 Proposed mechanism for radical elimination and methyl migration.

Aldehyde species?

It was clear from ^{1}H NMR analyses that two coupled doublets at 9.52 and 3.63 ppm were present. The very low-field shift at 9.52 ppm suggested the presence of an aldehyde proton coupled to a proton on the neighbouring carbon atom. Additionally, the IR stretch at ν_{max} 1723 cm^{-1} was within the approximate range for an exocyclic aldehyde. The most likely structure that corresponded to these observations was thus determined to be aldehyde **39**, and the proposed mechanism for its formation is

shown in Scheme 10. It was thought that the presence of a significant amount of moisture in the large volume of solvent required for eluting compound **31** from the alumina pad may have contributed to formation of the aldehyde product.

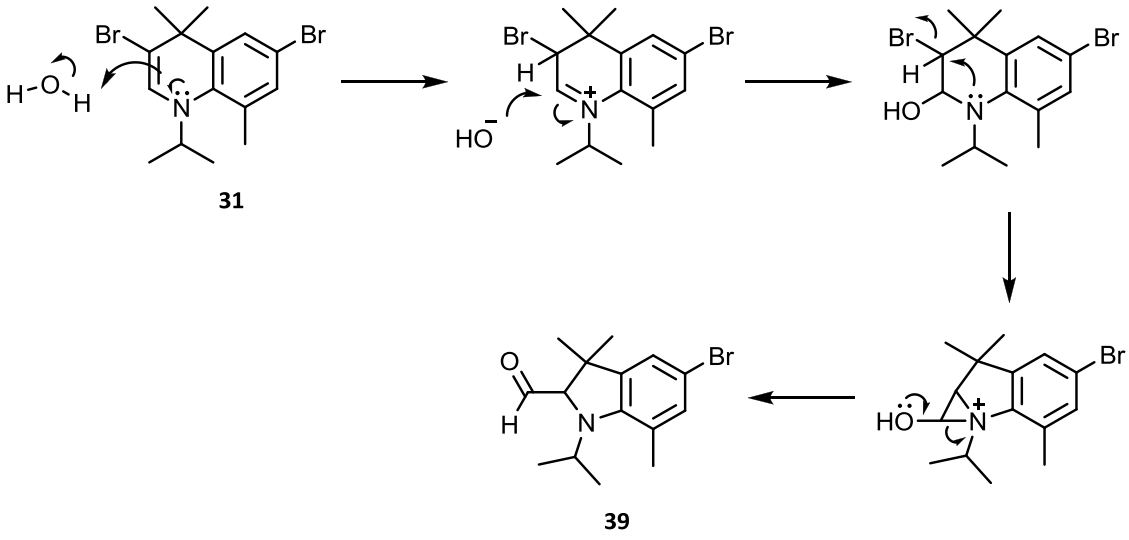

Scheme 10 Proposed mechanism for formation of aldehyde **39**.

The Brady's test using 2,4-dinitrophenylhydrazine (DNPH, Equation 12) was performed in order to assess if the aldehyde was indeed present. However, after overnight stirring at room temperature, no precipitate (indicative of product formation) was observed, neither was the expected mass of the adduct (**40**) found by GC-MS analysis. This lack of reaction was perhaps unsurprising, due to the unfavourable hindered approach of DNPH to the purported aldehyde. It is recognised that conclusive structural proof for formation of compound **39** is still required.

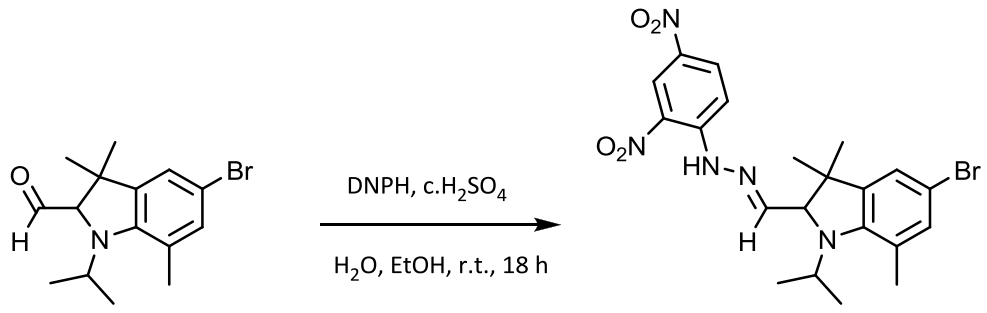

39 **40**

Equation 12

Carbenoid species?

It was also possible that dibromide **31** could possess a degree of carbene-like character, as shown in Scheme 11.

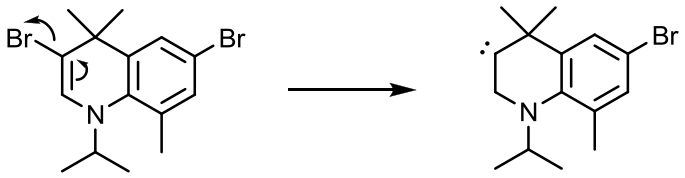

31 **41**

Scheme 11 Proposed generation of a carbenoid species (**41**).

Therefore, in order to examine the nature of **31**, as well as to derivatise and/or stabilise the molecule, a substitution reaction with allyltrimethylsilane was attempted using various Lewis acids (Equation 13).

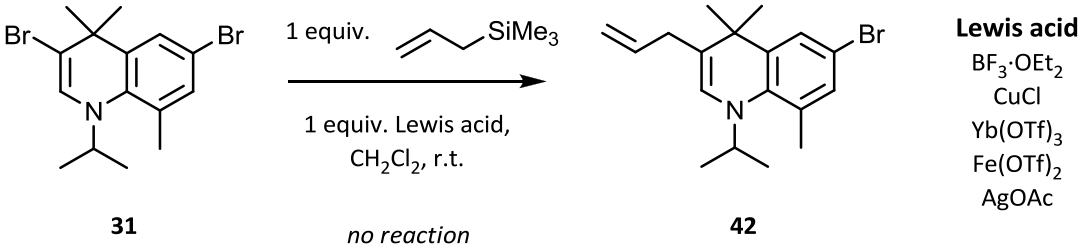

31 **42**

Equation 13

Compound **31** was dissolved in dry dichloromethane under an inert argon atmosphere, after which 1 equivalent of Lewis acid was added, and the solution was stirred for 10 min prior to the addition of 1 equivalent of allyltrimethylsilane. When $BF_3{\cdot}OEt_2$ was used as the catalyst, TLC analyses after 1, 2.5, and 18 h showed only starting material was present. The mixture was then heated gently to reflux (40 °C): after 2 h, no product was observed by TLC analysis; after 6 h, there was substantial decomposition of dibromide **31** as observed in the ^{1}H NMR spectrum, and the expected product peak of compound **42** was not detected by GC-MS analysis. Reactions using CuCl, $Yb(OTf)_3$,

$Fe(OTf)_2$, or AgOAc as catalyst were similarly unsuccessful. This lack of reactivity of the enamine bromide was surprising, and necessitates further investigation.

Future work

There could be an inherent instability of dibromide **31** that accounted for the unexpected side-products observed: these may be formed spontaneously following reaction workup, or could be produced during the purification process, either due to exposure to light, air, or moisture, or by reaction with alumina. Further investigations would be necessary in order to ascertain how and at which point the side-products are formed, as well as to definitively determine their structures. Given these findings, perhaps the best course of action would be to repeat the synthesis of the dibromide, and to take precautions during purification, handling, and storage (*i.e.* where possible to exclude light, air, and moisture) in order to avoid side-product formation.

The crude dibromide product was nevertheless employed for the synthesis of a bromine-containing retinoid (discussed in section 4.6.); however, it was not possible to achieve satisfactory purification of this compound.

Synthesis of the polar terminus

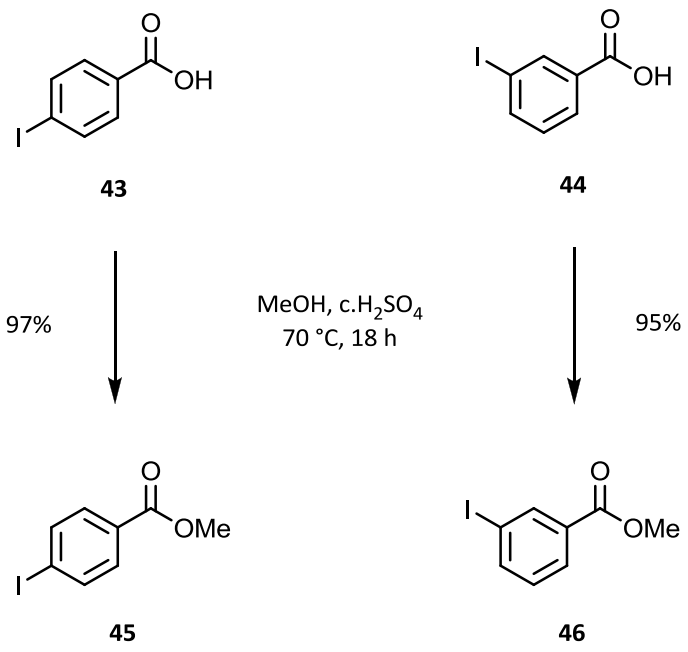

Scheme 12 Esterification reactions of 4-iodo (**43**)- and 3-iodo (**44**)-benzoic acid.

Preparation of the aryl alkyne region of the molecule was then carried out: 4-iodo- and 3-iodo-benzoic acids were used, with the aim of producing retinoids containing the carboxylic acid terminus in the *para*- and *meta*-positions, respectively. Thus, esterification reactions of 4-iodo (**43**)- and 3-iodo (**44**)-benzoic acids were carried out by refluxing the starting material in methanol, along with a catalytic amount of concentrated sulphuric acid. After overnight reaction, the corresponding methyl esters (**45** and **46**) were obtained in excellent yields following aqueous workup and recrystallisation (Scheme 12).

Next, Sonogashira coupling reactions were performed with esters **45** and **46** in order to afford the trimethylsilyl-protected aryl alkynes **47** and **48** in good yields (Scheme 13).

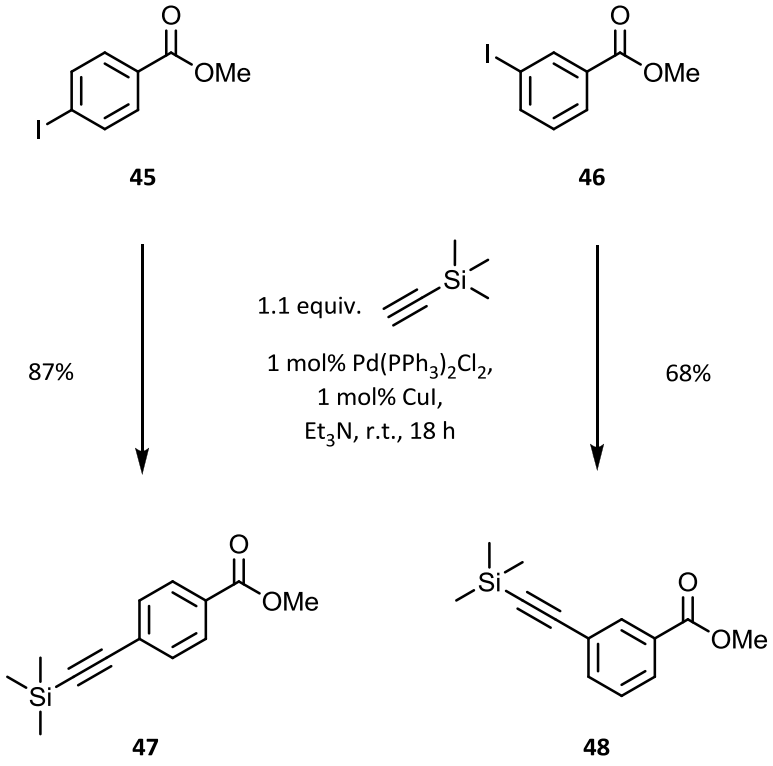

Scheme 13 Sonogashira coupling reactions with trimethylsilylacetylene (TMSA).

Finally, base deprotection of compounds **47** and **48** was carried out by stirring with 4 equivalents of sodium carbonate in a solution of methanol and water at ambient

temperature (Scheme 14). Alkynes **16** and **49** were thus obtained in good yields (79% and 63%, respectively).

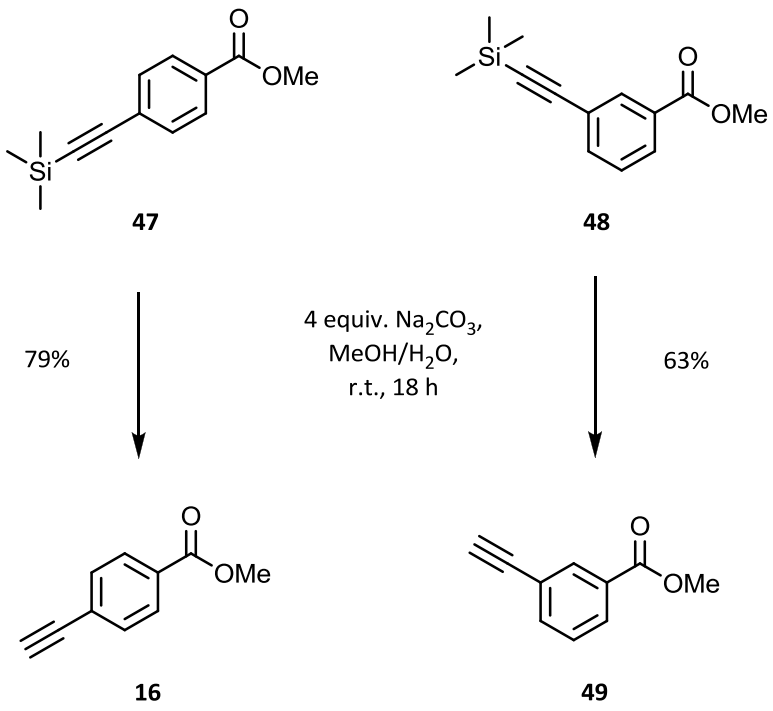

Scheme 14 Base deprotection reactions to provide alkynes **16** and **49**.

Halogen-exchange reaction

Having probed the various outcomes of the aromatic bromination reaction, namely, formation of the enamine and dibromide side-products, efforts were then directed towards synthesis of the original fluorescent retinoid target (compound **21**), using pure monobromide **28**, which was synthesised according to Equation 8. Thus, a halogen-exchange reaction to produce the desired iodide was attempted, using a procedure which had been previously reported as successful for the conversion of aromatic bromides (Equation 14).[182]

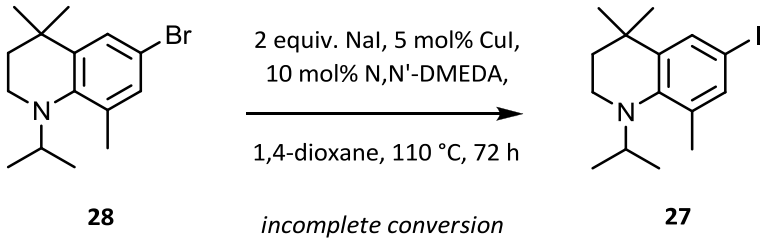

28 *incomplete conversion* **27**

Equation 14

Previously, when a sample of compound **28** containing approximately 10% of the enamine product (before conditions to obtain pure **28** were developed) was used in the halogen-exchange reaction, full conversion to iodide **27** was observed by GC-MS analysis. The subsequent Sonogashira coupling reaction with aryl alkyne **16** was successful in providing the desired (methyl-protected) retinoid compound, which, when dissolved in chloroform, was observed to be highly fluorescent under long-wave UV light. However, attempts at purification by column chromatography and recrystallisation were unsuccessful in separating the desired product from the enamine species.

When pure compound **28** was used, the halogen-exchange reaction proved sluggish, and after heating for 3 days, predominately unreacted starting material was observed by GC-MS analysis. Various factors were considered that may have hindered the reaction, including moisture in the solvent and/or reagents, the presence of oxygen, and stirring issues. However, even after these issues were addressed, less than 20% conversion to iodide **27** was observed by GC-MS analysis after 3 days. The addition of a further 5 mol% CuI and 10 mol% *N*,*N*'-DMEDA, followed by overnight heating, improved product conversion slightly to 30%. Addition of more catalyst and ligand (up to 15 mol% CuI and 30 mol% *N*,*N*'-DMEDA), as well as heating for up to 1 week, produced an eventual 90% conversion to the iodide compound. Evidently, given the high catalyst and ligand loadings, as well as the long reaction time required, this was an inefficient means of producing the desired product. It would appear, therefore, that the success of the procedure depended on a number of factors, and efforts to

optimise the reaction proved insufficiently effective. Furthermore, due to their similar R_f values, it was not possible to separate iodide **27** from the bromide starting material.

Sonogashira reactions with an aromatic bromide

Since synthesis of the desired iodide proved unsuccessful, alternative routes for obtaining the target fluorescent retinoid **21** were considered, and these are discussed in the following paragraphs.

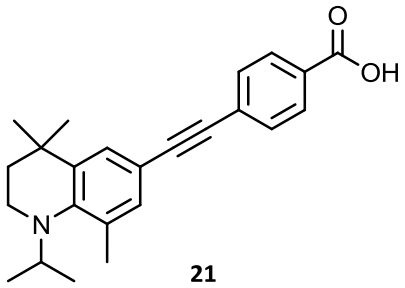

21

<u>*Reaction with aryl alkyne **16***</u>

First, a Sonogashira reaction between bromide **28** and alkyne **16** was attempted (Equation 15). The reaction was expected to be slow given the electron-rich nature of compound **28**, as well as the decreased reactivity of the aryl alkyne; nevertheless, if successful, this would provide a more direct route to the desired target retinoid. In order to improve reactivity, 10 mol% of CuI and $Pd(PPh_3)_2Cl_2$ catalysts, as well as 50 mol% triphenylphosphine (as a catalyst stabiliser), were employed. However, after heating to 80 °C for 3 days, no conversion to the product was observed by GC-MS analysis, and only starting materials were present. This lack of reaction was thought to be due to the deactivating nature of the inductively donating *N*-isopropyl and ring methyl groups, rendering bromide **28** a poor substrate for the Sonogashira reaction.

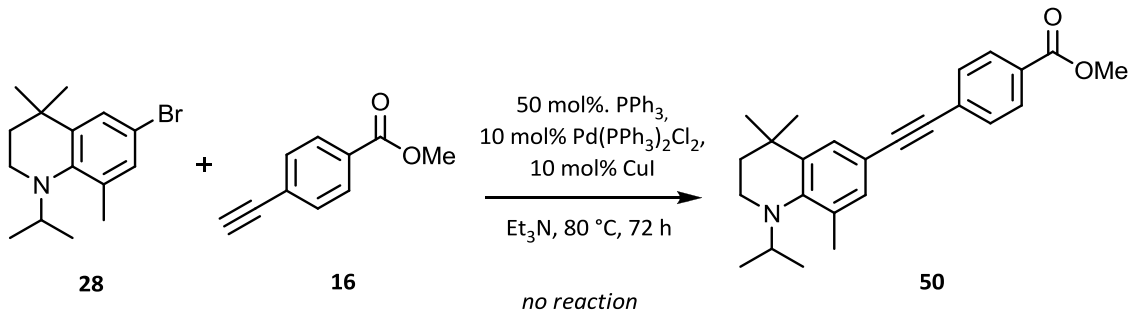

28 **16** *no reaction* **50**

Equation 15

Reaction with TMSA

Next, a Sonogashira reaction between bromide **28** and TMSA was attempted (Equation 16). The procedure was based on the synthesis of EC23,[115] and the bromide was expected to be more amenable to coupling with this more reactive alkyne.

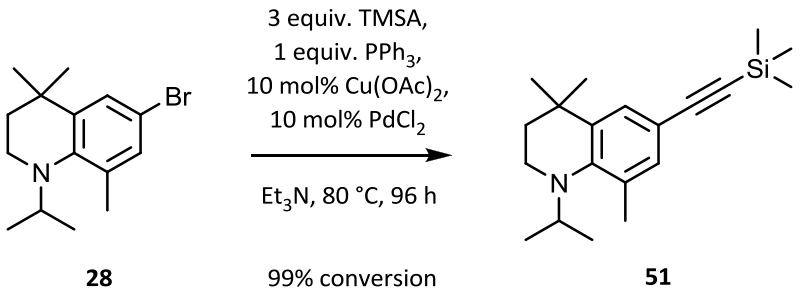

28 99% conversion **51**

Equation 16

In addition to 3 equivalents of TMSA, 1 equivalent of PPh_3 was used along with 10 mol% of $Cu(OAc)_2$ and $PdCl_2$ catalysts. The mixture was heated to 80 °C, and the reaction was monitored by GC-MS analysis: after 4 days, 99% conversion to alkyne **51** was observed. Following *in vacuo* solvent removal, the residue was filtered through a pad of silica, and the crude product was obtained as a dark yellow oil/low melting point solid. This material consisted mainly of compound **51** and triphenylphosphine oxide (Ph_3P=O), and slowly crystallised over a period of a few days. There was some evidence of instability at this point, as the enamine-type structure **52** was observed after leaving the oil for a few days at room temperature. It remains to be seen if this may be attributed to an inherent instability of the compound, or if the presence of oxidising impurities may have promoted loss of H_2 from the structure.

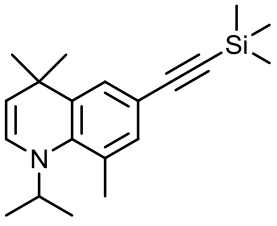

52

The significant quantity of $Ph_3P=O$ produced as a result of using 1 equivalent of PPh_3 in the coupling reaction proved problematic to separate from the desired product: Co-elution of $Ph_3P=O$ with alkyne **51** was observed during attempts at purification by silica-gel chromatography. Recrystallisation from various polar and non-polar solvents also did not effectively separate $Ph_3P=O$. Finally, recrystallisation of compound **51** from ethanol provided some pure product in the form of yellow needle-like crystals, albeit in a low yield (16%). When the reaction was repeated and the residue recrystallised from hexane, an improved yield of 59% was obtained; however, ^{1}H NMR analysis showed that the enamine product **52** was also present (approx. 10%). Thus, in future, the reaction and subsequent purification steps should be performed as quickly as possible in order to minimise the potential for oxidation. When PPh_3 was not used in the coupling reaction, poor conversion to alkyne **51** was observed by GC-MS analysis after 96 h reaction. It would appear that in this case, PPh_3 played an important role in the coupling reaction, possibly in stabilising the catalyst. Since the presence of $Ph_3P=O$ was not expected to affect subsequent reactions, crude **51** was used for the synthesis of the target retinoid compound (see Equation 18).

Microwave-assisted method

In order to reduce the reaction time required for the Sonogashira reaction between bromide **28** and TMSA, as well as to reduce the amount of PPh_3 required, microwave (MW) conditions were also assessed (Equation 17).

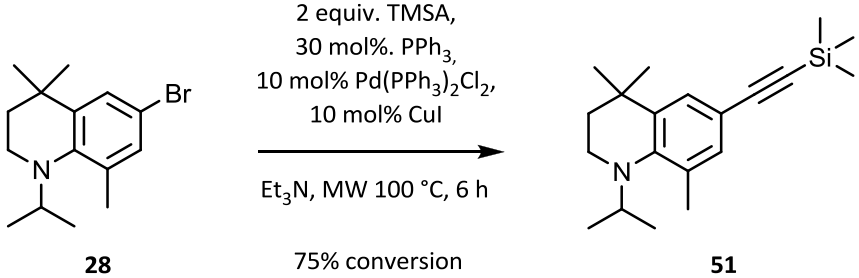

28 **51**

Equation 17

After heating to 100 °C for 6 h, 75% conversion to product **51** was observed by GC-MS analysis. Repeating the reaction with more catalyst, alkyne, as well as increasing the reaction time did not significantly improve conversion to the product. After *in vacuo* removal of Et_3N, filtration of the residue through a pad of silica (hexane:EtOAc, 9:1, as eluent) was effective in purifying the product, and some triphenylphosphine oxide still remained. Evidently there is scope for reaction optimisation, and the use of a polymer-supported PPh_3, or an alternative reagent, should be considered for ease of separation.

Base desilylation

Stirring compound **51** at room temperature with 4 equivalents of Na_2CO_3 in a solution of MeOH/Et_2O and 10% H_2O was ineffective in removing the trimethylsilyl group, so a stronger base, NaOH, was employed which resulted in complete conversion to compound **53** (Equation 18). Due to the presence of residual $Ph_3P{=}O$ from the previous Sonogashira reaction, it was not possible to carry out satisfactory purification of compound **53**.

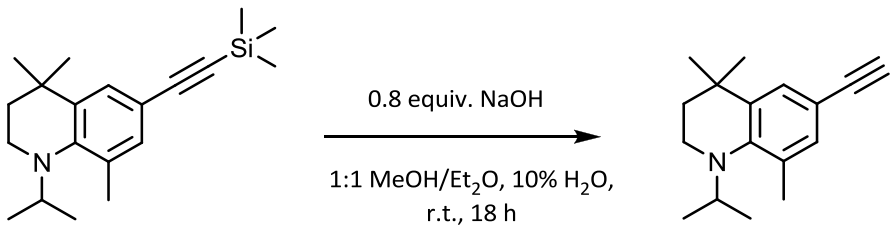

51 **53**

100% conversion

Equation 18

Second Sonogashira coupling

Synthesis of ester **50** was achieved by combining alkyne **53**, 0.95 equivalents of aryl iodide **45**, and 1 mol% of CuI and $Pd(PPh_3)_2Cl_2$ catalysts in Et_3N in a nitrogen-filled glovebox (Equation 19). After stirring at room temperature for 72 h, complete conversion to ester **50** was observed by GC-MS analysis. Following *in vacuo* removal of

the solvent, the residue was recrystallised from hexane to provide bright yellow needle-like crystals of pure compound **50**.

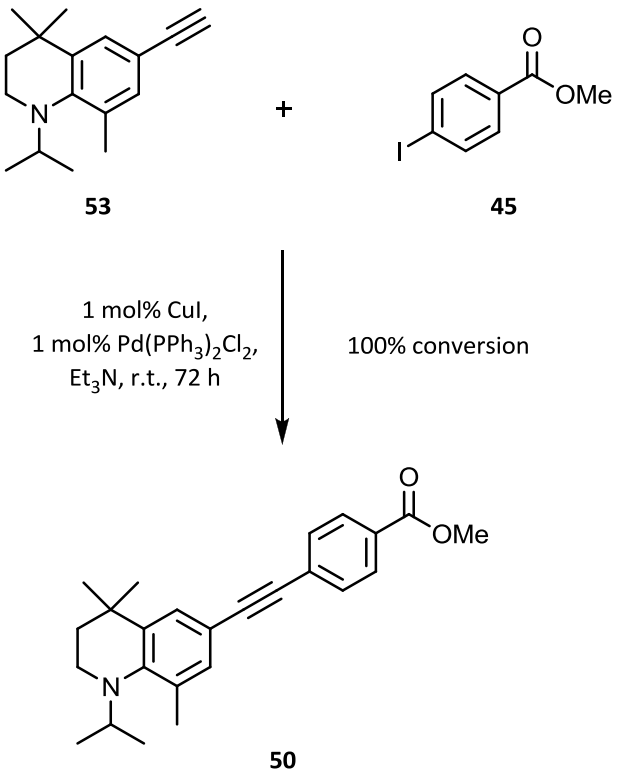

Equation 19

Ester hydrolysis

Compound **50** was hydrolysed according to Equation 20; following aqueous workup and recrystallisation from ethanol, the target retinoid was obtained in the form of neon-yellow fluffy crystals in high yield (89%).

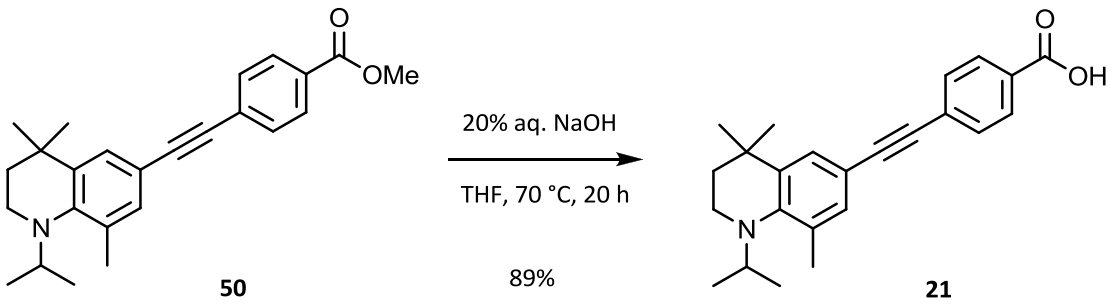

Equation 20

4.4. Stability and purification of GZ108

Photodehydrogenation

Upon completed synthesis of target retinoid **21**, a side-product resulting from the loss of H_2 from the molecule to give an enamine-type structure (**30**, Scheme 15) was observed, and constituted approximately 10% of the mixture.

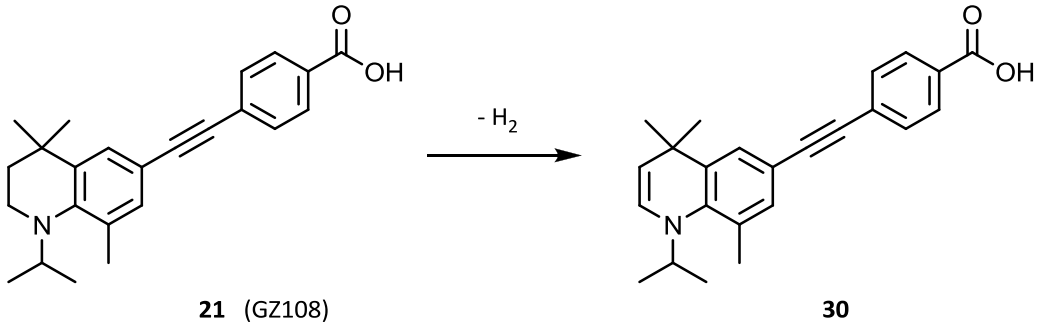

21 (GZ108) **30**

Scheme 15 Loss of H_2 from retinoid **21** to give the enamine-type structure **30**.

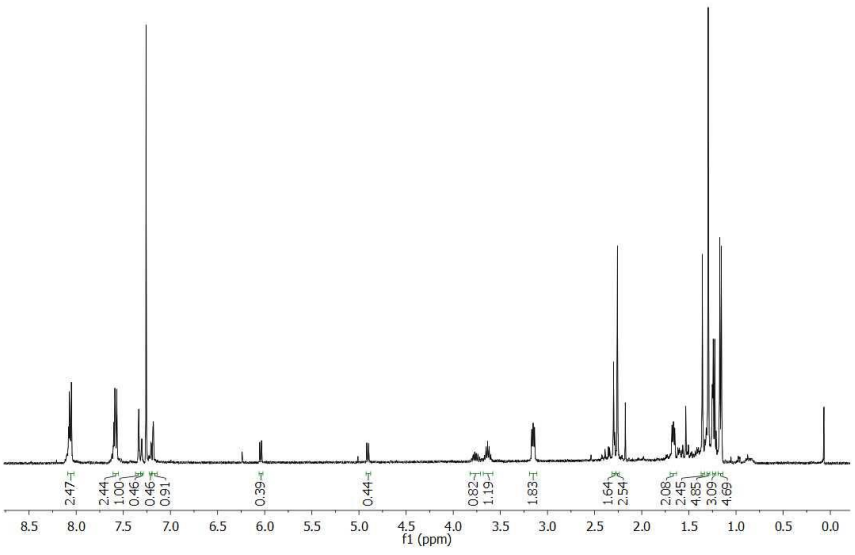

Fig. 41 Representative ^{1}H NMR spectrum of compound **21** in $CDCl_3$ (recorded at 400 MHz) exposed to a white fluorescent light source at a distance of 40 cm. Note the presence of doublet peaks in the alkene region, consistent with enamine **30**, the relative integral values of which increased over the course of the light experiment.

Steps had previously been taken to avoid this oxidation reaction during synthesis of the intermediates; however, it was now apparent that this could be an inherent instability of the molecule. It was thought that the dehydrogenation process could be induced by exposure to light: in order to test this theory, a sample of compound **21** was dissolved in $CDCl_3$ and placed under a white fluorescent lamp at a distance of 40 cm for up to 30 days; ^1H NMR analyses were carried out at various time intervals (Fig. 41).

By plotting a graph of the relative integral values of enamine **30** (two doublet peaks in the alkene region, as well as two singlets at 5.02 and 6.26 ppm, possibly due to intermediate side-products) compared to those for retinoid **21**, it was evident that the proportion of side-product in the sample increased steadily over the 30 day observation period (Fig. 42).

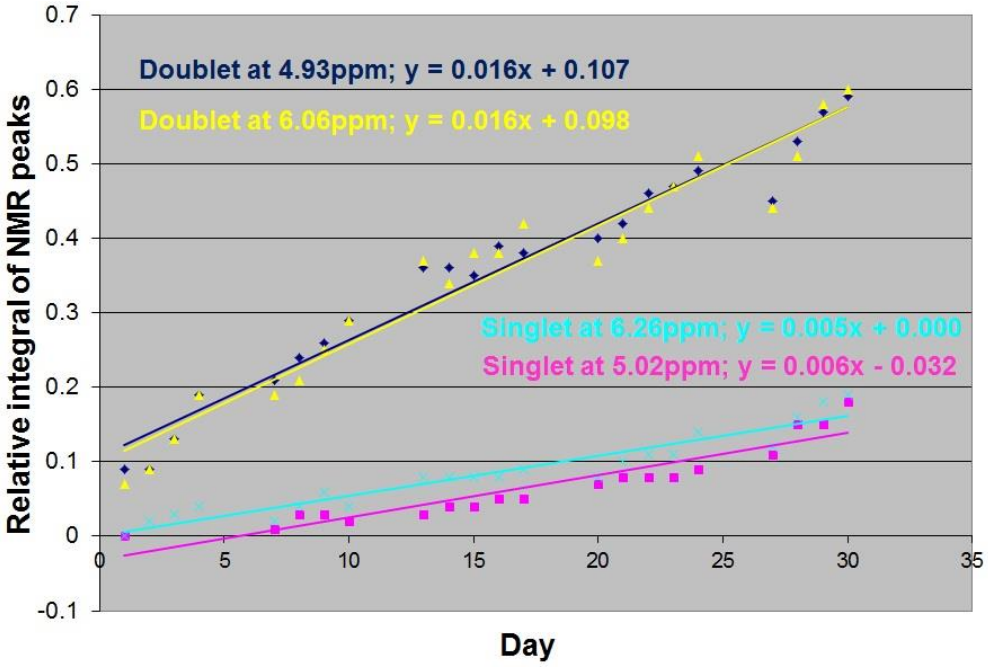

Fig. 42 Plot of the relative integral values of ^1H NMR peaks of the enamine side-product when a sample of retinoid **21** in $CDCl_3$ was exposed to a white fluorescent light source at a distance of 40 cm for up to 30 days.

An occurrence known as photo-dehydrogenation has previously been reported in the literature, whereby loss of H_2 from dihydropyrimidinones (**54**) was observed after irradiating samples that had been dissolved in chloroform (Equation 21).[183]

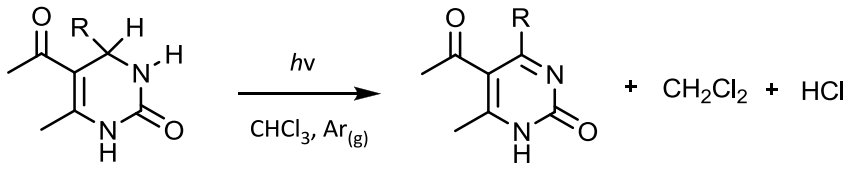

54 **55**

Equation 21

Interestingly, while reactions carried out in an oxygen atmosphere produced complex mixtures, an argon atmosphere provided the desired product (**55**), with chloroform being an important electron transfer agent; thus, a proposed route for photo-dehydrogenation was suggested (Scheme 16). This mechanism was supported by analysis of the acidity of the solution following irradiation, as well as detection of dichloromethane by GC analysis.

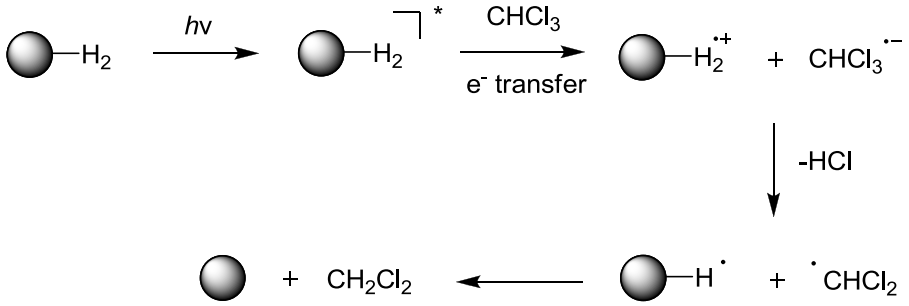

Scheme 16 Proposed mechanism for dehydrogenation *via* light-induced electron-transfer.

It was, therefore, feasible that such a process could account for the light-induced dehydrogenation observed with retinoid **21.** Since this occurrence was assumed to be due to the purported redox potential of chloroform, an analogous light study with

compound **21** dissolved in DMSO-d_6 was established in order to ascertain if photodehydrogenation would still be observed (Fig. 43).

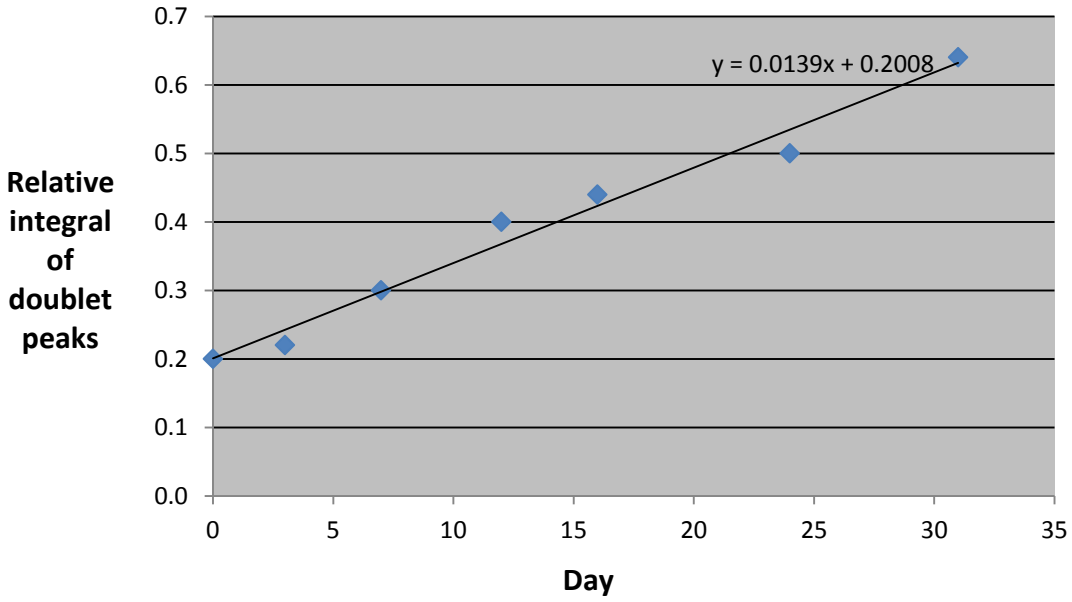

Fig. 43 Plot of the relative ^{1}H NMR integral values of the side-product formed when a sample of retinoid **21** in DMSO-d_6 was exposed to a white fluorescent light source at a distance of 40 cm for up to 30 days.

^{1}H NMR analyses were carried out over a period of 30 days, and a plot of the relative integral values of the doublet peaks associated with the side-product showed quite clearly that dehydrogenation was still occurring in DMSO-d_6 at a rate comparable to that of the compound in $CDCl_3$. (It was interesting to note, however, that in this solvent, no singlet peaks associated with a second side-product/intermediate were observed.) From these findings, it can be inferred that the major promoting factor for enamine formation was the presence of light, rather than any effects induced by the solvent. Indeed, when a sample of retinoid **21** in $CDCl_3$ was stored in the dark for a few weeks, no increase in the relative integrals of the side-product(s) was apparent by ^{1}H NMR analysis.

Despite the susceptibility of compound **21** towards light-induced dehydrogenation, the integrity of the structure remained otherwise intact, with no significant degradation observed over the course of the light experiments. However, when the NMR sample

was exposed to light for up to three months in an attempt to promote complete conversion to the enamine product, a more complex proton NMR spectrum was observed, which was indicative of product degradation or side-product formation. In any case, given the slow process, this was evidently an inefficient means of obtaining the desired product.

Proposed light-promoted radical mechanisms

Due to their unsaturated nature, retinoids are believed to be efficient scavengers of peroxyl radicals, which could account for their antioxidant properties.[184] Since formation of enamine **30** was proposed to occur in response to light and air, a mechanism for this process is outlined below, involving the formation of a hydroperoxyl radical (Schemes 17 and 18).

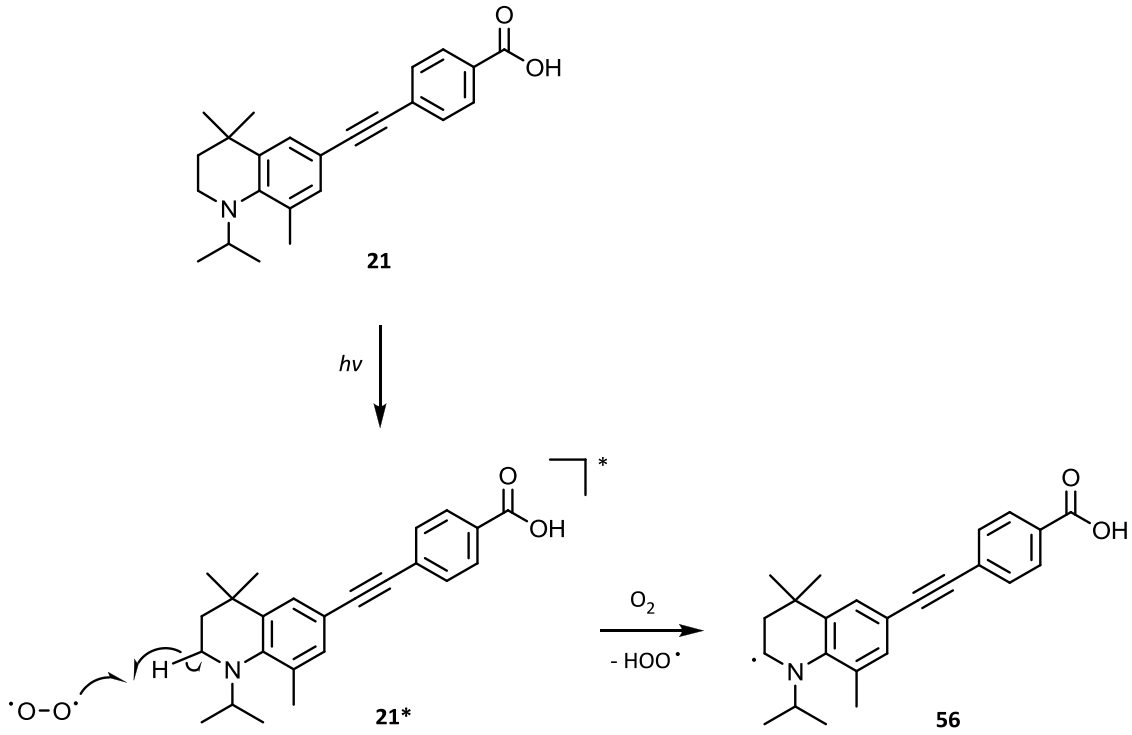

Scheme 17 Proposed mechanism for light-induced interaction of compound **21** with triplet oxygen.

Since the extended conjugated structure of retinoid **21** meant that the molecule was particularly susceptible to excitation by light, it was proposed that the α-hydrogen could be activated towards reaction with molecular oxygen, to form a radical-type structure (**56**, Scheme 17). The hydroperoxyl radical formed as a result could either be involved in a β-elimination (Scheme 18, green arrows), or an E1 elimination from the addition product **57** (Scheme 18, purple arrows).

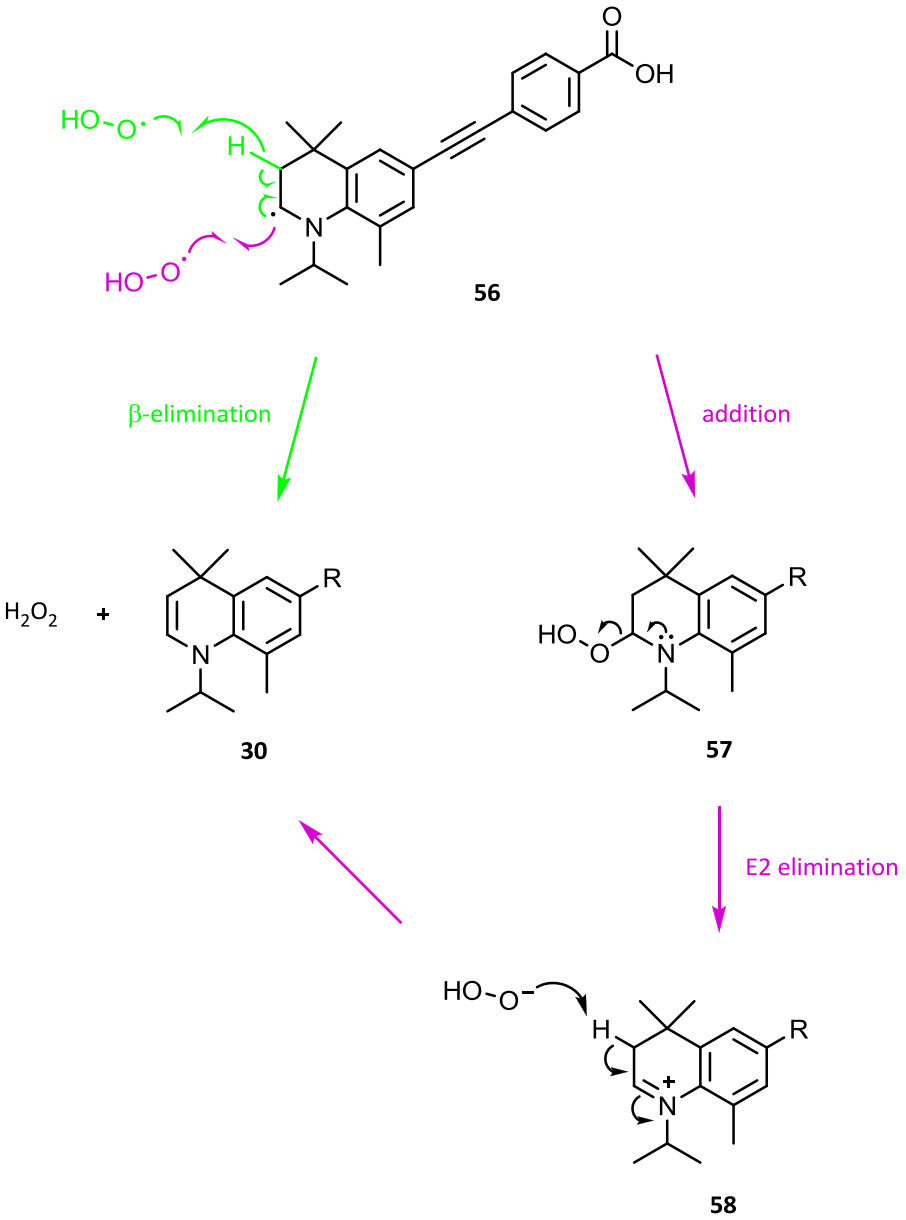

Scheme 18 Proposed mechanisms for generation of enamine **30** through reaction with a hydroperoxyl radical.

These could be plausible mechanisms for formation of the quinoline-type structure **30**. Given that the radical reaction steps were expected to be fast, the rate-limiting step was, therefore, likely to be excitation of the chromophore by light, thereby accounting for the slow dehydrogenation process observed.

In order to affirm if the mechanism suggested above was the process through which dehydrogenation of retinoid **21** occurred, a test for the presence of peroxides in the reaction mixture could be performed. If positive, the exclusion of oxygen from future experiments could be carried out, which should prevent oxidation to the enamine species. In addition, direct light irradiation of retinoid **21** (rather than through the glass of the NMR tube) using a photolysis lamp could be attempted as a more efficient method for synthesising enamine **30**.

Oxidation reactions

In order to ascertain if complete elimination from the tetrahydroquinoline core could be achieved, direct synthesis of the enamine product was attempted using oxidising agents. Given the availability of starting materials, these reactions were carried out using bromide **28**. First, 1 equivalent of the mild oxidising agent *N*-bromoacetamide (NBA) was added to a solution of compound **28** in chloroform (Equation 22).

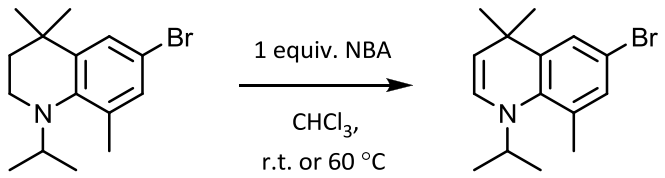

28 *no reaction* **29**

Equation 22

After stirring for 2 h at room temperature, an aqueous workup was performed on an aliquot of the reaction mixture, and a mixture of products was evident by ^{1}H NMR analysis, with signals corresponding to the starting material **28**, and compounds **31** and **33**. When the reaction was repeated with heating to 60 °C, only the starting material and dibromide **31** were observed by ^{1}H NMR analysis, and no enamine

product **29** was present (this observation may be explained by the mechanisms outlined in section 4.3. [see schemes 6 and 7]).

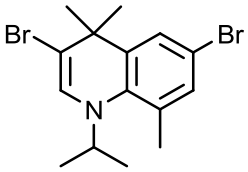

31

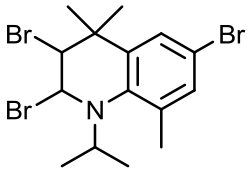

33

Oxidation of compound **28** using 2,3-dichloro-5,6-dicyano-1,4-benzoquinone (DDQ) was then attempted (Equation 23): a flask containing the bromide and 1 equivalent of DDQ was evacuated and filled with argon three times, after which dry dichloromethane was added and the mixture stirred at room temperature.

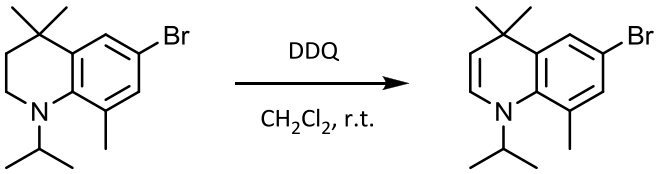

28 *no reaction* **29**

Equation 23

DDQ was still present by TLC analyses after 2, 4, and 6 h, and had not been consumed in the reaction. The mixture was then heated to reflux overnight, however, no change was observed by TLC analysis. After removal of the solvent, ^{1}H NMR analysis showed a mixture of products, with no enamine product present. Similarly, using 2 equivalents of DDQ also did not provide the desired product. It would be interesting to repeat these reactions with retinoid **21**, to assess if the presence of the extended conjugated system would induce a more favourable result.

Separation by HPLC

Given that synthetic routes to the enamine product **29** proved unyielding, efforts then turned towards purification of compound **21** and its enamine side-product **30** *via* HPLC. This would enable the fluorescence characterisation and biological testing of the

two compounds to be performed separately, thereby enabling definitive conclusions to be drawn concerning the properties of the individual compounds. Since the sample (consisting of a mixture of compound **21** and approximately 10% of enamine **30**) proved insoluble in either acetonitrile or methanol, it was first dissolved in a minimal volume of dichloromethane prior to making up to a 1 mL solution in methanol for HPLC analysis.

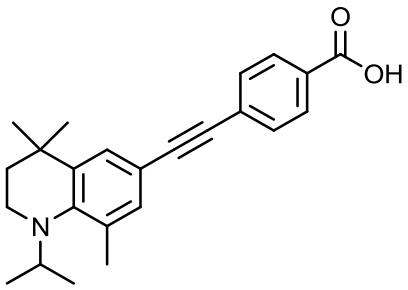

21

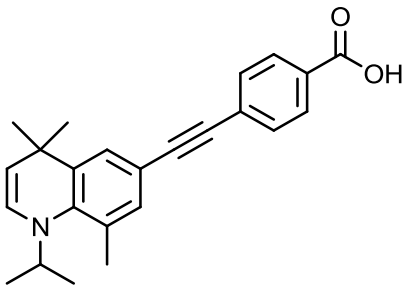

30

Elution with acetonitrile

When the sample was run using a standard gradient of acetonitrile (water:acetonitrile, 90:10 → water:acetonitrile, 10:90, over 20 min), compounds **21** and **30** were observed as two peaks in the mass spectrum, with similar retention times (11.77 and 12.23 min, respectively). A second analysis using a gradient of acetonitrile:water (50:50) → acetonitrile (100%) over 10 min was used in order to reduce the retention times, and led to the elution of compounds **21** and **30** after 9.29 and 10.26 min, respectively. The similar, as well as late, elution times observed with the acetonitrile solvent systems were not ideal, and the products risked being lost in the column wash.

Elution with methanol

A 50 → 100% gradient of methanol (with water as co-solvent) over 10 min was also trialled; however, long retention times were again observed (10.88 min and 11.34 min for compounds **30** and **21**, respectively). When the sample was run with 90% isocratic methanol, enamine **30** eluted more quickly, with a retention time of 2.80 min, and compound **21** at 3.58 min. With 85% isocratic methanol, compound **21** eluted after 8.09 min, and enamine **30** eluted at both 6.01 and 9.06 min (in order to avoid this, the

less polar solvent tetrahydrofuran, rather than dichloromethane, should be used for initial dissolution of the sample). Given these findings, 87% isocratic methanol should, therefore, prove the best solvent system for satisfactory product elution time and separation.

However, before HPLC could be carried out on a preparative scale in order to provide sufficient quantities of the compounds for fluorescence and biological evaluation, retinoid **21** needed to be synthesised *via* a route that would employ a Sonogashira reaction with an iodide substrate (see sections 4.7. and 4.8.). This was expected to be a more facile and higher-yielding reaction than the original procedure of using a bromide compound, and thus eliminate the need for use of triphenylphosphine as a catalyst stabiliser.

4.5. Initial fluorescence data and biological evaluation

This section outlines findings from Alex Palmer (Chemistry) and Rachel Wilson (Biological Sciences) as part of their BSI summer projects, with the co-operation of Dr. Carrie Ambler (Department of Biological Sciences) and Prof. John Girkin (Department of Physics) of Durham University. Full information concerning experimental procedures may be found in their respective project reports.[185,186]

Due to the difficulties in synthesising, purifying, and separating compounds **21** and **30** (discussed in the previous section), a sample containing a mixture of products (approx. 10% of the enamine compound) was used for initial fluorescence characterisation and stem cell testing. Given their highly similar nature, the activities of both compounds were not expected to be significantly different.

Fluorescence spectra of ester **50** and acid **21** (the latter containing approx. 10% of the enamine product) were obtained in various solvents (Fig. 44 and 45, respectively). The fluorescence of the compounds was easily detected, and solvent-dependent effects were observed (*i.e.* fluorescence maxima shifted to longer wavelengths as solvent

polarity increased), with significant fluorescence quenching observed in the more polar solvents (for example, in ethanol, DMSO, and cell culture media). This meant that when applied to cells, the fluorescence of the compounds could be expected to be discernable in discrete cellular locations, depending on the local polarity.

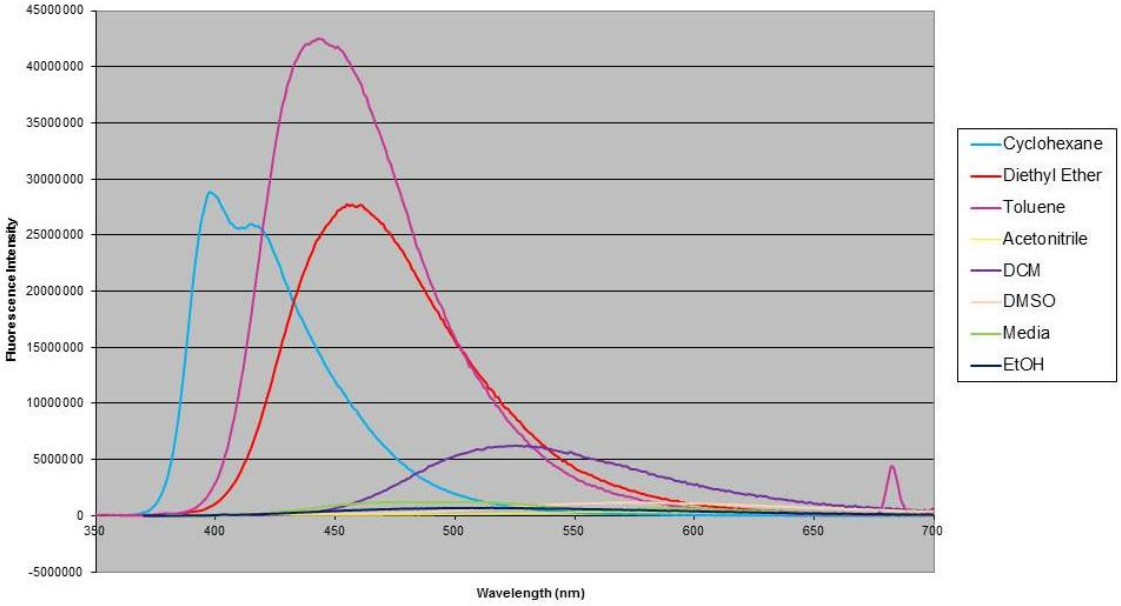

Fig. 44 Fluorescence emission spectra of ester **50** recorded in various solvents (excitation wavelength: 350 nm).[185]

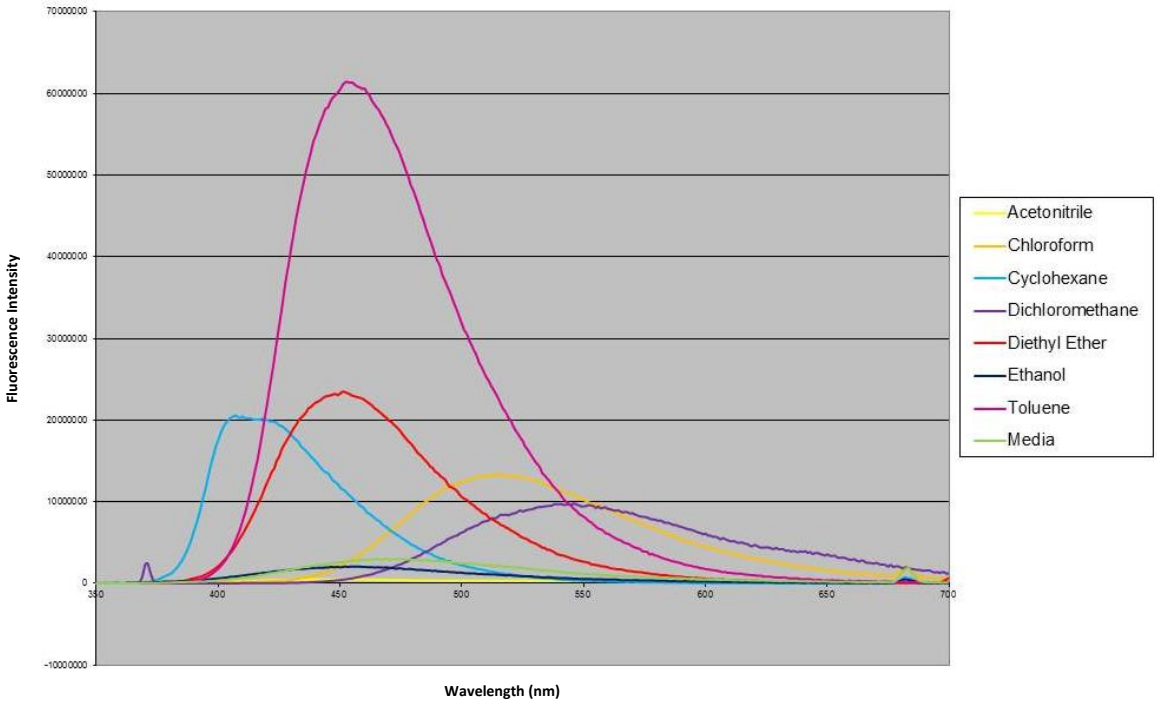

Fig. 45 Fluorescence emission spectra of retinoid **21** recorded in various solvents (excitation wavelength: 350 nm).[185]

Next, a preliminary cell-culture experiment was performed in which keratinocyte stem cells were incubated on glass cover slips using media supplemented with different concentrations of the sample - retinoid **21** with 10% enamine **30** - (1, 10, 25 and 100 μg/mL). The initial objectives were as follows: firstly, to determine if, at the concentrations used for cell testing, fluorescence may still be observed; then, to ascertain the extent, if any, of cellular uptake of the sample, and finally, to assess if the sample demonstrated any ability to induce changes in cell growth and morphology. Collectively, this information would enable a decision to be made regarding the viability of the compound as a visual cellular probe.

In the event of cell differentiation, keratinocyte cells would be expected to detach from the growth substratum; therefore, in order to ensure some cells may still be collected for visualisation (rather than risk losing cells into the incubation media), some of the keratinocytes exposed to 1 and 100 μg/mL of the retinoid sample were fixed and sealed onto microscope slides after 3 h exposure. After 18 h, the remaining cover slips were also fixed and sealed.

The slides were viewed using a fluorescence microscope fitted with a 20/0.75 objective lens. The findings were as follows:

- At the lowest concentration used (1 μg/mL), the fluorescence of the sample was still highly visible.
- After 3 h, cellular uptake of the sample was apparent, and at lower doses the compound(s) had not yet reached the nucleus.
- After 18 h, localisation of the sample within the nucleus was evident.
- Cells treated with higher doses of the sample appeared less healthy than those at lower concentrations: nuclei appeared saturated with the sample, fewer cell numbers were observed, and there was evidence of dead ‘exploded’ cells.
- When lower concentrations of the sample were used, increased cell numbers were observed, and distinct changes in cell morphology were apparent.

However, the limitations of this initial study were fully recognised: namely, the need for negative (untreated cells) and positive (cells treated with a retinoid known to induce differentiation) controls. Also, any cells that may have detached (and, by extension, differentiated in response to retinoid treatment) need also to be collected for analysis.

(a)

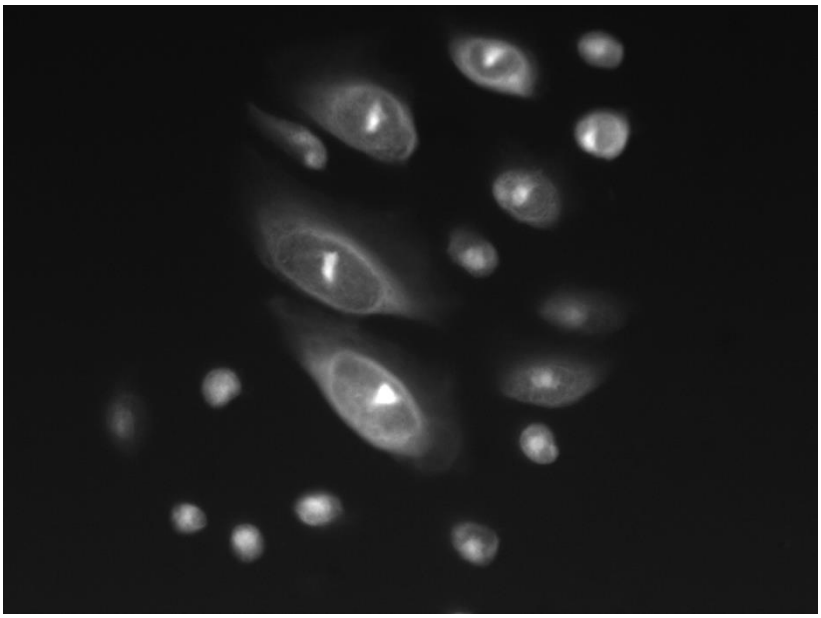

(b)

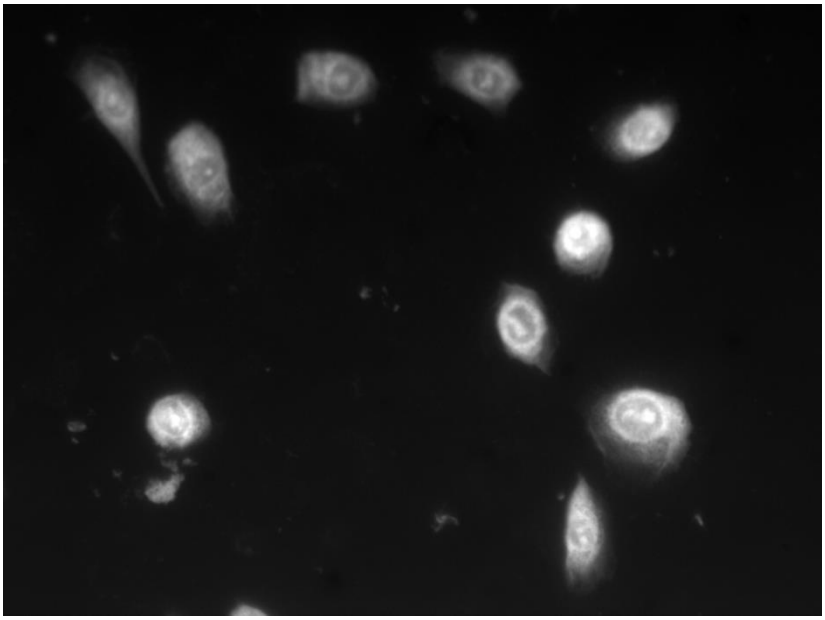

Fig. 46 Fluorescence images of keratinocyte cells incubated with 100 μg/mL of compound **21** (containing approx. 10% of the enamine product **30**) in the culture media for 3 h (a), and 18 h (b).

These initial studies demonstrated that the sample of compound **21** (with 10% of enamine **30**) was indeed able to act as a fluorescent probe in cell-culture experiments, which, in future, will allow for more extensive testing to be carried out, including visualisation at the organelle level, and assessment of the effects of the compound on inducing cell differentiation. Since the compounds appeared to be stable to photobleaching, this will likely greatly assist in the acquisition of fluorescence images, as well as in following the uptake and transport of the compound in live-cell tracking studies.

4.6. Synthesis of a bromine-containing retinoid

The dibromide compound **31** was successfully synthesised (see section 4.3., Equation 11), despite difficulties in purification, as well as in derivatising and stabilising the structure at the 3-position. It was nevertheless recognised that this moiety could be used to obtain the bromine-containing retinoid (**59**, Scheme 19), using a route analogous to that for the synthesis of retinoid **21**. This could potentially provide a structure possessing novel properties, and it would be interesting to determine to what extent the presence of a bromine atom would affect both the fluorescence and biological activity of the molecule.

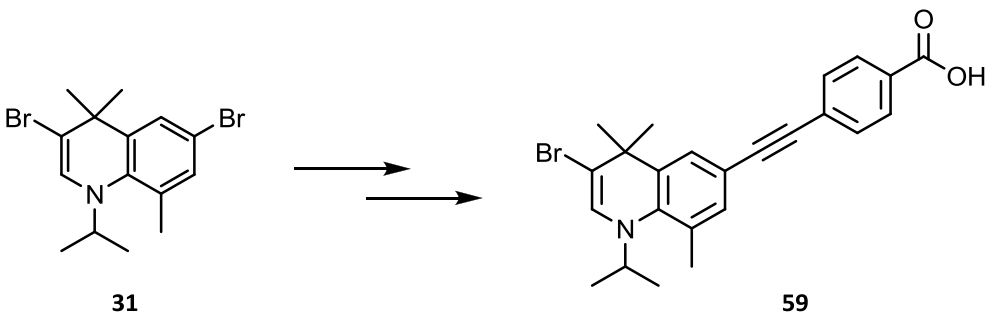

31 **59**

Scheme 19 Use of dibromide **31** to synthesise the bromine-containing retinoid, **59**.

Thus, a Sonogashira reaction with compound **31** and TMSA was performed. When an oil bath was used to heat the mixture to 80 °C, the reaction required 60 h for completion, and it was difficult to obtain the product in pure form (crude yield of 47%, estimated from ^{1}H NMR analysis). A greatly improved reaction time was achieved when a microwave-assisted method was used: after 6 h, 84% conversion to alkyne **60** was observed by GC-MS analysis (Equation 24).

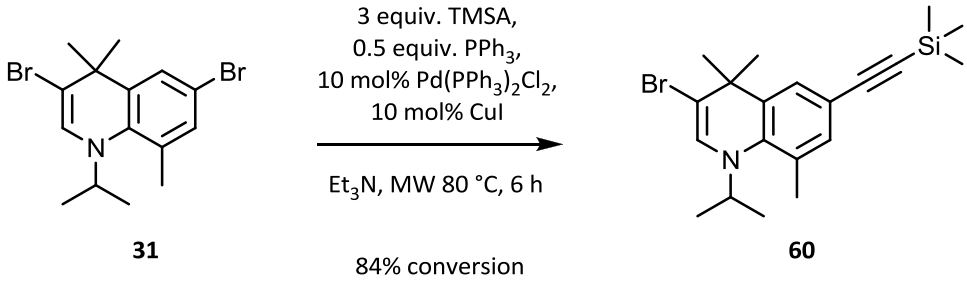

31 **60**

Equation 24

In addition to the desired product, some unreacted starting material (**31**) was present (8%), as well as the dicoupled product **61** (8%). Triethylamine was removed *in vacuo*, and the residue was filtered through a pad of silica (hexane:EtOAc, 9:1, as eluent, with 1% Et_3N). ^{1}H NMR and GC-MS analyses of the material obtained following *in vacuo* solvent removal showed that a 50:50 ratio of compound **60** and the debrominated product **52** was present.

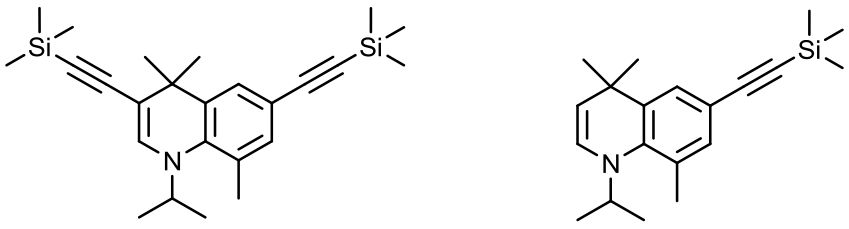

61 **52**

It was thought that debromination was triggered by purification on silica gel, thus, the Sonogashira reaction was repeated, and crude alkyne **60** was used in the subsequent reactions, with purification to be attempted following the last step in order to obtain

retinoid **59** in pure form. Thus, removal of the trimethylsilyl group from crude product **60** was carried out according to Equation 25 in order to provide the free alkyne (**62**).

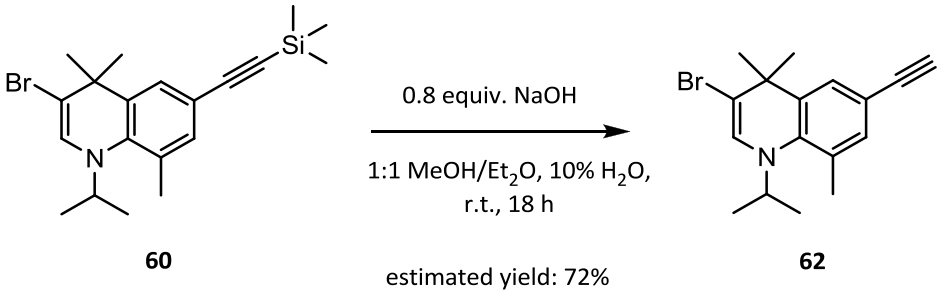

Equation 25

A Sonogashira reaction was then performed using alkyne **62** and 4-iodobenzoic acid methyl ester **45** (Equation 26).

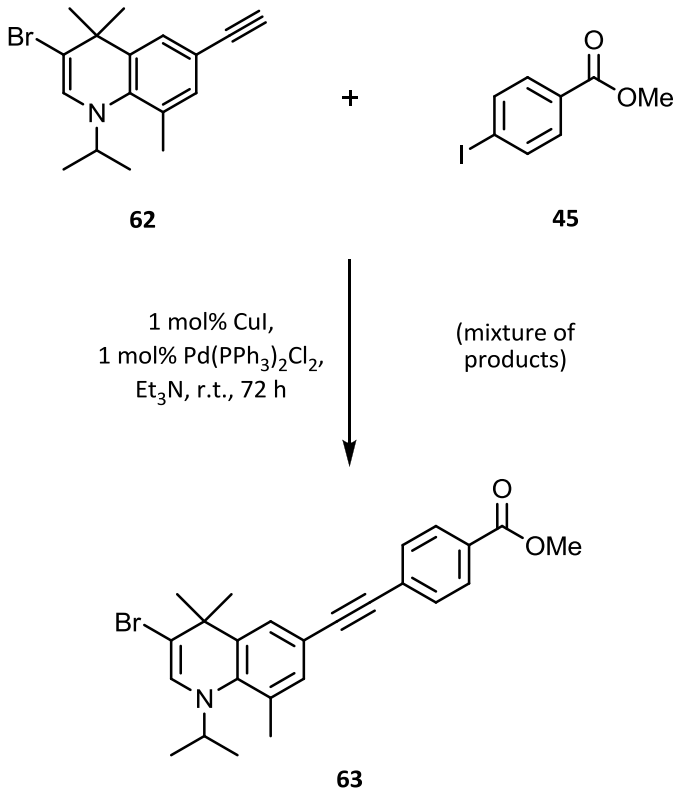

Equation 26

Formation of ester **63** was confirmed by ^{1}H NMR analysis, and TLC analyses on both alumina and silica gel plates (hexane:EtOAc, 9:1, as eluent, with and without 1% Et_3N) were performed to determine the appropriate solvent system for purification. Visualisation of the plates under long-wave UV light showed that, as expected, the material was highly fluorescent; however, significant streaking and spotting was observed on the plates regardless of the solvent system used, and was indicative of product instability towards purification by chromatographic means.

Despite this, purification of ester **63** was performed *via* vacuum filtration through a short pad (3 cm height, 4 cm diameter) of silica with solvent (hexane:EtOAc, 9:1, as eluent) that had been chilled in the freezer for 30 min before use. These steps were intended to reduce the extent of compound degradation, and to improve product recovery; however, ^{1}H NMR analysis showed no significant improvement in purity was attained when compared to the crude material, and a mixture of products remained. Perhaps, as appropriate equipment and purification systems become available, separation of compound **63** may be possible at a future date.

4.7. Synthesis of a fluorescent retinoid *via* an *N*-acetyl compound

Given that it was not possible to synthesise iodide **27** *via* a halogen-exchange reaction with bromide **28**, or direct iodination with compound **26** (Scheme 20; for a discussion, see section 4.3.), as well as the difficulty in carrying out the Sonogashira cross-coupling reaction using the bromide (requiring high loadings of PPh_3, palladium and copper catalysts, in addition to heating at a high temperature for a prolonged period), an alternative route to the desired iodide **27** was considered.

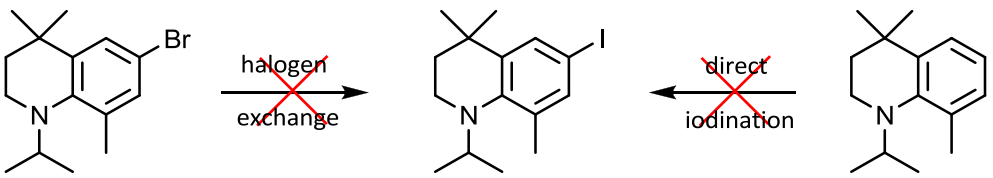

28 **27** **26**

Scheme 20

Proposed synthetic route

Since iodination of the *N*-methyl derivative (for synthesis of aza-EC23, see section 4.2.) proceeded relatively easily, it was thought that the presence of the *N*-isopropyl moiety, as well as a methyl group on the aromatic ring, deactivated compound **26** towards electrophilic aromatic substitution (a proposed explanation for this observation that takes into account the lowest energy conformations of the molecules is provided at the end of this section). Thus, the synthetic route to iodide **27** *via* an *N*-acetyl compound is outlined in Scheme 21: with the acetyl group in place of the isopropyl, the propensity for compound **66** to undergo aromatic iodination could then be assessed. Following removal of the acetyl group, alkylation with 2-iodopropane would then provide iodide **27**, the desired substrate in the Sonogashira coupling reaction for synthesis of the target fluorescent retinoid (**21**; GZ108).

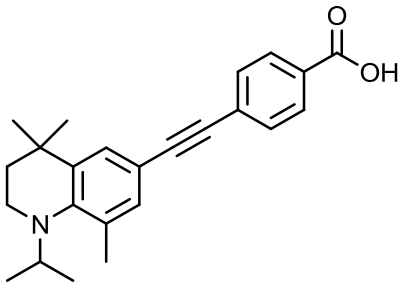

21 (GZ108)

The ability to remove the acetyl group would also enable the tetrahydroquinoline core to be derivatised on the nitrogen atom, thus allowing for the synthesis of new retinoid compounds. In addition, by attaching long alkyl chains (C12-C18) at this position, structures with emulsion-type properties could also be produced, and would enable investigation into the area of targeted retinoid delivery to specific cell types.

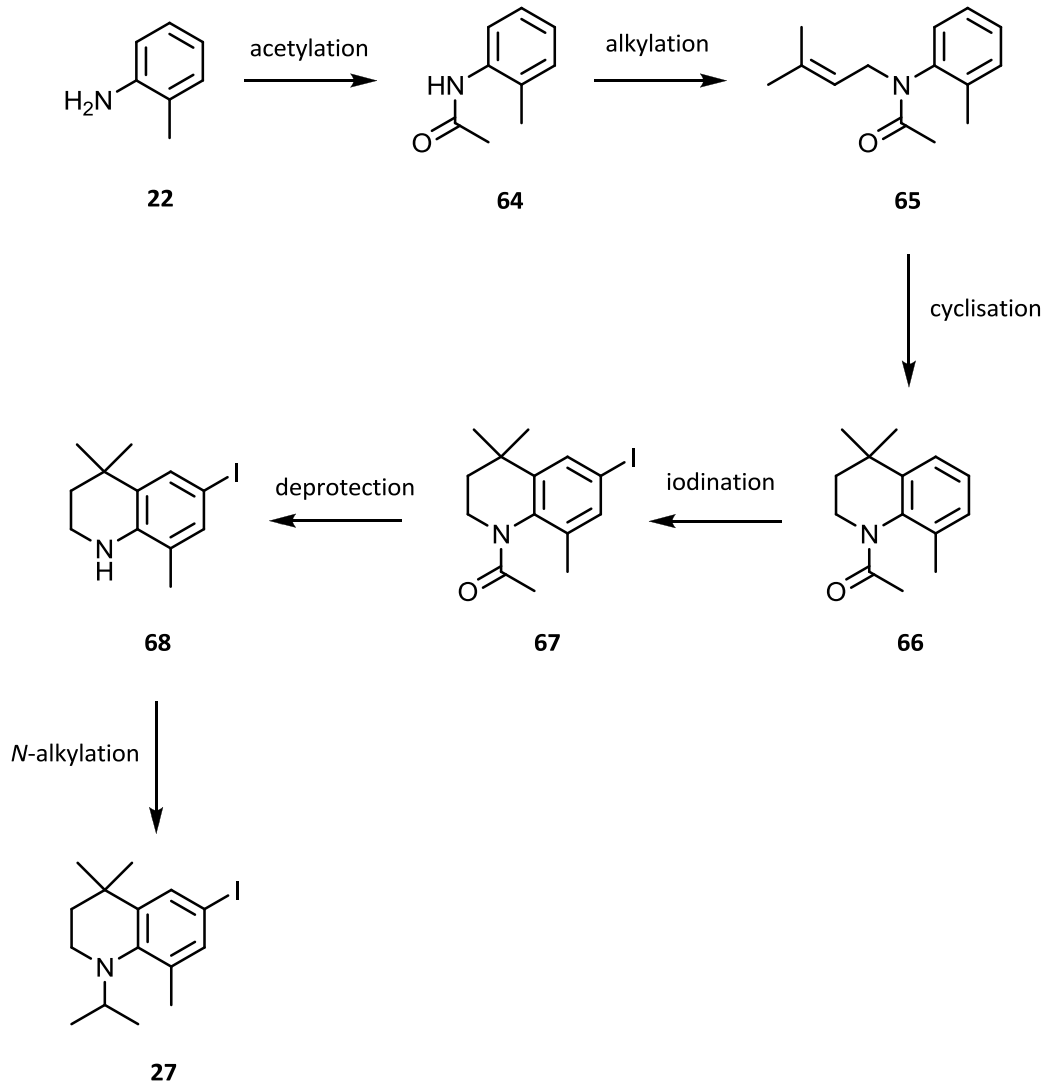

Scheme 21 Proposed synthetic route to iodide **27** *via* *N*-acetylation of *o*-toluidine.

Acetylation

Acetylation of *o*-toluidine was achieved by the dropwise addition of a solution of acetyl chloride (1.1 equivalents) in dichloromethane to a stirred solution of the amine and pyridine (2.5 equivalents) in dichloromethane, with the flask maintained at 0 °C (Equation 27). The reaction was monitored by TLC analysis, and found to be complete after stirring for 2 h. The product was obtained as a fluffy white crystalline solid following aqueous workup and recrystallisation. For a larger scale preparation (>10 g), residual pyridine proved difficult to remove completely by evaporation, becoming

trapped with the product as a hard residue at the bottom of the flask. In this case, a trituration was performed in which the product, along with residual pyridine, was redissolved in dichloromethane, and an equal volume of hexane was added. Dichloromethane was then removed *in vacuo*, at which point compound **64** crystallised from hexane, and was filtered out.

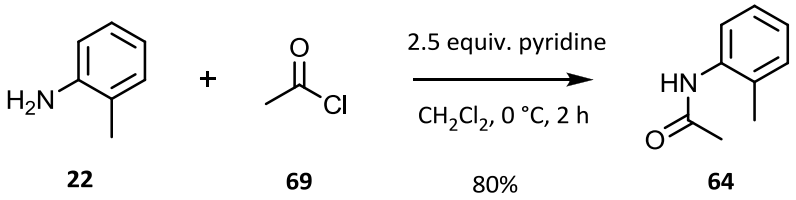

22 **69** 80% **64**

Equation 27

Alkylation

N-Alkylation of compound **64** with 3,3'-dimethylallyl bromide **12** using K_2CO_3 as base (as for the reaction with the *N*-isopropyl analogue) was not successful in promoting product formation. Thus, a stronger base, sodium hydride, was added slowly to a solution of compound **64** in dry DMF, and the mixture heated to 65 °C for 1 h. 3,3'-Dimethylallyl bromide (1.2 equivalents) was then added to the cooled solution, and the mixture was heated to 70 °C overnight. Following aqueous workup and purification by silica-gel chromatography, product **65** was obtained as a brown oil, albeit in poor yield (28%).

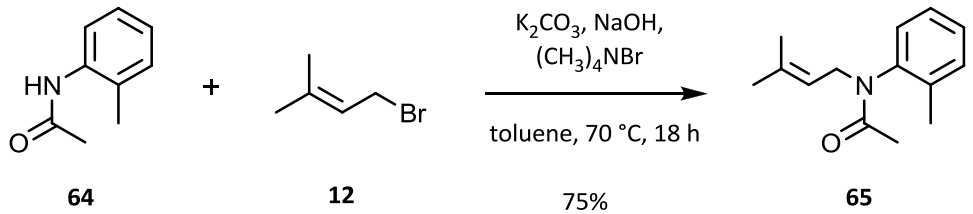

64 **12** 75% **65**

Equation 28

Compound **65** was finally obtained by heating a suspension of compound **64**, K_2CO_3 (1.1 equivalents), NaOH (1.1 equivalents), $(CH_3)_4NBr$ (3 mol%), and 3,3'-dimethylallyl bromide (1.2 equivalents) in toluene to 70 °C overnight with vigorous stirring (Equation 28). An aqueous workup was then performed, and the crude product purified by column chromatography on silica gel to give compound **65** in 75% yield (Fig. 47).

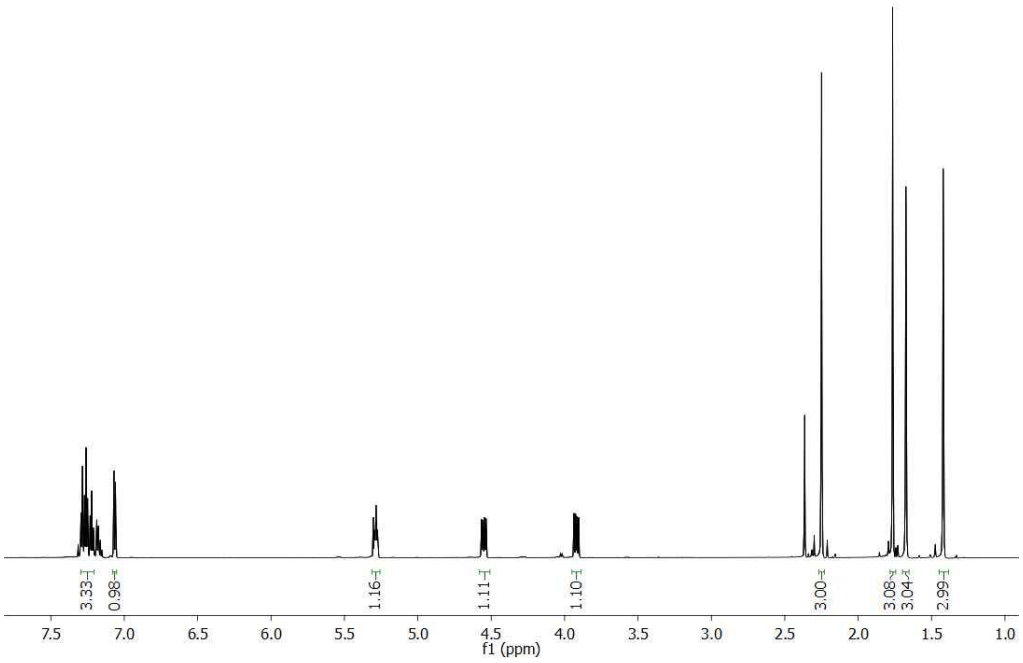

Fig. 47 ^{1}H NMR spectrum of allylated product **65** (recorded in $CDCl_3$ at 400 MHz).

Cyclisation

A literature procedure employing $AlCl_3$ in chlorobenzene was attempted for cyclisation of compound **65** (Equation 29).[187] However, after heating with 2.2 equivalents of the Lewis acid to 110 °C for 1 h, only starting material was present by ^{1}H NMR analysis. Heating for a further 5 h succeeded in converting approximately 10% of the starting material; similarly, heating to reflux (130 °C) overnight only resulted in a slight increase in conversion (15%).

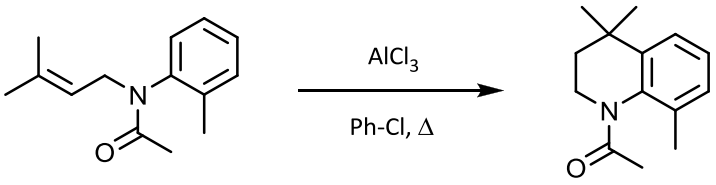

65 **66**

Equation 29

The reaction was repeated with heating to 120 °C, and consumption of the starting material was monitored by TLC analysis: after 5 h, a single product spot was observed. Following aqueous workup, ^{1}H NMR and COSY analyses of the red/brown residue showed a complex spectrum in which two major products were observed in a 3:1 ratio (Fig. 48).

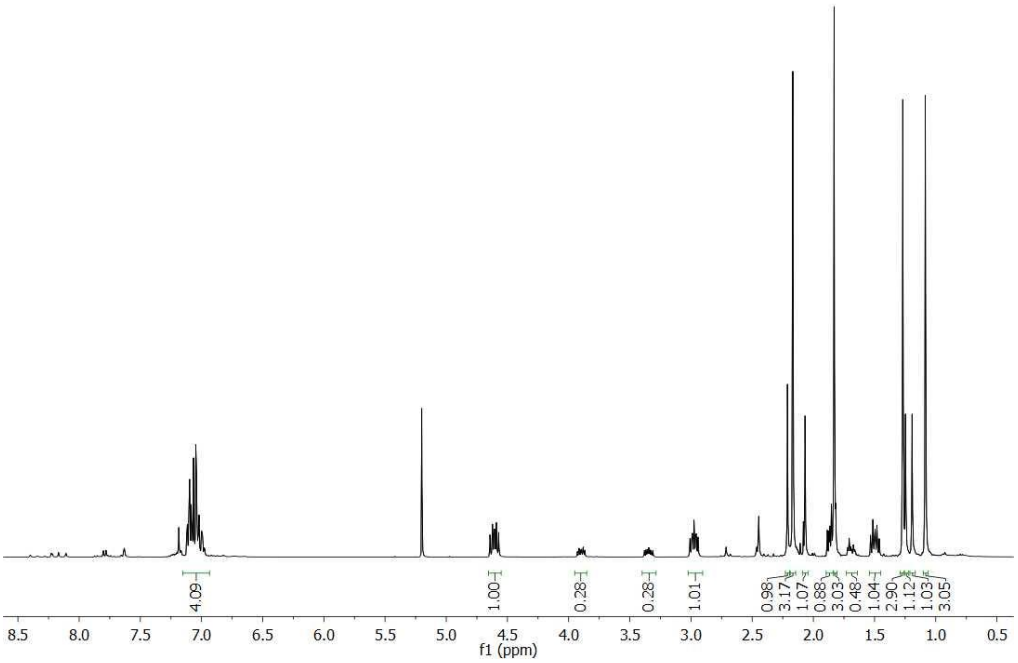

Fig. 48 ^{1}H NMR spectrum of material obtained (following aqueous workup) from heating compound **65** with 2.2 equivalents of $AlCl_3$ in chlorobenzene to 120 °C for 5 h in chlorobenzene - *recorded in $CDCl_3$ at 400 MHz*.

GC-MS analyses of the crude material found two peaks possessing the same mass: the two products should therefore be isomers, and it was possible that, as well as a methyl shift, a 5-membered ring compound could have been formed (*i.e.* resulting in the possible structures **70** to **72**; Fig. 49).

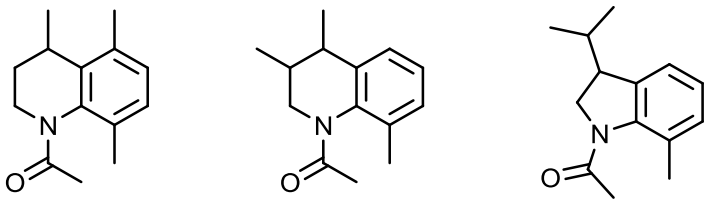

70 **71** **72**

Fig. 49 Possible isomers from cyclisation of compound **65**.

Purification of this mixture by silica-gel chromatography was attempted, using hexane:EtOAc, 9:1, as eluent. Coloured fractions were initially obtained, which provided an orange oil and a red solid; however, the desired product **66** was not present by ^{1}H NMR analysis. The polarity was increased (hexane:EtOAc, 3:1, as eluent), and a single product eluted over more than twenty fractions (Fig. 50). This compound was obtained in 25% yield (compared to the starting material), and ^{1}H NMR analyses of subsequent fractions from the column showed that the original mixture of products remained, which were not easily separated.

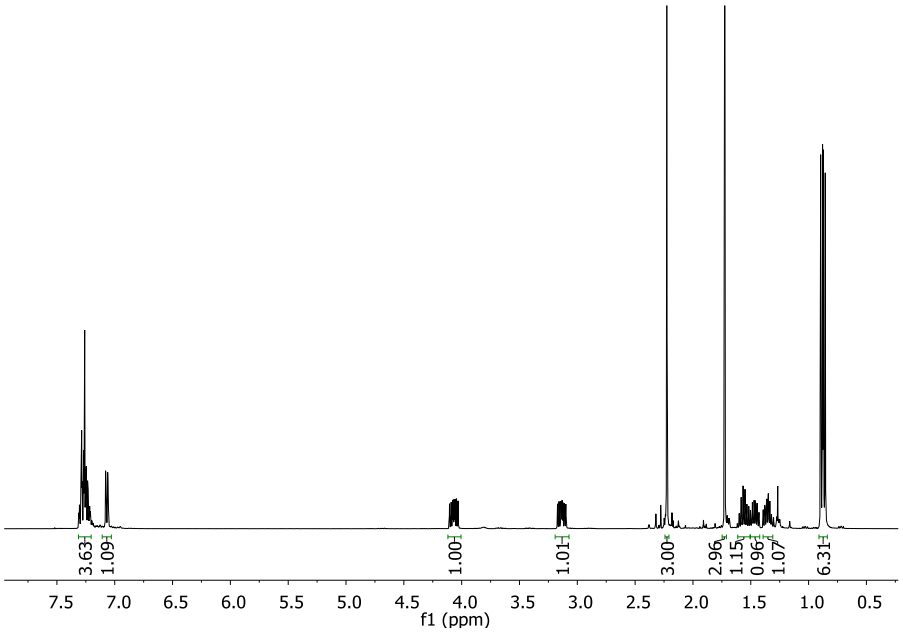

Fig. 50 ^{1}H NMR spectrum of product obtained (following column chromatography) from the attempted cyclisation of compound **65** by heating to 120 °C for 5 h in chlorobenzene with 2.2 equivalents $AlCl_3$ - *recorded in $CDCl_3$ at 400 MHz*.

^{1}H NMR analysis of the pure product showed that, while the alkane/alkene region of this material differed to that of the starting material, indicating that reaction had occurred, the five separate multiplet peaks that each integrated to one proton were inconsistent with the spectrum expected for the cyclised product.

The presence of the acetyl group may produce diastereotopic protons on the adjacent carbon atom, thereby accounting for the non-equivalent proton signals observed; however, no discernible coalescence of peaks was observed when variable temperature ^{1}H NMR studies were carried out with the compound in DMSO-d_6 (up to 80 °C), suggesting a fixed, stable, or rigid conformation. Notwithstanding this observation, the aromatic region of the product remained unchanged from the starting material, and still integrated to four protons, suggesting that cyclisation onto the ring had not occurred. Thus, alternative ways in which compound **65** may have reacted in the presence of $AlCl_3$ were considered.

Particularly interesting was a literature reference[188] that proposed a Lewis acid-promoted intramolecular carbonyl-ene reaction, and Scheme 22 outlines an analogous reaction with compound **65**.

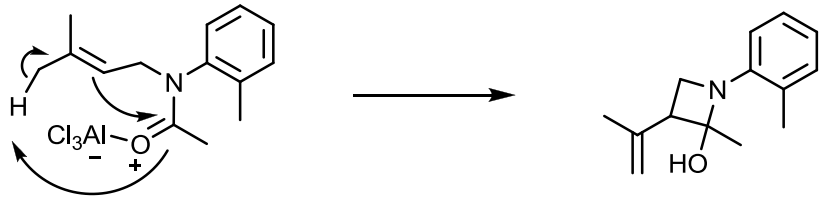

65 **73**

Scheme 22 Proposed Lewis acid-catalysed 4-*exo*-trig cyclisation of compound **65**.

The resulting product (compound **73**) would therefore contain a 4-membered ring, along with an isolated double bond and a carbinolamine. To determine if the latter was indeed present, a few drops of D_2O were added to the NMR tube containing the purified product of the $AlCl_3$-catalysed cyclisation reaction (Fig. 50); however, no exchangeable protons were observed. Given the strained 4-membered ring system present in the structure, as well as the probable instability of carbinolamines, further

reaction of compound **73**, specifically, an intramolecular ring expansion followed by dehydration, could also be possible (Scheme 23).

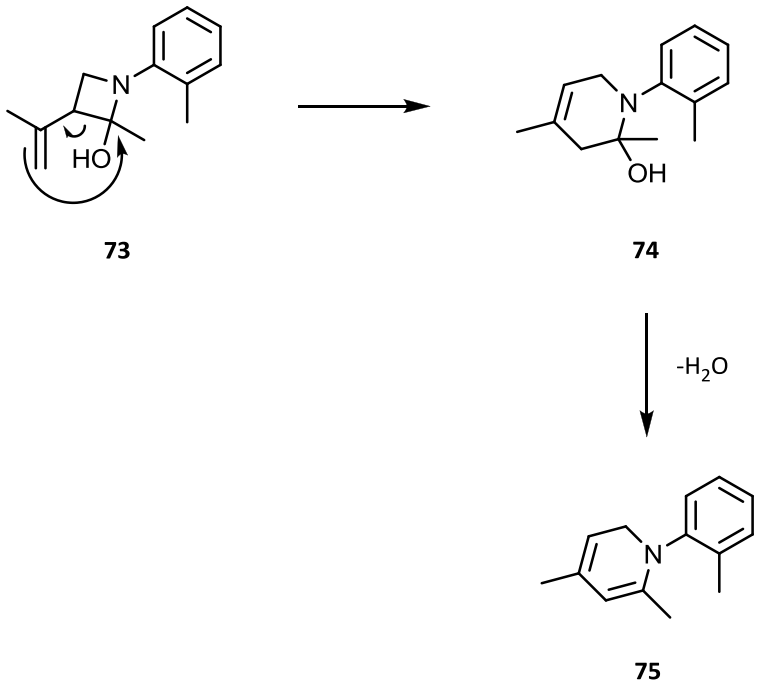

73 **74** **75**

Scheme 23 Proposed ring expansion of compound **73** followed by dehydration.

While the reactions outlined in Schemes 22 and 23 were feasible, none of the expected products from these transformations were identified by ^{1}H NMR analysis. A more simple explanation for the presence of the five individual proton peaks in the purified material could be the addition of H_2 across the alkene double bond to give the reduced product (**76**). HRMS analysis of the material supported this suggestion; however, given that no reducing agent was present in the reaction mixture, the mechanism for such an occurrence remains unknown.

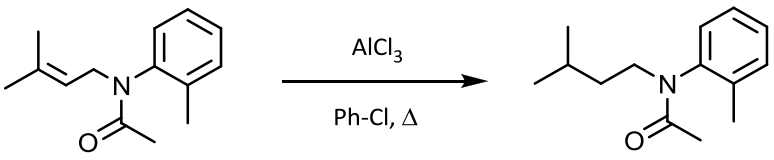

65 25% isolated yield **76**

Equation 30

In an effort to produce the desired cyclised product **66**, various reactions were set up between compound **65** and $AlCl_3$ under different conditions in dichloromethane (Table 3). The reactions were assessed for completion by ^1H NMR analysis of the reaction mixtures following aqueous workup. Despite using different numbers of equivalents of the Lewis acid, as well as varying the reaction time and temperature, in all cases where a reaction had occurred, the same 3:1 ratio of major to minor product was always observed by ^1H NMR analysis (see Fig. 48).

Table 3 Cyclisation conditions attempted with compound **65**.

Reaction	$AlCl_3$	Temp.	Time (h)	3:1 mix of products?
1	3 equiv.	r.t.	2.5	yes
2	3 equiv.	r.t.	1	yes
3	2 equiv.	r.t.	1	yes
4	2 equiv.	-78 °C	1	no reaction
5	2 equiv.	0 °C	0.5	yes
6	1 equiv.	r.t.	0.5	no reaction
7	1 equiv.	r.t.	1	mainly **65**
8	1 equiv.	r.t.	2	**65** (major) + 3:1 mix (minor)
9*	1 equiv.	130 - 85 °C	2	yes

*No solvent: $AlCl_3$ heated to 130 °C until molten, followed by addition of compound **65** and reducing the temperature to 85 °C.

Evidently, it was not possible to control the reaction outcome, and LCMS analysis of the mixture found that no chloride **77** (the result of simple addition of HCl across the alkene double bond) was present. Furthermore, given that the components of the mixture could not be easily separated (except to obtain, in low yield, the purported reduced compound shown in Fig. 50), the structures of the products from the reaction of compound **65** with $AlCl_3$ thus remain undetermined.

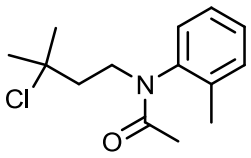

77

Cyclisation of compound **65** using PPA was also attempted; however, the reaction proved to be slow, and ^{1}H NMR analyses of the mixture showed that the reaction did not go to completion, despite heating to 120 °C for up to one week.

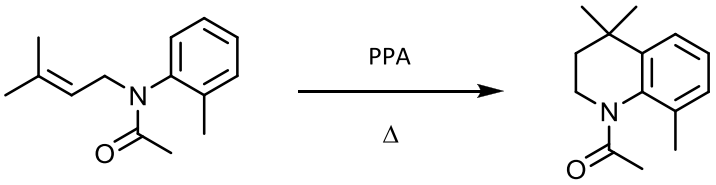

65 **66**

Equation 31

A modified approach was used: PPA was heated to 120 °C prior to the addition of neat compound **65**. After stirring for 15 min, an aqueous workup was performed to obtain an orange-coloured oil in approximately 40% yield (compared to the starting material), which was observed to be a single product by ^{1}H NMR analysis (Fig. 51).

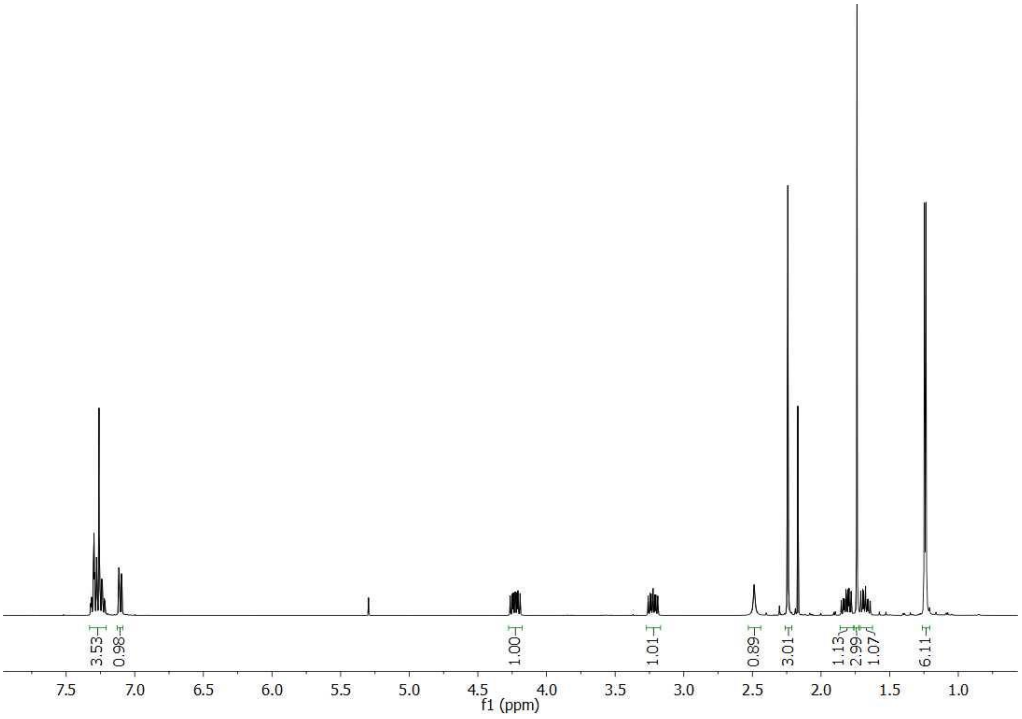

Fig. 51 ^{1}H NMR spectrum of product obtained from the reaction of compound **65** with PPA for 15 min at 120 °C - *recorded in $CDCl_3$ at 400 MHz.*

Nonetheless, a comparison of the spectrum to the aromatic region of compound **65** led to the conclusion that cyclisation onto the ring had not occurred. The presence of an exchangeable proton signal, at approx. 2.5 ppm, suggested that attack of the acetyl group may instead have occurred (Scheme 24).

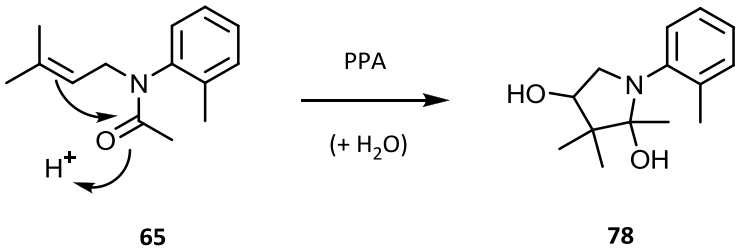

65 **78**

Scheme 24 Proposed cyclisation of compound **65** to give compound **78**.

However, simple addition of H_2O across the double bond could also be possible (Scheme 25).

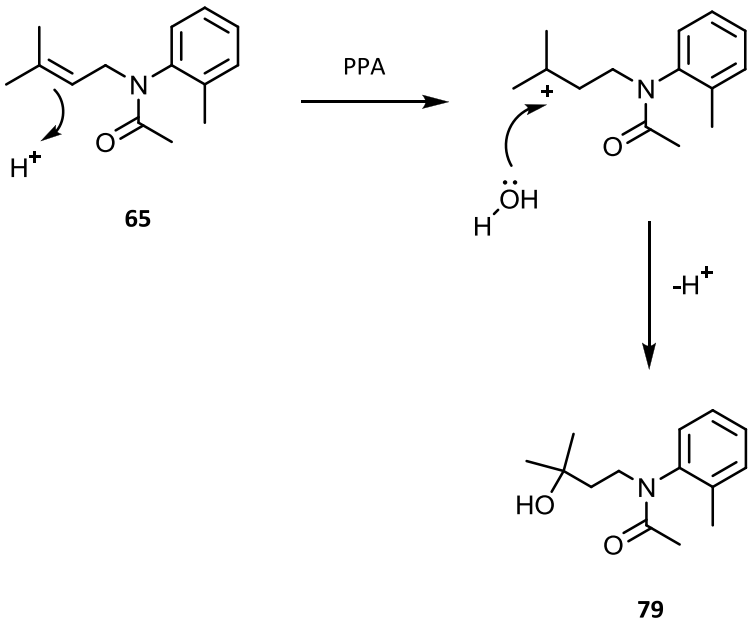

Scheme 25 Hydrolysis of compound **65** to give compound **79**.

This would then be consistent with the ^{13}C NMR spectrum of the material, which indicated that a carbonyl group was present; HRMS analysis also supported the structure of compound **79** as the product. As previously suggested, the presence of the acetyl group could give rise to the individual alkane proton peaks observed, and the great disparity between the proton chemical shifts (namely at 3.25 and 4.25 ppm, Fig. 51) could be further explained by hydrogen bonding within the molecule (Fig. 52), which would mean that the substituents on the nitrogen atom could remain in a relatively fixed conformation, and the alkane protons in question would experience considerably different chemical environments than if free bond rotation were possible.

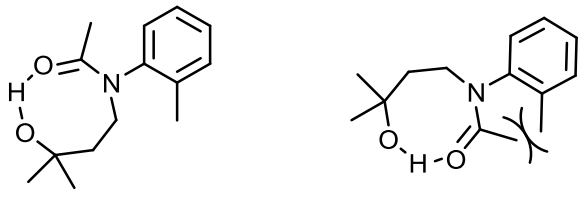

Fig. 52 Proposed hydrogen-bonding conformations of hydrolysis product **79**, with the less hindered (*i.e.* favoured) conformation shown on the left.

In order to determine if compound **79** would eventually react to provide the desired cyclised product, the reaction was repeated with heating for a longer period: compound **65** was added to a flask containing PPA that had been heated to 120 °C, and the mixture was stirred for 2 h. The resulting black/brown viscous oil was difficult to extract; however, some material was isolated following aqueous workup (approx. 50%), and three separate peaks, each integrating to one proton, were observed in the aromatic region of the ^{1}H NMR spectrum (Fig. 53). It appeared, therefore, that cyclisation had indeed occurred; however, it was apparent that the product had also deacetylated to give compound **80**.

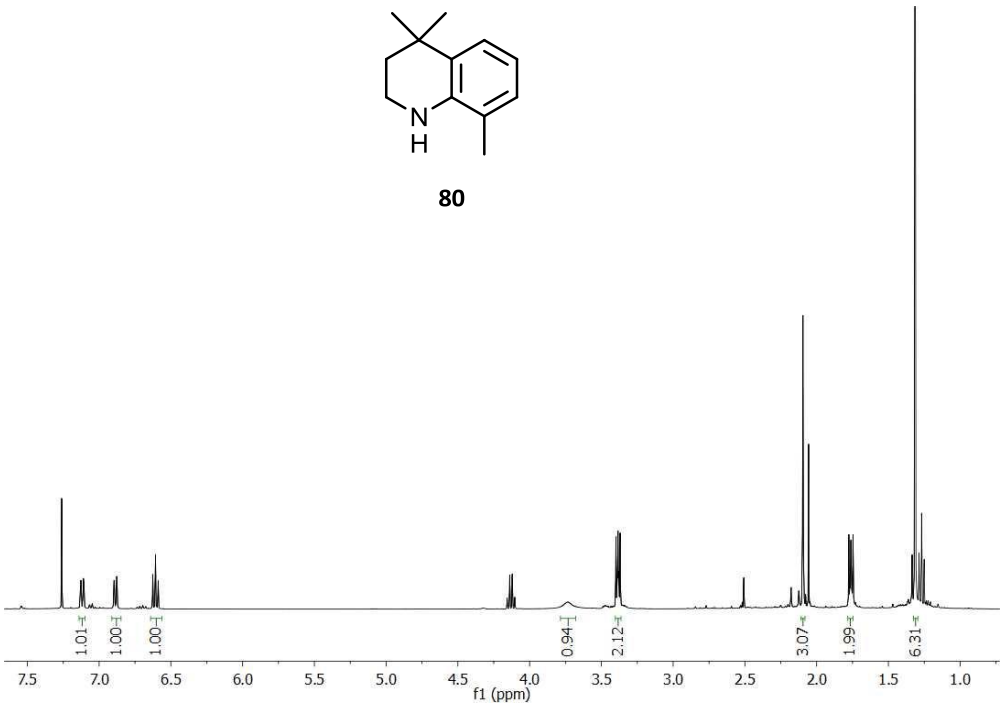

80

Fig. 53 ^{1}H NMR spectrum of product obtained from the reaction of compound **65** with PPA for 2 h at 120 °C - *recorded in $CDCl_3$ at 400 MHz*. (Note change in aromatic region - *residual ethyl acetate present*).

Since cyclisation of compound **65** using $AlCl_3$ and PPA had proved unsuccessful, alternative methods were considered: a literature procedure of cyclising a similar compound using concentrated sulphuric acid was attempted (Equation 32).[189]

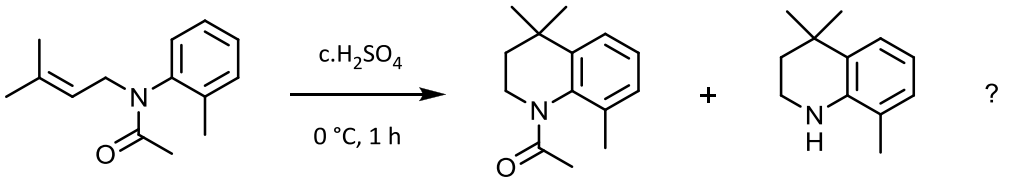

65 **66** **80**

Equation 32

The reaction mixture was stirred at 0 °C for 1 h, and an aqueous workup was performed. The resulting yellow oil proved to be a complex mixture of products as observed by ^{1}H NMR analysis. Perhaps, given the presence of the acetyl group, a strong acid was not an appropriate reagent to use for cyclisation of compound **65**.

Cyclisation using the weaker Lewis acid $BF_3{\cdot}OEt_2$ was also attempted (Equation 33): however, despite refluxing the mixture for 2 h, no reaction was observed by ^{1}H NMR analysis, and only starting material was recovered.

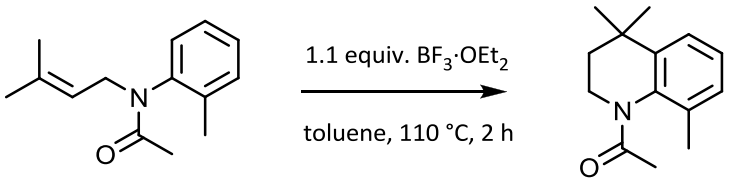

65 *no reaction* **66**

Equation 33

Finally, cyclisation of compound **65** was attempted using a catalytic amount of $Sc(OTf)_3$ (Equation 34), but this likewise proved unyielding, with only starting material present by ^{1}H NMR analysis.

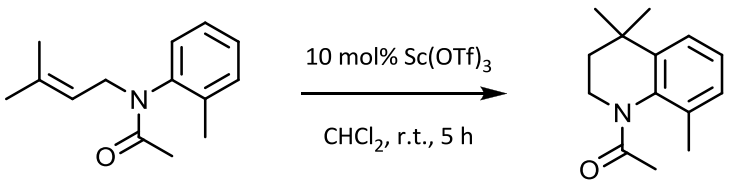

65 *no reaction* **66**

Equation 34

Iodination

Various iodination reactions were attempted on material that was originally thought to be the cyclised product (compound **66**); however, it was later apparent that the substrate used was in fact likely to be compound **78**, or more likely, the hydrolysis product **79** (see Fig. 51 for ^{1}H NMR spectrum).

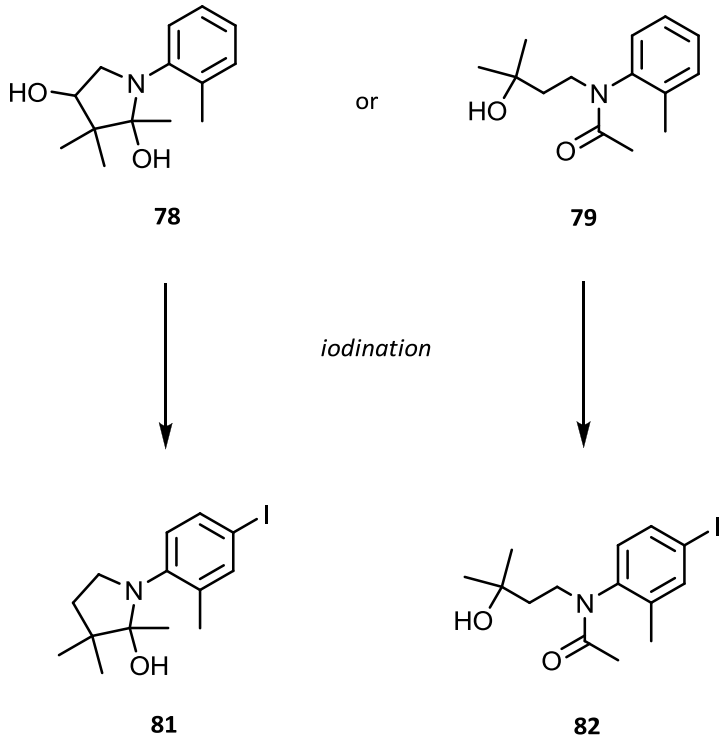

Equation 35

The iodination conditions attempted are outlined in Table 4; in all cases, care was taken to exclude light from the reactions. Following aqueous workup of the reaction mixtures, ^{1}H NMR analyses were performed to assess if iodination had occurred. A literature-reported method of using ICl and $In(OTf)_3$ to carry out mild and efficient direct aromatic iodination of acid-sensitive substrates[190] was attempted, both with and without heating (Table 4, Reactions 1-3), but only the starting material was observed by ^{1}H NMR analysis. Similarly, stirring the substrate with equimolar amounts of iodine and mercury(II) oxide (Table 4, Reactions 4 and 5), using iodine (Table 4, Reactions 6 and 7), or *N*-iodosuccinimide (Table 4, Reaction 8), were all ineffective in

promoting formation of the desired product: evidently, the substrate appeared to be highly deactivated towards electrophilic aromatic substitution.

Table 4 Iodination conditions attempted with the purified product from the reaction of compound **65** with PPA (see Fig. 51).

Reaction	Reagents	Solvent	Temp. (°C)	Time (h)	Product observed?
1	$In(OTf)_3$ (1.0 equiv.) ICl (1.5 equiv.)	MeCN	20	0.5	no
2	$In(OTf)_3$ (1.0 equiv.) ICl (1.5 equiv.)	MeCN	85	2.5	no
3	$In(OTf)_3$ (1.0 equiv.) ICl (1.0 equiv.)	MeCN	20	24	no
4	I_2 (1.0 equiv.) HgO (1.0 equiv.)	DCM	20	0.5	no
5	I_2 (1.0 equiv.) HgO (1.0 equiv.)	DCM	20	18	no
6	I_2 (0.95 equiv,)	CH_3Cl	-60 to -30	1	no
7	I_2 (0.95 equiv,)	CH_3Cl	20	60	no
8	NIS (1.1 equiv.)	MeCN	85	2.5	no

*NIS - *N*-iodosuccinimide

Low-energy conformation calculations

Spartan 10 was used to perform an equilibrium conformation calculation (with AM1 semi-empirical settings - which, on systems consisting of only C, H, N and O, provides sufficient accuracy to give a good indication of geometry *vs* energy - to generate 5000 conformers) to predict the lowest energy conformation for compound **79** (Fig. 54). As expected, hydrogen bonding between the carbonyl and hydroxyl groups was evident, and the alkyl chain was arranged away from the aromatic methyl group in order to reduce steric crowding. As a result of this arrangement, the lone pair of the nitrogen atom was in an orthogonal position relative to the aromatic π-system, and, therefore, seemed unable to activate the molecule towards electrophilic iodination (by donating electron density into the aromatic ring). This likely accounted for the lack of reactivity

of the compound, and a similar orthogonal arrangement of the nitrogen lone-pair could also be expected for the 5-membered ring-containing compound, **78**.

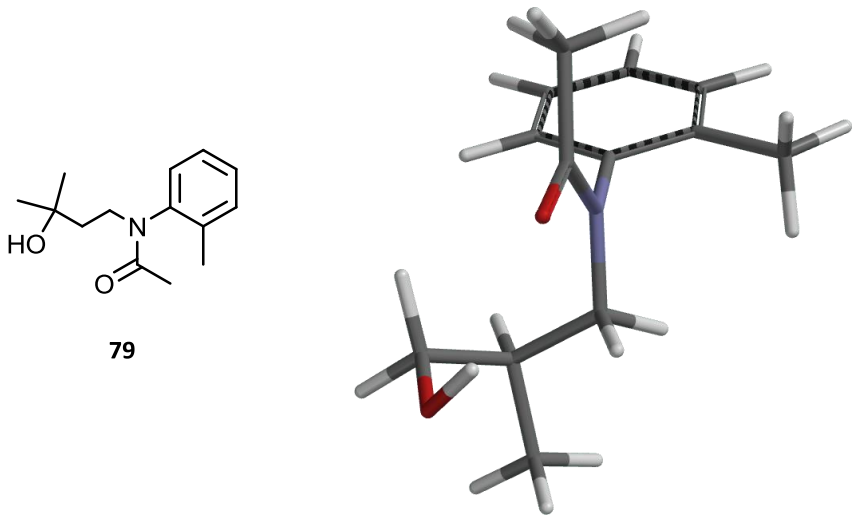

79

Fig. 54 Predicted lowest energy conformation of tertiary alcohol **79**, as calculated by Spartan 10.

AM1 (as implemented in Spartan 10) was also used to predict the lowest energy conformations of the tetrahydroquinoline structures **14** and **26**, in order to determine whether a similar explanation could be made for the great difficulty in performing an aromatic iodination reaction with the latter more substituted compound compared to its less substituted analogue.

Thus, the favoured low-energy conformations are shown in Fig. 55. In compound **26**, it could clearly be observed that the *N*-isopropyl moiety was arranged in a *pseudo*-axial position in order to reduce steric effects with the neighbouring *ortho*-methyl group. The latter thus appeared to play a significant role in deactivating compound **26** towards iodination, since the resulting conformation meant that the nitrogen lone-pair was less available to donate into the π-system, thereby rendering the molecule less susceptible towards electrophilic aromatic substitution. Conversely, in compound **14**, without the steric-hindering effects of an aromatic methyl substituent, the *N*-methyl group was able to lie in a more equatorial position. In this case, the activating effects

of the nitrogen lone-pair may be expected to come into play, thereby accounting for the relative ease with which this substrate undergoes aromatic iodination.

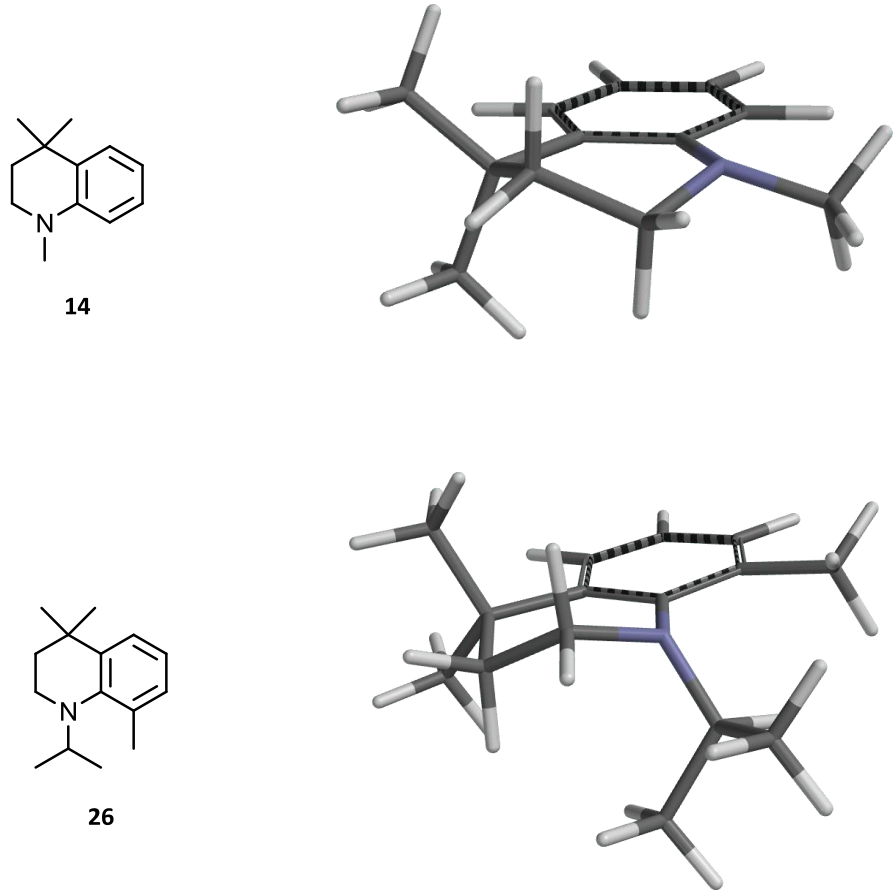

Fig. 55 Predicted lowest energy conformations of compounds **14** and **26**, as calculated by Spartan 10. *Note the pseudo-axial position of the N-isopropyl group in compound **26**, compared to the more equatorial position of the N-methyl group of compound **14**.*

It was further noted that, in compound **26**, due to the *pseudo*-axial arrangement of the *N*-isopropyl group, the nitrogen lone-pair was consequently more available for performing nucleophilic attack (for example, of oxidising species), which would explain the susceptibility of the molecule for forming an enamine side-product (discussed in section 4.3.).

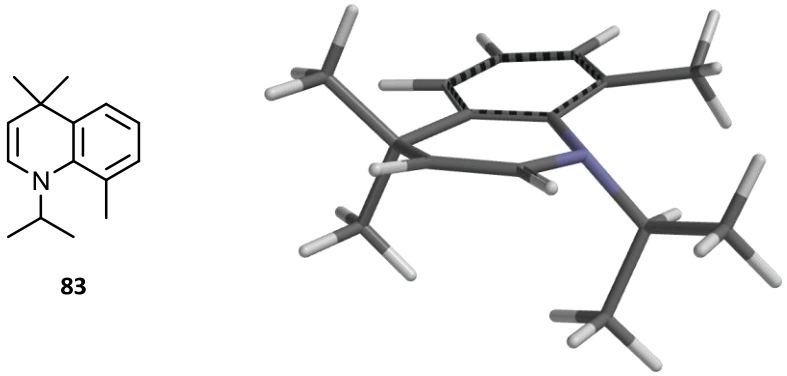

83

Fig. 56 Predicted lowest energy conformation of the oxidised derivative of compound **26**, as calculated by Spartan 10.

4.8. Synthesis of an amide-containing retinoid

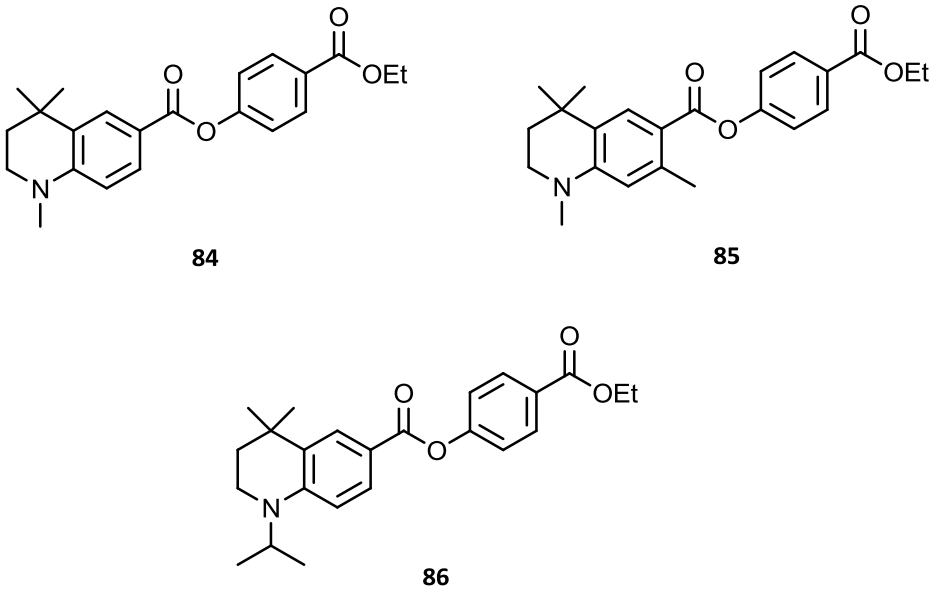

84 **85** **86**

Fig. 57 Flexible heteroarotinoids in which hydrophobicity of the molecule was increased through the incorporation of additional methyl groups.[191]

A series of heteroarotinoids (Fig. 57) was synthesised and evaluated for biological activity and RAR/RXR receptor specificity. The presence of the two-atom linkers (C-O) between the two aromatic rings increased the flexibility of the heteroarotinoids, and

these compounds were found to possess increased potency and specificity for retinoic acid receptors compared with analogues containing alkenyl linkers.[85] Synthesis of these heteroarotinoids were *via* cyclic amide structures, which were subsequently reduced to provide the tetrahydroquinoline cores.

Target hydrophobic core

Thus, synthesis of the cyclic amide-containing compound **87** (Fig. 58) was proposed, which was thought to possess desirable properties for incorporation into retinoids developed for fluorescence imaging applications.

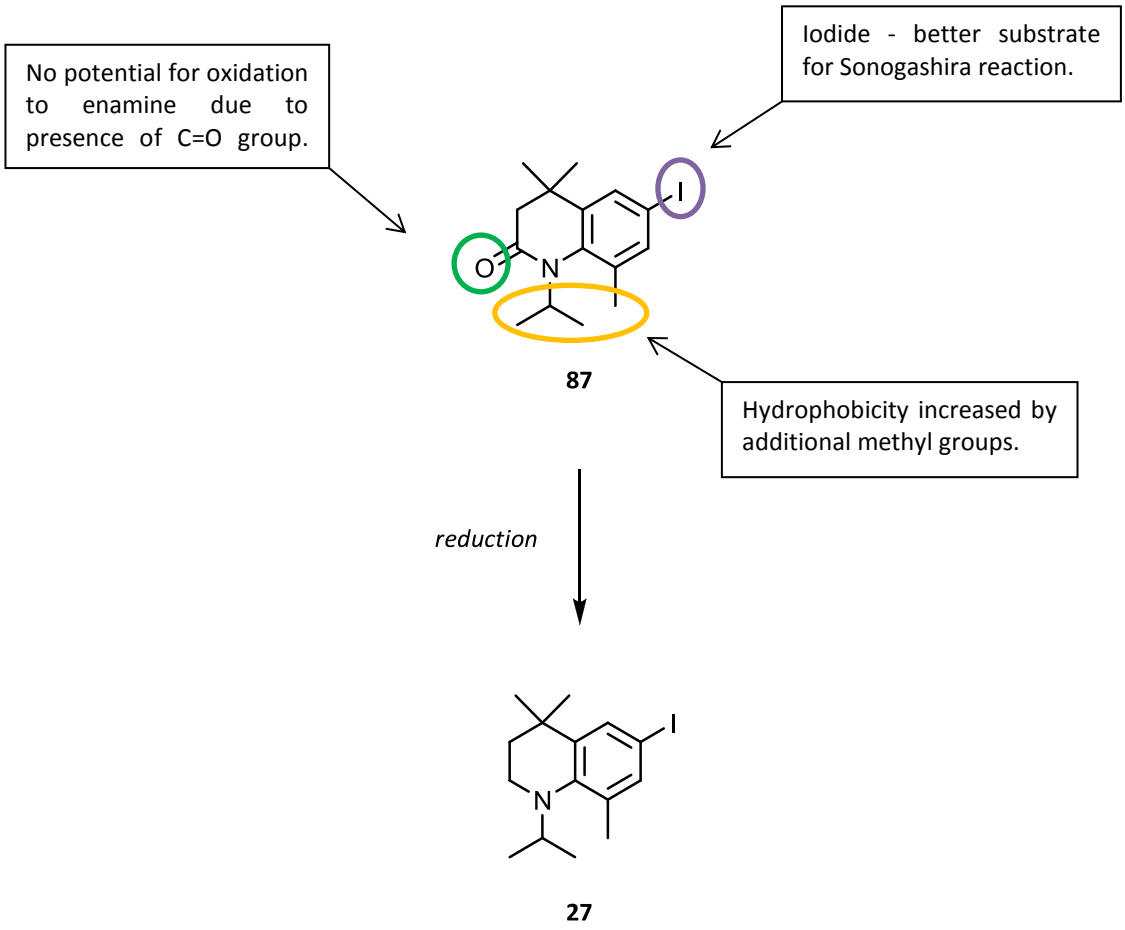

Fig. 58 Desired target substrate **87** for Sonogashira coupling reaction, which, if desired, may be reduced to provide the original target iodide **27**.

With compound **87** in hand, synthesis of retinoid **88** would then be possible, and it would be interesting to evaluate the fluorescence and biological properties of the amide-containing molecule.

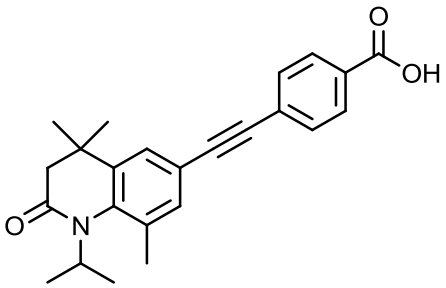

88

N-Alkylation

Reaction with acetone

The proposed reaction scheme for the synthesis of iodide **87** was based on a similar procedure reported in the literature (Scheme 26).[191]

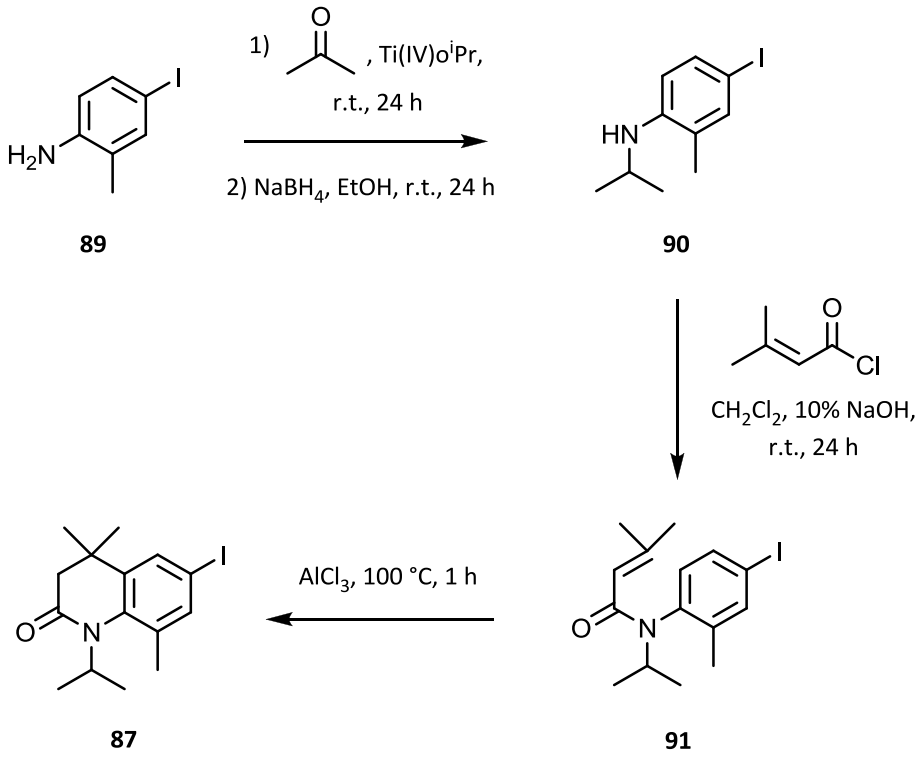

Scheme 26

4-Iodo-2-methylaniline (**89**) may be purchased from Sigma-Aldrich, however, it was synthesised *via* a straightforward procedure employing *o*-toluidine and 3 equivalents of iodine in a solution of pyridine and dioxane (Equation 36).[192] After stirring for 1 h at 0 °C, the mixture was allowed to warm to room temperature and stirred for a further 1 h. An aqueous workup was then performed, and the desired product was obtained in 61% yield after recrystallisation.

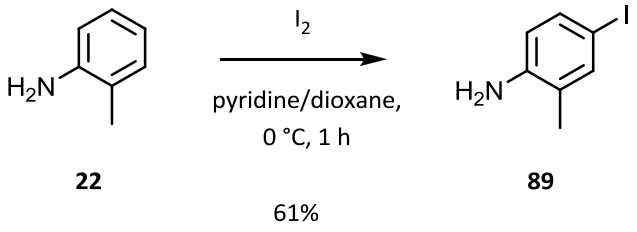

22 **89**

61%

Equation 36

In order to synthesise the *N*-isopropyl compound **90**, 1.5 equivalents of acetone and 1 equivalent of Ti(IV)o^{i}Pr were stirred with iodide **89** in ethanol for 24 h. However, a TLC analysis followed by a ninhydrin stain showed that only (the primary amine) starting material was present. The temperature was increased to 35 °C, and the mixture was stirred for a further 2 h; however, no product was observed by TLC analysis. The addition of more acetone (1.5 equivalents) followed by stirring at 35 °C for 5 h, also did not result in product formation. Given that this was reported as a successful procedure for performing *N*-alkylation of 4-bromoaniline, perhaps the presence of the *ortho*-methyl group played a role in hindering the approach of the electrophile, thereby disfavouring product formation.

Reaction with acryloyl chloride

An alternative route was then considered, which involved first performing *N*-alkylation of iodide **89** using 3,3'-dimethylacryloyl chloride,[85] after which cyclisation of the product may be carried out, and finally an *N*-isopropylation reaction would provide substrate **87**. Accordingly, the first *N*-alkylation reaction of compound **89** was performed according to Equation 37, and product **92** was obtained as a white

crystalline solid in 79% yield following aqueous workup and recrystallisation (Equation 37).

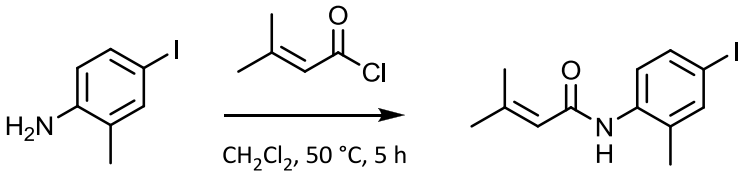

89 79% **92**

Equation 37

Cyclisation reactions

Cyclisation of compound **92** according to the reported literature method was then attempted (Equation 38).[85] This involved heating the starting material to 130 °C, prior to the addition of 1.5 equivalents of $AlCl_3$ over 1 h. The flask was then cooled to 80 °C, and a further 0.2 equivalents of $AlCl_3$ were added. The mixture for stirred for 30 min, then cooled to room temperature, and an aqueous workup was performed. However, ^{1}H NMR analysis revealed significant deiodination had taken place so that the desired compound **93** and the deiodinated product **94** were obtained in approx. 1:2 ratio, respectively (as observed by ^{1}H NMR analysis), which were not easily separated by column chromatography.

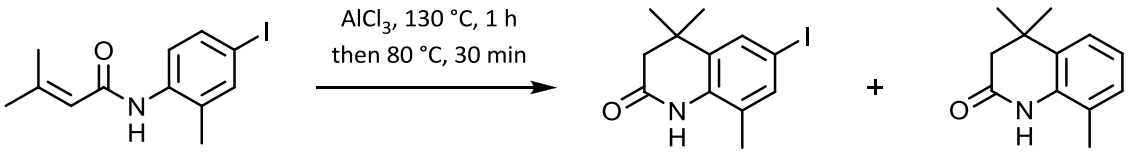

92 **93** (1 : 2) **94**

Equation 38

In order to obtain compound **93** as the sole product, iodination of the mixture of compounds **93** and **94** was attempted by the addition of 1.1 equivalents of ICl in acetic acid. Following overnight stirring at room temperature, this was successful in

increasing the proportion of the iodide product to approximately 62%. When the reaction was left stirring for a further 72 h, up to 78% of compound **93** was observed by ^{1}H NMR analysis.

It was thought that the iodination reaction may proceed more efficiently if carried out on a single compound, rather than with a mixture of products; therefore, reaction of *o*-toludine with 3,3-dimethylacryloyl chloride was performed according to Equation 39, which provided compound **95** as a white crystalline solid in 89% yield following aqueous workup and recrystallisation.

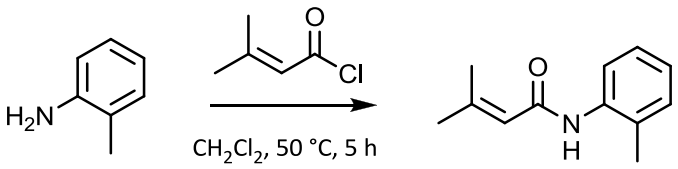

22 89% **95**

Equation 39

Next, cyclisation of compound **95** using $AlCl_3$ was carried out, with dichloromethane as the solvent (Equation 40). This was preferred over the solvent-free method, since the reaction proceeded more quickly, and given that no viscous black oil was produced, the product proved more facile to extract. Thus, pure compound **94** was obtained in 91% yield following aqueous workup and recrystallisation.

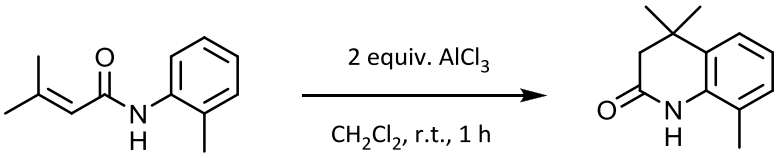

95 91% **94**

Equation 40

Compound **94** was then stirred with 1.1 equivalents of ICl in acetic acid at room temperature: following overnight reaction, approximately 62% conversion to the

iodide product was observed by ^{1}H NMR analysis. When the reaction was repeated using 2 equivalents of ICl, an improved conversion to the desired product (approximately 81%) was observed following overnight stirring. However, again, due to the highly similar nature of the starting material and product, it was not possible to obtain iodide **93** in pure form.

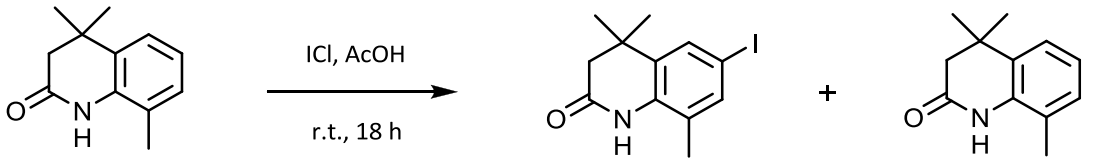

94 **93** **94**

Equation 41

At this point, it was recognised that cyclisation of the iodine-containing compound **92** could likewise be performed with $AlCl_3$ using a solvent. Perhaps, by avoiding high temperatures (as in the solvent-free method), deiodination may be less likely to occur. Compound **92** was accordingly stirred with 2 equivalents of $AlCl_3$ in dry dichloromethane for 1 h at room temperature: following aqueous workup, only 10% deiodination was observed by ^{1}H NMR analysis. Compound **93** was eventually obtained as the sole product when 1.5 equivalents of $AlCl_3$ were used; in this case, the reaction proceeded more slowly, and required 3 h for completion (Equation 42).

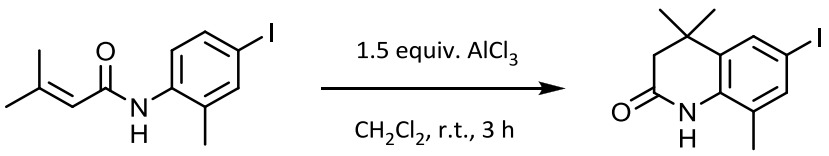

92 81% **93**

Equation 42

Derivatisation reactions

Next, reduction and *N*-alkylation of compound **93** were attempted in order to assess the ease of performing such reactions (Equation 43).

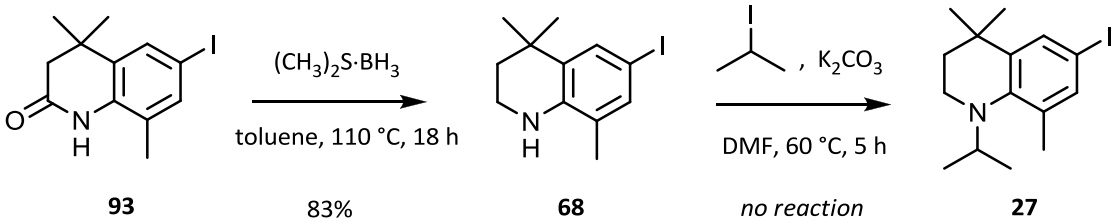

93 83% **68** *no reaction* **27**

Equation 43

Reduction of the carbonyl group with borane-dimethyl sulfide was successful, and provided compound **68** in 83% yield after reaction workup. This was then used for the subsequent alkylation reaction with 2-iodopropane, with K_2CO_3 as base; however, following heating to 60 °C in DMF for 5 h, only starting material was recovered. A stronger base, such as sodium hydride, may be more effective in promoting formation of the *N*-alkylated product.

Sonogashira coupling and hydrolysis

A Sonogashira reaction was carried out between iodide **93** and alkyne **16** in order to provide the cyclic amide-containing ester **96** (Equation 44). Following overnight heating, the mixture was filtered, and the solvent was removed *in vacuo*. The product proved unstable to purification *via* chromatographic means (streaking on the column was observed, and only a minimal amount of the product was recovered, regardless of the solvent system used), therefore, trituration of the product was performed using ethanol as the solvent, and compound **96** was thus obtained in 66% yield.

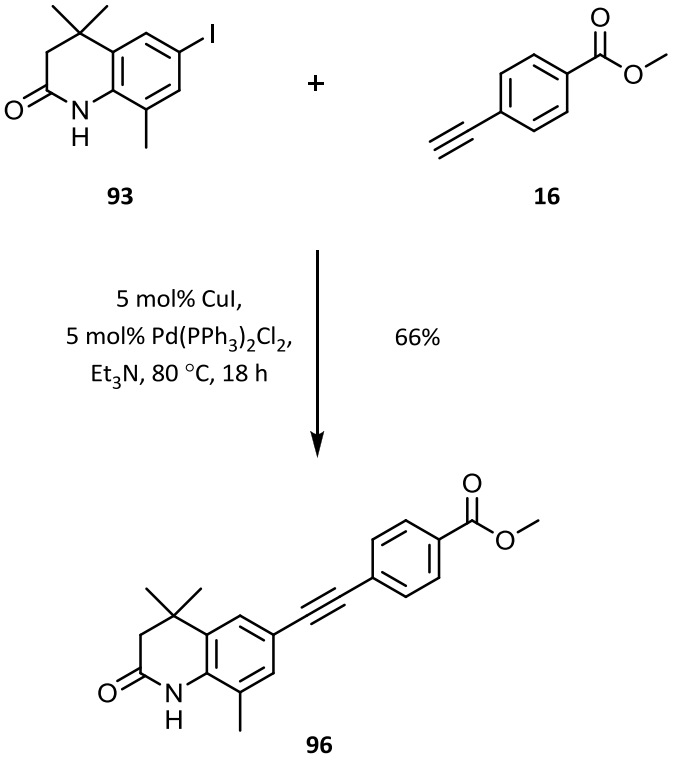

Equation 44

Next, ester hydrolysis was carried out according to Equation 45: after 4 h, some starting material was still observed by TLC analysis, so the reaction was heated for a further 4 h, after which a second TLC analysis showed only a single product spot was present.

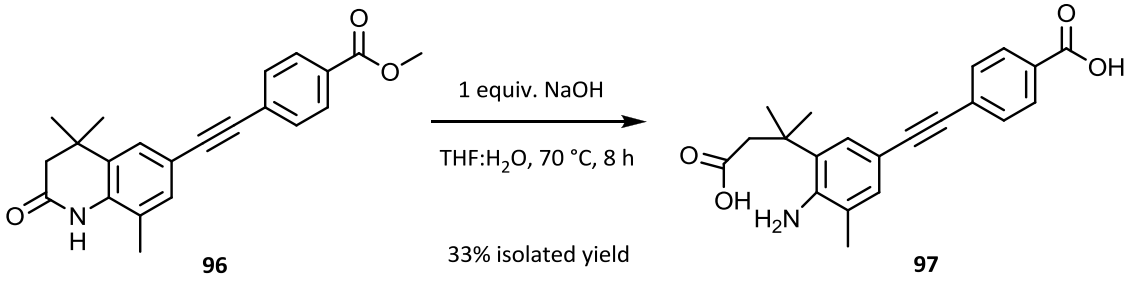

Equation 45

An aqueous workup was performed by adding diethyl ether and water to the cooled reaction mixture, followed by acidification of the aqueous layer to pH 1 using 1 M HCl. At this point, an insoluble white precipitate was formed, which did not dissolve when the mixture was extracted with diethyl ether. The combined organic extracts were dried over $MgSO_4$, however, following *in vacuo* removal of the solvent, only a minimal amount (approx. 15%) of product was recovered. A significant quantity of the insoluble material remained in the aqueous portion, and did not dissolve in any of the organic solvents that were added to the mixture (methanol, ethanol, diethyl ether, ethyl acetate, dichloromethane, acetone). Thus, it was thought that ring-opening of the cyclic amide must have occurred.

Given that the product of the hydrolysis reaction of compound **96** proved insoluble in any of the organic solvents used in an attempt to dissolve the material, the product was thought to exist in the zwitterionic form (Fig. 59).

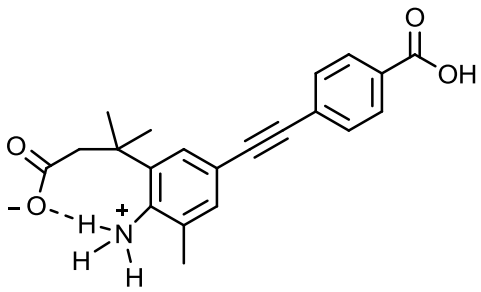

Fig. 59 Proposed ammonium carboxylate salt produced from the hydrolysis reaction of compound **96**. An intramolecular hydrogen-bonded structure is suggested.

^{1}H NMR analysis of the material in DMSO-d_6 revealed that a low-field singlet peak (at 9.66 ppm, which was consistent with a proton of a carboxylic acid group) corresponding to one proton was present, which disappeared when a D_2O exchange was carried out. An additional singlet peak was also present (at 3.87 ppm) that integrated to approximately 1.5 protons. However, in a D_2O exchange experiment, this signal remained unchanged, even after leaving the sample for a few days. It was, therefore, unlikely that this signal was caused by a proton attached to an oxygen or nitrogen atom. It was interesting to note, however, that the chemical shift value of this

singlet peak, along with its corresponding ^{13}C NMR signal, were highly similar to those observed for the methyl ester group in the starting material. The products of the hydrolysis reaction could, therefore, be the ring-opened compound **97** and its methyl ester analogue. Despite the ^{1}H NMR spectrum of the material giving no indication that a second product was present, it could be feasible that, due to their highly similar structure, the two compounds would appear essentially identical by ^{1}H NMR analysis.

N-Isopropyl derivative

Synthesis of the original target compound **87** was carried out by performing *N*-alkylation of compound **93** according to Equation 46.

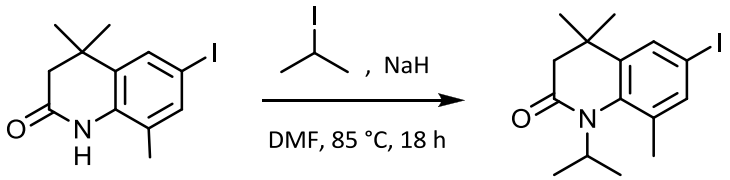

93 69% **87**

Equation 46

Next, a Sonogashira coupling reaction between compound **87** and alkyne **16** was performed: following overnight heating, the mixture was filtered, and the solvent was removed *in vacuo*. It was possible to purify this *N*-substituted compound by silica-gel chromatography, and pure compound **98** was thus obtained in 89% yield.

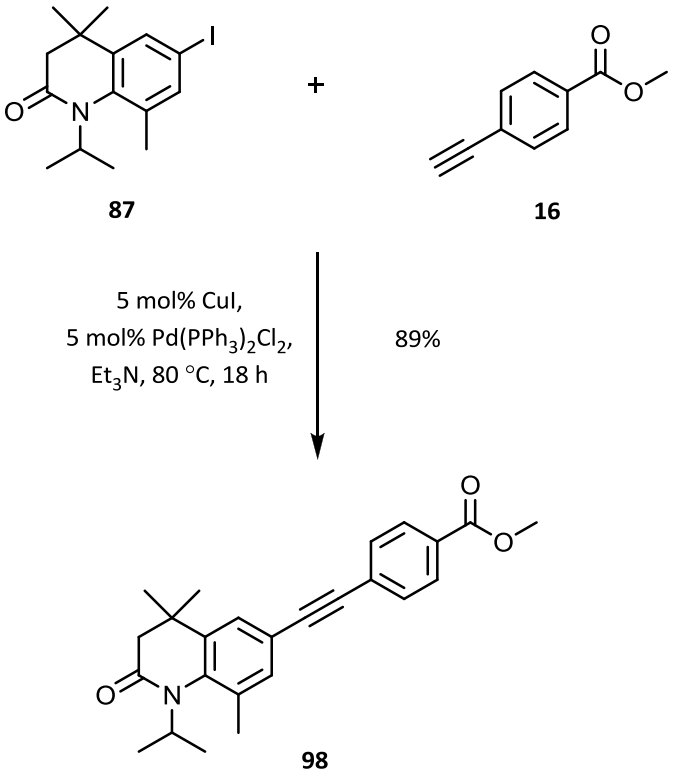

Equation 47

Ester hydrolysis of compound **98** was attempted using the conditions shown in Equation 48. However, in both cases, an insoluble material was obtained that proved to be consistent with the amide ring-opened product by ^{1}H NMR analysis.

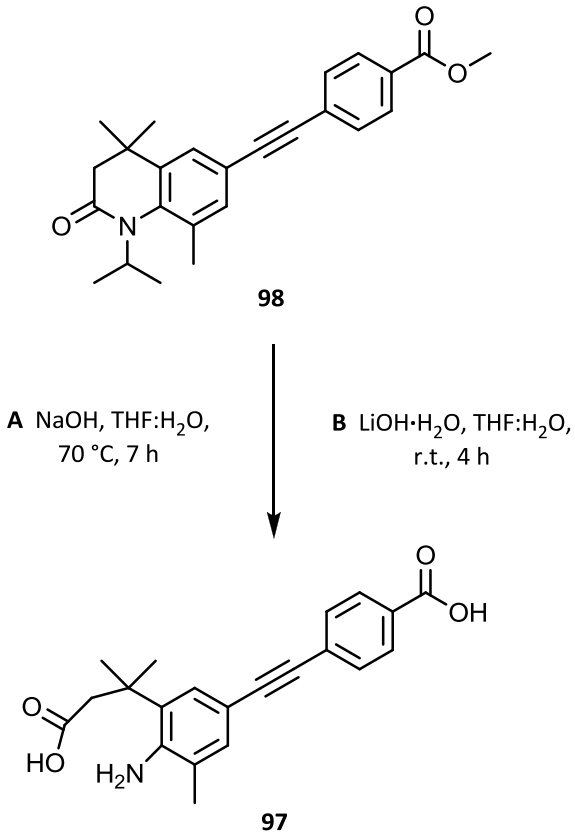

Equation 48

4.9. Synthesis of an amide retinoid *via* an oxazoline compound

Since hydrolysis of the methyl ester compounds in the previous section resulted in ring-opening of the cyclic amide, the synthesis of an oxazoline-containing analogue, which may be converted to the desired carboxylic acid product using milder conditions, is outlined in Scheme 27.

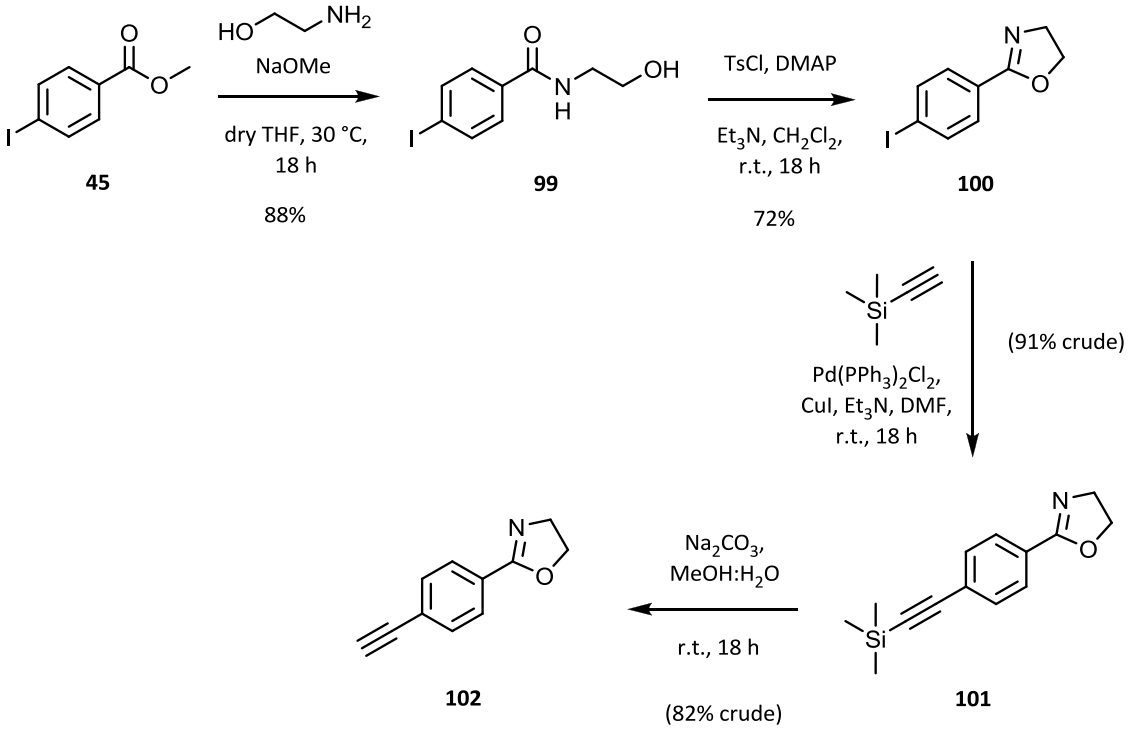

Scheme 27 Synthetic route to oxazoline compound.

Reaction of compound **45** with ethanolamine, followed by cyclisation of compound **99** using tosyl chloride and 4-dimethylaminopyridine, proved straightforward, and provided the oxazoline-containing aryl iodide **100** in a good yield (72%) following purification by silica-gel chromatography.

Next, a Sonogashira coupling reaction between compound **100** and TMSA was attempted according to the previously-established method of heating with palladium and copper catalysts in neat triethylamine. However, this led to a poor product recovery, and it was later thought that this was likely due to decomposition of the oxazoline moiety in the highly basic environment. The reaction was repeated using DMF as the solvent, with 2 equivalents of triethylamine as base. In addition, an acidic workup should be avoided for future repeats of the reaction, since the oxazoline group also appeared unstable to a 5% HCl wash. Nevertheless, removal of the trimethylsilyl group was carried out on the crude material to provide the free alkyne, compound **102**.

A final Sonogashira reaction was then carried out to obtain the oxazoline retinoid analogue **103** (Equation 49; for improved product yield, heating in neat triethylamine should be avoided for future repeats of this reaction).

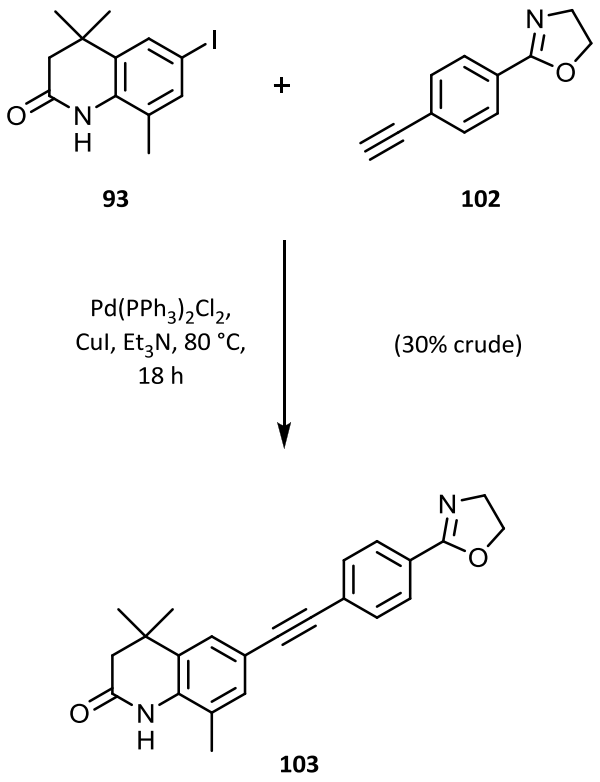

Equation 49

Conversion of compound **103** to the desired carboxylic acid product was attempted according to a reported literature method of stirring with NBu_4HSO_4 and 5% NaOCl in ethyl acetate at room temperature (Equation 50).[193] However, the reaction was slow, requiring a long reaction time (96 h) for consumption of the starting material. Following aqueous workup, an insoluble material was recovered, and it was apparent from ^{1}H NMR analysis that this was again the amide ring-opened product.

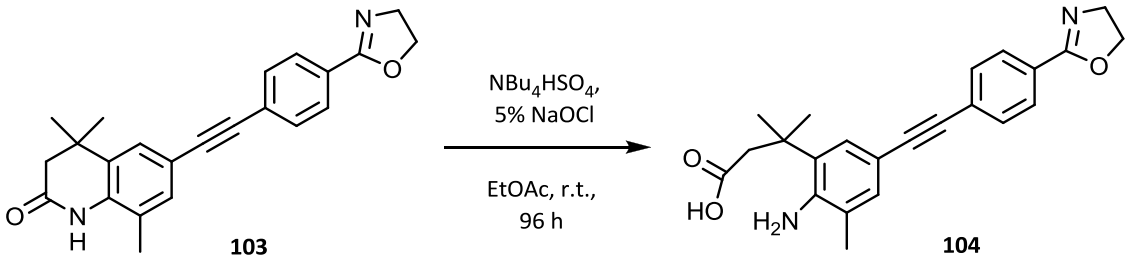

Equation 50

4.10. Conclusions and Outlook

It is evident that the synthetic route towards a cyclic amide-containing retinoid requires some optimisation in order to provide the desired carboxylic acid product, without causing ring-opening of the hydrophobic part of the molecule. Thus, a screening of procedures for milder hydrolysis of the methyl ester compounds could be carried out, as well as assessing different methods for conversion of the oxazoline group to the carboxylic acid. With the amide-containing retinoid in hand, it would then be possible to perform an evaluation of the stability, fluorescence, and biological properties of the molecule.

5. CONCLUDING REMARKS AND FUTURE WORK

5.1. Concluding remarks

These studies have demonstrated that minor changes to the structure of small molecules can have profound impacts on their biological activity. This was clear from evaluation of the thiazole-containing molecules **A**, **1**, and **2**: while the alkoxy (**A**)- and phenyl (**1**)-containing derivatives did not induce differentiation of TERA2.cl.SP12 EC cells, the more bulky tetramethyltetrahydronaphthyl (**2**)-substituted analogue displayed significant retinoid activity in this cell line, and promoted enhanced neurite outgrowth compared to ATRA. The relationship between activation of a particular receptor and the inducement of specific biological outcomes remains to be fully elucidated, and could provide an interesting area for further study.

In addition, the synthesis, characterisation, and initial biological evaluation of the fluorescent retinoid, **GZ108**, provided encouraging results to support the concept that fluorescence incorporated within an active small molecule could constitute a highly useful tool for the unprecedented real-time visual exploration of retinoid uptake, transport, and activity in biological cells and systems.

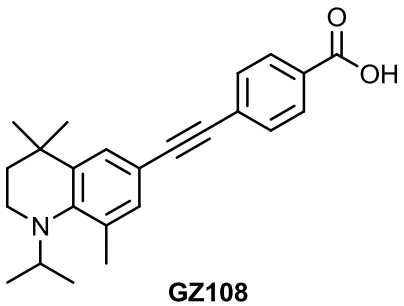

GZ108

Nevertheless, the propensity of the molecule for forming an enamine side product remains to be fully understood. This occurrence was proposed to be due to exposure of the fluorophore to light, resulting in overall dehydrogenation *via* a purported radical-mediated process. Furthermore, the predicted low-energy conformations calculated by Spartan 10 revealed the surprising effects of the *N*-substituent, which should be taken into account for future synthetic work. Briefly, the presence of the *N*-isopropyl group appeared to have a significant impact on the resulting conformation of

the molecule: in order to reduce steric effects with the aromatic methyl group, the isopropyl moiety was arranged such that the nitrogen lone-pair was no longer in conjugation with the rest of the molecule, and could not, therefore, play an electron donating/activating role. This would account for the great difficulty in performing aromatic iodination reactions with the hydrophobic core, which in turn affected the ease of carrying out the remaining reactions in the synthetic scheme, leading to a suboptimal product yield. Perhaps a simple substitution of an *N*-methyl group would be sufficient to stabilise the molecule towards *N*-oxidation or degradation, while allowing the nitrogen lone-pair to lie in a coplanar conformation.

Finally, the synthetic route to a cyclic-amide containing retinoid was successful; however, reactions to remove the protecting group (methyl or oxazoline moiety) in order to provide the free carboxylic acid terminus resulted in ring-opening of the cyclic amide; it is hoped that reaction optimisation would lead to a more favourable result.

5.2. Future work

Based on the findings from this project, the synthesis of novel structures to incorporate into fluorescent retinoid design is proposed in Fig. 60. The presence of the additional methyl groups adjacent to the nitrogen atom (compounds **105**-**107**) would increase the hydrophobicity, as well as stabilise the molecule by preventing oxidation to an enamine structure. The incorporation of a second aromatic group (compounds **107** and **108**) is based on the structures of known RARβ-selective ligands, and the additional conjugation would be expected to increase the fluorescence properties of the molecule.

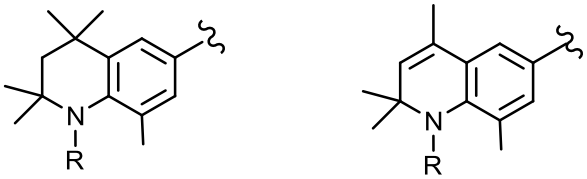

105

106

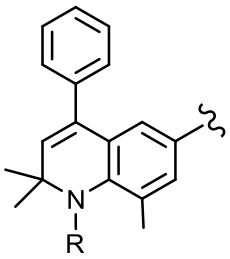

107

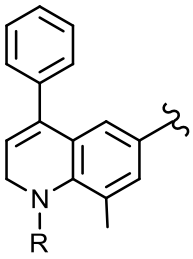

108

Fig. 60 Proposed novel building blocks for synthesis of fluorescent retinoids. The additional methyl groups increase hydrophobicity of the molecule while preventing oxidation to the enamine product. Fluorescence is increased by the additional conjugation in compounds **106**-**108**. The more bulky structures of compounds **107** and **108** are expected to provide selectivity for RARβ.

6. EXPERIMENTAL

6.1. General experimental

Reagents were purchased from Sigma-Aldrich, Acros or Alfa-Aesar, and used without further purification unless otherwise stated. Dry solvents were purchased from the supplier. Where indicated, reagents were combined in an Innovative Technology Inc. (UK; http://www.innovative-technology.co.uk) nitrogen-filled (BOC, UK; http://www.boconline.co.uk) glovebox. All glassware was oven-dried (130 °C) prior to use and cooled under a positive pressure of argon. Microwave (MW)-assisted reactions were carried out in an Emrys™ Optimizer (Personal Chemistry, Biotage, Sweden; http://www.biotage.com) in septum-containing, crimp-capped, sealed vials with automatic wattage adjustment to maintain the desired temperature for a specified period of time. Reactions were monitored in situ by TLC, GC-MS or 1H NMR spectroscopy to ensure consumption of starting materials before reaction workup. Thin layer chromatography (TLC) was performed on Polygram SIL G/UV_{254} plastic-backed silica gel plates with visualisation achieved using a UV lamp. Column chromatography was performed with Davisil Silica gel, 60 mesh. GC-MS was performed using an Agilent Technologies 6890 N gas chromatograph equipped with a 5973 inert mass selective detector and a 10 m fused silica capillary column (5% cross-linked phenylmethylsilicone) using the following operating conditions: injector temperature 250 °C, detector temperature 300 °C, oven temperature was ramped from 70 °C to 280 °C at 20 °C $min^{-}1$. UHP helium was used as the carrier gas. All NMR spectra were recorded on either Bruker Avance-400, Varian Mercury-400, Varian Inova-500 or Varian VNMRS 700 spectrometers at the following frequencies: ^{1}H: 200, 400, 500 and 700 MHz; ^{13}C: 126, 151 and 176 MHz; ^{19}F: 658.4 MHz. NMR spectra were recorded in $CDCl_3$ (where tetramethylsilane (TMS) was used as the internal standard), CD_3OD, or DMSO-d_6. The chemical shifts are reported in ppm relative to the residual protic solvent peak as reference, and spin multiplicities are indicated by the following symbols: s (singlet), d (doublet), dd (doublet of doublets), ddd (doublet of doublet of doublets), t (triplet), m (multiplet); J coupling constants are given in Hz. ES-MS was performed by the Durham University departmental service using an Acquity TQD (Waters UK Ltd) mass spectrometer and accurate mass measurements were obtained

on a Thermo LTQ-FT spectrometer. Elemental analyses were carried out using an Exeter Analytical E440 machine. Samples for HPLC analysis were submitted to the Durham University departmental service, and run on a C18 column at 20 °C, with a flow rate of 1 mL/min, and a wavelength of 254 nm was used for sample detection. IR spectra were recorded on a Perkin Elmer FT-IR spectrometer with an ATR attachment. Melting point values were measured on a Sanyo Gallenkamp apparatus and are uncorrected. Predicted low-energy conformation calculations were performed using Spartan 10, version 1.1.0 (Wavefunction Inc., 18410 Von Karman Ave., Suite 370, Irvine, CA 92612, USA; www.wavefun.com).

6.2. Synthetic procedures for thiazole-containing retinoids

4-(4-Hydroxy-5-methyl-thiazol-2-yl)-benzoic acid ethyl ester (5)

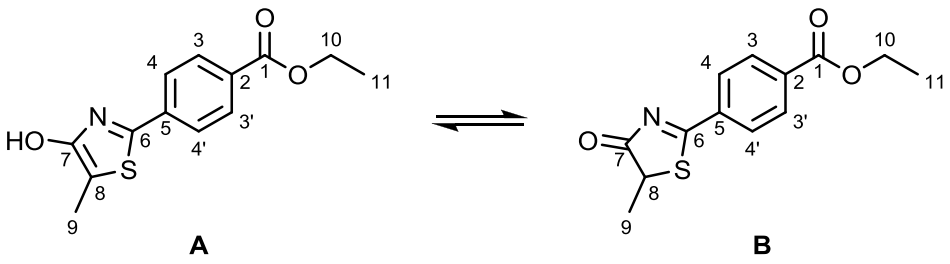

Ethyl 4-cyanobenzoate (1.29 g, 7.4 mmol), 2-mercaptopropionic acid (0.64 mL, 7.4 mmol) and pyridine (0.59 mL, 7.4 mmol) were thoroughly mixed in a MW vial and heated at 150 °C for 75 min (5 × 15 min periods). The resulting yellow solid was dissolved in ethyl acetate (60 mL). Undissolved material was removed by filtration, and recrystallisation from ethyl acetate produced yellow crystals that were washed with acetonitrile to provide compound **5** as a yellow crystalline solid (1.50 g, 77%): m.p. 203-205 °C;

A: ^{1}H NMR (700 MHz; $CDCl_3$) δ 8.11 (unsymmet. d, J = 8.4, 2H, $H_{3+3'}$), 7.88 (unsymmet. d, J = 8.4, 2H, $H_{4+4'}$), 4.40 (q, J = 7.0, 2H, H_{10}), 2.36 (s, 3H, H_9), 1.42 (t, J = 7.0, 3H, H_{11}); ^{13}C NMR (176 MHz; $CDCl_3$) δ 166.0 (C_1), 159.3 (C_6), 158.7 (C_7), 136.5 (C_5), 131.1 (C_2), 130.3 ($C_{3+3'}$), 125.4 ($C_{4+4'}$), 105.6 (C_8), 61.7 (C_{10}), 14.3 (C_{11}), 9.4 (C_9);

B: ^{1}H NMR (700 MHz; $CDCl_3$) δ 8.20-8.13 (m, 4H, H_{3+4}), 4.41 (q, J = 7.0, 2H, H_{10}), 4.29 (q, J = 7.0, 1H, H_9), 1.76 (d, J = 7.0, 3H, H_9), 1.43 (t, J = 7.0, 3H, H_{11}); ^{13}C NMR (176 MHz, $CDCl_3$) δ 193.8 (C_7), 165.3 (C_1), 159.1 (C_6), 135.9 (C_5), 135.5 (C_2), 130.0 ($C_{3+3'}$), 128.6 ($C_{4+4'}$), 61.7 (C_{10}), 49.4 (C_8), 18.1 (C_9), 14.2 (C_{11});

IR (neat) ν_{max}/cm^{-1} 2980w (C-$H_{aliphatic}$), 1709s (C=O_{ester}), 1580w (C=$C_{ar.}$), 1514w (C=$C_{ar.}$), 1466w (C=$C_{ar.}$), 1271s (C-O_{ester}), 1104s (C-O_{ester}), 856m (C-$H_{ar.}$); MS (ES): *m/z* = 264 [M + 1]$^{+}$; UV-vis (EtOH) λ_{max}/nm (ε/M^{-1} cm^{-1}): 204 (5 770), 244 (4 950), 356 (5 000). Anal. calcd for $C_{13}H_{13}NO_3S$: C, 59.30; H, 4.98; N, 5.32. Found: C, 58.99; H, 4.97; N, 5.34.

4-(5-Methyl-4-trifluoromethanesulfonyloxy-thiazol-2-yl)-benzoic acid ethyl ester (6)

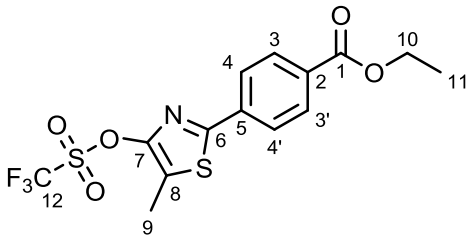

N,*N*-Diisopropylethylamine (2.65 mL, 15.2 mmol) was added to a stirred solution of 4-(4-hydroxy-5-methyl-thiazol-2-yl)-benzoic acid ethyl ester **5** (2.0 g, 7.60 mmol) in dichloromethane (30 mL). The flask was cooled to -78 °C, after which trifluoromethanesulfonic anhydride (4.4 g, 15.2 mmol) was carefully added. The reaction was allowed to warm slowly to room temperature and was stirred overnight under a nitrogen atmosphere. Dichloromethane (30 mL) and water (30 mL) were added, and the product extracted with dichloromethane (3 x 50 mL). The organic extracts were combined and washed three times with water (3 x 100 mL). After drying with $MgSO_4$, the solvent was removed *in vacuo* and the brown residue purified by flash chromatography to give a yellow oil, R_f. 0.32 (hexane:EtOAc, 8:2, as eluent). Recrystallisation from hexane provided compound **6** as an off-white crystalline solid (2.1 g, 70%): m.p. 48-50 °C; ^{1}H NMR (700 MHz; $CDCl_3$) δ 8.10 (unsymmet. d, J = 8.4, 2H, $H_{3+3'}$), 7.91 (unsymmet. d, J = 8.4, 2H, $H_{4+4'}$), 4.40 (q, J = 7.0, 2H, H_{10}), 2.49 (s, 3H, H_9), 1.42 (t, J = 7.0, 3H, H_{11}); ^{13}C NMR (176 MHz; $CDCl_3$) δ 165.9 (C_1), 161.2 (C_6), 148.3 (C_7),

136.2 (C_5), 132.4 (C_2), 130.4 ($C_{3+3'}$), 125.7 ($C_{4+4'}$), 122.4 (C_8), 119.7 (C_{12}), 61.5 (C_{10}), 14.5 (C_{11}), 10.2 (C_9); ^{19}F NMR (658.4 MHz; $CDCl_3$) δ 72.5; IR (neat) ν_{max}/cm^{-1} 1712s (C=O_{ester}), 1550m (C=$C_{ar.}$), 1422s (C=$C_{ar.}$), 1274m (C-O_{ester}), 1221s (C-O_{ester}), 1137s (C-F), 1093s (C-F), 769s (C-$H_{ar.}$), 694s (C-$H_{ar.}$) , 602s (C-$H_{ar.}$); MS (ES$^+$): *m/z* = 263 [M - CF_3SO_2]$^+$, 396 [M + 1]$^+$, 418 [M + Na]$^+$; UV-vis (EtOH) λ_{max}/nm (ε/M^{-1} cm^{-1}): 312 (23 100). Anal. calcd for $C_{14}H_{12}F_3NO_5S_2$: C, 42.53; H, 3.06; N, 3.54. Found: C, 42.50; H, 3.07; N, 3.48.

4-(5-Methyl-4-phenyl-thiazol-2-yl)-benzoic acid ethyl ester (9)

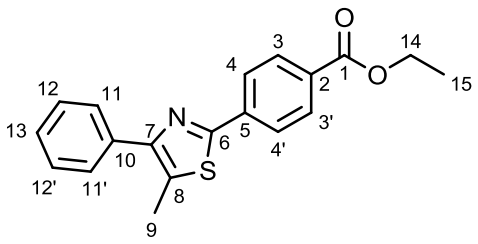

4-(5-Methyl-4-trifluoromethanesulfonyloxy-thiazol-2-yl)-benzoic acid ethyl ester **6** (500 mg, 1.26 mmol), phenylboronic acid pinacol ester (284 mg, 1.39 mmol), K_3PO_4 (537 mg, 2.53 mmol) and Pd(dppf)Cl_2 (28 mg, 0.0383 mmol, 3 mol%) were combined in DMF and H_2O (10 mL, 10:1) in a Schlenk tube under an inert nitrogen atmosphere and heated at 80 °C for 18 h. The mixture was dissolved in diethyl ether and washed twice with water. The organic layer was dried using $MgSO_4$ and the solvent removed *in vacuo* to give an orange/brown residue that was purified by column chromatography (3→5% EtOAc:hexane) to give a white solid following *in vacuo* removal of the solvent, R_f. 0.28 (hexane:EtOAc, 9:1, as eluent). Recrystallisation from ethanol provided compound **9** as a white crystalline solid (246 mg, 60%): m.p. 85-87 °C; ^{1}H NMR (700 MHz; $CDCl_3$) δ 8.10 (unsymmet. d, *J* = 8.4, 2H, $H_{3+3'}$), 8.03 (unsymmet. d, *J* = 8.4, 2H, $H_{4+4'}$), 7.73 (unsymmet d, *J* = 7.0, 2H, $H_{11+11'}$), 7.47 (unsymmet. t, *J* = 7.7, 2H, $H_{12+12'}$), 7.38 (unsymmet. t, *J* = 7.7, 1H, H_{13}), 4.40 (q, *J* = 7.0, 2H, H_{14}), 2.64 (s, 3H, H_9), 1.42 (t, *J* = 7.0, 3H, H_{15}); ^{13}C NMR (176 MHz; $CDCl_3$) δ 166.3 (C_1), 162.4 (C_6), 152.8 (C_7), 137.7 (C_5), 135.0 (C_{10}), 131.3 (C_2), 130.3 ($C_{3+3'}$), 129.8 (C_8), 128.8 ($C_{11+11'}$), 128.6 ($C_{12+12'}$), 127.9 (C_{13}), 126.2 ($C_{4+4'}$), 61.3 (C_{14}), 14.5 (C_{15}), 13.1 (C_9); IR (neat) ν_{max}/cm^{-1} 1706s (C=O_{ester}), 1278s (C-O_{ester}), 1101s (C-O_{ester}), 860s (C-$H_{ar.}$), 768s (C-$H_{ar.}$), 699s (C-$H_{ar.}$) ; MS (ES$^+$): *m/z*

= 324 $[M + 1]^+$, 325 $[M + 2]^+$, 670 $[2M + Na]^+$; UV-vis (EtOH) λ_{max}/nm (ε/M^{-1} cm^{-1}): 254 (22 400), 330 (18 100). Anal. calcd for $C_{19}H_{17}NO_2S$: C, 70.56; H, 5.30; N, 4.33. Found: C, 70.62; H, 5.32; N, 4.44.

4-[5-Methyl-4-(5,5,8,8-tetramethyl-5,6,7,8-tetrahydro-naphthalen-2-yl)-thiazol-2-yl]-benzoic acid ethyl ester (10)

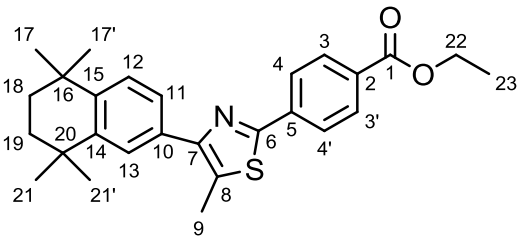

4-(5-Methyl-4-trifluoromethanesulfonyloxy-thiazol-2-yl)-benzoic acid ethyl ester **6** (500 mg, 1.26 mmol), 1,1,4,4-tetramethyl-1,2,3,4-tetrahydronaphthylboronic acid pinacol ester (477 mg, 1.52 mmol), K_3PO_4 (537 mg, 2.53 mmol) and $Pd(dppf)Cl_2$ (28 mg, 0.0383 mmol, 3 mol%) were combined in DMF and H_2O (10 mL, 10:1) in a Schlenk tube under an inert nitrogen atmosphere. After heating to 80 °C for 18 hours, the cooled mixture was dissolved in diethyl ether (20 mL) and washed with water (2 x 20 mL) and the organic layer was dried using $MgSO_4$. The solvent was removed *in vacuo*, and the residue was purified by flash chromatography, R_f. 0.33 (hexane:EtOAc, 9:1, as eluent). Following *in vacuo* removal of the solvent, recrystallisation of the resulting white solid from ethanol afforded the title product in the form of fluffy white crystals (410 mg, 75%): m.p. 161-162 °C; ^{1}H NMR (700 MHz; $CDCl_3$) δ 8.09 (unsymmet. d, J = 8.4, 2H, $H_{3+3'}$), 8.03 (unsymmet. d, J = 8.4, 2H, $H_{4+4'}$), 7.61 (d, J = 1.4, 1H, H_{11}), 7.49 (dd, J = 8.4 and 2.1, 1H, H_{12}), 7.40 (unsymmet. d, J = 8.4, 1H, H_{13}), 4.40 (q, J = 7, 2H, H_{22}), 2.63 (s, 3H, H_9), 1.73 (s, 4H, H_{18+19}), 1.42 (t, J = 7, 3H, H_{23}), 1.34 (s, 6H, $H_{17+17'}$), 1.32 (s, 6H, $H_{21+21'}$); ^{13}C NMR (176 MHz; $CDCl_3$) δ 166.3 (C_1), 162.1 (C_6), 153.3 (C_7), 144.9 (C_{15}), 144.7 (C_{10}), 137.9 (C_5), 132.1 (C_{14}), 131.2 (C_2), 130.2 ($C_{3+3'}$), 129.2 (C_8), 127.0 (C_{11}), 126.9 (C_{13}), 126.2 ($C_{4+4'}$), 126.0 (C_{12}), 61.3 (C_{22}), 35.2 (C_{18+19}), 34.5 (C_{16}), 34.4 (C_{20}), 32.1 ($C_{17+17'}$), 32.0 ($C_{21+21'}$), 14.5 (C_{23}), 13.1 (C_9); IR (neat) ν_{max}/cm^{-1} 1707s (C=O_{ester}), 1270s (C-O_{ester}), 1102s (C-O_{ester}), 772s (C-$H_{ar.}$); MS (ES^+): *m/z* = 434 $[M + 1]^+$; UV-vis (EtOH)

λ_{max}/nm (ε/M^{-1} cm^{-1}): 262 (27 400), 335 (17 600). Anal. calcd for $C_{27}H_{31}NO_2S$: C, 74.79; H, 7.21; N, 3.23. Found: C, 74.67; H, 7.22; N, 3.17.

4-(5-Methyl-4-phenyl-thiazol-2-yl)-benzoic acid (1)

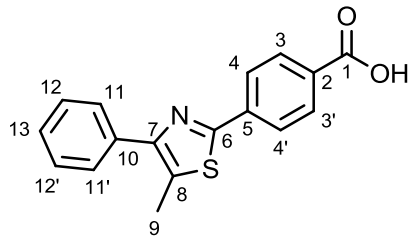

4-(5-Methyl-4-phenyl-thiazol-2-yl)-benzoic acid ethyl ester **9** (100 mg, 0.31 mmol) and $LiOH{\cdot}H_2O$ (39 mg, 0.93 mmol) were mixed in THF:H_2O (2 mL, 3:1 ratio) in a MW vial and irradiated at 160 °C for 15 min, after which the cooled reaction mixture was acidified with 1 M HCl and ethyl acetate (5 mL) was added. The organic layer was washed with brine (2 x 5 mL) and dried with $MgSO_4$. After *in vacuo* solvent removal, the residue was recrystallised from ethanol to give the title compound as a white crystalline solid (81 mg, 88%): m.p. 267-269 °C; ^{1}H NMR (500 MHz; DMSO-d_6) δ 8.05 (s, 4H, H_{3+4}), 7.76 (dd, J = 8.0 and 1.5, 2H, $H_{11+11'}$), 7.51 (td, J = 7.5 and 1.5, 2H, $H_{12+12'}$), 7.42 (tt, J = 7.5 and 1.5, 1H, H_{13}), 2.64 (s, 3H, H_9): ^{13}C (125.6 MHz, DMSO-d_6) 167.7 (C_1), 162.3 (C_6), 152.5 (C_7), 137.5 (C_5), 135.3 (C_{10}), 131.2 (C_2), 131.1 (C_8), 129.4 (C_{11}), 129.2 (C_{12}), 128.8 (C_{13}), 126.8 (C_{3+4}), 13.6 (C_9); IR (neat) ν_{max}/cm^{-1} 2847s (O-H), 1674s (C=O), 1284s (C-O), 858s (C-$H_{ar.}$), 771s (C-$H_{ar.}$), 700s (C-$H_{ar.}$), 681s (C-$H_{ar.}$); MS (ES^-): *m/z* = 294 $[M - H]^-$; UV-vis (EtOH) λ_{max}/nm (ε/M^{-1} cm^{-1}): 255 (23 000), 329 (19 000). Anal. calcd for $C_{17}H_{13}NO_2S$: C, 69.13; H, 4.44; N, 4.74. Found C, 68.79; H, 4.46; N, 4.74.

4-[5-Methyl-4-(5,5,8,8-tetramethyl-5,6,7,8-tetrahydro-naphthalen-2-yl)-thiazol-2-yl]-benzoic acid (2)

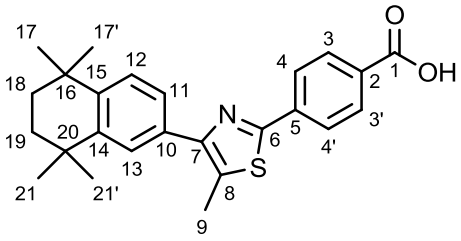

4-[5-Methyl-4-(5,5,8,8-tetramethyl-5,6,7,8-tetrahydro-naphthalen-2-yl)-thiazol-2-yl]-benzoic acid ethyl ester **10** (100 mg, 0.23 mmol) and $LiOH \cdot H_2O$ (29 mg, 0.69 mmol) were mixed in THF:H_2O (2 mL, 3 : 1 ratio) in a MW vial. After irradiation at 160 °C for 15 min, the reaction mixture was acidified with 1 M HCl and ethyl acetate (5 mL) was added. The organic layer was washed with brine (2 x 5 mL) and dried with $MgSO_4$. After *in vacuo* removal of the solvent, the residue was recrystallised from ethanol to give the title compound as a white crystalline solid (80 mg, 85%); m.p. 276-278 °C; ^{1}H NMR (500 MHz; DMSO-d_6) δ 8.07-8.02 (m, 4H, H_{3+4}), 7.63 (d, J = 2, 1H, H_{11}), 7.49 (dd, J = 8.0 and 2.0, 1H, H_{12}), 7.44 (unsymmet. d, J = 8.5, 1H, H_{13}), 2.62 (s, 3H, H_9), 1.69 (s, 4H, H_{18+19}), 1.31 (s, 6H, $H_{17+17'}$), 1.29 (s, 6H, $H_{21+21'}$); ^{13}C NMR (125.6 MHz; DMSO-d_6) δ 166.8 (C_1), 161.2 (C_6), 152.1 (C_7), 144.3 (C_{15}), 144.1 (C_{10}), 136.6 (C_5), 131.6 (C_{14}), 130.3 (C_2), 129.7 (C_{3+4}), 126.6 (C_8), 126.3 (C_{11}), 125.9 (C_{13}), 125.7 (C_{12}), 34.6 (C_{18+19}), 34.5 (C_{16}), 34.0 (C_{20}), 31.7 ($C_{17+17'}$), 31.6 ($C_{21+21'}$), 12.7 (C_9); IR (neat) ν_{max}/cm^{-1} 2929s (O-H), 1681s (C=O), 1279s (C-O), 773s (C-$H_{ar.}$); MS (ES^+): *m/z* = 404 $[M + H]^+$; UV-vis (EtOH) λ_{max}/nm (ε/M^{-1} cm^{-1}): 261 (27 000), 333 (17 000). Anal. calcd for $C_{25}H_{27}NO_2S$: C, 74.04; H, 6.71; N, 3.45. Found: C, 73.42; H, 6.75; N, 3.53.

6.3. Biological procedures

Tissue culture

Stock solutions of ATRA (Sigma-Aldrich, UK), EC23 (Reinnervate, Sedgefield, UK), compound **1**, and compound **2** were prepared in dimethyl sulfoxide (DMSO, Sigma) to concentrations of 10 mM. Aliquots of these stock solutions were stored at -80 °C in the

dark and thoroughly defrosted in a water bath set at 37 °C prior to use. Unless otherwise stated, all plastic-ware was purchased from Becton, Dickinson and Company. Phase contrast images of cultures were obtained using a light microscope (Nikon Diaphot 300) and photomicrographs were captured using digital photography (Nikon). Scale bars were calibrated and added to images using ImageJ. Human pluripotent TERA2.cl.SP12 embryonal carcinoma stem cells were cultured in DMEM (Sigma) supplemented with 10% FCS (Lonza, UK; http://www.lonza.com), 2 mM L-glutamine (Lonza) and 100 active units each of penicillin and streptomycin (Lonza). Cells were maintained in a humidified atmosphere of 5% CO_2 in air at 37 °C in a Sanyo CO2 incubator and handled under sterile conditions in a Class 1 microbiological safety cabinet. Cultures were passaged using sterile acid-washed glass beads (VWR, UK; https://uk.vwr.com) or trypsinised using a solution of 0.25% (w/v) trypsin (Life Technologies, UK; https://www.lifetechnologies.com) and 2 mM EDTA in PBS to obtain a single-cell suspension for counting. 96-Well plates were used for cell viability studies, and cultures intended for flow cytometric analyses were set up in T25 flasks. Human neural progenitor ReNcell 197VM cells (Millipore, UK; http://www.millipore.com) were maintained under the laboratory conditions described above. Before establishing cell cultures, a 20 µg mL^{-1} concentration of laminin solution was applied to all plastic-ware, which was incubated at 37 °C for 6 h then rinsed once with culture medium. Cells were maintained in serum-free conditions with DMEM:F12 (1:1, Gibco, Life Technologies) supplemented with B27 (Invitrogen, Life Technologies), 2 mM L-glutamine, gentamycin (Gibco), and 50 mg mL^{-1} heparin solution (Sigma). For proliferation, 10 ng mL^{-1} fibroblast growth factor (FGF) and 20 ng mL^{-1} epidermal growth factor (EGF) were added to the culture media before applying to cells. Cells were trypsinised as described above.

Neurite outgrowth assay

TERA2.cl.SP12 EC cells were maintained as described above. Aggregates of TERA2.cl.SP12 EC cells were produced by creating a single-cell suspension and adding 1.5×10^6 cells per 20 mL of maintenance media to a 90 mm un-treated Petri dish. The

cells were left to aggregate overnight and subsequently treated with the test compound. Aggregates were cultured for 21 d in the presence of the test compound to induce neural commitment and the production of neurospheres prior to analysis of neurite outgrowth. To induce neurite outgrowth, a 48-well tissue culture plate was used: the well was coated with a solution of 10 μg mL^{-1} laminin (Sigma) and poly-D-lysine (Sigma) overnight. The tissue culture was washed three times with sterile PBS prior to the addition of the neurospheres, which were added to the permissive substrate in the presence of the mitotic inhibitors: 5-fluoro-2-deoxyuridine (10 μM), uridine (10 μM), and cytosine-arabinoside (1 μM) in the TERA2.cl.SP12 maintenance media described previously, and incubated at 37 °C under 5% CO_2 for 10 d. Neurospheres where then fixed in 4% PFA and visualised by immunocytochemical staining of the TUJ-1 antibody. Neurites were imaged using the Nikon Diaphot 300 and quantified using Image J.

Cell viability assay

Cells were assessed for viability by combining a single-cell suspension (achieved by the addition of 1 mL, 0.25% trypsin/EDTA solution) of live cells with detached dead cells contained in the culture medium from each flask. Cell numbers were determined using a haemocytometer. Cells were required to be diluted 1:20 in a staining solution for the Viacount assay and added to a 96-well plate. The number of viable cells, percentage viabilities, and total cell numbers were recorded in triplicate for each experimental condition.

Flow cytometric analysis of pluripotent TERA2.cl.SP12 EC cells

At each time point (except for the negative control flasks, which were processed for analysis after 3 d), cultures were washed with PBS and treated with trypsin to obtain a single-cell suspension as described above. Cells were washed three times with PBS to ensure complete removal of trypsin. After centrifugation of the cell mixture and removal of the supernatant, the cell pellet was re-suspended in 0.1% bovine serum albumin (BSA) solution and counted using a haemocytometer. 200 000 cells per well

were added to a 96-well plate according to the experimental plan. After centrifugation of the plate at 1000 rpm for 3 min, and removal of the supernatant, cells were re-suspended in 50 µL of the appropriate primary antibody. Each triplicate set of culture conditions (ATRA, compounds **1** and **2**, as well as the DMSO-supplemented flasks [on day 3 only]) was analysed at each time point for expression of the following three antigens: SSEA-3 (antibody diluted 1:5 in 0.1% BSA), TRA-1-60 (diluted 1:10) and A2B5 (diluted 1:40). These primary monoclonal antibodies were used as they recognise specific cell surface antigens associated with globoseries glycolipids, glycoproteins and ganglioseries, displaying highly regulated expression profiles in response to differentiation of human EC cells. One well containing undifferentiated control cells was incubated with the mouse myeloma marker anti-P3X as a negative control. The plate was incubated on ice for 1 h, after which excess unbound antibody was removed by the addition of 100 µL ice-cold 0.1% BSA, centrifugation was performed as above and the supernatant was removed. Two further washings were carried out with 180 µl 0.1% BSA, after which cells were re-suspended with the fluorescent secondary antibody FITC (fluorescein isothiocyanate-conjugated) goat anti-mouse IgM (ICN Pharmaceuticals, Inc.; Aurora, OH; http://www.icnpharm.com) diluted 1:100 in 0.1% BSA. After incubating the plate in the dark for 1 h on ice, cells were washed three times with 0.1% BSA as described above, and re-suspended in 200 µL 0.1% BSA for analysis. Cell surface antigen expression on TERA2.cl.SP12 stem cells and their compound-induced derivatives was observed by indirect immunofluorescence and quantified using a flow cytometer (Guava Easycyte). A fluorescence threshold was set such that cells fluorescing with a greater intensity than approximately 95% of the cells incubated with the negative control antibody P3X were counted as antigen positive.

Immunocytochemistry with human pluripotent TERA2.cl.SP12 EC cells and neuroprogenitor ReN197 VM cells

Cells were fixed in 4% paraformaldehyde (PFA) in PBS (Sigma) for 30 min at r.t. and rinsed with PBS. Cell membranes were permeabilised by treatment with 1% Triton-X-100 (Sigma) in PBS for 10 min at r.t. Non-specific labelling was blocked by incubation

on a bench-top shaker (Fisher Scientific, UK; http://www.fisher.co.uk) for 1 h at r.t. with a solution of 1% goat serum (Sigma) containing 0.2% Tween-20 (Sigma) in PBS. Primary antibodies were diluted in blocking solution and incubated with cells for 1 h at r.t. [β-III tubulin antibody (TUJ1, Covance, UK; http://www.covance.com, diluted 1:600); NF-200 antibody (AbCam, Cambridge, MA; http://www.abcam.com, diluted 1:200)]. After washing three times for 15 min with PBS cells were incubated for 1 h in the dark with FITC-conjugated (anti-mouse Alexafluor 488, Invitrogen, diluted 1:600), Cy3-conjugated (anti-rabbit Cy3, JacksonLabs, UK; http://www.jireurope.com, diluted 1:600) fluorescently-labelled secondary antibodies and Hoechst 33342 nuclear staining dye (Molecular Probes, Life Technologies, diluted 1:1000) in blocking solution. Cells were washed twice more with PBS and left in the final wash for immediate imaging. Fluorescence micrographs, including Hoecsht 3342, were acquired using the appropriate filter sets and an adapted digital camera (Nikon).

6.4. Synthetic procedures for a fluorescent retinoid

2-Methyl-*N*-(propan-2-yl)aniline (24)

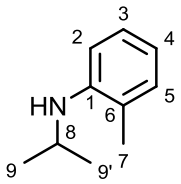

2-Iodopropane (40 mL, 400 mmol) was added to a refluxing mixture (105 °C) of *o*-toluidine (21.4 mL, 200 mmol) and powdered sodium hydroxide (20 g, 500 mmol). This was heated to reflux for 12 h under an inert argon atmosphere. The mixture was filtered, diluted with diethyl ether (100 mL), and washed with water (3 x 30 mL). The solvent was removed *in vacuo* and the residue purified by column chromatography on basic alumina (hexane:EtOAc, 95:5, as eluent), to afford compound **24** as a yellow oil (24.6 g, 82%): R_f. 0.51 (hexane:EtOAc, 95:5, as eluent); ^{1}H NMR (500 MHz; $CDCl_3$) δ 7.18 (dt, J = 7.5 and 1.5, 1H, H_3), 7.11 (dd, J = 7.5 and 0.5, 1H, H_5), 6.71-6.67 (m, 2H, H_{2+4}), 3.74 (septet, J = 6.5, 1H, H_8), 3.36 (br s, 1H, NH), 2.18 (s, 3H, H_7), 1.31 (d, J = 6.5,

6H, $H_{9+9'}$); ^{13}C NMR (176 MHz; $CDCl_3$) δ 145.5 (C_1), 130.3 (C_5), 127.2 (C_3), 121.8 (C_6), 116.5 (C_2), 110.3 (C_4), 44.1 (C_8), 23.3 ($C_{9+9'}$), 17.7 (C_7); IR (neat) ν_{max}/cm^{-1} 2965m (C-H_{methyl}), 1606s (C=$C_{ar.}$), 1512s (C=$C_{ar.}$), 1478m (C=$C_{ar.}$), 1382m (C-H_{methyl}); MS (ES^+): *m/z* = 150 $[M + H]^+$; UV-vis ($CHCl_3$) λ_{max}/nm ($\varepsilon/M^{-1}\,cm^{-1}$): 246 (42 900), 297 (11 000); HRMS (ES) calcd for $C_{10}H_{16}N$ $[M + H]^+$: 150.1279, found: 150.1283.

2-Methyl-*N*-(3-methylbut-2-en-1-yl)-*N*-(propan-2-yl)aniline (25)

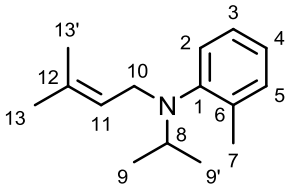

2-Methyl-*N*-(propan-2-yl)aniline **24** (11.3 g, 76 mmol) and 3,3-dimethylallyl bromide (9.7 mL, 84 mmol) were dissolved in acetonitrile (200 mL). Powdered potassium carbonate (11.6 g, 84 mmol) was added and the flask heated to reflux (70 °C) overnight under an inert argon atmosphere. The mixture was filtered and the solvent removed *in vacuo* to give a dark residue that was purified by column chromatography on basic alumina, providing compound **25** as a yellow oil (11.5 g, 70%): R_f. 0.55 (hexane as eluent); ^1H NMR (700 MHz; $CDCl_3$) δ 7.19 (unsymmet. d, *J* = 7.7, 1H, H_5), 7.11 (unsymmet. t, *J* = 7.7, 1H, H_3), 7.04 (unsymmet. d, *J* = 7.7, 1H, H_2), 6.96 (unsymmet. t, *J* = 7.7, 1H, H_4), 5.02 (t, *J* = 6.3, 1H, H_{11}), 3.60 (d, *J* = 6.3, 2H, H_{10}), 3.22 (septet, *J* = 7.0, 1H, H_8), 2.31 (s, 3H, H_7), 1.61 and 1.60 (s, 3H, $H_{13+13'}$), 1.10 (d, *J* = 7.0, 6H, $H_{9+9'}$); ^{13}C NMR (176 MHz; $CDCl_3$) δ 150.1 (C_1), 135.7 (C_6), 132.6 (C_{12}), 130.9 (C_5), 125.6 (C_3), 123.7 (C_2), 123.1 (C_4), 123.0 (C_{11}), 53.0 (C_8), 44.2 (C_{10}), 25.8 and 18.5 ($C_{13+13'}$), 19.7 ($C_{9+9'}$), 18.5 (C_7); IR (neat) ν_{max}/cm^{-1} 2968s (C-H_{methyl}), 2929m (C-H_{vinyl}), 1598m (C=$C_{ar.}$), 1490s (C=$C_{ar.}$), 1449m (C=$C_{ar.}$), 1380m (C-H_{methyl}), 1360m (C-H_{methyl}); MS (ES^+): *m/z* = 218 $[M + H]^+$; UV-vis ($CHCl_3$) λ_{max}/nm ($\varepsilon/M^{-1}\,cm^{-1}$): 260 (13 700), 243sh (11 600); HRMS (ES) calcd for $C_{15}H_{24}N$ $[M + H]^+$: 218.1903, found: 218.1906.

1-Isopropyl-4,4,8-trimethyl-1,2,3,4-tetrahydroquinoline (26)

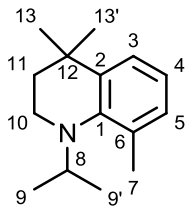

2-Methyl-*N*-(3-methylbut-2-en-1-yl)-*N*-(propan-2-yl)aniline **25** (10.6 g, 49 mmol) and polyphosphoric acid (60 g) were heated to 120 °C for 24 h. The mixture was diluted with water (50 mL), and aqueous potassium hydroxide carefully added until neutral. The reaction mixture was extracted with diethyl ether (500 mL) , and the combined organic layers were washed with water (3 x 100 mL). After drying with $MgSO_4$, the mixture was filtered, and the solvent removed *in vacuo* to give a crude oil which was purified by flash chromatography on silica gel (hexane:EtOAc, 9:1, as eluent), to afford compound **26** as a yellow oil (8.2 g, 78%): R_f. 0.64 (hexane:EtOAc, 9:1, as eluent); ^{1}H NMR (700 MHz; $CDCl_3$) δ 7.15 (dd, J = 7.7 and 1.4, 1H, H_3), 6.97 (dd, J = 7.0 and 0.7, 1H, H_5), 6.79 (t, J = 7.7, 1H, H_4), 3.55 (septet, J = 7.0, 1H, H_8), 3.15-3.12 (m, 2H, H_{10}), 2.26 (s, 3H, H_7), 1.68-1.65 (m, 2H, H_{11}), 1.28 (s, 6H, $H_{13+13'}$), 1.15 (d, J = 7.0, 6H, $H_{9+9'}$); ^{13}C NMR (176 MHz; $CDCl_3$) δ 146.0 (C_1), 138.0 (C_2), 130.1 (C_6), 129.6 (C_5), 124.1 (C_3), 120.0 (C_4), 53.0 (C_8), 38.5 (C_{10}), 37.8 (C_{11}), 32.5 (C_{12}), 32.2 ($C_{13+13'}$), 20.8 ($C_{9+9'}$), 20.5 (C_7); IR (neat) ν_{max}/cm^{-1} 2959s (C-H_{methyl}), 1591w (C=$C_{ar.}$), 1464s (C=$C_{ar.}$), 1426s (C=$C_{ar.}$), 1130s (C-N); MS (ES$^+$): *m/z* = 218 [M + H]$^+$; UV-vis ($CHCl_3$) λ_{max}/nm (ε/M^{-1} cm^{-1}): 261 (20 000), 298sh (6 600); HRMS (ES) calcd for $C_{15}H_{24}N$ [M + H]$^+$: 218.1903, found: 218.1904.

6-Bromo-1-isopropyl-4,4,8-trimethyl-1,2,3,4-tetrahydroquinoline (28)

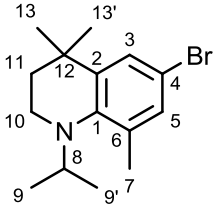

A stirred solution of 1-isopropyl-4,4,8-trimethyl-1,2,3,4-tetrahydroquinoline **26** (2.30 g, 10.6 mmol) in chloroform (20 mL) was cooled in an acetone bath fitted with a cryostat set at a temperature of -60 °C. Bromine liquid (515 µl, 10.1 mmol, 0.95 equiv.) was then added dropwise to the stirred reaction mixture. The temperature was raised gradually to -30 °C over a period of 1 h, after which the mixture was washed with a saturated solution of $NaHCO_3$ (3 x 20 mL), and the organic phase dried with $MgSO_4$. Following *in vacuo* removal of the solvent, the crude oil was purified by filtering through a pad of neutral alumina (hexane:EtOAc, 9:1, as eluent). Monobromide **28** was obtained as a colourless oil (1.95 g, 62%) after *in vacuo* removal of the solvent: R_f. 0.46 (hexane as eluent); ^{1}H NMR (600 MHz; $CDCl_3$) δ 7.21 (d, J = 2.4, 1H, H_3), 7.08 (d, J = 2.4, 1H, H_5), 3.48 (septet, J = 6.6, 1H, H_8), 3.12-3.09 (m, 2H, H_{10}), 2.22 (s, 3H, H_7), 1.65-1.62 (m, 2H, H_{11}), 1.26 (s, 6H, $H_{13+13'}$), 1.13 (d, J = 6.6, 6H, $H_{9+9'}$); ^{13}C NMR (151 MHz; $CDCl_3$) δ 145.2 (C_1), 140.2 (C_2), 132.4 (C_6), 132.0 (C_5), 126.8 (C_3), 112.6 (C_4), 53.1 (C_8), 38.4 (C_{10}), 37.3 (C_{11}), 32.8 (C_{12}), 31.9 ($C_{13+13'}$), 20.7 ($C_{9+9'}$), 20.3 (C_7); IR (neat) ν_{max}/cm^{-1} 2960s (C-H_{methyl}), 1468s (C=$C_{ar.}$), 860s (C-$H_{ar.}$), 829m (C-$H_{ar.}$), 742m (C-$H_{ar.}$); MS (EI): *m/z* = 296 and 298 $[M + H]^+$; UV-vis (EtOH) λ_{max}/nm (ε/M^{-1} cm^{-1}): 272 (16 500); HRMS (ES) calcd for $C_{15}H_{23}BrN$ $[M + H]^+$: 296.1014, found: 296.1004.

3,6-Dibromo-1-isopropyl-4,4,8-trimethyl-1,4-dihydroquinoline (31)

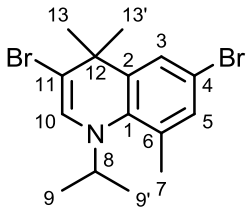

2,6-Lutidine (2.23 mL, 19.1 mmol) and Br_2 liquid (490 µl, 9.57 mmol) were added to a stirred solution of 1-isopropyl-4,4,8-trimethyl-1,2,3,4-tetrahydroquinoline **26** (520 mg, 2.39 mmol) in chloroform (20 mL). The mixture was heated to 60 °C and stirred overnight. Starting material consumption was indicated by ^{1}H NMR analysis, after which chloroform (50 mL) was added and the organic layer washed with 2.5% aqueous HCl (3 x 50 mL), and 1M aqueous $NaHCO_3$ (3 x 50 mL). After drying with $MgSO_4$, and

removal of the solvent *in vacuo*, a brown oil was obtained (976 mg) consisting mainly of dibromide **31**: ^{1}H NMR (400 MHz; $CDCl_3$) δ 7.21 (d, J = 1.6, 1H, H_3), 7.13 (d, J = 1.6, 1H, H_5), 6.35 (s, 1H, H_{10}), 3.59 (septet, J = 6.4, 1H, H_8), 2.24 (s, 3H, H_7), 1.49 (s, 6H, $H_{13+13'}$), 1.20 (d, J = 6.4, 6H, $H_{9+9'}$); ^{13}C NMR (176 MHz; $CDCl_3$) δ 140.2 (C_1), 138.0 (C_2), 132.7 (C_5), 130.4 (C_6), 128.4 (C_{10}), 127.6 (C_3), 115.7 (C_{11}), 115.5 (C_4), 53.7 (C_8), 39.7 (C_{12}), 32.1 ($C_{13+13'}$), 20.4 ($C_{9+9'}$), 20.2 (C_7); IR (neat) ν_{max}/cm^{-1} 2972s (C-H_{methyl}), 1464s (C=$C_{ar.}$), 1432s (C=$C_{ar.}$), 754s (C-$H_{ar.}$); MS (ES$^+$): *m/z* = 296 [M - Br]$^+$; UV-vis (EtOH) λ_{max}/nm (ε/M^{-1} cm^{-1}): 296 (4 900).

Methyl 4-iodobenzoate (45)

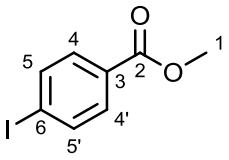

4-Iodobenzoic acid (12.2 g, 49 mmol) was dissolved in methanol (300 mL) with concentrated H_2SO_4 (2 mL), and refluxed at 70 °C overnight. Water (250 mL) was added and the mixture extracted with diethyl ether (3 x 150 mL). The organic layers were combined, washed with water (2 x 200 mL), dried over $MgSO_4$ and the solvent removed *in vacuo* to afford compound **45** in the form of white needles (12.5 g, 97%), which were sufficiently pure to be used without further purification: m.p. 116-117 °C (lit.,[194] 115-116 °C); R_f. 0.30 (hexane:EtOAc, 9:1, as eluent); ^{1}H NMR (700 MHz; $CDCl_3$) δ 7.80 (unsymmet. d, J = 8.4, 2H, $H_{5+5'}$), 7.74 (unsymmet. d, J = 8.4, 2H, $H_{4+4'}$), 3.91 (s, 3H, H_1); ^{13}C NMR (176 MHz; $CDCl_3$) δ 166.8 (C_2), 137.9 ($C_{5+5'}$), 131.2 ($C_{4+4'}$), 129.8 (C_3), 100.8 (C_6), 52.4 (C_1); IR (neat) ν_{max}/cm^{-1} 2948w (C-H_{methyl}), 1710s (C=O_{ester}), 1585s (C=$C_{ar.}$), 1436s (C=$C_{ar.}$), 1284s (C-H_{methyl}), 1272s (C-O_{ester}), 1107s (C-O_{ester}), 845s (C-$H_{ar.}$), 827s (C-$H_{ar.}$); MS (EI): *m/z* = 262 [M]$^+$, 231 [M - OCH_3]$^+$; UV-vis (EtOH) λ_{max}/nm (ε/M^{-1} cm^{-1}): 256 (12 100). Anal. calcd for $C_8H_7IO_2$: C, 36.67; H, 2.69. Found: C, 36.76; H, 2.71.

Methyl 3-iodobenzoate (46)

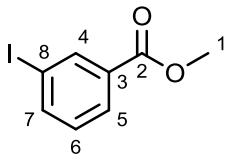

Procedure as for compound **45**, using 3-iodobenzoic acid (10.2 g, 41 mmol) to provide ester **46** as a white crystalline solid (10.2 g, 95%), which was sufficiently pure to be used without further purification: m.p. 49-50 °C (lit.,[195] 49-50 °C); R_f. 0.40 (hexane:EtOAc, 9:1, as eluent); ^{1}H NMR (500 MHz; $CDCl_3$) δ 8.38 (t, J = 1.5, 1H, H_4), 8.00 (dt, J = 7.5 and 1.5, 1H, H_5), 7.88 (dt, J = 7.5 and 1.5, 1H, H_7), 7.19 (t, J = 7.5, 1H, H_6), 3.92 (s, 3H, H_1); ^{13}C NMR (126 MHz; $CDCl_3$) δ 165.8 (C_2), 141.9 (C_7), 138.6 (C_4), 132.2 (C_3), 130.2 (C_6), 128.9 (C_5), 93.9 (C_8), 52.5 (C_1); IR (neat) ν_{max}/cm^{-1} 2948w (C-H_{methyl}), 1704s (C=O_{ester}), 1589w (C=$C_{ar.}$), 1567m (C=$C_{ar.}$), 1440s (C=$C_{ar.}$), 1277s (C-H_{methyl}), 1299s (C-O_{ester}), 1115s (C-O_{ester}), 740s (C-$H_{ar.}$), 704s (C-$H_{ar.}$); MS (EI): *m/z* = 262 $[M]^+$; UV-vis (EtOH) λ_{max}/nm (ε/M^{-1} cm^{-1}): 200 (19 700), 220 (22 400). Anal. calcd. for $C_8H_7IO_2$: C, 36.67; H, 2.69. Found: C, 36.75; H, 2.68.

Methyl 4-((trimethylsilyl)ethynyl)benzoate (47)

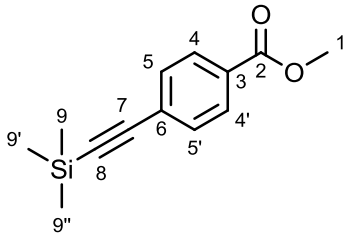

Methyl 4-iodobenzoate **45** (12.5 g, 48 mmol), Cu(I)I (0.09 g, 0.48 mmol), and $Pd(PPh_3)_2Cl_2$ (0.33 g, 0.48 mmol) were slurried in triethylamine (200 mL) in a nitrogen purged flask. Nitrogen gas was bubbled through the mixture for 10 min prior to the addition of TMSA (5.4 g, 55 mmol) under a nitrogen atmosphere. The flask was sealed, and the mixture left to stir overnight at room temperature. Reaction completion was monitored by GC-MS, after which the solvent was removed under a high vacuum. The residue was dissolved in hexane and filtered through a silica pad (hexane:EtOAc, 9:1,

as eluent). After *in vacuo* removal of the solvent, compound **47** was obtained in the form of yellow needles (9.7 g, 87%), which were sufficiently pure to be used without further purification: m.p. 56-57 °C (lit.,[196] 55-56 °C); R_f. 0.35 (hexane:EtOAc, 9:1, as eluent); ^{1}H NMR (700 MHz; $CDCl_3$) δ 7.97 (unsymmet. d, J = 8.4, 2H, $H_{4+4'}$), 7.52 (unsymmet. d, J = 8.4, 2H, $H_{5+5'}$), 3.91 (s, 3H, H_1), 0.26 (s, 9H, $H_{9+9'+9''}$); ^{13}C NMR (176 MHz; $CDCl_3$) δ 166.7 (C_2), 132.0 ($C_{5+5'}$), 129.8 (C_3), 129.5 ($C_{4+4'}$), 127.9 (C_6), 104.2 (C_7), 97.8 (C_8), 52.4 (C_1), 0.0 ($C_{9+9'+9''}$); IR (neat) ν_{max}/cm^{-1} 2953m (C-H_{methyl}), 2160m (C≡$C_{disub.}$), 1718s (C=O_{ester}), 1603s (C=$C_{ar.}$), 1560w (C=$C_{ar.}$), 1497w (C=$C_{ar.}$), 1443s (C=$C_{ar.}$), 1275s (C-O_{ester}), 1246s (C-H_{methyl}), 1110s (C-O_{ester}), 837s (C-H_{ar}), 759s (C-H_{ar}); MS (GC): *m/z* = 232 $[M]^+$, 217 $[M - CH_3]^+$; UV-vis (EtOH) λ_{max}/nm (ε/M^{-1} cm^{-1}): 200 (33 200), 268 (29 400). Anal. calcd. for $C_{13}H_{16}O_2Si$: C, 67.20; H, 6.94. Found: C, 67.25; H, 6.96.

Methyl 3-((trimethylsilyl)ethynyl)benzoate (48)

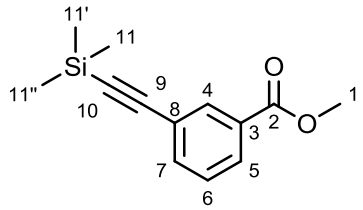

Procedure as for compound **47**, using methyl 3-iodobenzoate **46** (4.5 g, 17 mmol) to give compound **48** as a pale yellow solid (2.7 g, 68%), which was sufficiently pure to be used without further purification: m.p. 52-53 °C (lit.,[197] 52 °C); R_f. 0.43 (hexane:EtOAc, 9:1, as eluent); ^{1}H NMR (700 MHz; $CDCl_3$) δ 8.14-8.13 (m, 1H, H_4), 7.97 (dt, J = 7.7 and 1.4, 1H, H_5), 7.63 (dt, J = 7.7 and 1.4, 1H, H_7), 7.38 (t, J = 7.7, 1H, H_6), 3.92 (s, 3H, H_1), 0.26 (s, 9H, $H_{11+11'+11''}$); ^{13}C NMR (176 MHz; $CDCl_3$) δ 166.5 (C_2), 136.2 (C_7), 133.3 (C_4), 130.5 (C_3), 129.6 (C_5), 128.5 (C_6), 123.8 (C_8), 104.0 (C_9), 95.5 (C_{10}), 52.4 (C_1), 0.0 ($C_{11+11'+11''}$); IR (neat) ν_{max}/cm^{-1} 2956m (C-H_{methyl}), 2159m (C≡$C_{disub.}$), 1725s (C=O_{ester}), 1598w (C=$C_{ar.}$), 1578w (C=$C_{ar.}$), 1484w (C=$C_{ar.}$), 1429m (C=$C_{ar.}$), 1298s (C-O_{ester}), 1208s (C-O_{ester}), 845s (C-$H_{ar.}$), 749s (C-$H_{ar.}$); MS (EI): *m/z* = 232 $[M]^+$, 217 $[M - CH_3]^+$; UV-vis

(EtOH) λ_{max}/nm (ε/M^{-1} cm^{-1}): 228 (37 300), 260 (20 100). Anal. calcd. for $C_{13}H_{16}O_2Si$: C, 67.20; H, 6.94. Found: C, 67.43; H, 7.03.

Methyl 4-ethynylbenzoate (16)

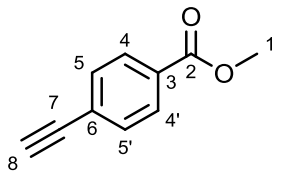

Methyl 4-((trimethylsilyl)ethynyl)benzoate (**47**, 9.2 g, 40 mmol) and sodium carbonate (17.0 g, 160 mmol) were mixed in 10:1 methanol and water (330 mL) and stirred overnight at room temperature. The mixture was diluted with diethyl ether (300 mL) and washed with water (2 x 150 mL). The aqueous phase was extracted with diethyl ether (2 x 150 mL) and the combined organic layers were dried over $MgSO_4$. After *in vacuo* removal of the solvent, alkyne **16** was obtained as a yellow crystalline solid (5.0 g, 79%), which was sufficiently pure to be used without further purification: m.p. 94-95 °C (lit.,[196] 93-94 °C); R_f. 0.27 (hexane:EtOAc, 9:1, as eluent); ^{1}H NMR (700 MHz; $CDCl_3$) δ 7.99 (unsymmet. d, J = 8.4, 2H, $H_{4+4'}$), 7.54 (unsymmet. d, J = 8.4, 2H, $H_{5+5'}$), 3.92 (s, 3H, H_1), 3.22 (s, 1H, H_8); ^{13}C NMR (176 MHz; $CDCl_3$) δ 166.6 (C_2), 132.2 ($C_{5+5'}$), 130.3 (C_3), 129.6 ($C_{4+4'}$), 126.9 (C_6), 82.9 (C_7), 80.2 (C_8), 52.4 (C_1); IR (neat) ν_{max}/cm^{-1} 3242s (C-H_{alkyne}), 2952w (C-H_{methyl}), 2104w (C≡$C_{term.}$), 1702s (C=O_{ester}), 1607m (C=$C_{ar.}$), 1560w (C=$C_{ar.}$), 1434s (C=$C_{ar.}$), 1288s (C-H_{methyl}), 1278s (C-O_{ester}), 1109s (C-O_{ester}), 860s (C-$H_{ar.}$), 772s (C-$H_{ar.}$), 721s (C-$H_{ar.}$), 678s (C-$H_{ar.}$); MS (EI): *m/z* = 342 $[2M + Na]^+$; UV-vis (EtOH) λ_{max}/nm (ε/M^{-1} cm^{-1}): 256 (22 300). Anal. calcd. for $C_{10}H_8O_2$: C, 74.99; H, 5.03. Found: C, 74.84; H, 5.14.

Methyl 3-ethynylbenzoate (49)

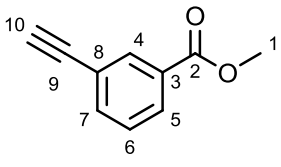

Procedure as for compound **16**, using methyl 3-((trimethylsilyl)ethynyl)benzoate **48** (1.8 g, 8 mmol) to give alkyne **49** as a yellow solid (0.79 g, 63%), which was sufficiently pure to be used without further purification: m.p. 55-56 °C (lit.,[197] 54-55 °C); R_f. 0.27 (hexane:EtOAc, 9:1, as eluent); ^{1}H NMR (600 MHz; $CDCl_3$) δ 8.17 (t, J = 1.8, 1H, H_4), 8.02 (dt, J = 7.8 and 1.2, 1H, H_5), 7.67 (dt, J = 7.8 and 1.2, 1H, H_7), 7.41 (t, J = 7.8, 1H, H_6), 3.93 (s, 3H, H_1), 3.12 (s, 1H, H_{10}); ^{13}C NMR (151 MHz; $CDCl_3$) δ 166.4 (C_2), 136.4 (C_7), 133.4 (C_4), 130.6 (C_3), 129.9 (C_5), 128.6 (C_6), 122.7 (C_8), 82.7 (C_9), 78.3 (C_{10}), 52.5 (C_1); IR (neat) ν_{max}/cm^{-1} 3255s (C-H_{alkyne}), 2956m (C-H_{methyl}), 2109w (C≡$C_{term.}$), 1714s (C=O_{ester}), 1598w (C=$C_{ar.}$), 1582m (C=$C_{ar.}$), 1482m (C=$C_{ar.}$), 1433s (C=$C_{ar.}$), 1294s (C-O_{ester}), 1274s (C-H_{methyl}), 1197s (C-O_{ester}), 749s (C-$H_{ar.}$), 716s (C-$H_{ar.}$), 664s (C-$H_{ar.}$); MS (EI): *m/z* = 343 [2M + Na]; UV-vis (EtOH) λ_{max}/nm (ε/M^{-1} cm^{-1}): 220 (32 800), 248 (16 700), 272 (18 500). Anal. calcd. for $C_{10}H_8O_2$: C, 74.99; H, 5.03. Found: C, 75.31; H, 5.10.

1-Isopropyl-4,4,8-trimethyl-6-((trimethylsilyl)ethynyl)-1,2,3,4-tetrahydroquinoline (51)

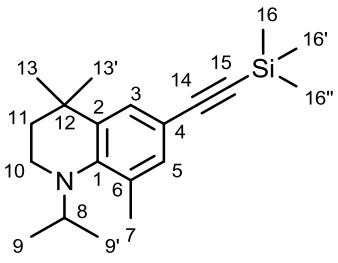

6-Bromo-1-isopropyl-4,4,8-trimethyl-1,2,3,4-tetrahydroquinoline **28** (523 mg, 1.77 mmol), PPh_3 (463 mg, 1.77 mmol), $PdCl_2$ (31 mg, 0.18 mmol) and $Cu(OAc)_2$ (32 mg, 0.18 mmol) were added to a Schlenk tube, which was then evacuated and filled with argon. This was repeated a further two times followed by addition of dry triethylamine (30 mL). After bubbling argon through the mixture for 10 min, trimethylsilylacetylene (754 µl, 5.30 mmol) was added. Argon was bubbled through the mixture for a further 5 min before the tube was sealed and heated at 80 °C. After 4 days, approximately 95% conversion to the product was found by GC-MS analysis. After *in vacuo* removal of the solvent, the residue was redissolved in hexane:ethyl acetate (95:5, with 1% Et_3N), and filtered through a silica pad to remove catalyst residue. Purification by column

chromatography was performed on silica gel treated with 1% Et_3N (hexane:EtOAc, 95:5, as eluent). Significant co-elution with PPh_3=O occurred, however, fractions containing mainly the desired product were obtained and provided the crude product as a yellow solid (345 mg, 62%) following *in vacuo* removal of the solvent. Recrystallisation from ethanol afforded some pure compound **51** as yellow needle-like crystals (88 mg, 16%), which was used for characterisation purposes: m.p. 78-80 °C; R_f. 0.46 (hexane:EtOAc, 95:5, with 1% Et_3N, as eluent); ^{1}H NMR (600 MHz, $CDCl_3$) δ 7.25 (d, J = 1.8, 1H, H_3), 7.10 (d, J = 1.8, 1H, H_5), 3.58 (septet, J = 6.6, 1H, H_8), 3.13-3.11 (m, 2H, H_{10}), 2.21 (s, 3H, H_7), 1.64-1.62 (m, 2H, H_{11}), 1.26 (s, 6H, $H_{13+13'}$), 1.12 (d, J = 6.6, 6H, $H_{9+9'}$), 0.23 (s, 9H, $H_{16+16'+16''}$); ^{13}C NMR (176 MHz; $CDCl_3$) δ 146.9 (C_1), 137.7 (C_2), 133.4 (C_5), 129.2 (C_6), 127.8 (C_3), 113.3 (C_4), 106.8 (C_{14}), 91.5 (C_{15}), 52.9 (C_8), 38.2 (C_{10}), 37.5 (C_{11}), 32.5 (C_{12}), 31.6 ($C_{13+13'}$), 20.5 ($C_{9+9'}$), 20.5 (C_7), 0.4 ($C_{16+16'+16''}$); IR (neat) ν_{max}/cm^{-1} 2957s (C-H_{methyl}), 2140w (C-C_{alkyne}); MS (EI): *m/z* = 314 $[M + H]^+$; UV-vis (EtOH) λ_{max}/nm (ε/M^{-1} cm^{-1}): 304 (39 800). Anal. calcd. for $C_{20}H_{31}NSi$: C, 76.61; H, 9.97; N, 4.47. Found: C, 76.63; H, 10.09; N, 4.41.

6-Ethynyl-1-isopropyl-4,4,8-trimethyl-1,2,3,4-tetrahydroquinoline (53)

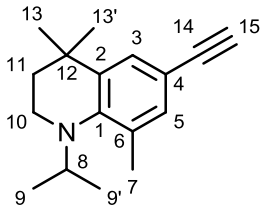

1-Isopropyl-4,4,8-trimethyl-6-((trimethylsilyl)ethynyl)-1,2,3,4-tetrahydroquinoline **51** (177 mg, 0.56 mmol) was dissolved in MeOH:Et_2O (1:1, 30 mL) followed by addition of NaOH (18 mg, 0.45 mmol) and H_2O (1 mL). After overnight stirring, a TLC analysis indicated that the starting material had been consumed. Diethyl ether (50 mL) was added, the organic layer was washed with H_2O (3 x 50 mL), dried with $MgSO_4$, and the solvent removed *in vacuo* to give the crude product **53** as a brown oil (142 mg, 109%): ^{1}H NMR (700 MHz, $CDCl_3$) δ 7.29 (s, 1H, H_3), 7.11 (s, 1H, H_5), 3.60 (septet, J = 6.3, 1H, H_8), 3.14-3.12 (m, 2H, H_{10}), 2.98 (s, 1H, H_{15}), 2.23 (s, 3H, H_7), 1.66-1.64 (m, 2H, H_{11}),

1.26 (d, *J* = 0.7, 6H, $H_{13+13'}$), 1.15 (dd, *J* = 6.3 and 0.7, 6H, $H_{9+9'}$); ^{13}C NMR (176 MHz; $CDCl_3$) δ 147.1 (C_1), 137.7 (C_2), 133.4 (C_5), 129.4 (C_6), 128.0 (C_3), 112.3 (C_4), 85.1 (C_{14}), 75.0 (C_{15}), 52.9 (C_8), 38.2 (C_{10}), 37.5 (C_{11}), 32.5 (C_{12}), 31.7 ($C_{13+13'}$), 20.6 ($C_{9+9'}$), 20.6 (C_7); IR (neat) ν_{max}/cm^{-1} 2954s (C-H_{methyl}), 2125w (C-C_{alkyne}); MS (ES^+): *m/z* 242 $[M + H]^+$.

Methyl 4-((1-isopropyl-4,4,8-trimethyl-1,2,3,4-tetrahydroquinolin-6-yl)ethynyl) benzoate (50)

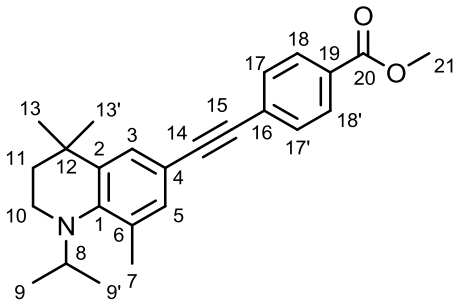

In a nitrogen-filled glovebox, crude 6-ethynyl-1-isopropyl-4,4,8-trimethyl-1,2,3,4-tetrahydroquinoline **53** (140 mg, 0.58 mmol), methyl 4-iodobenzoate (144 mg, 0.55 mmol), $Pd(PPh_3)Cl_2$ (4 mg, 1 mol%) and CuI (1 mg, 1 mol%) were dissolved in triethylamine (10 mL) in a Schlenk flask. The flask was sealed and the mixture stirred at room temperature for 3 days, after which GC-MS analysis showed complete conversion to the product. The solvent was removed *in vacuo* to give a golden-yellow solid (92 mg, 40%) consisting mainly of the desired ester, which, for characterisation purposes was recrystallised from hexane to give yellow needle-like crystals of pure ester **50** (40 mg, 18%): m.p. 126-127 °C; ^1H NMR (700 MHz; $CDCl_3$) δ 7.99 (unsymmet. d, *J* = 8.4, 2H, $H_{18+18'}$), 7.55 (unsymmet. d, *J* = 8.4, 2H, $H_{17+17'}$), 7.33 (s, 1H, H_3), 7.17 (s, 1H, H_5), 3.92 (s, 3H, H_{21}), 3.63 (septet, *J* = 6.3, 1H, H_8), 3.17-3.13 (m, 2H, H_{10}), 2.25 (s, 3H, H_7), 1.68-1.65 (m, 2H, H_{11}), 1.29 (s, 6H, $H_{13+13'}$), 1.16 (d, *J* = 6.3, 6H, $H_{9+9'}$); ^{13}C NMR (176 MHz; $CDCl_3$) δ 166.9 (C_{20}), 147.3 (C_1), 137.9 (C_2), 133.2 (C_5), 131.3 ($C_{17+17'}$), 129.6 ($C_{18+18'}$), 129.4 (C_6), 129.1 (C_{16}), 128.8 (C_{19}), 127.7 (C_3), 112.8 (C_4), 94.3 (C_{14}), 87.2 (C_{15}), 53.0 (C_8), 52.3 (C_{21}), 38.2 (C_{10}), 37.5 (C_{11}), 32.6 ($C_{13+13'}$), 31.6 (C_{12}), 20.7 (C_7), 20.6 ($C_{9+9'}$); IR (neat) ν_{max}/cm^{-1} 2957s (C-H_{methyl}), 2196s (C-C_{alkyne}), 1716s (C=O_{ester}), 1272s (C-O_{ester});

MS (ES^+): *m/z* = 376 $[M + H]^+$; UV-vis (EtOH) λ_{max}/nm ($\varepsilon/M^{-1}\,cm^{-1}$): 360 (42 900). Anal. calcd. for $C_{25}H_{29}NO_2$: C, 79.96; H, 7.78; N, 3.73. Found: C, 79.56; H, 7.65; N, 3.62.

Methyl 4-((1-isopropyl-4,4,8-trimethyl-1,2,3,4-tetrahydroquinolin-6-yl)ethynyl) benzoic acid (21)

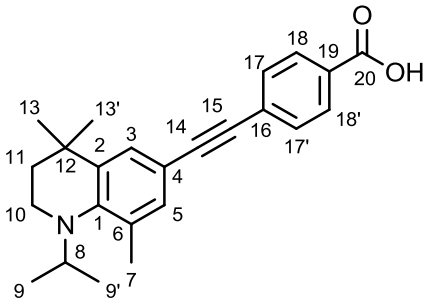

Methyl 4-((1-isopropyl-4,4,8-trimethyl-1,2,3,4-tetrahydroquinolin-6-yl)ethynyl) benzoate **50** (40 mg, 0.1 mmol) was dissolved in THF (2 mL) and 20% aq. NaOH (2 mL). The mixture was heated to reflux (70 °C) for 20 h under an inert argon atmosphere to give a colourless solution and a TLC analysis indicated consumption of the ester. Diethyl ether (10 mL) and H_2O (10 mL) were added and the solution acidified to pH 1 with 1 M HCl upon which yellow crystals precipitated out of the aqueous layer. Diethyl ether was added (30 mL) to extract the product, the organic layer was separated, dried using $MgSO_4$ and the solvent removed *in vacuo* to give a yellow solid. This was recrystallised from ethanol to provide acid **21** as a neon-yellow crystalline solid (32 mg, 89%): ^1H NMR (600 MHz; $CDCl_3$) δ 8.06 (unsymmet. d, *J* = 8.4, 2H, $H_{18+18'}$), 7.58 (unsymmet. d, *J* = 8.4, 2H, $H_{17+17'}$), 7.34 (s, 1H, H_3), 7.19 (s, 1H, H_5), 3.64 (septet, *J* = 6.0, 1H, H_8), 3.18-3.13 (m, 2H, H_{10}), 2.26 (s, 3H, H_7), 1.69-1.65 (m, 2H, H_{11}), 1.30 (s, 6H, $H_{13+13'}$), 1.17 (d, *J* = 6.0, 6H, $H_{9+9'}$); ^{13}C NMR (176 MHz; $CDCl_3$) δ 169.9 (C_{20}), 147.4 (C_1), 137.9 (C_2), 133.3 (C_5), 131.4 ($C_{17+17'}$), 130.2 ($C_{18+18'}$), 130.1 (C_{16}), 129.4 (C_6), 127.7 (C_3), 127.6 (C_{19}), 112.7 (C_4), 95.0 (C_{14}), 87.2 (C_{15}), 53.0 (C_8), 38.2 (C_{10}), 37.5 (C_{11}), 32.6 (C_{12}), 31.6 ($C_{13+13'}$), 20.7 (C_7), 20.6 ($C_{9+9'}$); IR (neat) ν_{max}/cm^{-1} 2962br (O-H_{acid}), 2190s (C-C_{alkyne}), 1683s (C=O_{acid}), 1592s (C=$C_{ar.}$), 1470m (C=$C_{ar.}$), 1273 (C-O_{acid}); MS (ES^+): *m/z* = 362 $[M + H]^+$; UV-vis ($CHCl_3$) λ_{max}/nm ($\varepsilon/M^{-1}\,cm^{-1}$): 371 (45 600). Anal. calcd. for $C_{24}H_{27}NO_2$: C, 79.74; H, 7.53; N, 3.87. Found: C, 79.18; H, 7.53; N, 3.75.

6.5. Synthetic procedures for a bromine-containing retinoid

3-Bromo-1-isopropyl-4,4,8-trimethyl-6-((trimethylsilyl)ethynyl)-1,4-dihydroquinoline (60)

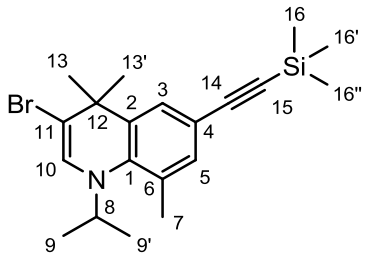

A Schlenk tube was charged with 3,6-dibromo-1-isopropyl-4,4,8-trimethyl-1,4-dihydroquinoline **31** (1.0 g, 2.7 mmol), PPh_3 (350 mg, 1.3 mmol), $Pd(PPh_3)_2Cl_2$ (190 mg, 0.3 mmol) and CuI (50 mg, 0.3 mmol), then evacuated and filled with argon. This was repeated a further two times, after which dry triethylamine (35 mL) was added. The mixture was stirred for 10 min before the dropwise addition of trimethylsilylacetylene (1.1 mL, 8.0 mmol). The flask was then sealed and heated to 80 °C for 60 h, after which a GC-MS analysis of the reaction mixture was performed to confirm reaction completion. The solvent was removed *in vacuo* to give crude **60** as a brown oil (1.21 g, crude yield estimated from ^{1}H NMR analysis: 47%): ^{1}H NMR (700 MHz; $CDCl_3$) δ 7.24 (d, J = 2.1, 1H, H_3), 7.14 (d, J = 2.1, 1H, H_5), 6.35 (s, 1H, H_{10}), 3.64 (septet, J = 6.3, 1H, H_8), 2.23 (s, 3H, H_7), 1.49 (s, 6H, $H_{13+13'}$), 1.19 (d, J = 6.3, 6H, $H_{9+9'}$), 0.24 (s, 9H, $H_{16+16'+16''}$); ^{13}C NMR (176 MHz; $CDCl_3$) δ 141.6 (C_1), 136.0 (C_2), 134.0 (C_5), 128.6 (C_3), 128.1 (C_{10}), 127.9 (C_6), 117.1 (C_4), 116.1 (C_{11}), 105.5 (C_{14}), 93.0 (C_{15}), 53.6 (C_8), 39.6 (C_{12}), 32.2 ($C_{13+13'}$), 20.5 ($C_{9+9'}$), 20.2 (C_7), 0.2 ($C_{16+16'+16''}$); IR (neat) ν_{max}/cm^{-1} 2960s (C-H_{methyl}), 2147s (C≡$C_{disub.}$), 1470s (C=$C_{ar.}$), 1436s (C=$C_{ar.}$); MS (GC): m/z = 389 [M^{79}Br - H]$^-$ and 391 [M^{81}Br - H]$^-$.

3-Bromo-6-ethynyl-1-isopropyl-4,4,8-trimethyl-1,4-dihydroquinoline (62)

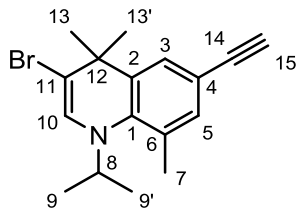

3-Bromo-1-isopropyl-4,4,8-trimethyl-6-((trimethylsilyl)ethynyl)-1,4-dihydroquinoline **60** (500 mg, 1.28 mmol), NaOH (41 mg, 1.02 mmol) and H_2O (0.8 mL) were dissolved in MeOH:Et_2O (1:1, 40 mL), and the mixture stirred at room temperature overnight, after which GC-MS analysis revealed the reaction to be complete. Diethyl ether (40 mL) was added and the organic layer washed with water (3 x 30 mL), dried with $MgSO_4$ and the solvent removed *in vacuo* to provide crude **62** as a brown viscous oil (420 mg, crude yield estimated from ^{1}H NMR analysis: 72%): ^{1}H NMR (700 MHz; $CDCl_3$) δ 7.27 (d, J = 1.4, 1H, H_3), 7.15 (d, J = 1.4, 1H, H_5), 6.36 (s, 1H, H_{10}), 3.66 (septet, J = 7.0, 1H, H_8), 2.24 (s, 3H, H_7), 1.49 (s, 6H, $H_{13+13'}$), 1.21 (d, J = 7.0, 6H, $H_{9+9'}$); ^{13}C NMR (176 MHz; $CDCl_3$) δ 141.8 (C_1), 136.0 (C_2), 133.9 (C_5), 128.9 (C_3), 128.1 (C_{10}), 128.0 (C_6), 116.1 (C_4), 115.9 (C_{11}), 84.0 (C_{14}), 76.2 (C_{15}), 53.5 (C_8), 39.5 (C_{12}), 32.2 ($C_{13+13'}$), 20.5 ($C_{9+9'}$), 20.3 (C_7); IR (neat) ν_{max}/cm^{-1} 2961s (C-H_{methyl}), 2060w (C≡$C_{term.}$), 1469s (C=$C_{ar.}$), 1436s (C=$C_{ar.}$); MS (GC): m/z = 317 [M^{79}Br - H]$^-$ and 319 [M^{81}Br - H]$^-$.

Methyl 4-((3-bromo-1-isopropyl-4,4,8-trimethyl-1,4-dihydroquinolin-6-yl)ethynyl)benzoate (63)

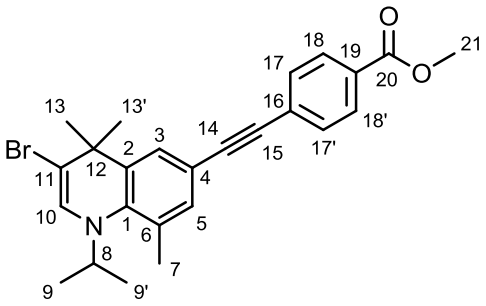

A Schlenk tube was charged with 3-bromo-6-ethynyl-1-isopropyl-4,4,8-trimethyl-1,4-dihydroquinoline **62** (200 mg, 0.63 mmol), 4-iodobenzoic acid methyl ester (156 mg,

0.60 mmol), $Pd(PPh_3)_2Cl_2$ (4 mg, 0.006 mmol) and CuI (1 mg, 0.006 mmol). After thrice evacuating and filling the flask with argon, dry triethylamine (10 mL) was added. The sealed flask was heated to 50 °C for 72 h, with reaction completion monitored by GC-MS analysis. The solvent was removed *in vacuo* to give crude **63** as a brown oil (307 mg, 108%): ^{1}H NMR (700 MHz; $CDCl_3$) δ 7.80 (unsymmet. d, J = 8.4, 2H, $H_{18+18'}$), 7.74 (unsymmet. d, J = 8.4, 2H, $H_{17+17'}$), 7.33 (d, J = 2.1, 1H, H_3), 7.22 (d, J = 2.1, 1H, H_5), 6.38 (s, 1H, H_{10}), 3.92 (s, 3H, H_{21}), 3.69 (septet, J = 6.3, 1H, H_8), 2.28 (s, 3H, H_7), 1.53 (s, 6H, $H_{13+13'}$), 1.23 (d, J = 6.3, 6H, $H_{9+9'}$); ^{13}C NMR (176 MHz; $CDCl_3$) δ 166.7 (C_{20}), 141.8 (C_1), 137.8 (C_2), 136.2 (C_5), 133.6 ($C_{17+17'}$), 132.0 ($C_{18+18'}$), 131.4 (C_6), 131.2 (C_{16}), 129.7 (C_{19}), 129.6 (C_3), 129.5 (C_{10}), 115.9 (C_4), 92.9 (C_{14}), 88.0 (C_{15}), 53.6 (C_8), 39.6 (C_{12}), 32.2 ($C_{13+13'}$), 20.6 ($C_{9+9'}$), 20.3 (C_7); IR (neat) ν_{max}/cm^{-1} 2966s (C-H_{methyl}), 2198w (C≡$C_{disub.}$), 1720s (C=O_{ester}), 1604s (C=$C_{ar.}$), 1470m (C=$C_{ar.}$), 1435s (C=$C_{ar.}$); MS (GC): *m/z* = 451 [M^{79}Br - H]$^-$ and 453 [M^{81}Br - H]$^-$.

6.6. Synthetic procedures for *N*-acetyl compounds

N-*o*-Tolylacetamide (64)

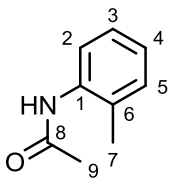

Acetyl chloride (22 mL, 308 mmol) was added slowly dropwise to a stirred solution of *o*-toluidine (30 g, 280 mmol) and pyridine (59 mL, 728 mmol) in dichloromethane (300 mL). The flask was maintained at 0 °C in an ice and methanol bath, and after stirring for 2 h, the mixture was allowed to warm to room temperature, then washed with water (180 mL), brine (2 x 180 mL), and the organic layer dried over $MgSO_4$. After filtering the mixture, a trituration was performed in which hexane (300 mL) was added to the filtrate, followed by *in vacuo* removal of dichloromethane. The resulting suspension was filtered to obtain the title compound as a fluffy white crystalline solid (33 g, 80%): m.p. 109-111 °C; ^{1}H NMR (700 MHz; $CDCl_3$) δ 7.77 (d, J = 7.7, 1H, H_3), 7.23-

7.21 (m, 1H, H_2), 7.20-7.18 (m, 1H, H_5), 7.08 (t, *J* = 7.7, 1H, H_4), 6.96 (br s, 1H, NH), 2.26 (s, 3H, H_7), 2.21 (s, 3H, H_9); ^{13}C NMR (176 MHz; $CDCl_3$) δ 168.4 (C_8), 135.8 (C_1), 130.6 (C_5), 129.3 (C_6), 126.9 (C_2), 125.5 (C_4), 123.5 (C_3), 24.5 (C_9), 17.9 (C_7); IR (neat) ν_{max}/cm^{-1} 3283m (N-H), 3220m (N-H), 1651s (C=O); MS (ES$^+$): *m/z* = 150 $[M + H]^+$; HRMS (ES$^+$) calcd. for $C_9H_{11}NO$ $[M + H]^+$: 150.0919, found: 150.0900.

_N_-(3-Methylbut-2-enyl)-_N_-_o_-tolylacetamide (65)

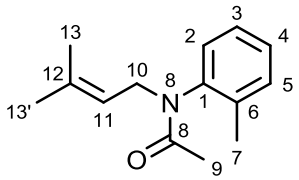

A mixture of *N*-*o*-tolylacetamide **64** (23.0 g, 154 mmol), K_2CO_3 (23.4 g, 170 mmol), NaOH (6.8 g, 170 mmol), $[CH_3(CH_2)_3]_4NBr$ (1.5 g, 4.6 mmol, 3 mol%) and 3,3'-dimethylallyl bromide (28.0 g, 185 mmol) in toluene (600 mL) was heated to 70 °C with vigorous stirring. After 18 h, the resulting yellow suspension was cooled to room temperature, water (1 L) was added, and the mixture extracted with toluene (3 x 600 mL). The combined organic layers were washed with 6 M HCl (600 mL), followed by brine (2 x 600 mL), and dried over $MgSO_4$. The mixture was filtered, the solvent removed *in vacuo*, and the residue purified by column chromatography on silica gel (hexane:EtOAc, 8:2, as eluent) to provide the title compound as a yellow oil (25.1 g, 75%): ^{1}H NMR (700 MHz; $CDCl_3$) δ 7.28 (unsymmet. d, *J* = 7.0, 1H, H_5), 7.26 (t, *J* = 7.7, 1H, H_4), 7.22 (t, *J* = 7.7, 1H, H_3), 7.07 (unsymmet. d, *J* = 7.7, 1H, H_2), 5.28 (t, *J* = 7.0, 1H, H_{11}), 4.55 (dd, *J* = 14.7 and 7.0, 1H, H_{10}), 3.92 (dd, *J* = 14.7 and 7.7, 1H, H_{10}), 2.25 (s, 3H, H_7), 1.77 (s, 3H, H_{13}), 1.68 (s, 3H, H_9), 1.42 (s, 3H, H_{13}); ^{13}C NMR (176 MHz; $CDCl_3$) δ 170.1 (C_8), 141.6 (C_1), 136.2 (C_{12}), 135.8 (C_6), 131.2 (5), 129.1 (C_2), 128.1 (C_4), 127.0 (C_3), 119.1 (C_{11}), 45.7 (C_{10}), 25.7 (C_9), 22.2 (C_{13}), 17.5 (C_7), 17.5 (C_{13}); IR (neat) ν_{max}/cm^{-1} 2918br (C-H_{alkyl}), 1656s (C=O); MS (ES$^+$): *m/z* = 218 $[M + H]^+$; HRMS (ES$^+$) calcd. for $C_{14}H_{20}NO$ $[M + H]^+$: 218.1545, found: 218.1547.

_N_-Isopentyl-_N_-_o_-tolylacetamide (76)

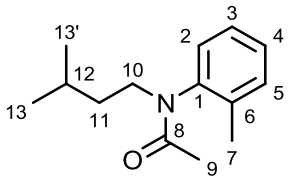

N-(3-Methylbut-2-enyl)-*N*-*o*-tolylacetamide **65** (2.0 g, 9.2 mmol) and $AlCl_3$ (2.7 g, 20.2 mmol) were heated in chlorobenzene (6 mL) to 120 °C for 5 h, after which a TLC analysis showed that the starting material had been consumed, and a single product spot was present. Water (10 mL) was added to the cooled reaction mixture, and the organic layer was extracted with toluene (2 x 50 mL). The combined organic layers were washed with 6 M HCl (50 mL), followed by brine (2 x 50 mL), then dried over $MgSO_4$. Following *in vacuo* removal of the solvent, the residue was purified by column chromatography on silica gel (hexane:EtOAc, 3:1, as eluent) to give an orange oil (490 mg, 25%): R_f. 0.61 (hexane:EtOAc, 4:1, as eluent); ^{1}H NMR (700 MHz; $CDCl_3$) δ 7.30 (dd, J = 7.7 and 1.4, 1H, H_5), 7.26 (td, J = 7.7 and 1.4, 1H, H_4), 7.23 (td, J = 7.7 and 1.4, 1H, H_3), 7.07 (dd, J = 7.7 and 1.4, 1H, H_2), 4.07 (ddd, J = 13.2, 10.7 and 5.6, 1H, H_{10}), 3.14 (ddd, J = 13.2, 10.7 and 5.2, 1H, H_{10}), 2.23 (s, 3H, H_7), 1.73 (s, 3H, H_9), 1.57 (nonet, J = 7.0, 1H, H_{12}), 1.50-1.44 (m, 1H, H_{11}), 1.38-1.32 (m, 1H, H_{11}), 0.89 (d, J = 7.0, 3H, H_{13}), 0.87 (d, J = 6.3, 3H, H_{13}); ^{13}C NMR (176 MHz; $CDCl_3$) δ 170.4 (C_8), 141.9 (C_1), 135.8 (C_6), 131.6 (C_5), 129.2 (C_2), 128.3 (C_4), 127.2 (C_3), 46.9 (C_{10}), 36.5 (C_{11}), 26.3 (C_{12}), 22.8 (C_{13}), 22.6 (C_{13}), 22.5 (C_9), 17.7 (C_7); IR (neat) ν_{max}/cm^{-1} 2954s (C-H_{alkyl}), 2869s (C-H_{alkyl}), 1657s (C=O); MS (ES$^+$): *m/z* = 220 [M + H]$^+$, 461 [2M + Na]; HRMS (ES$^+$) calcd. for $C_{14}H_{22}NO$ [M + H]$^+$: 220.1701, found: 220.1704; calcd. for $C_{28}H_{42}N_2O_2Na$ [2M + Na]: 461.3144, found: 461.3164.

_N_-(3-Hydroxy-3-methylbutyl)-_N_-_o_-tolylacetamide (79)

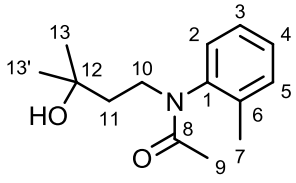

Polyphosphoric acid (15 g) was heated to 120 °C in a conical flask, and *N*-(3-methylbut-2-enyl)-*N*-*o*-tolylacetamide **65** (2.77 g, 12.7 mmol) was added dropwise with stirring. After 15 min, ice water (20 mL) was added, followed by cautious addition of aqueous NaOH until the solution was basic. The mixture was extracted with ethyl acetate (50 mL), washed with water (2 x 50 mL), and the organic layer dried over $MgSO_4$. The mixture was filtered, and the solvent was removed *in vacuo* to provide the title compound as an orange oil (1.20 g, 40%): ^{1}H NMR (400 MHz; $CDCl_3$) δ 7.32-7.29 (m, 1H, H_5), 7.28-7.25 (m, 1H, H_4), 7.23 (dd, *J* = 7.2 and 2, 1H, H_3), 7.10 (dd, *J* = 7.6 and 1.6, 1H, H_2), 4.23 (ddd, *J* = 13.6, 9.2 and 6.4, 1H, H_{10}), 3.22 (ddd, *J* = 13.6, 8.8 and 5.6, 1H, H_{10}), 2.45 (br s, 1H, OH), 2.24 (s, 3H, H_7), 1.82 (ddd, *J* = 14.4, 8.8 and 6.4, 1H, H_{11}), 1.74 (s, 3H, H_9), 1.68 (ddd, *J* = 14.4, 8.8 and 5.6, 1H, H_{11}), 1.25 (s, 3H, H_{13}), 1.24 (s, 3H, H_{13}); ^{13}C NMR (176 MHz; $CDCl_3$) δ 171.2 (C_8), 141.9 (C_1), 135.6 (C_6), 131.8 (C_5), 129.0 (C_2), 128.5 (C_4), 127.3 (C_3), 69.7 (C_{12}), 44.7 (C_{10}), 40.8 (C_{11}), 29.8 (C_{13}), 29.6 (C_{13}), 22.5 (C_9), 17.7 (C_7); IR (neat) ν_{max}/cm^{-1} 3400s br (O-H), 2972s (C-H_{alkyl}), 1633s (C=O); MS (ES$^+$): *m/z* = 258 [M + Na], 493 [2M + Na]; HRMS (ES$^+$) calcd. for $C_{14}H_{21}NO_2Na$ [M + Na]: 258.1470, found: 258.1470; calcd. for $C_{28}H_{42}N_2O_4Na$ [2M + Na]: 493.3042, found: 493.3046.

4,4,8-Trimethyl-1,2,3,4-tetrahydroquinoline (80)

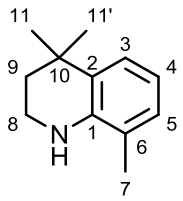

Polyphosphoric acid (15 g) was heated to 120 °C in a conical flask, and *N*-(3-methylbut-2-enyl)-*N*-*o*-tolylacetamide **65** (3.72 g, 17.1 mmol) was added dropwise with stirring. After 2 h, ice water (20 mL) was added to the black mixture, followed by cautious addition of aqueous NaOH until the solution was basic. The mixture was extracted with ethyl acetate (50 mL), washed with water (2 x 50 mL), dried over $MgSO_4$ and the solvent removed *in vacuo* to provide the title compound as a viscous black oil (1.50 g,

50%): ^{1}H NMR (600 MHz; $CDCl_3$) δ 7.11 (dd, J = 7.8 and 1.2, 1H, H_3), 6.89 (dq, J = 7.8 and 1.2, 1H, H_5), 6.61 (t, J = 7.8, 1H, H_4), 3.40-3.37 (m, 2H, H_8), 2.10 (s, 3H, H_7), 1.78-1.75 (m, 2H, H_9), 1.32 (s, 6H, $H_{11+11'}$); ^{13}C NMR (176 MHz; $CDCl_3$) δ 141.7 (C_1), 139.8 (C_6), 127.9 (C_5), 124.5 (C_3), 121.1 (C_2), 116.5 (C_4), 38.7 (C_8), 37.4 (C_9), 32.0 (C_{10}), 31.4 ($C_{11+11'}$), 17.7 (C_7); IR (neat) ν_{max}/cm^{-1} 3428s br (N-H), 2957s (C-H_{alkyl}), 2924s (C-H_{alkyl}), 2854s (C-H_{alkyl}), 1598s (C=$C_{ar.}$); MS (ES^+): m/z = 176 $[M + H]^+$; HRMS (ES^+) calcd. for $C_{12}H_{18}N$ $[M + H]^+$: 176.1439, found: 176.1437.

6.7. Synthetic procedures for amide-containing retinoids

4-Iodo-2-methylaniline (89)

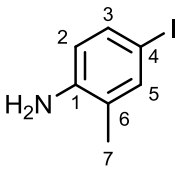

Commercially available from Sigma-Aldrich, otherwise, synthesis was follows: a solution of *o*-toluidine (10.0 g, 93 mmol) in pyridine and dioxane (500 mL, 1:1) was cooled to 0 °C in an ice bath. Iodine (71.0 g, 280 mmol) was added in one portion and the brown mixture stirred for 1 h at 0 °C followed by 1 h at room temperature. A saturated aqueous solution of sodium thiosulfate was then added until the brown colour disappeared. The mixture was extracted with dichloromethane (500 mL), washed with water (2 x 300 mL), and dried over $MgSO_4$. After *in vacuo* removal of the solvent, the residue was recrystallised from methanol to provide the title compound as a light-brown crystalline solid (13.1 g, 61%): m.p. 107-110 °C; ^{1}H NMR (600 MHz; $CDCl_3$) δ 7.34 (d, J = 1.6, 1H, H_5), 7.30 (dd, J = 8.4 and 2.0, 1H, HI_3), 6.44 (d, J = 8.0, 1H, H_2), 3.61 (br s, 2H, NH), 2.11 (s, 3H, H_7); ^{13}C NMR (100.6 MHz; $CDCl_3$) δ 144.4 (C_1), 138.8 (C_5), 135.7 (C_3), 125.1 (C_6), 117.0 (C_2), 79.6 (C_4), 17.2 (C_7). All other spectroscopic data were identical to those reported in the literature.[198]

N-(4-Iodo-2-methylphenyl)-3-methylbut-2-enamide (92)

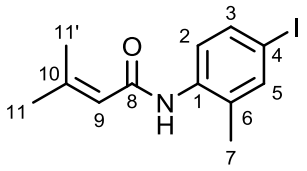

3,3-Dimethylacryloyl chloride (6.20 mL, 56 mmol) in dichloromethane (40 mL) was added slowly dropwise to a stirred solution of 4-iodo-2-methylaniline **89** (25.9 g, 111 mmol) in dichloromethane (850 mL). The mixture was heated to reflux (50 °C) for 5 h, then cooled to room temperature. The precipitate was removed by vacuum filtration, and the filtrate was washed with 2 M HCl (500 mL), sat. $NaHCO_3$ (500 mL), brine (500 mL), and the organic layer was dried over $MgSO_4$. Following *in vacuo* removal of the solvent, the residue was recrystallised from methanol to provide the title compound as a white crystalline solid (14.0 g, 79%): m.p. 119-121 °C; ^{1}H NMR (700 MHz; $CDCl_3$) δ 7.72 (s, 1H, H_5), 7.51-7.49 (m, 1H, H_2), 7.49-7.48 (m, 1H, H_3), 6.83 (br s, 1H, OH), 5.72 (s, 1H, H_9), 2.21 (s, 3H, $H_{11'}$), 2.19 (s, 3H, H_7), 1.90 (s, 3H, H_{11}); ^{13}C NMR (176 MHz; $CDCl_3$) δ 165.1 (C_8), 154.4 (C_{10}), 139.3 (C_2), 136.3 (C_4), 136.0 (C_3), 130.8 (C_6), 124.5 (C_5), 118.7 (C_9), 88.7 (C_1), 27.8 ($C_{11'}$), 20.4 (C_{11}), 17.8 (C_7); IR (neat) ν_{max}/cm^{-1} 3289br (N-H), 2357br (N-H), 1636s (C=O); MS (ES$^+$): *m/z* = 338 $[M + Na]^+$; HRMS (ES$^+$) calcd. for $C_{12}H_{15}INO$ $[M + H]^+$: 316.0198, found: 316.0203. Anal. calcd. for $C_{12}H_{14}INO$: C, 45.73; H, 4.48; N, 4.44. Found: C, 45.89; H, 4.48; N, 4.35.

6-Iodo-4,4,8-trimethyl-3,4-dihydroquinolin-2(1*H*)-one (93)

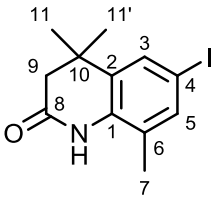

A solution of $AlCl_3$ (3.65 g, 27.4 mmol) in dry dichloromethane (100 mL) was stirred for 20 min at room temperature, followed by the addition of *N*-(4-iodo-2-methylphenyl)-3-methylbut-2-enamide **92** (5.76 g, 18.3 mmol) in dry dichloromethane (50 mL) *via*

cannula. After 3 h, ice water (150 mL) was added, and the mixture was extracted into dichloromethane (200 mL). The organic layer was separated, washed with 2 M HCl (300 mL), water (2 x 300 mL), 10% $Na_2S_2O_3$ (300 mL), and brine (300 mL). After drying the organic layer over $MgSO_4$, the solvent was removed *in vacuo*, and the product triturated from ethanol to provide the title compound as a white crystalline solid (4.66 g, 81%): m.p. 186-188 °C; ^{1}H NMR (600 MHz; $CDCl_3$) δ 7.63 (br s, 1H, NH), 7.44 (d, J = 1.8, 1H, H_3), 7.38 (d, J = 1.8, 1H, H_5), 2.45 (s, 2H, H_9), 2.20 (s, 3H, H_7), 1.30 (s, 6H, $H_{11+11'}$); ^{13}C NMR (176 MHz; $CDCl_3$) δ 170.2 (C_8), 137.7 (C_5), 134.9 (C_1), 134.2 (C_2), 131.5 (C_3), 125.5 (C_4), 86.5 (C_6), 45.1 (C_9), 34.2 (C_{10}), 27.6 ($C_{11+11'}$), 16.8 (C_7); IR (neat) ν_{max}/cm^{-1} 3193m (N-H), 3120m(N-H), 2949m (C-H_{alkyl}), 1678s (C=O); MS (ES^+): *m/z* = 338 [M + Na]$^+$; HRMS (ES^+) calcd. for $C_{12}H_{15}INO$ [M + H]$^+$: 316.0198, found: 316.0211. Anal. calcd. for $C_{12}H_{14}INO$: C, 45.73; H, 4.48; N, 4.44. Found: C, 45.54; H, 4.38; N, 4.35.

3-Methyl-*N*-*o*-tolylbut-2-enamide (95)

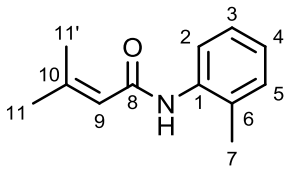

3,3-Dimethylacryloyl chloride (2.60 mL, 23.3 mmol) in chloroform (10 mL) was added slowly dropwise to a stirred solution of *o*-toluidine (5.00 g, 46.7 mmol) in chloroform (200 mL). The mixture was heated to reflux (70 °C) for 5 h, then cooled to room temperature. The precipitate was removed by vacuum filtration, and the filtrate was washed with 2 M HCl (200 mL), sat. $NaHCO_3$ (200 mL), brine (200 mL), dried over $MgSO_4$, and the solvent removed *in vacuo* to provide the title compound as a white crystalline solid following recrystallisation from methanol (3.92 g, 89%): m.p. 99-101 °C; ^{1}H NMR (700 MHz; $CDCl_3$) δ 7.86 (s, 1H, H_2), 7.19 (unsymmet. d, J = 7.0, 1H, H_3), 7.16 (unsymmet. d, J = 8.4, 1H, H_4), 7.08-7.04 (m, 1H, H_5), 6.98 (br s, 1H, NH), 5.76 (s, 1H, H_9), 2.24 (s, 3H, H_7), 2.21 and 1.90 (2 x s, 3H, $H_{11+11'}$); ^{13}C NMR (176 MHz; $CDCl_3$) δ 165.1 (C_8), 153.1 (C_{10}), 136.1 (C_1), 130.5 (C_4), 128.9 (C_6), 126.7 (C_3), 124.9 (C_5), 123.1 (C_2), 118.8 (C_9), 27.4 and 20.1 ($C_{11+11'}$), 17.9 (C_7); IR (neat) ν_{max}/cm^{-1} 3294s (N-H), 1667s

(C=O), 1640s (C=$C_{ar.}$); MS (ES^+): *m/z* = 190 $[M + H]^+$. Anal. calcd. for $C_{12}H_{15}NO$: C, 76.16; H, 7.99; N, 7.40. Found: C, 76.00; H, 7.89; N, 7.29.

4,4,8-Trimethyl-3,4-dihydroquinolin-2(1*H*)-one (94)

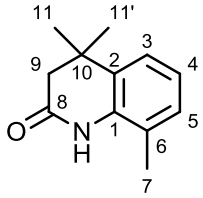

A solution of $AlCl_3$ (4.90 g, 37.0 mmol) in dry dichloromethane (200 mL) was stirred for 15 min at room temperature, followed by the addition of 3-methyl-*N*-*o*-tolylbut-2-enamide **95** (3.50 g, 18.5 mmol) in dry dichloromethane (20 mL). After stirring for 1 h, ice water (100 mL) was added, and the mixture was extracted into dichloromethane (200 mL). The organic layer was separated, washed with 2 M HCl (200 mL), water (2 x 200 mL) and dried over $MgSO_4$. The solvent was removed *in vacuo*, and the residue recrystallised from acetonitrile to provide the title compound as a white crystalline solid (3.20 g, 91%): m.p. 133-135 °C; ^{1}H NMR (600 MHz; $CDCl_3$) δ 7.50 (br s, 1H, NH), 7.17 (unsymmet. d, *J* = 7.8, 1H, H_3), 7.06-7.03 (m, 1H, H_5), 6.97 (t, *J* = 7.8, 1H, H_4), 2.48 (s, 2H, H_9), 2.25 (s, 3H, H_7), 1.33 (s, 6H, $H_{11+11'}$); ^{13}C NMR (176 MHz; $CDCl_3$) δ 170.5 (C_8), 134.2 (C_2), 132.6 (C_1), 129.2 (C_5), 123.3 (C_4), 122.9 (C_6), 122.5 (C_3), 45.3 (C_9), 34.2 (C_{10}), 27.8 ($C_{11+11'}$), 17.2 (C_7); IR (neat) ν_{max}/cm^{-1} 3220br (N-H), 2963m (C-H_{alkyl}), 1669s (C=O); MS (ES^+): *m/z* = 212 $[M + Na]^+$. Anal. calcd. for $C_{12}H_{15}NO$: C, 76.16; H, 7.99; N, 7.40. Found: C, 76.00; H, 7.89; N, 7.29.

6-Iodo-4,4,8-trimethyl-1,2,3,4-tetrahydroquinoline (68)

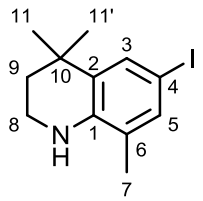

A solution of 6-iodo-4,4,8-trimethyl-3,4-dihydroquinolin-2(1*H*)-one **93** (740 mg, 2.35 mmol) in dry toluene (10 mL) was cooled to 0 °C in an ice bath. Borane-dimethyl sulfide (1.23 mL of a 2.0 M solution in toluene, 2.47 mmol) was added dropwise and the mixture stirred at 0 °C for 15 min, then refluxed (110 °C) overnight. After cooling to room temperature, 10% Na_2CO_3 (15 mL) was added, and the solution stirred for a further 30 min. The organic layer was separated, washed with water (2 x 10 mL), dried over $MgSO_4$, and concentrated *in vacuo* to provide the title compound as a dark orange oil (590 mg, 83%): ^{1}H NMR (400 MHz; $CDCl_3$) δ 7.35 (s, 1H, H_3), 7.20 (s, 1H, H_5), 3.78 (br s, 1H, NH), 3.43-3.35 (m, 2H, H_8), 2.05 (s, 3H, H_7), 1.75-1.67 (m, 2H, H_9), 1.29 (s, 6H, $H_{11+11'}$); MS (ES^+): *m/z* = 347 $[M + 2Na]^+$; HRMS (ES^+) calcd. for $C_{12}H_{17}IN$ $[M + H]^+$: 302.0406, found: 302.0414.

Methyl 4-((4,4,8-trimethyl-2-oxo-1,2,3,4-tetrahydroquinolin-6-yl)ethynyl)benzoate (96)

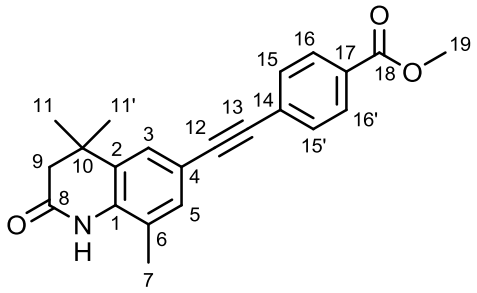

6-Iodo-4,4,8-trimethyl-3,4-dihydroquinolin-2(1*H*)-one **93** (1.00 g, 3.17 mmol) and methyl 4-ethynylbenzoate **16** (483 mg, 3.01 mmol) were mixed in triethylamine (50 mL) under an inert nitrogen atmosphere in a Schlenk tube. Nitrogen gas was bubbled through the mixture for 10 min, then $Pd(PPh_3)_2Cl_2$ (111 mg, 0.16 mmol, 5 mol%) and CuI (30 mg, 0.16 mmol, 5 mol%) were added, and the mixture was purged with nitrogen for a further 10 min. The flask was sealed, and the mixture heated to 80 °C overnight, after which the solvent was removed under high vacuum. Given that the product proved unstable to purification *via* chromatographic means, the residue was dissolved in ethanol (10 mL), and the insoluble title product was filtered out as a green-coloured powdery solid (690 mg, 66%): m.p. 222-224 °C; ^{1}H NMR (700 MHz; $CDCl_3$) δ 8.02 (unsymmet. d, *J* = 8.4, 2H, $H_{16+16'}$), 7.67 (br s, 1H, NH), 7.57 (unsymmet. d,

J = 8.4, 2H, $H_{15+15'}$), 7.36 (s, 1H, H_3), 7.27 (s, 1H, H_5), 3.93 (s, 3H, H_{19}), 2.50 (s, 2H, H_9), 2.26 (s, 3H, H_7), 1.35 (s, 6H, H_{11}); ^{13}C NMR (176 MHz; $CDCl_3$) δ 170.3 (C_8), 166.7 (C_{18}), 134.9 (C_1), 132.9 (C_2), 132.6 (C_5), 131.5 ($C_{15+15'}$), 129.7 ($C_{16+16'}$), 129.5 (C_{17}), 128.2 (C_{14}), 126.3 (C_3), 123.3 (C_6), 117.2 (C_4), 92.6 (C_{12}), 88.1 (C_{13}), 52.4 (C_{19}), 45.1 (C_9), 34.3 (C_{10}), 27.7 ($C_{11+11'}$), 17.1 (C_7); IR (neat) ν_{max}/cm^{-1} 2962m (C-H_{alkyl}), 2209m (C≡$C_{disub.}$), 1713s (C=O_{ester}), 1673s (C=O_{amide}), 1599s (C=$C_{ar.}$), 1475s (C=$C_{ar.}$); MS (ES^+): *m/z* = 348 $[M + H]^+$; UV-vis (EtOH) λ_{max}/nm (ε/M^{-1} cm^{-1}): 324 (33 800). Anal. calcd. for $C_{22}H_{21}NO_3$: C, 76.06; H, 6.09; N, 4.03. Found: C, 75.17; H, 6.08; N, 4.05.

4-((4-Amino-3-(1-carboxy-2-methylpropan-2-yl)-5-methylphenyl)ethynyl)benzoic acid (97)

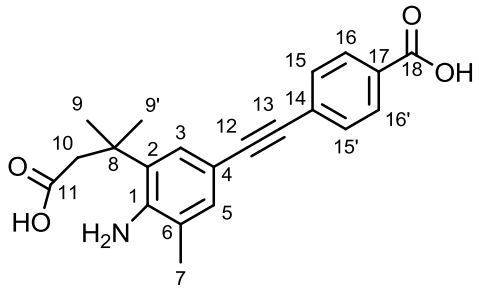

Methyl 4-((4,4,8-trimethyl-2-oxo-1,2,3,4-tetrahydroquinolin-6-yl)ethynyl)benzoate **96** (300 mg, 0.86 mmol) was dissolved in THF/H_2O (3:1, 24 mL), and NaOH (35 mg, 0.86 mmol) was added. The mixture was heated to 70 °C overnight, after which diethyl ether (20 mL) and water (10 mL) were added to the cooled mixture. The aqueous layer was acidified to pH 1, which resulted in a white suspension that was insoluble in organic solvents. The solution was basified to pH 5-7 with aqueous KOH, then extracted with ethyl acetate (3 x 20 mL). The combined organic layers were dried over $MgSO_4$, and following *in vacuo* removal of the solvent, the title compound was obtained as a white solid (100 mg, 33%): ^{1}H NMR (700 MHz; DMSO-d_6) δ 9.66 (d, *J* = 4.2, 1H, OH), 7.98 and 7.95 (2 x d, *J* = 8.4, 1H, $H_{16+16'}$), 7.66 and 7.62 (2 x d, *J* = 8.4, 1H, $H_{15+15'}$), 7.36 (d, *J* = 4.2, 1H, H_3), 7.29 (s, 1H, H_5), 3.87 (s, 1.5H, OMe), 2.38 (s, 2H, H_{10}), 2.24 (s, 3H, H_7), 1.26 (s, 6H, $H_{9+9'}$); ^{13}C NMR (176 MHz; DMSO-d_6) δ 170.2 (C_{11}), 166.9 (C_{18}), 166.0 (C_{COOMe}), 136.2 (C_1), 133.6 (C_2), 132.4 (C_5), 131.6 ($C_{15+15'}$), 129.7 ($C_{16+16'}$),

129.1 (C_{17}), 127.7 (C_{14}), 125.8 (C_3), 124.8 (C_6), 115.5 (C_4), 93.3 (C_{12}), 87.7 (C_{13}), 52.5 (C_{COOMe}), 44.7 (C_{10}), 33.8 (C_8), 27.2 ($C_{9+9'}$), 17.4 (C_7); IR (neat) ν_{max}/cm^{-1} 3200m br (N-H), 2960w (C-H_{alkyl}), 2180w (C≡$C_{disub.}$), 1694s (C=O_{acid}), 1674s (C=O_{amide}), 1644s (N-H), 1599s (C=$C_{ar.}$), 1476s (C=$C_{ar.}$); MS (ES^-): *m/z* = 332 $[M - H^+ - H_2O]^-$; UV-vis (EtOH) λ_{max}/nm ($\varepsilon/M^{-1}\ cm^{-1}$): 316 (5 300). HRMS ($ES^+$) calcd. for $C_{21}H_{18}NO_3$ $[M - H^+ - H_2O]^-$: 332.1287, found: 332.1286.

6-Iodo-1-isopropyl-4,4,8-trimethyl-3,4-dihydroquinolin-2(1*H*)-one (87)

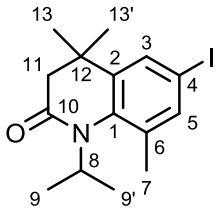

6-Iodo-4,4,8-trimethyl-3,4-dihydroquinolin-2(1*H*)-one **93** (1.50 g, 4.76 mmol) and NaH - 60% dispersion in mineral oil - (476 mg, 11.9 mmol) were added to a Schlenk flask. The flask was evacuated and purged with nitrogen three times, then dry DMF (25 mL) was added and the mixture heated to 85 °C for 1 h. 2-Iodopropane (950 µl, 9.52 mmol) was added to the cooled mixture, followed by heating to 85 °C. After overnight reaction, the reaction mixture was cooled, and water (20 mL) was added. The mixture was then extracted with dichloromethane (3 x 30 mL), and the combined organic layers were washed with water (50 mL), followed by brine (50 mL), and dried over $MgSO_4$. The solvent was removed *in vacuo*, and the residue was purified by flash chromatography on silica gel (hexane:EtOAc, 9:1, as eluent) to provide the title compound as a pale yellow solid (1.18 g, 69%) following *in vacuo* removal of the solvent: m.p. 91-93 °C; ^{1}H NMR (700 MHz; $CDCl_3$) δ 7.40 (unsymmet. d, *J* = 1.4, 1H, H_5), 7.39 (unsymmet. d, *J* = 2.1, 1H, H_3), 5.39 (septet, *J* = 6.3, 1H, H_8), 2.30 (s, 3H, H_7), 2.19 (s, 2H, H_{11}), 1.33 (d, *J* = 6.3, 6H, $H_{9+9'}$), 1.21 (s, 6H, $H_{13+13'}$); ^{13}C NMR (176 MHz; $CDCl_3$) δ 164.6 (C_{10}), 141.6 (C_1), 138.0 (C_2), 137.4 (C_5), 135.7 (C_4), 130.1 (C_3), 88.2 (C_6), 68.4 (C_8), 40.0 (C_{11}), 33.8 (C_{12}), 27.6 ($C_{13+13'}$), 21.9 ($C_{9+9'}$). 17.6 (C_7); IR (neat) ν_{max}/cm^{-1} 2968s (C-H_{alkyl}), 1621s (C=O); MS (ES^+): *m/z* = 358 $[M + H]^+$; HRMS (ES^+) calcd. for $C_{15}H_{21}INO$ [M +

H]$^+$: 358.0668, found: 358,0657. Anal. calcd. for $C_{15}H_{20}INO$: C, 50.43; H, 5.64; N, 3.92. Found: C, 49.61; H, 5.54; N, 3.72.

Methyl 4-((1-isopropyl-4,4,8-trimethyl-2-oxo-1,2,3,4-tetrahydroquinolin-6-yl)ethynyl)benzoate (98)

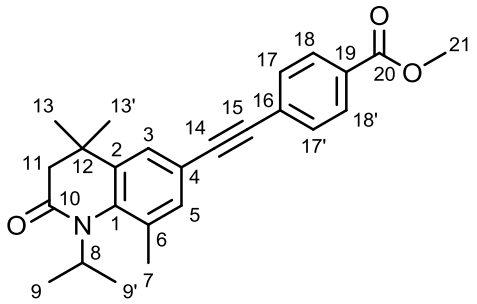

6-Iodo-1-isopropyl-4,4,8-trimethyl-3,4-dihydroquinolin-2(1*H*)-one **87** (240 mg, 0.67 mmol) and methyl 4-ethynylbenzoate **16** (108 mg, 0.67 mmol) were dissolved in triethylamine (10 mL) in a Schlenk tube, and nitrogen gas was bubbled through the mixture for 10 min. $Pd(PPh_3)_2Cl_2$ (24 mg, 0.03 mmol, 5 mol%) and CuI (6 mg, 0.03 mmol, 5 mol%) were added, and the mixture was purged with nitrogen for a further 10 min. The sealed flask was heated to 80 °C overnight, after which the solvent was removed under high vacuum, and the residue purified by column chromatography on silica gel (hexane:EtOAc, 93:7, as eluent). Following *in vacuo* removal of the solvent, the title compound was obtained as a yellow solid (233 mg, 89%): m.p. 85-87 °C; ^{1}H NMR (700 MHz; $CDCl_3$) δ 8.00 (d, J = 8.4, 2H, $H_{18+18'}$), 7.58 (d, J = 8.4, 2H, $H_{17+17'}$), 7.31 (d, J = 1.4, 1H, H_3), 7.28 (d, J = 1.4, 1H, H_5), 5.43 (septet, J = 6.3, 1H, H_8), 3.93 (s, 3H, H_{21}), 2.36 (s, 3H, H_7), 2.24 (s, 2H, H_{11}), 1.35 (d, J = 6.3, 6H, $H_{9+9'}$), 1.25 (s, 6H, $H_{13+13'}$); ^{13}C NMR (176 MHz; $CDCl_3$) δ 166.8 (C_{20}), 165.2 (C_{10}), 142.7 (C_1), 135.8 (C_2), 133.3 (C_6), 132.2 (C_5), 131.5 ($C_{17+17'}$), 129.6 ($C_{18+18'}$), 129.2 (C_{19}), 128.7 (C_{16}), 124.9 (C_3), 117.6 (C_4), 93.8 (C_{14}), 87.8 (C_{15}), 68.5 (C_8), 52.3 (C_{21}), 40.1 (C_{11}), 33.9 (C_{12}), 27.7 ($C_{13+13'}$), 21.9 ($C_{9+9'}$), 17.9 (C_7); IR (neat) ν_{max}/cm^{-1} 2962s (C-H_{alkyl}), 2925s (C-H_{alkyl}), 2203m (C≡$C_{disub.}$), 1726s (C=O_{ester}), 1633s (C=O_{amide}), 1587s (C=$C_{ar.}$), 1463s (C=$C_{ar.}$), 1434s (C=$C_{ar.}$); MS (ES$^+$): *m/z* = 390 [M + H]$^+$; UV-vis (EtOH) λ_{max}/nm (ε/M^{-1} cm^{-1}): 332 (22 900). Anal. calcd. for $C_{25}H_{27}NO_3$: C, 77.09; H, 6.99; N, 3.60. Found: C, 76.98; H, 7.00; N, 3.41.

6.8. Synthetic procedures for oxazoline-containing compounds

N-(2-Hydroxyethyl)-4-iodobenzamide (99)

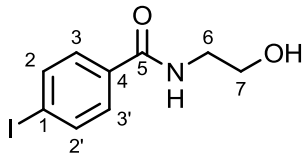

Methyl 4-iodobenzoate **45** (7.7 g, 29.4 mmol) was dissolved in dry tetrahydrofuran (50 mL), after which ethanolamine (3.5 mL, 58.8 mmol) and sodium methoxide (222 mg, 4.11 mmol) were added. The flask was sealed, and the mixture stirred at 30 °C for 18 h, with reaction completion monitored by TLC analysis. Water (250 mL) was added, and the resulting precipitate was filtered, washed with water (50 mL), and dried *in vacuo* to provide the product as a white crystalline solid (7.5 g, 88%): m.p. 161-163 °C; ^{1}H NMR (700 MHz; CD_3OD) δ 7.83 (unsymmet. d, J = 8.4, 2H, $H_{2+2'}$), 7.59 (unsymmet. d, J = 8.4, 2H, $H_{3+3'}$), 3.70 (t, J = 5.6, 2H, H_7), 3.49 (t, J = 5.6, 2H, H_6); ^{13}C NMR (176 MHz; CD_3OD) δ 169.6 (C_5), 138.9 ($C_{2+2'}$), 135.2 (C_4), 130.0 ($C_{3+3'}$), 99.1 (C_1), 61.5 (C_6), 43.6 (C_7); IR (neat) ν_{max}/cm^{-1} 3294s br (O-H), 2872m (C-H_{alkyl}), 1625s (C=O_{amide}), 1589s (C=$C_{ar.}$), 1552s (C=$C_{ar.}$); MS (ES$^+$): *m/z* = 292 [M + 1]$^+$, 314 [M + Na]$^+$. Anal. calcd. for $C_9H_{10}INO_2$: C, 37.14; H, 3.46; N, 4.81. Found: C, 37.21; H, 3.46; N, 4.76.

2-(4-Iodophenyl)-4,5-dihydrooxazole (100)

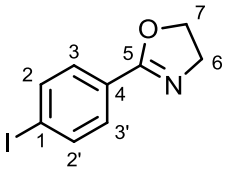

N-(2-Hydroxyethyl)-4-iodobenzamide **99** (7.50 g, 25.8 mmol), 4-dimethylaminopyridine (630 mg, 5.2 mmol) and triethylamine (10.2 mL, 73.2 mmol) were stirred in dry dichloromethane (200 mL). 4-Toluenesulfonyl chloride (8.35 g, 43.8 mmol) was added, the flask sealed, and the mixture stirred at 30 °C for 18 h, with reaction completion monitored by TLC analysis. The mixture was poured onto water (200 mL) and the organic layer was separated. The aqueous layer was extracted with chloroform (3 x

150 mL). The combined organic layers were dried over $MgSO_4$, and the solvent removed *in vacuo*. The residue was then dissolved in methanol (200 mL), and NaOH (3.1 g, 77.5 mmol) was added. After stirring the mixture at room temperature for 2 h, chloroform (200 mL) and water (200 mL) were added. The organic layer was separated, and the aqueous layer was extracted with chloroform (3 x 150 mL). The combined organic layers were dried over $MgSO_4$ and the solvent removed *in vacuo*. The residue was then filtered through a pad of silica (CH_2Cl_2:MeOH, 95:5, as eluent) to obtain the product as a pale yellow crystalline solid (5.11 g, 72%) following *in vacuo* removal of the solvent: m.p. 108-110 °C; ^{1}H NMR (700 MHz; $CDCl_3$) δ 7.76 (unsymmet. d, J = 8.4, 2H, $H_{2+2'}$), 7.65 (unsymmet. d, J = 8.4, 2H, $H_{3+3'}$), 4.42 (t, J = 9.8, 2H, H_7), 4.04 (t, J = 9.8, 2H, H_6); ^{13}C NMR (176 MHz; $CDCl_3$) δ 164.2 (C_5), 137.7 ($C_{2+2'}$), 129.8 ($C_{3+3'}$), 127.4 (C_4), 98.3 (C_1), 67.9 (C_6), 55.1 (C_7); IR (neat) ν_{max}/cm^{-1} 2926m (C-H_{alkyl}), 2871m (C-H_{alkyl}), 1640s (C=N), 1587s (C=$C_{ar.}$); MS (ES^+): *m/z* = 274 $[M + H]^+$. Anal. calcd. for C_9H_8INO: C, 39.59; H, 2.95; N, 5.13. Found: C, 39.48; H, 3.03; N, 5.04.

2-(4-((Trimethylsilyl)ethynyl)phenyl)-4,5-dihydrooxazole (101)

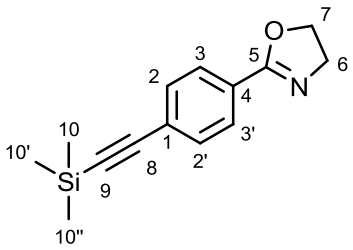

A Schlenk tube was charged with 2-(4-iodophenyl)-4,5-dihydrooxazole **100** (2.0 g, 7.3 mmol), CuI (70 mg, 0.37 mmol) and $Pd(PPh_3)_2Cl_2$ (257 mg, 0.37 mmol). After evacuating and filling the flask with argon three times, dry DMF (20 mL) was added, and argon was bubbled through the stirred mixture for 10 minutes. Triethylamine (2.04 mL, 14.6 mmol) and trimethylsilylacetylene (2.07 mL, 14.6 mmol) were added, the flask was sealed, and the mixture stirred at room temperature for 18 hours. Ethyl acetate (50 mL) was added, and the mixture was washed with water (3 x 50 mL). The organic layer was dried over $MgSO_4$ and the solvent removed *in vacuo* to provide a brown solid (purified yield not yet available): ^{1}H NMR (700 MHz; $CDCl_3$) δ 7.87

(unsymmet. d, *J* = 8.4, 2H, $H_{3+3'}$), 7.49 (unsymmet. d, *J* = 8.4, 2H, $H_{2+2'}$), 4.42 (t, *J* = 9.8, 2H, H_7), 4.05 (t, *J* = 9.8, 2H, H_6), 0.25 (s, 9H, $H_{10+10'+10''}$); ^{13}C NMR (176 MHz; $CDCl_3$) δ 164.2 (C_5), 132.0 ($C_{2+2'}$), 128.1 ($C_{3+3'}$), 127.6 (C_4), 126.1 (C_1), 104.5 (C_8), 96.9 (C_9), 67.8 (C_7), 55.1 (C_6), 0.00 ($C_{10+10'+10''}$); MS (GC): *m/z* = 243 $[M]^+$.

2-(4-Ethynylphenyl)-4,5-dihydrooxazole (102)

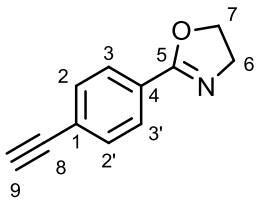

2-(4-((Trimethylsilyl)ethynyl)phenyl)-4,5-dihydrooxazole **101** (380 mg, 1.6 mmol) and Na_2CO_3 (662 mg, 6.3 mmol) were mixed in methanol and water (11 mL, 10:1) and stirred overnight at room temperature. Diethyl ether (10 mL) was then added, and the mixture was washed with water (3 x 10 mL), the aqueous layers were combined and extracted with diethyl ether (2 x 20 mL). The combined organic extracts were dried over $MgSO_4$ and the solvent removed *in vacuo* to give a yellow crystalline solid (220 mg, 82%): ^{1}H NMR (700 MHz; $CDCl_3$) δ 7.90 (unsymmet. d, *J* = 8.4, 2H, $H_{3+3'}$), 7.52 (unsymmet. d, *J* = 8.4, 2H, $H_{2+2'}$), 4.43 (t, *J* = 9.8, 2H, H_7), 4.07 (t, *J* = 9.8, 2H, H_6), 3.18 (s, 1H, H_9); ^{13}C NMR (176 MHz; $CDCl_3$) δ 164.2 (C_5), 132.2 ($C_{2+2'}$), 128.2 ($C_{3+3'}$), 128.1 (C_4), 125.1 (C_1), 83.2 (C_8), 79.4 (C_9), 67.9 (C_7), 55.2 (C_6); MS (ES^+): *m/z* = 172 $[M + H]^+$.

6-((4-(4,5-dihydrooxazol-2-yl)phenyl)ethynyl)-4,4,8-trimethyl-3,4-dihydroquinolin-2(1H)-one (103)

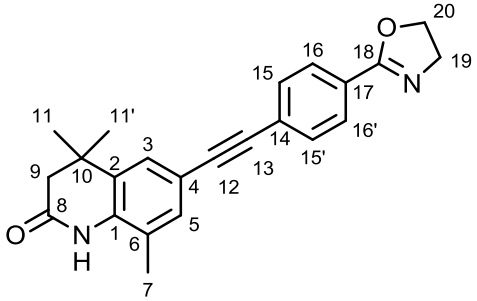

*In order to reduce compound degradation/decomposition, and to improve the yield, this procedure should be repeated using DMF as the solvent (see procedure for synthesis of compound **101**), and purification via chromatographic means should be avoided.*

A Schlenk tube was charged with 6-iodo-4,4,8-trimethyl-3,4-dihydroquinolin-2(1*H*)-one **93** (386 mg, 1.22 mmol), 2-(4-ethynylphenyl)-4,5-dihydrooxazole **102** (220 mg, 1.29 mmol), $Pd(PPh_3)_2Cl_2$ (43 mg, 0.06 mmol, 5 mol%) and CuI (12 mg, 0.06 mmol, 5 mol%). The flask was evacuated and filled with argon three times, after which dry triethylamine (10 mL) was added, and argon was bubbled through the stirred mixture. After 10 min, the flask was sealed and heated to 80 °C overnight. The cooled mixture was filtered, and triethylamine was removed *in vacuo*. The product was triturated from acetonitrile to provide compound **103** as an orange solid (160 mg, 37%): m.p. 224-226 °C; ^{1}H NMR (700 MHz; $CDCl_3$) δ 7.92 (d, J = 8.4, 2H, $H_{16+16'}$), 7.55 (d, J = 8.4, 2H, $H_{15+15'}$), 7.45 (br s, 1H, NH), 7.36 (s, 1H, H_3), 7.26 (s, 1H, H_5), 4.45 (t, J = 9.1, 2H, H_{20}), 4.08 (t, J = 9.1, 2H, H_{19}), 2.50 (s, 2H, H_9), 2.25 (s, 3H, H_7), 1.35 (s, 6H, $H_{11+11'}$); ^{13}C NMR (176 MHz; $CDCl_3$) δ 170.2 (C_8), 164.3 (C_{18}), 134.7 (C_1), 132.8 (C_2), 132.5 (C_5), 131.5 ($C_{15+15'}$), 128.3 ($C_{16+!6'}$), 127.3 (C_{17}), 126.5 (C_{14}), 126.3 (C_3), 123.1 (C_6), 117.5 (C_4), 91.8 (C_{12}), 88.4 (C_{13}), 67.9 (C_{20}), 55.2 (C_{19}), 45.1 (C_9), 34.3 (C_{10}), 27.8 ($C_{11+11'}$), 17.0 (C_7); IR (neat) ν_{max}/cm^{-1} 3236m br (N-H), 2960m (C-H_{alkyl}), 1674s (C=N), 1650s (C=O), 1600m (C=$C_{ar.}$), 1511m (C=$C_{ar.}$), 1475s (C=$C_{ar.}$); MS (ES^+): *m/z* = 359 $[M + H]^+$; UV-vis (EtOH) λ_{max}/nm (ε/M^{-1} cm^{-1}): 324 (34 700). Anal. calcd. for $C_{23}H_{22}N_2O_2$: C, 77.07; H, 6.19; N, 7.82. Found: C, 76.24; H, 6.10; N, 7.63.

7. REFERENCES

1. L. J. Gudas, *J. Biol. Chem.*, 1994, **269**, 15399-15402.
2. J. L. Napoli, *Clin. Immunol. Immunopathol.*, 1996, **80**, S52-S62.
3. R. Blomhoff and H. K. Blomhoff, *J. Neurobiol.*, 2006, **66**, 606-630.
4. Shmarakov, M. K. Fleshman, D. N. D'Ambrosio, R. Piantedosi, K. M. Riedl, S. J. Schwartz, R. W. Curley Jr, J. von Lintig, L. P. Rubin, E. H. Harrison and W. S. Blaner, *Arch. Biochem. Biophys*, 2010, **504**, 3-10.
5. R. Kawaguchi, J. Yu, J. Honda, J. Hu, J. Whitelegge, P. Ping, P. Wiita, D. Bok and H. Sun, *Science*, 2007, **315**, 820-825.
6. L. Wu and A. C. Ross, *J. Lipid Res.*, 2010, **51**, 378-387.
7. P. Bouillet, V. Sapin, C. Chazaud, N. Messaddeq, D. Decimo, P. Dolle and P. Chambon, *Mech. Dev.*, 1997, **63**, 173-186.
8. L. L. Sandell, B. W. Sanderson, G. Moiseyev, T. Johnson, A. Mushegian, K. Young, J. P. Rey, J. X. Ma, K. Staehling-Hampton and P. A. Trainor, *Genes Dev.*, 2007, **21**, 1113-1124.
9. M. Donovan, B. Olofsson, A. L. Gustafson, L. Dencker and U. Eriksson, *J. Steroid Biochem. Mol. Biol.*, 1995, **53**, 459-465.
10. T. T. Schug, D. C. Berry, N. S. Shaw, S. N. Travis and N. Noy, *Cell*, 2007, **129**, 723-733.
11. S. A. Kliewer, K. Umesono, D. J. Mangelsdorf and R. M. Evans, *Nature*, 1992, **355**, 446-449.
12. M. Maden, *Nature Rev. Neurosci.*, 2007, **8**, 755-765.
13. B. Appel and J. S. Eisen, *Neuron*, 2003, **40**, 461-464.
14. M. Kim, A. Habiba, J. M. Doherty, J. C. Mills, R. W. Mercer and J. E. Huettner, *Dev. Biol.*, 2009, **328**, 456-471.
15. P. W. Andrews, *Dev. Biol.*, 1984, **103**, 285-293.
16. E. M. V. Jones-Villeneuve, M. W. McBurney, K. A. Rogers and V. I. Kalnins, *J. Cell. Biol.*, 1982, **94**, 253-262.
17. J. Mey and P. McCaffery, *Neuroscientist*, 2004, **10**, 409-421.
18. H. Wichterle, I. Lieberam, J. A. Porter and T. M. Jessell, *Cell*, 2002, **110**, 385-397.

19. X.-J. Li, B.-Y. Hu, S. A. Jones, Y.-S. Zhang, T. LaVaute, Z.-W. Du and S.-C. Zhang, *Stem Cells*, 2008, **26**, 886-893.
20. R. C. Moon, G. J. Kelloff, C. J. Detrisac, V. E. Steele, C. F. Thomas and C. C. Sigman, *Anticancer Res.*, 1994, **14**, 5-11.
21. Y. Li, Y. Zhang, J. Hill, H. T. Kim, Q. Shen, R. P. Bissonnette, W. W. Lamph and P. H. Brown, *Br. J. Cancer*, 2008, **98**, 1380-1388.
22. Y. Wang, W. Wen, Y. Yi, Z. Zhang, R. A. Lubet and M. You, *Cancer Prev. Res.*, 2009, **2**, 1059-1064.
23. R. K. Shah, T. A. Valdez, Z. Wang and S. M. Shapshay, *Laryngoscope*, 2001, **111**, 1203-1208.
24. C. Pisano, L. Vesci, R. Fodera, F. F. Ferrara, C. Rossi, M. De Cesare, V. Zuco, G. Pratesi, R. Supino and F. Zunino, *Ann. Oncol.*, 2007, **18**, 1500-1505.
25. B. Liu, K. W. Lee, H. Li, L. Ma, G. L. Lin, R. A. Chandraratna and P. Cohen, *Cancer Res.*, 2005, **11**, 4851-4856.
26. M. H. Bukhari, S. S. Qureshi, S. Niazi, M. Asef, M. Naheed, S. A. Kahn, N. A. Chaudhry, M. Tayyab and M. Hasan, *Int. J. Dermatol.*, 2007, **46**, 1160-1165.
27. A. Yamane, N. Tsukamoto, T. Saitoh, H. Uchiumi, H. Handa, M. Karasawa, Y. Nojima and H. Murakami, *Intern. Med.*, 2009, **48**, 1691-1694.
28. M. J. Edelman, R. Smith, P. Hausner, L. A. Doyle, K. Kalra, J. Kendall, M. Bedor and S. Bisaccia, *J. Clin. Oncol.*, 2005, **23**, 5774-5778.
29. Y. Muto, H. Moriwaki and Y. Shiratori, *Digestion*, 1998, **59** (Suppl 2), 89-91.
30. F. Recchia, G. Sica, G. Candeloro, S. Necozione, R. Bisegna, M. Bratta and S. Rea, *Oncol. Rep.*, 2009, **21**, 1011-1016.
31. S. Alvarez, P. Germain, R. Alvarez, F. Rodriguez-Barrios, H. Gronemeyer and A. R. de Lera, *Int. J. Biochem. Cell Biol.*, 2007, **39**, 1406-1415.
32. M. Petkovich, N. J. Brand, A. Krust and P. Chambon, *Nature*, 1987, **330**, 444-450.
33. P. Chambon, *FASEB J.*, 1996, **10**, 940-954.
34. P. Dolle, *Nucl. Recept. Signal.*, 2009, **7**, e006.

35. T. Lufkin, D. Lohnes, M. Mark, A. Dierich, P. Gorry, M. P. Gaub, M. LeMeur and P. Chambon, *Proc. Natl. Acad. Sci. USA*, 1993, **90**, 7225-7229.

36. N. B. Ghyselinck, V. Dupe, A. Dierich, N. Messaddeq, J. M. Garnier, C. Rochette-Egly, P. Chambon and M. Mark, *Int. J. Dev. Biol.*, 1997, **41**, 425-447.

37. D. Lohnes, P. Kastner, A. Dierich, M. Mark, M. LeMeur and P. Chambon, *Cell*, 1993, **73**, 643-658.

38. H. M. Sucov, E. Dyson, C. L. Gumeringer, J. Price, K. R. Chien and R. M. Evans, *Genes Dev.*, 1994, **8**, 1007-1018.

39. P. Kastner, J. M. Grondona, M. Mark, A. Gansmuller, M. LeMeur, D. Decimo, J. L. Vonesch, P. Dolle and P. Chambon, *Cell*, 1994, **78**, 987-1003.

40. H. M. Sucov, J. C. Izpisua-Belmonte, Y. Ganan and R. M. Evans, *Development*, 1995, **121**, 3997-4003.

41. P. Kastner, M. Mark, M. Leid, A. Gansmuller, W. Chin, J. M. Grondona, D. Decimo, W. Krezel, A. Dierich and P. Chambon, *Genes Dev.*, 1996, **10**, 80-92.

42. B. Mascrez, N. B. Ghyselinck, M. Watanabe, J. S. Annicotte, P. Chambon, J. Auwerx and M Mark, *EMBO Rep.*, 2004, **5**, 285-290.

43. W. Krezel, V. Dupe, M. Mark, A. Dierich, P. Kastner and P. Chambon, *Proc. Natl. Acad. Sci. USA*, 1996, **93**, 9010-9014.

44. C. Mendelsohn, D. Lohnes, D. Decimo, T. Lufkin, M. LeMeur, P. Chambon and M. Mark, *Development*, 1994, **120**, 2749-2771.

45. C. Mendelsohn, M. Mark, P. Dolle, A. Dierich, M. P. Gaub, A. Krust, C. Lampron and P. Chambon, *Dev. Biol.*, 1994, **166**, 246-258.

46. E. Li, H. M. Sucov, K. F. Lee, R. M. Evans and R. Jaenisch, *Proc. Natl. Acad. Sci. U. S. A.*, 1993, **90**, 1590-1594.

47. T. J. Desai, F. Chen, J. Lu, J. Qian, K. Niederreither, P. Dolle, P. Chambon and W. V. Cardoso, *Dev. Biol.*, 2006, **291**, 12-24.

48. Y. Liu, M. O. Lee, H. G. Wang, Y. Li, Y. Hashimoto, M. Klaus, J. C. Reed and X. Zhang, *Mol. Cell. Biol.*, 1996, **16**, 1138-1149.

49. Y. Li, M. I. Dawson, A. Agadir, M. O. Lee, L. Jong, P. D. Hobbs and X. K. Zhang, *Int. J. Cancer*, 1998, **75**, 88-95

50. R. Pergolizzi, V. Appierto, M. Crosti, E. Cavadini, L. Cleris, A. Guffanti and F. Formelli, *Int. J. Cancer*, 1999, **81**, 829-834.

51. M. J. Campbell, S. Park, M. R. Uskokovic, M. I. Dawson and H. P. Koeffler, *Endocrinology*, 1998, **139**, 1972-1980.

52. N. Ferrari, M. Pfahl and G. Levi, *Mol. Cell. Biol.*, 1998, **18**, 6482-6492.

53. A. D. Hoffman, D. Engelstein, T. Bogenrieder, C. N. Papandreou, E. Steckelman, A. Dave, R. J. Motzer, E. Dmitrovsky, A. P. Albino and D. M. Nanus, *Clin. Cancer Res.*, 1996, **2**, 1077-1082.

54. A. Kaiser, H. Herbst, G. Fisher, M. Koenigsmann, W. E. Berdel, E. O. Riecken and S. Rosewicz, *Gastroenterology*, 1997, **113**, 920-929.

55. C. Li and Y. J. Wan, *Cancer Lett.*, 1998, **124**, 205-211.

56. R. J. Shaw, T. Liloglou, S. N. Rogers, J. S. Brown, E. D. Vaughan, D. Lowe, J. K. Field and J. M. Risk, *Cancer*, 2006, **94**, 561-568.

57. L. Di Croce, V. A. Raker, M. Corsaro, F. Fazi, M. Fanelli, M. Faretta, F. Fuks, F. Lo Coco, T. Kouzarides, C. Nervi, S. Minucci and P. G. Pelicci, *Science*, 2002, **295**, 1079-1082.

58. S. M. Sirchia, M. Ren, R. Pili, E. Sironi, G. Somenzi, R. Ghidoni, S. Toma, G. Nicolo and N. Sacchi, *Cancer Res.*, 2002, **62**, 2455-2461.

59. S. E. Touma, J. S. Goldberg, P. Moench, X. Guo, S. K. Tickoo, L. J. Gudas and D. M. Nanus, *Clin. Cancer Res.*, 2005, **11**, 3558-3566.

60. S. P. Si, X. Lee, H. C. Tsou, R. Buchsbaum, E. Tibaduiza and M. Peacocke, *Exp. Cell Res.*, 1996, **223**, 102-111.

61. V. L. Seewaldt, B. S. Johnson, M. B. Parker and S. J. Collins, *Cell Growth & Differ.*, 1995, **6**, 1077-1088.

62. E. Weber, R. K. Ravi, E. S. Knudsen, J. R. Williams, L. E. Dillehay, B. D. Nelkin, G. P. Kalemkerian, J. R. Feramisco and M. Mabry, *Int. J. Cancer*, 1999, **80**, 935-943.

63. Y. Zhuang, T. N. Faria, P. Chambon and L. J. Gudas, *Mol. Cancer Res.*, 2003, **1**, 619-630.

64. H. de The, M. Vivanco-Ruiz, P. Tiollais, H. Stunnenberg and A. Dejean, *Nature*, 1990, **343**, 177-180.

65. C. A. Martin, L. M. Ziegler and J. L. Napoli, *Proc. Natl. Acad. Sci. U. S. A.*, 1990, **87**, 4804-4808.

66. J. Corcoran, B. Shroot, J. Pizzey and M. Maden, *J. Cell. Sci.*, 2000, **113**, 2567-2574.

67. P. L. So, P. K. Yip, S. Bunting, L. F. Wong, N. D. Mazarakis, S. Hall, S. McMahon, M. Maden and J. P. Corcoran, *Dev. Biol.*, 2006, **298**, 167-175.

68. J. Corcoran, P.-L. So, R. D. Barber, K. J. Vincent, N. D. Mazarakis, K. A. Mitrophanous, S. M. Kingsman and M. Maden, *J. Cell. Sci.*, 2002, **115**, 3779-3786.

69. L. F. Wong, P. K. Yip, A. Battaglia, J. Grist, J. Corcoran, M. Maden, M. Azzouz, S. M. Kingsman, A. J. Kingsman, N. D. Mazarakis and S. B. McMahon, *Nat. Neurosci.*, 2006, **9**, 243-250.

70. P. K. Yip, L. F. Wong, D. Pattinson, A. Battaglia, J. Grist, E. J. Bradbury, M. Maden, S. B. McMahon and N. D. Mazarakis, *Hum. Mol. Genet.*, 2006, **15**, 3107-3118.

71. M. Agudo, P. Yip, M. Davies, E. Bradbury, P. Doherty, S. McMahon,. M. Maden and J. P. Corcoran, *Neurobiol. Dis.*, 2010, **37**, 147-155.

72. M. B. Goncalves, M. Agudo, S. Connor, S. McMahon, S. L. Minger, M. Maden and J. P. Corcoran, *Dev. Biol.*, 2009, **326**, 305-313.

73. L. H. Camacho, *J. Biol. Regul. Homeost. Agents*, 2003, **17**, 98-114.

74. A. K. Silverman, C. N. Ellis and J. J. Voorhees, *J. Am. Acad. Dermatol.*, 1987, **16**, 1027-1039.

75. R. M. Russell, J. L. Boyer, S. Bagheri and Z. Hruban, *N. Engl. J. Med.*, 1974, **291**, 435-440.

76. J. K. Ellis, R. M. Russell, F. L. Makrauer and E. J. Schaefer, *Ann. Intern. Med.*, 1986, **105**, 877-879.

77. T. O. Carpenter, J. M. Pettifor, R. M. Russell, J. Pitha, S. Mobarhan, M. S. Ossip, S. Wainer and C. S. Anast, *J. Pediatr.*, 1987, **111**, 507-512.

78. E. Z. Szuts and F. I. Harosi, *Arch. Biochem. Biophys.*, 1991, **287**, 297-304.

79. A. Stephens-Jarnagin, D. A. Miller and H. F. DeLuca, *Arch. Biochem. Biophys.*, 1985, **237**, 11-16.

80. M. I. Dawson, P. D. Hobbs, K. Derdzinski, R. L.-S. Chan, J. Gruber, W.-R. Chao, S. Smith, R. W. Thies and L. J. Schiff, *J. Med. Chem.*, 1984, **27**, 1516-1531.

81. T. Yamakawa, H. Kagechika, E. Kawachi, Y. Hashimoto and K. Shudo, *J. Med. Chem.*, 1990, **33**, 1430-1437.

82. M. Teng, T. T. Duong, E. S. Klein, M. E. Pino and R. A. S. Chandraratna, *J. Med. Chem.*, 1996, **39**, 3035-3038.

83. B. P. Klaholz, J.-P. Renaud, A. Mitschler, C. Zusi, P. Chambon, H. Gronemeyer and D. Moras, *Nat. Struct. Biol.*, 1998, **5**, 199-202.

84. K. M. Waugh, K. D. Berlin, W. T. Ford, E. M. Holt, J. P. Carroll, P. R. Schomber and L. J. Schiff, *J. Med. Chem.*, 1985, **27**, 116-124.

85. D. M. Benbrook, M. M. Madler, L. W. Spruce, P. J. Birckbichler, E. C. Nelson, S. Subramanian, G. M. Weerasekare, J. B. Gale, M. K. Patterson Jr, B. Wang, W. Wang, S. Lu, T. C. Rowland, P. DiSilvestro, C. Lindamood III, D. L. Hill and K. D. Berlin, *J. Med. Chem.*, 1997, **40**, 3567-3583.

86. D. M. Benbrook, S. Subramanian, J. B. Gale, S. Liu, C. W. Brown, M. F. Boehm and K. D. Berlin, *J. Med. Chem.*, 1998, **41**, 3753-3757.

87. T. Okitsu, D. Nakazawa, K. Nakagawa, T. Okano and A. Wada, *Chem. Pharm. Bull.*, 2010, **58**, 418-422.

88. T. Okitsu, K. Sato, K. Iwatsuka, N. Sawada, K. Nakagawa, T. Okano, S. Yamada, H. Kakuta and A. Wada, *Bioorg. Med. Chem.*, 2011, **19**, 2939-2949.

89. M. Ebisawa, E. Kawachi, H. Fukasawa, Y. Hashimoto, A. Itai, K. Shudo and H. Kagechika, *Biol. Pharm. Bull.*, 1998, **21**, 547-549.

90. M. Ebisawa, K. Ohta, E. Kawachi, H. Fukasawa, Y. Hashimoto and H. Kagechika, *Chem. Pharm. Bull. (Tokyo)*, 2001, **49**, 501-503.

91. J. Charton, R. Deprez-Poulain, N. Hennuyer, A. Tailleux, B. Staels and B. Deprez, *Bioorg. Med. Chem. Lett.*, 2009, **19**, 489-492.

92. P. Germain, P. Chambon, G. Eichele, R. M. Evans, M. A. Lazar, M. Leid, A. R. de Lera, R. Lotan, D. J. Mangelsdorf and H. Gronemeyer, *Pharmacol. Rev.*, 2006, **58**, 712-725.

93. S. Nagpal, S. M. Thacher, S. Patel, S. Friant, M. Malhotra, J. Shafer, G. Krasinski, A. T. Asano, M. Teng, M. Duvic and R. A. S. Chandraratna, *Cell Growth Differ.*, 1996, **7**, 1783-1791.

94. J. Look, J. Landwehr, F. Bauer, A. S. Hoffmann, H. Bluethmann and P. LeMotte, *Am. J. Physiol.*, 1995, **269**, 91-98.

95. A. M. Standeven, R. L. Beard, A. T. Johnson, M. F. Boehm, M. Escobar, R. A. Heyman and R. A. S. Chandraratna, *Fund. Appl. Toxicol.*, 1996, **33**, 264-271.

96. K. Shimono, W. Tung, C. Macolino, A. H. Chi, J. H. Didizian, C. Mundy, R. A. Chandraratna, Y. Mishina, M. Enomoto-Iwamoto, M. Pacifici and M. Iwamoto, *Nature Med.*, 2011, **17**, 454-461.

97. J. Rees, *Br. J. Dermatol.*, 1992, **126**, 97-104.

98. S. Nagpal and R. A. S. Chandraratna, *Curr. Pharm. Des.*, 1996, **2**, 295-316.

99. P. Germain, S. Kammerer, E. Pérez, C. Peluso-Iltis, D. Tortolani, F. C. Zusi, J. Starrett, P. Lapointe, J.-P. Daris, A. Marinier, A. R. de Lera, N. Rochel and H. Gronemeyer, *EMBO Rep.*, 2004, **5**, 877-882.

100. B. P. Klaholz, A. Mitschler and D. Moras, *J. Mol. Biol.*, 2000, **302**, 155-170.

101. B. W. Lund, F. Piu, N. K. Gauthier, A. Eeg, E. Currier, V. Sherbukhin, M. R. Brann, U Hacksell and R. Olsson, *J. Med. Chem.*, 2005, **48**, 7517-7519.

102. B. W. Lund, A. E. Knapp, F. Piu, N. K. Gauthier, M. Begtrup, U. Hacksell and R. Olsson, *J. Med. Chem.*, 2009, **52**, 1540-1545.

103. (*a*) K. Umemura, K. Watanabe, K. Ono, M. Yamaura and J. Yoshimura, *Tetrahedron Lett.*, 1997, **38**, 4811-4814; (*b*) R. A. Hughes, S. P. Thompson, L. Alcaraz and C. J. Moody, *J. Am. Chem. Soc.*¸ 2005, **127**, 15644-15651.

104. (*a*) J. Mulzer, A. Mantoulidis and E. Öhler, *Tetrahedron Lett.*, 1997, **38**, 7725-7728; (*b*) C. J. Moody and J. C. A. Hunt, *J. Org. Chem.*, 1999, **64**, 8715-8717; (*c*) S. Kehraus, G. M. Konig, A. D. Wright and G. Woerheide, *J. Org. Chem.*, 2002, **67**, 4989-4992.

105. (*a*) M. J. Remuiñán and G. Pattenden, *Tetrahedron Lett.*, 2000, **41**, 7367-7371; (*b*) D. Romo, N. S. Choi, S. Li, I. Buchler, Z. Shi and J. O. Liu, *J. Am. Chem. Soc.*, 2004, **126**, 10582-10588; (*c*) M.-Y. Jang, Y. Lin, S. D. Jonghe, L.-J. Gao, B. Vanderhoydonck, M. Froeyen, J. Rozenski, J. Herman, T. Louat, K. V. Belle, M. Waer and P. Herdewijn, *J. Med. Chem.*, 2011, **54**, 655-668.

106. G.-L. Zhou, *"Synthesis and evaluation of small molecules for stem cell differentiation"*, MSci project, 2010, Durham University.

107. F. A. J. Kedersky, J. H. Holms, J. L. Moore, R. L. Bell, R. D. Dyer, G. W. Carter, D. W. Brooks, *J. Med. Chem.*, 1991, **34**, 2158–2165.

108. R. M. Rzasa, M. R. Kaller, G. Lia, E. T. Magal, T. Nguyen, T. D. Osslund, D. Powers, V. S. Satora, V. N. Viswanadhan, H.-L. Wang, X. Xiong, W. Zhong, H.M. Norman, *Bioorg. Med. Chem.*, 2007, **15**, 6574–6595.

109. G. C. Barrett, *Tetrahedron,* 1980, **36**, 2023-2058.

110. E. Täuscher, D. Weiß, R. Beckert, J. Fabian, A. Assumpção, H. Görls, *Tetrahedron Lett.*, 2011, **52**, 2292-2294.

111. A. Arcadi, O. A. Attanasi, B. Guidi, E. Rossi, S. Santeusanio, *Eur. J. Org. Chem.*, **1999**, 3117-3126.

112. S. M. Ronkin, M. Badia, S. Bellon, A.-L. Grillot, C. H. Gross, T. H. Grossman, N. Mani, J. D. Parsons, D. Stamos, M. Trudeau, Y. Wei, P. S. Charifson, *Bioorg. Med. Chem. Lett.*, 2010, **20**, 2828-2831.

113. S. A. Przyborski, *Stem Cells*, 2001, **19**, 500-504.

114. R. Stewart, V. Christie and S. A. Przyborski, *Stem Cells*, 2003, **21**, 248-256.

115. (*a*) V. B. Christie, J. H. Barnard, A. S. Batsanov. C. E. Bridgens, E. B. Cartmell, J. C. Collings, D. J. Maltman, C. P. F. Redfern, T. B. Marder, S. A. Przyborski, A. Whiting, *Org. Biomol. Chem.*, 2008, **6**, 3497-3507; (*b*) V. B. Christie, D. J. Maltman, A. P. Henderson, A. Whiting, T. B. Marder, M. Lako and S. A. Przyborski, *J. Neurosci. Methods*¸ 2010, **193**, 239-245.

116. D. J. Maltman, V. B. Christie, J. C. Collings, J. H. Barnard, S. Fenyk, T. B. Marder, A. Whiting, S. A. Przyborski, *Mol. BioSyst.*, 2009, **5**, 458-471.

117. K. Rurack and U. Resch-Genger, *Chem. Soc. Rev.*, 2002, **31**, 116-127.

118. S. Suresh, *Acta Mater.*, 2007, **55**, 3989-4014.

119. B. N. G. Giepmans, S. R. Adams, M. H. Ellisman and R. Y. Tsien, *Science*, 2006, **312**, 217-224.

120. L. A. Ernst, R. K. Gupta, R. B. Mujumdar and A. S. Waggoner, *Cytometry*, 1989, **10**, 3-10.

121. R. F. Kubin and A. N. Fletcher, *J. Lumin.*, 1982, **27**, 455-462.

122. R. Y. Tsien, *Annu. Rev. Biochem.*, 1998, **67**, 509-544.

123. M. V. Matz, Y. A. Labas and J. Ugalde, *Methods Biochem. Anal.*, 2006, **47**, 139-161.

124. D. M. Chudakov, S. Lukyanov and K. A. Lukyanov, *Trends Biotechnol.*, 2005, **23**, 605-613.

125. N. C. Shaner, P. A. Steinbach and R. Y. Tsien, *Nat. Methods*, 2005, **2**, 905-909.

126. M. Ormö, A. B. Cubitt, K. Kallio, L. A. Gross, R. Y. Tsien and S. J. Remington, *Science*, 1996, **273**, 1392-1395.

127. T. Suzuki, T. Nishimaki-Mogami, H. Kawai, T. Kobayashi, Y. Shinozaki, Y. Sato, T. Hashimoto, Y. Asakawa, K. Inoue, Y. Ohno, T. Hayakawa and T. Kawanishi, *Phytomedicine*, 2006, **13**, 401-411.

128. M. A. Walling J. A. Novak and J. R. E. Shepard, *Int. J. Mol. Sci.*, 2009, **10**, 441-491.

129. B. Ballou, B. C. Lagerholm, L. A. Ernst, M. P. Bruchez and A. S. Waggoner, *Bioconjugate Chem.*, 2004, **15**, 79-86.

130. X. Michalet, F. F. Pinaud, L. A. Bentolila, J. M. Tsay, S. Doose, J. J. Li, G. Sundaresan, A. M. Wu, S. S. Gambhir and S. Weiss, *Science*, 2005, **307**, 538-544.

131. B. Dubertret, P. Skourides, D. J. Norris, V. Noireaux, A. H. Brivanlou and A. Libchaber, *Science*, 2002, **298**, 1759-1762.

132. A. M. Derfus, W. C. W. Chan and S. N. Bhatia, *Nano Lett.*, 2004, **4**, 11-18.

133. L. Song, C. A. Varma, J. W. Verhoeven and H. J. Tanke, *Biophys. J.*, 1996, **70**, 2959-2968.

134. R. A. Hoebe, C. H. Van Oven, T. W. Gadella Jr, P. B. Dhonukshe, C. J. F. Van Noorden and E. M. Manders, *Nat. Biotechnol.*, 2007, **25**, 249-253.

135. C. Eggeling, J. Widengren, L. Brand, J. Schaffer, S. Felekyan and C. A. M. Seidel, *J. Phys. Chem. A*, 2006, **110**, 2979-2995.

136. X. Kong, E. Nir, K. Hamadani and S. Weiss, *J. Am. Chem. Soc.*, 2007, **129**, 4643-4654.

137. G. Donnert, C. Eggeling and S. W. Hell, *Nat. Methods*, 2007, **4**, 81-86.

138. R. E. Benesch and R. Benesch, *Science*, 1953, **118**, 447-448.

139. I. Rasnik, S. A. McKinney and T. Ha, *Nat. Methods*, 2006. **3**, 891-893.

140. F. Köhn, J. Hofkens, R. Gronheid, M. Van der Auweraer and F. C. De Schryver, *J. Phys. Chem. A*, 2002, **106**, 4808-4814.

141. J. Widengren and P. Schwille, *J. Phys. Chem. A*, 2000, **104**, 6416-6428.

142. J. Lippincott-Schwartz, E. Snapp and A. Kenworthy, *Nat. Rev. Mol. Cell Biol.*, 2001, **2**, 444-456.

143. J. Zheng, *Methods Mol. Biol.*, 2006, **337**, 65-77.

144. X. S. Xie, J. Yu and W. Y. Yang, *Science*, 2006, **312**, 228-230.

145. G. S. Harms, L. Cognet, P. H. M. Lommerse, G. A. Blab and T. Schmidt, *Biophys. J.*, 2001, **80**, 2396-2408.

146. C. Joo, H. Balci, Y. Ishitsuka, C. Buranachai and T. Ha, *Annu. Rev. Biochem.*, 2008, **77**, 51-76.

147. R. Iino, I. Koyama and A. Kusumi, *Biophys. J.*, 2001, **80**, 2667-2677.

148. Y. Sako, S. Minoghchi and T. Yanagida, *Nat. Cell Biol.*, 2000, **2**, 168-172.

149. M. Ueda, Y. Sako, T. Tanaka, P. Devreotes and T. Yanagida, *Science*, 2001, **294**, 864-867.

150. M. Vrljic, S. Y. Nishimura, S. Brasselet, W. E. Moerner and H. M. McConnell, *Biophys. J.*, 2002, **83**, 2681-2692.

151. M. Dahan, S. Levi, C. Luccardini, P. Rostaing, B. Riveau and A. Triller, *Science*, 2003, **302**, 442-445.

152. M. D. Wang, M. J. Schnitzer, H. Yin, R. Landick, J. Gelles and S. M. Block, *Science*, 1998, **282**, 902-907.

153. S. C. Blanchard, R. L. Gonzalez Jr., H. D. Kim. S. Chu and J. D. Puglisi, *Nat. Struct. Mol. Biol.*, 2004, **11**, 1008-1014.

154. J. Elf, G. W. Li and X. S. Xie, *Science*, 2007, **316**, 1191-1194.

155. B. Fahrenkrog and U. Aebi, *Nat. Rev. Mol. Cell Biol.*, 2003, **4**, 757-766.

156. W. Yang, J. Gelles and S. M. Musser, *Proc. Natl. Acad. Sci. USA*, 2004, **101**, 12887-12892.

157. C. Kural, H. Kim, S. Syed, G. Goshima, V. I. Gelfand and P. R. Selvin, *Science*, 2005, **308**, 1469-1472.

158. D. Fusco, N. Accornero, B. Lavoie, S. M. Shenoy, J.-M. Blanchard, R. H. Singer and E. Bertrand, *Curr. Biol.*, 2003, **13**, 161-167. 394.

159. A. Bashirullah, R. L. Cooperstock and H. D. Lipshitz, *Annu. Rev. Biochem.*, 1998, **67**, 335-

160. B. J. Cha, B. S. Koppetsch and W. E. Theurkauf, *Cell*, 2001, **106**, 35-46.

161. G. S. Wilkie and I. Davies, *Cell*, 2001, **105**, 209-219.

162. B. Sodeik, M. W. Ebersold and A. Helenius, *J. Cell Biol.*, 1997, **136**, 1007-1021.

163. J. S. Bartlett and R. J. Samulski, *Nature Med.*, 1998, **4**, 635-637.

164. G. Seisenberger, M. U. Reid, T. Endreß, H. Büning, M. Hallek and C. Bräuchle, *Science*, 2001, **294**, 1929-1932.

165. K. M. Laginha, S. Verwoert, G. J. R. Charrois and T. M. Allen, *Clin. Cancer Res*, 2005, **11**, 6944-6949.

166. K. K. Karukstis, E. H. Thompson, J. A. Whiles and R. J. Rosenfeld, *Biophys. Chem.*, 1998, **73**, 249-263.

167. O. Hovorka, V. Subr, D. Větvička, L. Kovář, J. Strohalm, M. Strohalm, A. Benda, M. Hof, K. Ulbrich and B. Ríhová, *Eur. J. Pharm. Biopharm.*, 2010, **76**, 514-524.

168. P. Mohan and N. Rapoport, *Mol. Pharm.*, 2010, **7**, 1959-1973.

169. J. H. Barnard, *unpublished results*, 2010, Durham University.

170. J. N. Norcliffe, MSci project, 2011, Durham University.

171. M. H. Bickel, *Pharmacol. Rev.*, 1969, **21**, 325-255.

172. R. M. Dawson, *Biochem. J.*, 1975, **149**, 293-295.

173. J. Subik, G. Takacsova, M. Psenak and F. Devinsky, *Antimicrob. Agents Chemother.*, **1977**, 139-146.

174. J. March, *Advanced Organic Chemistry*, 4th ed., **2000**, Wiley-Interscience, New York.

175. T. Mukaiyama, H. Kitagawa and J. Matsuo, *Tetrahedron Lett.*, 2000, **41**, 9383-9386.

176. A.-S. Castanet, F. Colobert and P.-E. Broutin, *Tetrahedron Lett.*, 2002, **43**, 5047-5048.

177. S. Adimurthy, G. Ramachandraiah, P. K. Ghosh and A. V. Bedekar, *Tetrahedron Lett.*, 2003, **44**, 5099-5101.

178. T. Yamamoto, K. Toyota and N. Morita, *Tetrahedron Lett.*, 2010, **51**, 1364-1366.

179. J. N. Kim, H. S. Kim, J. H. Gong and Y. M. Chung, *Tetrahedron Lett.,* 2001**, 42**, 8341-8344.

180. L. Foucout, F. Gourand, M. Dhilly, P. Bohn, G. Dupas, J. Costentin, A. Abbas, F. Marsais, L. Barré and V. Levacher, *Org. Biomol. Chem.*, 2009**, 7**, 3666-3673.

181. R. M. G. Roberts, D. Ostović and M. M. Kreevoy, *J. Org. Chem.*, 1983**, 48**, 2053-2056.

182. A. Klapars and S. L. Buchwald, *J. Am. Chem. Soc.*, 2002**, 124**, 14844-14845.

183. H. R. Memarian, A. Farhadi, H. Sabzyan and M. Soleymani, *J Photochem. Photobiol. A: Chem.*, 2010, **209**, 95-103.

184. M. Rózanowska, A. Cantrell, R. Edge, E. J. Land, T. Sarna and T. G. Truscott, *Free Radic. Biol. Med.*, 2005, **39**, 1399-1405.

185. R. Wilson, BSI project report, 2012, Durham University.

186. A. Palmer, BSI project report, 2012, Durham University.

187. S. Sakami, K. Kawai, M. Maeda, T. Aoki, H. Fujii, H. Ohno, T. Ito, A. Saitoh, K. Nakao, N. Izumimoto, H. Matsuura, T. Endo, S. Ueno, K. Natsume and H. Nagase, *Bioorg. Med. Chem.*, 2008, **16**, 7956-7967.

188. T. Narender, S. Sarkar, K. Rajendar and S. Tiwari, *Organic Lett.*, 2011, **13**, 6140-6143.

189. A. Orchard, G. A. Schamerhorn, B. D. Calitree, G. A. Sawada, T. W. Loo, M. C. Bartlett, D. M. Clarke and M. R. Dettya, *Bioorg. Med. Chem.*, 2012, **20**, 4290-4302.

190. R. Johnsson, A. Meijer and U. Ellervik, *Tetrahedron*, 2005, **61**, 11657-11663.

191. A. Dhar, S. Liu, J. Klucik, K. D. Berlin, M. M. Madler, S. Lu, R. T. Ivey, D. Zacheis, C. W. Brown, E. C. Nelson, P. J. Birckbichler and D. M. Benbrook, *J. Med. Chem.*, 1999, **42**, 3602-3614.

192. C. Monnereau, E. Blart and F. Odobel, *Tetrahedron Lett.*, 2005, **46**, 5421-5423.

193. J. I. Levin and S. M. Weinreb, *Tetrahedron Lett.*, 1982, **23**, 2347-2350.

194. Y. Kato, M. M. Conn and J. Rebek Jr., *J. Am. Chem. Soc.*, 1994, **116**, 3279-3284.

195. A. L. S. Thompson, G. W. Kabalka, R. M. Akula and J. W. Huffman, *Synthesis*, 2005, **4**, 547-550.

196. Q. Li, A. V. Rukavishnikov, P. A. Petukhov, T. O. Zaikova, C. Jin and J. F. W. Keana, *J. Org. Chem.*, 2003, **68**, 4862-4869.

197. G. T. Crisp and P. D. Turner, *Tetrahedron*, 2000, **56**, 407-415.

198. D. W. Slocum, K. C. Kristen, Q. Nguyen, P. E. Whitley, T. K. Reinscheld and B. Fouzia, *Tetrahedron Lett.*, 2011, **52**, 7141-7145.